National Library
of Canada

Bibliothèque nationale
du Canada

Canadian Theses Service

Service des thèses canadiennes

Ottawa, Canada
K1A 0N4

NOTICE

The quality of this microform is heavily dependent upon the quality of the original thesis submitted for microfilming. Every effort has been made to ensure the highest quality of reproduction possible.

If pages are missing, contact the university which granted the degree.

Some pages may have indistinct print especially if the original pages were typed with a poor typewriter ribbon or if the university sent us an inferior photocopy.

Reproduction in full or in part of this microform is governed by the Canadian Copyright Act, R.S.C. 1970, c. C-30, and subsequent amendments.

AVIS

La qualité de cette microforme dépend grandement de la qualité de la thèse soumise au microfilmage. Nous avons tout fait pour assurer une qualité supérieure de reproduction.

S'il manque des pages, veuillez communiquer avec l'université qui a conféré le grade.

La qualité d'impression de certaines pages peut laisser à désirer, surtout si les pages originales ont été dactylographiées à l'aide d'un ruban usé ou si l'université nous a fait parvenir une photocopie de qualité inférieure.

La reproduction, même partielle, de cette microforme est soumise à la Loi canadienne sur le droit d'auteur, SRC 1970, c. C-30, et ses amendements subséquents.

NL-339 (r. 88/04) c

Canada

THE UNIVERSITY OF ALBERTA

TIME-DEPENDENT INSTABILITY IN FISSURED, OVER-CONSOLIDATED CLAYS AND MUDSTONES

BY

NOBUYUKI YOSHIDA

©

A THESIS
SUBMITTED TO THE FACULTY OF GRADUATE STUDIES AND
RESEARCH IN PARTIAL FULFILMENT OF THE REQUIREMENTS FOR
THE DEGREE OF
DOCTOR OF PHILOSOPHY

DEPARTMENT OF CIVIL ENGINEERING

EDMONTON, ALBERTA
SPRING, 1990

National Library of Canada

Bibliothèque nationale du Canada

Canadian Theses Service

Service des thèses canadiennes

Ottawa, Canada
K1A 0N4

NOTICE

The quality of this microform is heavily dependent upon the quality of the original thesis submitted for microfilming. Every effort has been made to ensure the highest quality of reproduction possible.

If pages are missing, contact the university which granted the degree.

Some pages may have indistinct print especially if the original pages were typed with a poor typewriter ribbon or if the university sent us an inferior photocopy.

Reproduction in full or in part of this microform is governed by the Canadian Copyright Act, R.S.C. 1970, c. C-30, and subsequent amendments.

AVIS

La qualité de cette microforme dépend grandement de la qualité de la thèse soumise au microfilmage. Nous avons tout fait pour assurer une qualité supérieure de reproduction.

S'il manque des pages, veuillez communiquer avec l'université qui a conféré le grade.

La qualité d'impression de certaines pages peut laisser à désirer, surtout si les pages originales ont été dactylographiées à l'aide d'un ruban usé ou si l'université nous a fait parvenir une photocopie de qualité inférieure.

La reproduction, même partielle, de cette microforme est soumise à la Loi canadienne sur le droit d'auteur, SRC 1970, c. C-30, et ses amendements subséquents.

ISBN 0-315-60332-1

NL-339 (r. 88/04) c

Canada

THE UNIVERSITY OF ALBERTA

RELEASE FORM

NAME OF AUTHOR: Nobuyuki Yoshida

TITLE OF THESIS: TIME-DEPENDENT INSTABILITY IN FISSURED, OVER-CONSOLIDATED CLAYS AND MUDSTONES

DEGREE FOR WHICH THESIS WAS PRESENTED: Doctor of Philosophy

YEAR THIS DEGREE GRANTED: Spring, 1990

Permission is hereby granted to THE UNIVERSITY OF ALBERTA LIBRARY to reproduce single copies of this thesis and to lend or sell such copies for private, scholarly or scientific research purposes only.

The author reserves other publication rights, and neither the thesis nor extensive extracts from it may be printed or otherwise reproduced without the author's written permission.

(SIGNED) Nobuyuki Yoshida

PERMANENT ADDRESS:

Naka 1-9, Suwanomori
Hamadera, Sakai
Osaka
JAPAN 592

DATE March 20, 1990

THE UNIVERSITY OF ALBERTA
FACULTY OF GRADUATE STUDIES AND RESEARCH

The undersigned certify that they have read, and recommend to the Faculty of Graduate Studies and Research for acceptance, a thesis entitled TIME-DEPENDENT INSTABILITY IN FISSURED, OVER-CONSOLIDATED CLAYS AND MUDSTONES submitted by Nobuyuki Yoshida in partial fulfilment of the requirements for the degree of Doctor of Philosophy.

Dr. N. R. Morgenstern (Supervisor)

Dave Chan
Dr. D. H. Chan

Dr. Z. Eisenstein

Dr. A. Elwi

K. Barron
Dr. K. Barron

Hoek
Dr. E. Hoek (External Examiner)

Date: March 15, 1990

Dedication

To my father and mother

Abstract

Stability problems in fissured, over-consolidated clays and mudstones are troublesome because of their time-dependent nature. This time-dependent instability has been attributed to softening and long-term pore water pressure effects.

A comprehensive review of time-dependent instability in fissured, over-consolidated clays and mudstones is presented. The mechanisms and effects of softening are discussed in detail. The effects of long-term pore water pressure equalization are also considered. The mechanism of softening described by Terzaghi appears to be valid. Weathering effects also contribute to softening. Softening may be classified into internal and external mechanisms. Field evidence for softening are collected from the literature. Softening effects can be seen to result in a decrease in the shear strength of a material with time, accompanied by a reduction in the dilatancy characteristics.

A simple non-linear failure criterion is proposed for materials of interest in this study. The usefulness of this failure criterion is demonstrated through comparisons with experimental data taken from the literature. The shear strength reduction due to softening may be described rationally from the initial to the fully-softened condition, using the proposed failure criterion together with time-dependent strength parameters.

It is proposed to analyze the effects of softening by means of the finite element method. This follows a conventional elastic-plastic formulation. The proposed failure criterion is used in its generalized form as a yield function, together with the time-dependent strength parameters. The constitutive models are elastic, perfectly-plastic and strain-softening relations. Analyses of examples illustrate the effectiveness of this finite element formulation.

Analytical methods to analyze softening effects are also derived by incorporating the proposed failure criterion with time-dependent strength parameters into various existing methods of analysis. These methods provide a simple and inexpensive means of evaluating the effect of softening.

A comprehensive finite element analysis of softening is presented and an example is analyzed, which portrays the essentials of the role of the softening mechanism in time-dependent instability.

Time-dependent deformations observed in fissured, over-consolidated clays and mudstones are often analyzed as creep or visco-plastic behaviour. However, considering the calculation results presented in this work, it can be said that the concepts presented here provide an alternate means to analyze time-dependent instability without losing physical insight.

Acknowledgements

The author would like to express deep gratitude and appreciation to his supervisor and mentor, Professor N. R. Morgenstern, for his invaluable guidance and immeasurable assistance during the course of the research and the preparation of the dissertation. His continuous interest and enthusiasm to the project are greatly acknowledged.

The author wishes to express sincere thanks to Dr. D. H. Chan for his valuable comments on the finite element formulation.

The author also wishes to thank Dr. Y. Tanaka for his continuous advice and encouragement on studying abroad.

The financial support from the Department of Civil Engineering at the University of Alberta and by the Natural Sciences and Engineering Research Council of Canada is very much appreciated. The computing facilities were provided by the University of Alberta and the University of Calgary.

For their valuable comments on this thesis, the author would like to acknowledge the contributions of his examiners, Drs. D. H. Chan, Z. Eisenstein, A. Elwi, K. Barron and E. Hoek.

A special note of gratitude goes to Messrs. Alan Gale, Richard Chalaturnyk and Ms. Sharon Mayan for their timely help and support during the preparation of the dissertation.

Acknowledgement is extended to Mr. Gerry Cyre, senior technician of the Geotechnical Engineering Division, who has always provided assistance and was instrumental in the pressuremeter program.

A note of thanks goes to my colleagues, Messrs. Flavio M. Kuwajima, Richard Wan, W. Simon Tortike, Drs. Heinrich Heinz, T. T. Wong who have made my life here memorable and enjoyable.

Finally, the author would like to express special gratitude to his parents, Nao and Yasuyuki, who have been always a source of emulation, encouragement and perseverance.

Table of Contents

Chapter Page

1. Introduction ____ 1
   - 1.1 General ____ 1
   - 1.2 Scope of work ____ 2
2. Review of literature ____ 5
   - 2.1 Introduction ____ 5
   - 2.2 Softening ____ 5
   - 2.3 Field evidence of softening ____ 7
     - 2.3.1 English clays ____ 7
     - 2.3.2 Upper Cretaceous bedrock (Western Canada) ____ 11
     - 2.3.3 Japanese mudstones ____ 12
   - 2.4 Softening mechanism ____ 14
   - 2.5 Rate of softening ____ 23
   - 2.6 Pore water pressure effect ____ 24
     - 2.6.1 Long-term pore water pressure equalization ____ 24
     - 2.6.2 Relation between pore water pressure and softening ____ 28
   - 2.7 Theoretical studies ____ 29
   - 2.8 Summary ____ 31
3. Failure criterion ____ 63

3.1 Introduction ____ 63

3.2 Failure criterion ____ 63

3.2.1 Non-linear failure criterion ____ 63

3.2.2 Characteristics of proposed failure criterion ____ 67

3.2.3 Applications ____ 70

3.3 Representation of softening ____ 70

3.4 Summary ____ 72

4. Finite element analysis ____ 110

4.1 Introduction ____ 110

4.2 Finite element method ____ 111

4.2.1 Elastic-plastic constitutive relation ____ 111

4.2.2 Finite element formulation ____ 115

4.2.3 Computational procedure ____ 117

4.3 Yield function ____ 118

4.3.1 Generalization of yield function ____ 118

4.3.2 Singular points treatment ____ 120

4.4 Computer program ____ 121

4.5 Examples ____ 121

4.5.1 Elastic, perfectly-plastic model ____ 122

4.5.2 Strip footing analysis ____ 123

4.5.3 Cut slope analysis ____ 124

4.5.4 Tunnel analysis ____ 126

4.6 Summary ____ 127

5. Finite element analysis with strain-softening model ____ 153

5.1 Introduction ____ 153

5.2 Strain-softening model ____ 154

5.2.1 Description ____ 154

5.2.2 Triaxial compression test simulation ____ 158

5.3 Softening analysis ____ 159

5.4 Example ____ 160

5.5 Summary ____ 162

6. Analysis of high rock pressure in tunnelling ____ 180

6.1 Introduction ____ 180

6.2 Noshiro Tunnel No. 4 ____ 180

6.2.1 Brief description of tunnel ____ 180

6.2.2 Geotechnical properties of bedrock material ____ 181

6.3 Finite element analysis ____ 182

6.3.1 Determination of input data ____ 182

6.3.2 Analysis procedure ____ 184

6.4 Results of analysis and discussion ____ 185

6.5 Summary ____ 187

7. Simple evaluation of softening effect in geotechnical engineering problems ____ 219

7.1 Introduction ____ 219

7.2 Slope stability ____ 220

7.2.1 Infinite slip surface ____ 220

7.2.2 Circular slip surface ____ 221

7.3 Rankine earth pressure ____ 223

7.4 Stresses and displacements around tunnel ____ 224

7.5 Examples ____ 227

7.5.1 Slope stability analysis with an infinite slip surface ____ 227

7.5.2 Slope stability analysis with a circular slip surface ____ 228

7.5.3 Calculation of Rankine lateral earth pressure ____ 229

7.5.4 Rock-support interaction analysis ____ 230

7.6 Summary ____ 231

8. A comprehensive softening analysis ____ 249

8.1 Introduction ____ 249

8.2 Further insight into softening ____ 249

8.2.1 Internal and external softening ____ 249

8.2.2 Restriction on softening ____ 251

8.3 Finite element analysis ____ 253

8.3.1 Preliminary consideration ____ 253

8.3.2 Softening analysis ____ 254

8.3.3 Results 256

8.4 Commentary 257

8.5 Summary 259

9. Conclusions 273

9.1 Conclusions 273

9.2 Suggestions for future research 276

References 278

Appendix 289

List of Tables

Table Page

2.1 Index properties of London Clay 33

2.2 Mineralogy of clay fraction of London Clay 34

2.3 Index properties of Upper Lias Clay 35

2.4 Mineralogy of clay fraction of Upper Lias Clay 36

2.5 Index properties of bedrock materials at Devon Side site 37

2.6 Index properties of mudstone at Noshiro Tunnel No. 4 38

3.1 Strength parameters 74

4.1 Various yield functions 128

4.2 Gradient vectors for various yield functions 129

4.3 Material properties for strip footing and cut slope analyses 130

4.4 Material properties for tunnel analysis 131

5.1 Index properties of Tohoku Mudstone 164

5.2 Input data for triaxial test simulation 165

5.3 Input data for cut slope analysis 166

6.1 Index properties of Japanese Tertiary mudstones 189

6.2 Material properties for analysis of Noshiro Tunnel No. 4 190

7.1 Material properties for slope stability analysis 232

Table Page

7.2 Material properties for calculation of lateral earth pressure ____ 233

7.3 Material properties for rock-support interaction analysis ____ 234

8.1 Material properties of clay for excavation analysis ____ 260

List of Figures

Figure Page

2.1 Relation between average shear strength along slip surface.and time for cuttings and retaining walls in London Clay (modified after Skempton, 1948) 39

2.2 Moisture content variation in vicinity of thin soft failure zone at Uxbridge (modified after Henkel, 1957) 40

2.3 Strength reduction with time for London Clay (modified after James, 1970) 41

2.4 Relation between average shear strength and average effective normal stress (modified after James, 1970) 42

2.5 Relation between mean shear strength and mean effective normal stress for cutting slope failures in Upper Lias Clay (modified after Chandler,1974) 43

2.6 Typical stress-strain curves for softened and unsoftened back slope materials (modified after Eigenbrod and Morgenstern, 1971) 44

2.7 Results of triaxial tests on back slope materials (modified after Eigenbrod and Morgenstern, 1971) 45

2.8 Water content distribution before and after drained direct shear tests on mudstone specimen taken from Noshiro Tunnel No. 4 (modified after Nakano, 1979) 46

2.9 Typical stress-strain curves for mudstone and fault gouge clay taken from Noshiro Tunnel No. 4 (modified after Nakano, 1981) 47

2.10 Typical results of drained triaxial compression tests on undisturbed Blue London Clay samples taken from Level E (modified after Bishop *et al.*, 1965) 48

Figure Page

2.11 Shear strength of Blue London Clay taken from Wraysbury (modified after Marsland, 1971) 50

2.12 Shear strength of model specimen having rough surfaces 51

2.13 Shear strength reduction due to softening in stiff, fissured clay (modified after Morgenstern, 1977) 52

2.14 Results of oedometer tests using different procedures (modified after Graham and Au, 1985) 53

2.15 Results of triaxial tests on Lake Agssiz clays in normalized p'-q space (modified after Graham and Au, 1985) 54

2.16 Results of swelling tests on shale samples (modified after Peterson and Peters, 1963) 55

2.17 Changes in pore water pressure and factor of safety during and after excavation in clay (modified after Bishop and Bjerrum, 1960) 56

2.18 Relation between measured pore pressure ratio and elapsed time after excavation in Brown London Clay 57

2.19 Pore water pressure measurements at Queens Avenue (modified after McGown *et al.*, 1987) 58

2.20 Pore water pressure equalization in undisturbed material, Queens Avenue (modified after McGown *et al.*, 1987) 59

2.21 Pore water pressure equalization in disturbed material, Queens Avenue (modified after McGown *et al.*, 1987) 60

Figure		Page
2.22	Relation between coefficient of permeability and depth for Blue London Clay and Upper Lias Clay (modified after Walbancke, 1975)	61
2.23	Variation in pore pressure ratio with time (modified after Vaughan and Walbancke, 1973)	62
3.1	Influence of parameter A on failure envelope	76
3.2	Influence of parameter B on failure envelope	77
3.3	Influence of parameter S on failure envelope	78
3.4	Mohr's diagram (modified after Balmer, 1952)	79
3.5	Influence of parameter A on Mohr failure envelope	80
3.6	Influence of parameter B on Mohr failure envelope	81
3.7	Influence of parameter S on Mohr failure envelope	82
3.8	Influence of normal stress on angle of friction and cohesion intercept	83
3.9	Comparison of failure criterion with triaxial test data for Blue London Clay (Bishop *et al.*, 1965)	85
3.10	Comparison of failure criterion with triaxial test data for Keuper Marl (Chandler, 1967)	86
3.11	Comparison of failure criterion with triaxial test data for Kobe Mudstone 1 (Yoshinaka and Yamabe, 1980)	87
3.12	Comparison of failure criterion with triaxial test data for Kobe Mudstone 2 (Yoshinaka and Yamabe, 1980)	88
3.13	Comparison of failure criterion with triaxial test data for Ohya-Ishi (Tuff) (Adachi *et al.*, 1981)	89

Figure Page

3.14 Comparison of failure criterion with triaxial test data for Indiana Limestone (Schwartz, 1964) ____ 90

3.15 Comparison of failure criterion with triaxial test data for Georgia Marble (Schwartz, 1964) ____ 91

3.16 Comparison of failure criterion with triaxial test data for Pottsville Sandstone (Schwartz, 1964) ____ 92

3.17 Comparison of failure criterion with triaxial test data for Stone Mountain Granite (Schwartz, 1964) ____ 93

3.18 Comparison of failure criterion with triaxial test data for Tennessee Marble (Wawersik, 1968) ____ 94

3.19 Comparison of failure criterion with triaxial test data for Panguna Andesite (Jaeger, 1970) ____ 95

3.20 Comparison of failure criterion with triaxial test data for Shimajiri Mudstone (Shinjo, 1976) ____ 96

3.21 Comparison of failure criterion with triaxial test data for Tohoku Mudstone (Watanabe *et al.*, 1988) ____ 97

3.22 Comparison of failure criterion with triaxial test data for Devon Granite (test data from Franklin and Hoek, 1970) ____ 98

3.23 Comparison of failure criterion with triaxial test data for Portland Limestone (Franklin and Hoek, 1970) ____ 99

3.24 Comparison of failure criterion with triaxial test data for Derbyshire Sandstone (Franklin and Hoek, 1970) ____ 100

3.25 Comparison of failure criterion with triaxial test data for Darley Dale Sandstone (Franklin and Hoek, 1970) ____ 101

Figure Page

3.26 Comparison of failure criterion with triaxial test data for Carrara Marble (Franklin and Hoek, 1970) 102

3.27 Comparison of failure criterion with triaxial test data for Pennant Sandstone (Franklin and Hoek, 1970) 103

3.28 Variations of parameter A with time for different values of **a** 104

3.29 Variations of parameter B with time for different values of **b** 105

3.30 Variations of parameter S with time for different values of **c** 106

3.31 Variation in failure envelope during softening 107

3.32 Variation of angle of friction during softening 108

3.33 Variation of cohesion intercept during softening 109

4.1 Proposed yield criterion in principal stress space 132

4.2 Variation of yield surface during softening 133

4.3 Variation of stress, strain and shear strength during softening 134

4.4 Finite element mesh for strip footing analysis 135

4.5 Variation of settlement at center line with time 136

4.6 Strength envelopes just before collapse of ground 137

4.7 Development of plastic zones under footing (associated flow rule) 138

Figure Page

4.8 Development of plastic zones under footing (non-associated flow rule) 139

4.9 Finite element mesh for cut slope analysis 140

4.10 Variation of vertical displacement at crest of slope with time 141

4.11 Variation of horizontal displacement at crest of slope with time 142

4.12 Strength envelopes just before collapse of slope 143

4.13 Development of plastic zones in slope (associated flow rule) 144

4.14 Development of plastic zones in slope (non-associated flow rule) 145

4.15 Variation of vertical displacement at crest of slope with time 146

4.16 Variation of horizontal displacement at crest of slope with time 147

4.17 Development of plastic zones in slope (associated flow rule) 148

4.18 Development of plastic zones in slope (non-associated flow rule) 149

4.19 Finite element mesh for tunnel analysis 150

4.20 Variation of tunnel wall displacement with time 151

4.21 Development of plastic zones around tunnel 152

5.1 Assumed variations of strength parameters for post-peak behaviour 167

Figure Page

5.2 Yield surface and plastic potential surface 168

5.3 Comparison of computation with experimental results for Tohoku Mudstone 169

5.4 Effect of $\overline{\varepsilon_{s}^{p}}$ on computed stress-strain relation 170

5.5 Effect of A* on computed stress-strain relation 171

5.6 Variation of stress, strain and strength during softening 172

5.7 Finite element mesh for cut slope analysis 173

5.8 Strength envelopes at 0, 40 and 100 years 174

5.9 Stress and strain relations at 0, 40 and 100 years 175

5.10 Variation of displacements at crest of slope with time 176

5.11 Development of plastic zones in slope 177

5.12 Distribution of accumulated equivalent plastic strains along horizontal plane 178

5.13 Variation of mobilized shear strength envelopes along horizontal plane 179

6.1 Geology and location of Noshiro Tunnel No. 4 (modified after Nakano, 1979) 191

6.2 Measured fibre stresses at floor, spring line and roof in steel supports (modified after Nakano, 1974) 192

6.3 Shear strength of mudstone of Noshiro Tunnel No. 4 194

6.4 Swelling of remoulded mudstone under various vertical pressures (modified after Nakano, 1979) 195

Figure Page

6.5 Relation among vertical pressure, water content and uniaxial compression strength of mudstone (modified after Nakano, 1979) ____ 196

6.6 Input stress-strain relations ____ 197

6.7 Softening of mudstone in terms of normalized uniaxial compression strength ____ 198

6.8 Input variation of shear strength with time ____ 199

6.9 Finite element mesh for analysis of Noshiro Tunnel No. 4 ____ 200

6.10 Variation of normal stress at floor with time (elastic, perfectly-plastic model) ____ 201

6.11 Variation of normal stress at spring line with time (elastic, perfectly-plastic model) ____ 202

6.12 Variation of normal stress at roof with time (elastic, perfectly-plastic model) ____ 203

6.13 Variation of tangential stress at floor with time (elastic, perfectly-plastic model) ____ 204

6.14 Variation of tangential stress at spring line with time (elastic, perfectly-plastic model) ____ 205

6.15 Variation of tangential stress at roof with time (elastic, perfectly-plastic model) ____ 206

6.16 Normal stress distribution along lining ($K_0 = 1.0$) ____ 207

6.17 Normal stress distribution along lining ($K_0 = 1.5$) ____ 208

6.18 Development of plastic zones around tunnel ($K_0 = 1.0$) ____ 209

Figure Page

6.19 Development of plastic zones around tunnel ($K_0 = 1.5$) 210

6.20 Variation of normal stress at floor with time (strain-softening model) 211

6.21 Variation of normal stress at spring line with time (strain-softening model) 212

6.22 Variation of normal stress at roof with time (strain-softening model) 213

6.23 Variation of tangential stress at floor with time (strain-softening model) 214

6.24 Variation of tangential stress at spring line with time (strain-softening model) 215

6.25 Variation of tangential stress at roof with time (strain-softening model) 216

6.26 Development of plastic zones around tunnel ($K_0 = 1.0$) 217

6.27 Development of plastic zones around tunnel ($K_0 = 1.5$) 218

7.1 Slope with infinite slip surface 235

7.2 Slope with circular slip surface 236

7.3 Rankine active and passive states of stresses in horizontal ground 237

7.4 Circular tunnel under hydrostatic stress field 238

7.5 Variation with time of mobilized shear strength along slip surface 239

Figure Page

7.6 Variation of factor of safety with time for different values of r_u 240

7.7 Variation of factor of safety with time for different slope angles 241

7.8 Variation of factor of safety with time 242

7.9 Critical slip circles at time of 0 and 50 years for Case 3 243

7.10 Variation of factor of safety with time for different values of r_u 244

7.11 Rankine wall with horizontal ground surface 245

7.12 Active earth pressure distribution with depth 246

7.13 Variations with time of radial and tangential stresses around tunnel 247

7.14 Variation with time of ground convergence curve 248

8.1 Stress paths and pore water pressure changes before and after excavation 261

8.2 Pore water pressure at end of construction in 1:3 cut slope (modified after Walbancke, 1975) 262

8.3 Calculation of variation in pore water pressure with time in cut slope 263

8.4 Time contour showing equi-time lines for 1:3 cut slope 264

8.5 Ground condition of cut slope for finite element analysis 265

8.6 Finite element discretization of cut slope 266

Figure Page

8.7 Softening zones in ground for finite element analysis _ 267

8.8 Input strength variation with time at σ_3'=0.05 MPa ____ 268

8.9 Variation with time in horizontal displacements at crest and toe of slope ____ 269

8.10 Variation with time in vertical displacements at crest and toe of slope ____ 270

8.11 Development of plastic zones in cut slope ____ 271

8.12 Flow chart of comprehensive swelling-softening analysis ____ 272

Nomenclature

A, B and S	Strength parameters of the proposed failure criterion
a, b and c	Strength reduction-parameters for A, B and S, respectively
A_0, B_0 and S_0	Initial strength parameters of the proposed failure criterion
A_{fs}, B_{fs} and S_{fs}	Fully-softened strength parameters of the proposed failure criterion
A_r, B_r and S_r	Residual strength parameters of the proposed failure criterion
c'	Cohesion intercept in terms of effective stress
C.F.	Clay fraction
c_i	Instantaneous cohesion intercept
CSL	Critical State Line
$d\varepsilon_{ij}$	Strain increment tensor
D_{ijkl}	Constitutive tensor
$d\sigma_{ij}$	Stress increment tensor
E	Young's Modulus

ε_{ij}	Strain tensor
ε_p	Equivalent plastic strain
ε_v	Vertical strain
F	Yield function
ϕ'	Angle of friction in terms of effective stress
ϕ_i	Instantaneous angle of friction
F_s	Factor of safety
G	Plastic potential function
γ	Unit weight
I_1	First stress invariant
J_2	Second deviatric stress invariant
J_3	Third deviatric stress invariant
κ	Hardening (softening) parameter
K_0	Initial earth pressure ratio
LL	Liquid limit
m and s	Strength parameters of Hoek-Brown failure criterion
ν	Poisson's Ratio

p	$(\sigma_1+\sigma_3)/2$ (or $(\sigma_1+2\sigma_3)/3$ in Fig. 2.15)
P, Q and R	Strength parameters of the proposed failure criterion in terms of σ and τ
PI	Plasticity index
PL	Plastic limit
q	$(\sigma_1-\sigma_3)/2$ (or $(\sigma_1-\sigma_3)$ in Fig. 2.15)
r_u	Pore pressure ratio
σ	Normal stress
σ_1	Major principal stress
σ_3	Minor principal stress
σ_c	Uniaxial compression strength
σ_{c0}	Initial uniaxial compression strength
σ_{ij}	Stress tensor
σ_v	Vertical stress
σ_v'	Effective vertical stress
σ_{vc}'	Effective pre-consolidation pressure
τ	Shear stress
t	Time
t_f	Time to a fully-softened condition

u	Pore water pressure
w	Water content
w_n	Natural water content
Y	Yield stress from uniaxial tests
ψ	Dilatancy angle

1. Introduction

1.1 General

It has long been known that cut slopes in fissured, overconsolidated clays and mudstones may fail some considerable time after the slope was constructed. Further, the failure is often a 'first-time' failure; that is, there has been no previous instability due to landsliding or other geological processes. Cuttings in London Clay, for instance, often failed with delay of several to many decades after excavation. This time-dependent instability is attributed to reduction with time in the shear strength of a material. Two factors - softening and pore water pressure equalization - contribute to this loss of shear strength. Throughout this thesis 'softening' does not mean 'strain-softening' unless otherwise stated.

Softening is time-dependent and leads to a reduction in shear strength of material. It can be triggered by unloading which may be imposed artificially or naturally. Weathering also contributes to softening. Softening has received increased attention since Terzaghi described it in 1936 in connection with failure of slopes in stiff, fissured clays; but most often attention is directed toward determination of the shear strength operative at failure from back-analyses of failed slopes rather than understanding of the mechanisms and effects of softening.

In spite of the lack of understanding of softening, the effect of softening has been recognized in geotechnical practice by employing fully-softened shear strength parameters which are determined on the remoulded, normally-consolidated clay or by considering the c' component to be zero in the shear strength parameters of the undisturbed clay. These fully-softened strength parameters have been widely used not only in stability analyses but also in the deformation analyses of earth structures constructed in these materials. However, the softening mechanisms and their effects remain poorly-understood. Further, the time-dependency is often neglected or dealt with using wrong mechanisms.

It has been recognized that pore water pressure immediately after excavation is much smaller than the ultimate equilibrium pressure due to development of negative excess pore water pressure and that this depressed pore water tends to equalize with time toward the ultimate equilibrium condition. This is accompanied by swelling of the material. This pore water pressure equalization leads to a gradual decrease in effective stresses in the ground, thus resulting in a reduction in the shear strength.

The purpose of the research encompassed by this dissertation is to gain a better understanding of time-dependent instability in fissured, over-consolidated clays and mudstones with special emphasis on softening and the numerical analysis of softening effects.

1.2 Scope of work

To achieve the objective stated above the following scope of work has been pursued:

1. Review of literature (Chapter 2)

The purpose of this review is to clarify mechanisms of time-dependent instability in fissured, over-consolidated clays and mudstones. The main emphasis is placed upon softening. The concept and mechanism of softening are discussed together with an overview of field evidence and experimental studies. Pore water pressure effects are also considered. Finally, theoretical studies regarding softening are reviewed.

2. Development of a failure criterion (Chapter 3)

A simple non-linear failure criterion is proposed to represent the effect of softening which is clarified in Chapter 2. Time-dependent strength parameters are also proposed. Effectiveness of the failure criterion is evaluated through comparisons with experimental data taken from the literature.

3. Development of a finite element method (Chapters 4 and 5)

In order to analyze softening effects, a finite element method is developed based upon an elastic-plastic formulation. The failure criterion and time-dependent strength parameters proposed in Chapter 3 are incorporated in this finite element method. The constitutive model considers an elastic, perfectly-plastic (Chapter 4) and strain-softening (Chapter 5) relations. Although pore water pressure effects are included in the finite element method for an effective stress analysis, the dissipation of pore water pressure is not taken into account.

4. Application of the finite element analysis of softening to a rock pressure problem (Chapter 6)

In order to evaluate the usefulness of the finite element method proposed in previous chapters, a rock pressure problem observed in a tunnel constructed in mudstone bedrock is analyzed. The setting of this problem is taken from a case history in Japan.

5. Performance of simple analyses of softening in geotechnical engineering problems (Chapter 7)

In order to appreciate the effect of softening in routine analyses in a simple and inexpensive manner, the proposed failure criterion and time-dependent strength parameters are incorporated in several existing analytical methods in geotechnical engineering.

6. Consideration of a comprehensive softening analysis (Chapter 8)

A more comprehensive finite element analysis of softening is presented based upon a further discussion on softening and the concepts of softening established in Chapter 2, and an example is analyzed.

7. Conclusions (Chapter 9)

The conclusions drawn from this research work are summarized. Suggestions for future research are also given.

2. Review of literature

2.1 Introduction

This chapter reviews mechanisms of long-term instability of cut slopes and tunnels in fissured, over-consolidated clays and mudstones. The main emphasis is placed upon softening. The concept of softening is first described, followed by field evidence of softening. The field evidence comes from case histories of cut slopes in England, Canada and of tunnels in Japan. The mechanism of softening is then discussed based upon experimental studies available in the literature. Long-term pore water pressure effects, another factor in time-dependent instability, is also considered. Finally, theoretical studies on softening are reviewed.

2.2 Softening

As early as 1884, softening of fissured, over-consolidated clays and its importance were noticed by some engineers, in field investigations in connection with stability of cuttings for railroads in England. A first, clear explanation of the mechanism of softening was put forward by Terzaghi in 1936, in relation to cut slope failures in stiff, fissured clays. It is summarized as follows. The fissures are almost closed as long as the clay is in its natural state. When a cut is made, the state of stress around the cut is changed and the clay expands, allowing some of the fissures to open. The fissures will remain open at considerable depths because of the high strength of the clay. When water such as rainfall infiltrates the openings and the clay along the faces of the fissures starts swelling, weakening of fragments of the clay results. More fissures may be opened or formed during softening. In this way, softening advances gradually and may lead eventually to failure of the cut slope.

Softening can occur in an underground excavation. When an opening is excavated in a rock mass, tangential stress concentrations are developed around the opening wall. As the stress level is high relative to the rock mass strength, an over-stressed zone is created near the opening, followed by stress redistribution. If the rock mass is composed of sedimentary soft rocks such as mudstone and shale, the rock material in the plastic zone can absorb water and soften. This leads to a gradual increase in tunnel deformations, for an unlined tunnel, or in the rock pressures imposed on the supports, for a lined tunnel. This point was illustrated by Nakano (1979, 1981) and is discussed in the next section. It should be noted in the above that not only fissures but also unloading plays an important role in softening.

Any differential displacements or shear strains which may occur locally due, for instance, to lateral expansion upon unloading also contribute to softening (Skempton, 1970). This can be seen easily from experimental observations that during shear, under drained conditions, an over-consolidated clay exhibits dilatancy accompanied by an increase in water content of the thin shear zone. As can be seen in the subsequent section, this has also been observed in the field (*e.g.*, Henkel, 1956; 1957).

Weathering contributes to softening. It causes the structural disintegration or physical breakdown of a rock mass and the decomposition or chemical alteration of the constituent minerals and matrix materials, contributing to the reduction of shear strength. The main physical weathering processes are cyclical wetting-drying and freezing-thawing. Oxidation, reduction and hydrolysis are typical examples of chemical weathering. These weathering processes affect the dilatancy characteristics and the frictional component of shear strength (*e.g.*, Chandler; 1969, 1972). More detail of the effect of physical weathering upon shear strength is discussed under the context of softening mechanisms in Section 2.4.

Softening can be classified into internal and external processes. The softening described by Terzaghi, Nakano and Skempton can be considered to be internal since no external agents are acting on the process except for the initial unloading. On the other hand, the softening due to weathering can be considered to be external because during the process the energy for disintegrating the material comes from outside of the ground. It should be noted that this softening may be restricted to the near ground surface since weathering effects are generally restricted to relatively shallow depths below the ground surface. It is reasonable to believe that softening is more severe and its rate is much higher near the ground surface than at depth because at shallow depths internal as well as external softening take place.

2.3 Field evidence of softening

2.3.1 English clays

London Clay

London Clay is probably the best known fissured, over-consolidated clay in geotechnical engineering. It is a marine clay deposited, following the sandy Oldhaven Beds, in Eocene age and was overlain by later Eocene sediments such as the Claygate, Bagshot, Bracklesham and Barton Beds. At least 150 m of the sediments have been removed by erosion in many areas of the London Basin. Thus, the clay is heavily over-consolidated. London Clay is generally blue-grey in colour (Blue London Clay) and highly fissured. The top 5 to 15 m of the clay, however, is oxidized to a brown colour due to weathering (Brown London Clay). The index properties of London Clay are known to be relatively uniform throughout the area. The typical index properties are summarized in Table 2.1. Table 2.2 shows the mineralogy of the clay fraction.

Softening of the clay along fissures upon percolation of rainwater was observed by engineers and geologists during the construction of railway cuttings in London in the mid nineteenth century. Later, Skempton (1948) investigated many cuttings and retaining walls which failed 10 to 47 years after construction. For instance, the detailed investigations of the slip of a retaining wall at Kensal Green, which was constructed in Brown London Clay in 1912 and failed 29 years later, revealed softened clay on the surfaces of the fissures. Free water was also found in the fissures. Based upon back-analyses of case histories, variation of the average shear strength along the slip surface with time is presented as shown in

Figure 2.1. The time dependent nature of softening is clearly indicated.

Henkel (1956, 1957) also reported the existence of very wet, soft clay in the slip zone during the investigation of three cut slope failures at Uxbridge, Wood Green and Northolt. These failures took place 19 to 55 years after excavation. At the Uxbridge site, for instance, a sample taken from a borehole crossing the slip zone was observed to have a soft zone about a quarter inch (6 mm) thick, and the water content distribution around the soft zone was measured as shown in Figure 2.2. It is seen that the water content varies from a peak value of 36% in the soft zone to the value of 28% in the surrounding zone. This softening was considered to be associated with the dilatancy observed during local shear displacements.

James (1970) analyzed about ninety case histories in English over-consolidated clays including London Clay. The analysis was conducted in a more rational manner than the previous studies by Skempton (1948) and Henkel (1957). He used the Morgenstern-Price method which can handle an arbitrarily-shaped slip surface in terms of effective stress. The study confirmed the softening effect suggested earlier by Skempton (1948) and Henkel (1957), and its time dependency. Figure 2.3 shows a plot of back-calculated cohesion intercepts associated with the Mohr-Coulomb failure criterion for cut slopes against their life time. The cohesion intercept for each failure was evaluated on the assumption that the angle of friction was 20° which is a typical value for the peak shear strength of undisturbed and remoulded London Clay. The results are also plotted in the form of a graph relating the average shear strength along the slip surface to the average effective normal stress as shown in Figure 2.4. Points of first-time slips are located above or on the line defined by $\phi' = 20°$ and $c' = 0$, depending upon their age. As the life time of a slope increases the point approaches the line, as would be expected from Figure 2.3. This shear strength can be considered to be that of the ultimate condition of softening and has been called the fully-softened strength (Skempton, 19[illegible]).

Upper Lias Clay

Upper Lias Clay is a fissured, over-consolidated clay of Jurassic age, which outcrops widely in the Midlands of England. It generally has a blue-grey colour in the unweathered state and a brown colour when weathered. Since the clay has been very heavily over-consolidated, the maximum, previous overburden thickness exceeding 1000 m, the natural water content of Lias Clay in the unweathered state is well below the plastic limit. Compared with London Clay, Lias Clay is less plastic. One of the significant features observed in the Lias Clay is weathering effects (Chandler, 1972). Weathering raises the natural water content of the clay to its plastic limit and reduces its shear strength markedly. Brecciation is often observed in the upper layer, which results from severe weathering. The index properties are summarized in Table 2.3 and Table 2.4.

Cassel (1948) observed softening of Upper Lias Clay. He investigated several failures of cuttings which were delayed 40 to 70 years from the completion of excavation. Wetter and softer clays were observed along the slip surfaces.

Chandler (1974) studied twelve first-time failures of cuts in the east Midlands. The failures occurred from 6 to 126 years after excavation. At the several sites where deep holes were drilled for investigation, softened clays were detected in samples taken at the elevation of the slip surface. Results of the back-analyses of these failures showed that the brecciated clay exhibited lower shear strength than the merely weathered clay (Figure 2.5). It should be noted that even brecciated clay does not reach its residual condition. Further, the typical laboratory value of ϕ' shown by a broken line agrees with the back-figured value.

2.3.2 Upper Cretaceous bedrock (Western Canada)

Two well-documented case histories, based upon extensive field investigations, are presented here: those of the Devon Slide (Eigenbrod and Morgenstern, 1971) and Edgerton Slide (Tweedie, 19[illegible]; Thomson and Tweedie, 1978).

The Devon slide, which is located south-east of Edmonton, Alberta, took place in bedrock of the Edmonton formation, two months after excavation. The Edmonton formation is a non-marine deposit and consists of mudstone, claystone, siltstone and sandstone with coal seams and bentonitic layers. About 600 m of sediments of the Paskapoo formation and the upper part of the Edmonton formation is believed to have been removed by subaerial erosion during the Oligocene age. Index properties of the bedrock materials at the site are summarized in Table 2.5. From an extensive investigation, including test pits and seven boreholes, the slip surface was found to be seated in a horizontal bentonitic layer and to cross mudstone and claystone layers in the back slope. Further, it was determined that the bedrock materials of the back slope had experienced softening in place. Figure 2.6 shows typical stress-strain curves obtained from drained triaxial tests on softened and unsoftened back slope materials. The corresponding failure envelopes are plotted in a p-q diagram as shown in Figure 2.7. It can be seen that the softened material possesses significantly lower stiffness and shear strength compared with the unsoftened material.

The Edgerton slide is located in eastern Alberta and is seated in bedrock of the Belly River formation which consists of poorly-indurated, interbedded sandstone, siltstone and clayshale of late Upper Cretaceous age. Weathering effects were observed down to a depth of 12 m below ground surface. Softening of clayshale along the joints was observed in core samples taken from the slope.

2.3.3 Japanese mudstones

Softening has been observed in mudstone bedrock around tunnels. Nakano (1979, 1981) conducted comprehensive studies on Tertiary mudstones in Japan in connection with heavy rock pressures observed in many tunnels. One of his case histories, Noshiro Tunnel No.4, is described here. This tunnel was driven through a Tertiary mudstone bedrock in the Fujikotogawa formation. It is reported that the mudstone disintegrates easily upon cyclical drying and wetting but that it shows little disintegration when merely immersed in water at its natural water content. The typical index properties are given in Table 2.6. During the construction of the tunnel, mudstone and gouge clay were exposed on the excavation faces. It was found that the mudstone experienced softening. The water content of the mudstone corresponded to that of the remoulded mudstone swollen under the overburden pressure, but the mudstone still exhibited strain-softening behaviour. The water content distribution in an undisturbed mudstone specimen before and after a drained direct shear test in a dry shear box is shown in Figure 2.8. A significant increase in water content can be seen in the thin shear zone. On the other hand, the gouge clay showed no over-consolidation effect and had a significantly higher water content which was considered to be due to dilatancy during tectonic shearing, reaching the fully-softened state. Figure 2.9 shows the typical stress-strain curves obtained in triaxial compression tests on mudstone and gouge clay sampled from a tunnel face. Considering that there was no free ground water around the tunnel sufficient for expansive clay minerals contained in the rock to swell such a large amount, it was suggested that the strength reduction of the rock mass to the fully-softened state could be the most likely cause for such high rock pressure. It is reasonable to consider that a significant amount of swelling was taking place due to physical disturbance provided during formation of the plastic zone around the tunnel and contributed to this high rock pressure. Water would be drawn from pores and fissures. Ohtsuka and Takano (1980) also reported similar observations during the construction of Nabetachiyama Tunnel.

2.4 Softening mechanism

Historically, the softening effect has been considered in terms of the fully-softened condition, *i.e.*, complete reduction of the cohesion intercept in the Mohr-Coulomb failure criterion. The following are typical values for the peak and residual shear strength parameters, in terms of effective stress, of undisturbed Brown London Clay. The peak shear strength parameters for the remoulded, normally-consolidated clay are also shown (Skempton, 1970; 1977).

Undisturbed samples

Peak shear strength

$c' = 15$ kPa $\quad \phi' = 20°$ on standard specimens

$c' = 7$ kPa $\quad \phi' = 20°$ on larger specimens

Residual shear strength

$c' = 0$ kPa $\quad \phi' = 14°$.

Remoulded samples

Peak shear strength

$c' = 0$ kPa $\quad \phi' = 20°$.

It should be noted here that the remoulded, normally-consolidated clay gives the same value of ϕ' as the undisturbed clay. This peak strength of the remoulded sample has been used as the fully-softened strength for Brown London Clay which agrees with the field strength as shown in Figure 2.4.

Fully-softened strength parameters are determined on the remoulded clay or by considering the c' component to be zero in the shear strength parameters of the undisturbed clay. These fully-softened strength parameters have been recommended and widely used in design of cuttings in fissured, over-consolidated clays and mudstones (Chandler and Skempton, 1974; Simpson *et al.*, 1979; Gibo, 1987). However, the mechanism of the reduction of shear strength due to softening has not been fully understood.

Before discussing the mechanism of softening in detail, it would be useful to review briefly the shear strength characteristics of fissured, over-consolidated clays. The typical characteristics can be summarized, referring to a comprehensive experimental study by Bishop *et al.* (1965) on undisturbed Blue London Clay (Figure 2.10), as follows:

(a) The stress-strain curve is of brittle type for low to medium stress levels and changes gradually from the brittle to ductile type as the effective confining pressure increases.
(b) The transition of the volume change from contraction to dilation occurs just before or when the peak stress is reached.
(c) The failure envelope is markedly non-linear at low stress levels.

Similar characteristics have also been observed on mudstones (Shinjo, 1976; Watanabe *et al.*, 1988).

The existence of fissures makes the shear behaviour of the material unique. Marsland (1971) studied this aspect in some detail. From a review of drained triaxial compression tests on large diameter (98 mm) specimens of Blue London Clay, it was found that at low effective stresses the fissured clay behaved like a blocky material separated by a system of fissures and that the shear plane passed through fissures between clay lumps within which the effect of high over-consolidation was retained. At higher effective stresses the shear took place through the hard clay lumps. The resulting failure envelope is curved as shown in Figure 2.11 (seen also in Figure 2.10(b)). Another important observation in the study was that specimens which were allowed to swell under very low stresses prior to shearing did not exhibit dilatancy or a pronounced peak in the stress-strain curve. This is an indication of the softening effect.

Similar observations have been made by Kjartanson (1978) and Thomson and Kjartanson (1985) from drained triaxial tests on an over-consolidated Lake Edmonton clay which had been subjected to weathering effects, creating nugget structures in the clay mass. The samples were observed to behave as a cohesionless material. At low stress levels shear took place around the hard nuggets and through the nuggets at stress levels higher than the effective overburden pressure. The failure envelope was approximated to be bi-linear.

The non-linear failure envelope observed in fissured, over-consolidated clays can be explained from the viewpoint of shear strength of discontinuities in a rock mass. Patton (1966) carried out an experimental study in which direct shear tests were conducted on plaster specimens having interlocking surfaces as shown in Figure 2.12. During shear, the specimen moves over the teeth at low normal stresses, resulting in a high angle of friction and high dilatancy. The angle of friction is due to the inclination of the teeth and the angle of internal friction of the material. As the normal stress increases the tendency for the teeth to be sheared off increases and dilatancy decreases. In the extreme, no dilatancy will occur and the shear plane will pass entirely through the intact material. The inclination of the teeth then contributes neither to the shear strength nor the dilatancy. A bi-modal failure envelope results as shown in Figure 2.12. In reality, even at low stresses, some asperities on discontinuities are sheared off and only at very high stresses can shear take place entirely through the intact rock. Thus, a non-linear failure envelope is obtained instead of the bi-modal failure envelope.

With the above discussion, the softening effect can be visualized as follows. Suppose that unloading is imposed on ground consisting of a fissured, over-consolidated clay. Suction is generated by the unloading, and some fissures open. The surface of the clay lumps adjacent to the fissures starts softening by absorption of water as discussed in Section 2.2, creating softer mantles around the hard cores. This results also in a weaker interlocking condition in the system of fissures. These softer mantles would be sheared before the hard cores are brought into contact and sheared, and less shear force would be required. This results in a reduction of the dilatancy property or the geometric component of resistance. As the softening advances, the degree and area of softening increase. Thus more softer zones would be involved in shearing, resulting in further reduction in the shear strength. Since the clay, in reality, is under a certain effective over-burden pressure, the clay at the ultimate condition of softening, the fully-softened condition, would be equivalent to the normally-consolidated clay (Skempton, 1970).

Botts (1986) attempted to explain the strength reduction due to softening from the viewpoint of the behaviour of joints in a rock mass. He related the softening of fissures to an increase in the thickness of soft fillings in joints and considered that the effect of the filling on the shear strength of a rough joint was similar to the softening effect.

A first, valuable remark on the effect of softening was made by Morgenstern in 1977, with the schematic view as shown in Figure 2.13:

> ". . . the results of softening may simply be to reduce the dilatancy characteristics of the fissured system at low effective stresses."

In order to clarify the mechanism of strength reduction due to softening, it is necessary to conduct an experimental study at low stress levels. There are only a few comprehensive experimental studies conducted at low stress levels. Graham and Au (1985), and Graham and Shields (1985) carried out a series of triaxial tests under undrained and drained conditions on samples: (a) undisturbed, (b) swollen under low effective stresses and (c) subjected to five cycles of freezing and thawing, of fissured, over-consolidated Lake Agssiz clays over a wide range of effective stress levels including very low stresses. The study of sample microstructure indicated cyclical freezing-thawing disturbed the soil structure more severely than mere swelling, and nugget structures were observed in the freeze-thaw cycled samples. The results of consolidation tests, conducted at the same time, confirmed this point. Freeze-thaw cycles and swelling increased the pre-yield compressibility but decreased the post-yield compressibility as shown in Figure 2.14. The freeze-thaw cycled samples exhibited no yield point, while the swollen samples still showed a clear yield point, suggesting much of the original soil structure was still retained after swelling. Regarding the shear behaviour, undisturbed samples exhibited strain-softening characteristics with high dilatancy under drained conditions. The freeze-thaw cycled samples, on the other hand, showed a less pronounced peak in their stress-strain curves with less dilatancy. The swollen samples exhibited intermediate characteristics. The strength envelopes are shown in Figure 2.15. Non-linearity is noticed in the strength envelopes. It is clearly shown in the figure that the effects of swelling and freeze-thaw cycles are to reduce the shear strength. The freeze-thaw cycled samples exhibit lower shear strength, which is consistent with the microscopic study on the test samples. It can be seen that the strength envelopes for these samples tend to become parallel to that for undisturbed samples at higher stress levels. Further, they appear to approach the critical state line. An examination of the effective stress paths during undrained tests indicates that the swollen and freeze-thaw cycled samples exhibit stress paths similar to those for undisturbed samples rather than for the remoulded samples. These results suggest that part of the original soil structure is retained in these samples. It should be noted that application of more than five cycles of freezing-thawing was reported to cause further damage to the soil structure of the test samples and to lead to further disintegration. Thus, lower failure envelopes could have resulted.

In the above study, it can be seen that the clay, when experiencing softening, displays smaller shear strength and less tendency to dilate. Further, the effect of softening appears as the lowering of the failure envelope and the reduction in the high curvature observed at low stresses. This appears to support the view of softening presented by Morgenstern (1977).

Experimental studies regarding the effects of swelling on shear strength at low stress levels have been carried out by Scarpelli and Calabresi (1984), Calabresi and Scarpelli (1985) and Calabresi and Rampello (1987). A series of undrained triaxial tests was conducted on fissured, over-consolidated Italian clay specimens subjected to swelling for periods of 20 days, 1 month (after desiccation of 8 hours at 30°) and 3 months. The 20-day specimens were observed to exhibit brittleness and significant negative pore water pressure during shear. The 3-month specimens showed lower shear strength, but was almost the same as that of the 1-month specimens. However, the shear strength envelopes for these specimens are somewhat above the peak shear strength envelope of the normally-consolidated specimens. The effective stress paths observed in the tests are similar to each other but are quite different from those of the normally-consolidated specimens. The results of oedometer tests on these specimens indicated that swelling disturbs the soil structure and reduces the yield stress but that all the samples tested still exhibited yield points. Thus, these specimens were not fully-softened by swelling.

A recent experimental study focussing on the effects of weathering on the shear strength of London Clay shows similar conclusions to the above (Chandler and Apted, 1988). Undrained triaxial compression tests were carried out on London Clay taken from clay pits at South Ockendon, Essex. The effects of weathering varies with depth. The sample taken from a shallow depth, 1 to 2.8 m from the ground surface, had been subjected to extensive weathering and showed lower shear strength. However, the shear strength of these samples was observed to be higher than that of the remoulded, normally-consolidated clay. The effective stress paths also confirm this point.

Since softening accompanies an increase in the water content of material, reduction in stiffness of the material results. Eigenbrod (1972) demonstrated a decrease in stiffness due to softening of a variety of fissured, over-consolidated clays and mudstones. It was observed that the slope of the initial portion of a stress-strain curve decreased and that the amount of reduction depended upon the degree of softening the test sample experienced. A similar observation was made by Botts (1986) on Pierre shale. After subjecting samples to longer periods of drying and wetting significantly lower values of Young's modulus were obtained. Considering the previous discussion, it can be considered that at the fully-softened condition, the deformation properties of a material would be equivalent to those of the remoulded, normally-consolidated clay.

In connection with strength reduction, slaking is an important phenomenon observed in fissured, over-consolidated clays and mudstones and has been the subject of intensive studies (*e.g.*, Eigenbrod, 1972; Moriwaki, 1974; Botts, 1986). In general, slaking is defined as the structural disintegration of soil and rock due to disruption or breakage of interparticle bonds by the action of repeated wetting and drying. This disruption can be caused by compression of entrapped air in the pores of clay upon wetting (Terzaghi and Peck, 1948; Ladd, 1960), or by physico-chemical reaction of clay minerals (Nakano, 1967; Moriwaki, 1974).

Most mudstones exhibit little disintegration upon mere immersion in water and some disintegrate when dried before immersion. A threshold value of the degree of dryness exists which appears to be necessary for mudstone to slake. When mudstone is dried beyond the threshold value, the slaking begins upon immersion in water, and the higher the dryness, the easier the mudstone slakes. Cyclic action of drying-wetting enhances slaking significantly. The degree of slaking depends upon the type of mineralogy in the mudstone and the induration. At the end of slaking, a remoulded clay or silt would result and the water content could be as high as its liquid limit (Morgenstern and Eigenbrod, 1974).

Slaking behaviour is stress-dependent. For instance, Figure 2.16 shows the relations between volume change and elapsed time obtained from swelling tests conducted by Peterson and Peters (1963) on shale samples, (a) dried to their shrinkage limits and (b) with their natural water contents before saturation, under vertical pressures of 1 psi (7 kPa) and 5 psi (35 kPa). It can be seen that under the lower vertical pressure significant volume increase takes place, but that under the higher pressure the volume change tends to be suppressed. It follows that the lower the confining pressure the material is subjected to the more severe the slaking effect. This indicates the importance of slaking in considering softening.

2.5 Rate of softening

The rate of softening should be estimated from field observations or analyses of case histories. Detailed studies on the rate of softening are rare. Thus, those studies on London Clay, by Skempton (1948), Henkel (1957) and James (1970), based upon case histories are very valuable. The results were already presented in Section 2.2 (Figures 2.1 and 2.2). From these figures, the strength reduction seems to follow an inverse-hyperbolic function of time. Further, the fully-softened condition seems to be reached in about 100 years, although there are also pore water pressure effects especially in younger slopes. Since they are based solely upon case histories in London Clay, the above observations may not be applied to softening in other geologic conditions.

An attempt was made by Hirano *et al.* (1983) to estimate the rate of softening from field observations, in connection with tunnelling. They deduced the rate of strength reduction due to softening from variations with time of tunnel wall convergence. The measurements were taken after the face had been advanced more than two diameters past the instrumented section. The effect of time-dependent movements due to excavation advance effect was then considered negligible and a linear function of time was assumed for the strength reduction.

In the subsequent chapters, shear strength parameters are assumed to decrease according to either an inverse-hyperbolic or a linear function during the softening process.

2.6 Pore water pressure effect

2.6.1 Long-term pore water pressure equalization

Excavation of a cutting causes a reduction in total stresses. Assuming that the excavation is rapid, sufficient for pore water not to migrate (*i.e.*, undrained unloading), depressed pore water pressures are developed just after excavation. This results in little change in effective stresses in the ground. Thus, the stability of the cut is apparently maintained. As time goes by, this depressed pore water pressure tends to equalize being accompanied by swelling and leading to a reduction in the stability of the cut. Bishop and Bjerrum (1960) presented a schematic diagram of the influence of the long-term equalization of pore water pressure after excavation upon the stability of a cut slope, as shown in Figure 2.17.

Field observations of depressed pore water pressure after excavation in fissured, over-consolidated clays have been reported at several sites. de Beer (1969) reported negative excess pore water pressures in cuts in Boom Clay, Belgium. Banks (1971) reported reduced pore water pressures below the canal water level in the Culebra clayshale at the Panama Canal. Some piezometer readings taken at the canal indicated equilibrium conditions had not been reached even after about 60 years (Lutton and Banks, 1970). An average permeability of 1.0×10^{-12} m/s and an average coefficient of consolidation on the order of 10^{-1} m^2/years were reported. Walbancke (1975) measured depressed pore water pressures in London Clay at Edgwarebury and Potters Bar cuttings sites. The measurements indicated that the equalization of the pore water pressure had progressed little 19 years after excavation. Burland and Hancock (1977) recorded the changes in pore water pressure during and after excavation in London Clay at House of Commons. During the stepped excavation, pore water pressure measured just outside the excavation decreased in response to the each excavation step. About 3 years after the completion of the excavation, negative excess pore water pressure was still observed. The in-situ permeability of the intact clay layer (Blue London Clay) was reported to be as low as 3.0×10^{-11} m/s. It was noted that this value agreed well with experimentally determined values for the clay which ranged from 2.0×10^{-11} to 8.0×10^{-10} m/s. It can be seen that the low rate pore water pressure equalization is associated with the low permeability of soil. Figure 2.18 shows a plot of measured r_u in cut slopes against elapsed time after excavation in Brown London Clay, in which data points are taken from Walbancke (1975) and Skempton (1977). It can be seen that pore water pressure equalization is a long-term process. It should be noted that these measurements are taken at depth and that the equalization of pore water pressure may be faster at surface.

Depressed pore water pressures are also brought about by natural causes such as natural erosion and landslides. Muir Wood (1971) observed depressed pore water pressures in the Gault Clay at Folkestone Warren at which the piezometric levels were below sea level. Several observations of depressed pore water pressures have been made at coastal cliffs in England. Since the long-term equalization of pore water pressure due to natural causes has not been paid much attention, case histories from the coastal cliffs at

Herne Bay, England are presented here. The investigations are reported in greater detail by Bromhead (1978) and McGown *et al.* (1987).

The coastal cliffs at Herne Bay consist mainly of London Clay overlying Oldhaven Sandstone. Major landslides took place at Miramar in 1883 and 1953, and at Queens Avenue in 1896 and 1937. Remedial works such as re-grading and drainage were done during 1969 and 1971 at both sites. During the field investigation, many piezometers were installed within and adjacent to the sliding mass, in 1969. In 1978, new sets of piezometers were installed at the both sites because of mechanical problems in some of the original piezometers. The piezometric readings were taken from 1969 to 1971 and from 1978 to 1986. Figure 2.19 shows the piezometric data from the Queens Avenue site. Figures 2.20 and 2.21 show the pore water pressure versus time relations for outside and within the sliding mass, respectively. A steady increase in the pore water pressure at Location A1 during 1969 and 1986 suggests that equalization of pore water pressure is under way but that it is a slow process. The time to attain a steady seepage condition is estimated as approximately 50 years, assuming that the lowest pore water pressure was created just after the major landslide in 1937. It can be seen from Figure 2.21 that the pore water pressure changes in the slide mass or disturbed mass are not easily interpreted because of the complex stress history.

Similar observations were also presented by Bromhead and Dixon (1984) in coastal cliffs at Warden Point, 18 km west of Herne Bay. The geologic conditions are similar to those of Herne Bay. It was suggested that the long-term depressed pore water pressures resulted from unloading due to erosion and landslides. In-situ permeability of 3.5×10^{-10} m/s was reported. A very long time, on the order of 2000 years, was estimated as necessary for the pore water pressure to reach its equilibrium condition.

Equalization of depressed pore water pressure is accompanied by swelling of the ground and the rate depends upon the bulk coefficient of swelling. The coefficient of swelling is proportional to the coefficient of permeability. A low value of the coefficient of permeability results in a low value of the coefficient of swelling.

Determination of a representative value of the coefficient of permeability is not a simple task because of the presence of fissures. Two types of permeability must be considered: a fissure permeability and permeability of the intact material. The latter could be determined without any difficulty by a conventional technique such as a swelling test on intact samples. On the other hand, finding the former is problematical. It is stress-dependent as seen in studies on water flow through discontinuities in a rock mass (*e.g.*, Hoek and Bray, 1981). Upon unloading due to excavation, fissures tend to open resulting in an increase in the permeability. Clay along the open fissures continues to swell upon entry of water and re-seals the openings. Coefficients of permeability measured for Blue London Clay and Upper Lias Clay are plotted against depth in Figure 2.22 (Walbancke, 1975). These coefficients of permeability were determined in-situ and in the laboratory. Stress-dependency of permeability can be seen in the Figure; that is, the coefficient of permeability decreases with depth. This also reflects change in weathering structure.

2.6.2 Relation between pore water pressure and softening

Long-term pore water pressure equalization can be modelled by using consolidation theory. Eigenbrod (1972, 1975) computed the changes in pore water pressure in a slope after excavation by solving a two-dimensional equation derived from Terzaghi's consolidation theory, using the finite element method. Several case histories of cut slope failures were analyzed including ones at the Panama Canal and in London Clay. Provided that reasonable values of the coefficient of swelling could be obtained, it was found that the computed pore water pressures agreed well with the measurements. Regarding failures in London Clay, it was suggested that long-term equalization of pore water pressure might be a main cause of the delayed failures; considering that the analysis results indicated that pore water pressure stabilization would be reached after 50 to 100 years.

Subsequently, from the viewpoint of pore water pressure effects, Vaughan and Walbancke (1973) re-analyzed many first-time failures of cuttings in London Clay. Average values of r_u required for the factor of safety to be unity were calculated using the Morgenstern-Price slope stability method, assuming that the shear strength parameters of $c' = 0$ MPa and $\phi' = 20°$ were mobilized. The relations between r_u and the lifetime of cut slopes are shown in Figure 2.23 together with some actual field measurements. It can be seen that computed r_u increases with time and that the computed and measured values are consistent for the Brown London Clay. The failures seem to be controlled by this long-term equilibration process. This point was further emphasized by Chandler (1984). He argued that first-time failures taking place within about 40 to 50 years were controlled by pore water pressure equalization, assuming that swelling was completed within 40 to 50 years. Further, it was concluded that for these delayed failures the softening effect was minimal. However, it was not explained why the shear strength had been reduced to the fully-softened condition, *i.e.*, $c' = 0$ MPa and $\phi' = 20°$.

In Section 2.6.1, a plot of measured r_u against elapsed time after excavation was presented for Brown London Clay. This plot demonstrates the long-term process of pore water pressure equalization. This increase in pore water pressure with time results in reduction of effective stresses, thus leading to instability of a cut, as discussed previously. However, as discussed in Section 2.4, swelling alone can not reduce the shear strength of a material such a large amount. Thus, it would be more reasonable to consider that the substantial reduction in shear strength resulted from the softening effect during pore water pressure equalization and that failure took place when the stress in the slope became greater than the shear strength of the material which was being affected by softening.

2.7 Theoretical studies

Numerous attempts have been made to analyze time-dependent instability in fissured, over-consolidated clays and mudstones. However, only a few studies take into account softening.

Hirano *et al.* (1983) analyzed long-term deformations around a tunnel driven through a Japanese Tertiary mudstone bedrock. An elastic, perfectly-plastic finite element model was used for the bedrock material, with the Mohr-Coulomb yield criterion. The softening effect was approximated by reducing the cohesion component in the yield function. The cohesion component was assumed to decrease linearly with time and the rate of reduction varied with stress level. The rate increased as stress conditions approached the failure surface. The parameter involved in the strength reduction was deduced from the relation between time and tunnel wall convergence obtained from field measurements. The computed displacement-time relations showed fairly good agreement with the field observations.

Kawamoto and Tanaka (1988) and Tanaka and Kawamoto (1989) take into account both softening effects and strain-softening properties in deformation analyses of cut slopes. An elastic-plastic finite element method was used with a Mohr-Coulomb yield criterion. Strain-softening was incorporated by a reduction with plastic deviator strains of the parameters, α and κ, in the equivalent Drucker-Prager yield function instead of reducing c' and ϕ'. Softening was considered by a reduction of the cohesion component, c', but the time factor was not handled.

It should be noted that the above studies assume softening as a reduction of c' component alone in the Mohr-Coulomb failure criterion. This is not a proper representation of softening as discussed in Section 2.4. Further, the dissipation of excess pore water pressure is not taken into account.

An interesting analytical method was used by Sidharta (1985), although it did not take into account softening effects. Following studies on creep failure by Nelson and Thompson (1974, 1977), he developed a method of predicting the time to failure of a cut slope, taking into account the effects of dissipation of negative pore water pressure, strain-softening properties and strength reduction due to creep. The method is basically a limit equilibrium analysis using Bishop's simplified method. For simplicity, information on stresses and pore water pressure distributions in the ground before and after excavation are deduced from existing published data. Further, excess pore water pressure is assumed to dissipate exponentially with time instead of solving differential equations, and the time to reach equilibrium is assumed to be given by Terzaghi's consolidation theory. Good agreement is obtained between the calculated and actual time to failure for two case histories.

2.8 Summary

The main purpose of this chapter was to review the mechanisms of long-term instability of slopes and tunnels in fissured, over-consolidated clays and mudstones. Great emphasis was placed upon softening.

Terzaghi appears to have described the core concept of softening. Here, softening is classified into internal and external processes. The importance of softening is supported by field evidence from England, Canada and Japan. The mechanism of softening was clarified based upon reviews of experimental studies available in the literature. These materials exhibit strain-softening behaviour and non-linear failure envelopes. The effect of softening is to decrease shear strength accompanied by a diminishing of the tendency to dilate. The reduction of shear strength due to softening can be represented as a lowering of the failure envelope and the reduction in the high non-linearity at low stress levels. The softening rate should be estimated from field observations or analyses of case histories.

Depressed pore water pressures generated by unloading tend to equalize over a long period of time, leading to long-term instability of cut slopes. The depressed pore water pressure can be created not only by man-made cuttings but also by natural erosion and landslides.

Long-term pore water pressure equalization seems to have controlled delayed failures observed in London Clay. However, since swelling alone is not sufficient for the shear strength of the clay to decrease significantly, it would be reasonable to consider that softening controlled those failures through substantial reduction in the shear strength.

A review of theoretical studies revealed that very few took the effect of softening into account in a comprehensive manner, and that there have been no studies which handle the softening effect, pore water pressures and strain-softening at the same time.

Table 2.1 Index properties of London Clay

	w (%)	LL (%)	PL (%)	PI (%)	C.F. (%)	References
Blue London Clay	21 - 26 (23)	61 - 80 (72)	21 - 31 (26)	-	-	Word *et al.* (1960)
	22 - 26 (24)	60 - 71 (67)	24 - 29 (27)	36 - 43 (40)	42 - 60 (53)	Bishop *et al.* (1965)
	28	69	26	43	58	Skempton and Petley (1967)
Brown London Clay	33	80	29	-	-	Skempton and Delory (1957)
	31	82	30	52	55	Skempton and Chandler (1974)

Note: A value in bracket is an average value.

Table 2.2 Mineralogy of clay fraction of London Clay

Montmorillonite	Illite	Kaolinite	Chlorite	Reference
35 - 47 (%)	41 - 47 (%)	12 - 15 (%)	3 (%)	Burnett and Fookes (1974) Chandler and Apted (1988)

Table 2.3 Index properties of Upper Lias Clay

	w (%)	LL (%)	PL (%)	PI (%)	C.F. (%)	References
Weathered	17 - 20	57 - 65	24 - 33	33 - 38	-	Cassel (1948)
	18 - 30	57 - 65	24 - 29	28 - 41	33 - 50	Chandler (1972)
Brecciated	20 - 35	61 - 68	27 - 31	29 - 41	42 - 62	Chandler (1974)

Table 2.4 Mineralogy of clay fraction of Upper Lias Clay

Montmorillonite	Illite	Kaolinite	Chlorite	Reference
20 - 25 (%)	40 - 45 (%)	30 - 50 (%)	< 5 (%)	Chandler (1972)

Table 2.5 Index properties of bedrock materials at Devon Slide site

Material	w (%)	LL (%)	PL (%)	PI (%)	C.F. (%)
Bentonitic Clay	4	100	39.8	60.2	47
Weathered Back Slope Clayey	31.8	84.8	20.1	64.7	52
Weathered Back Slope Sandy Silty	26.6	44.9	20.6	24.3	32
Unweathered Back Slope Sandy Siltstone	20.9	43	20.5	22.7	22

(Taken from Eigenbrod and Morgenstern, 1971)

Table 2.6 Index properties of mudstone at Noshiro Tunnel No.4

w (%)	LL (%)	PL (%)	PI (%)	C.F. (%)
-	96	48	48	-

(Taken from Nakano, 1979)

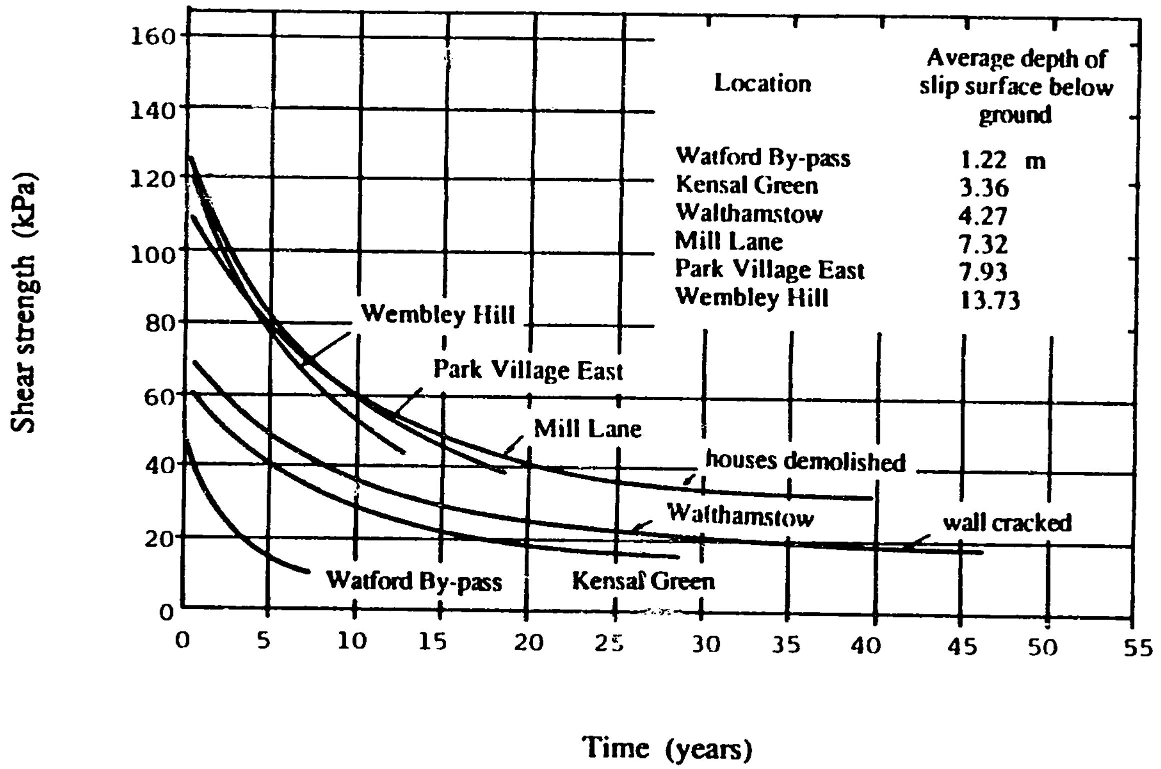

Figure 2.1 Relation between average shear strength along slip surface and time for cuttings and retaining walls in London Clay (modified after Skempton, 1948)

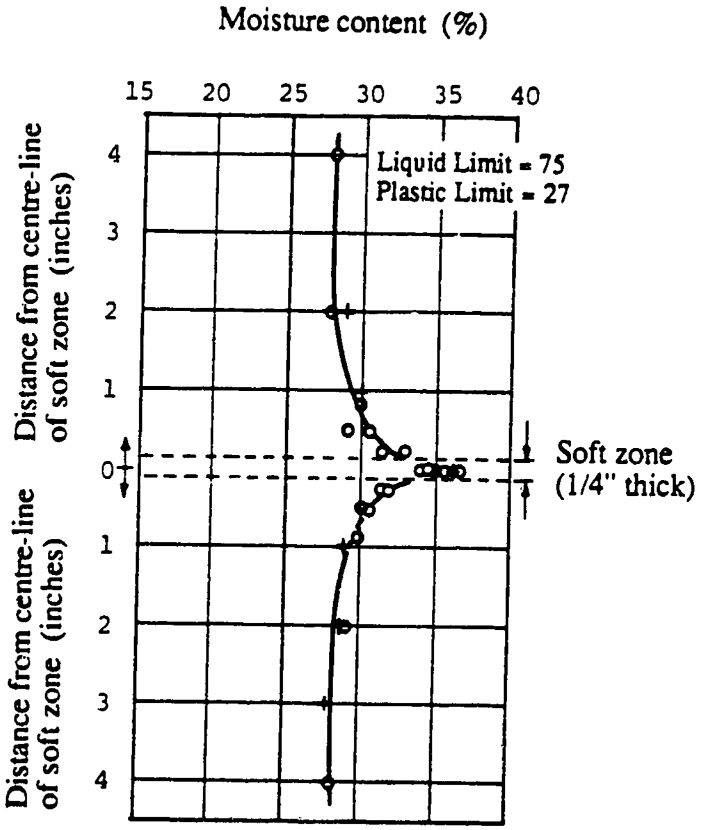

Figure 2.2 Moisture content variation in vicinity of thin soft failure zone at Uxbridge (modified after Henkel, 1957)

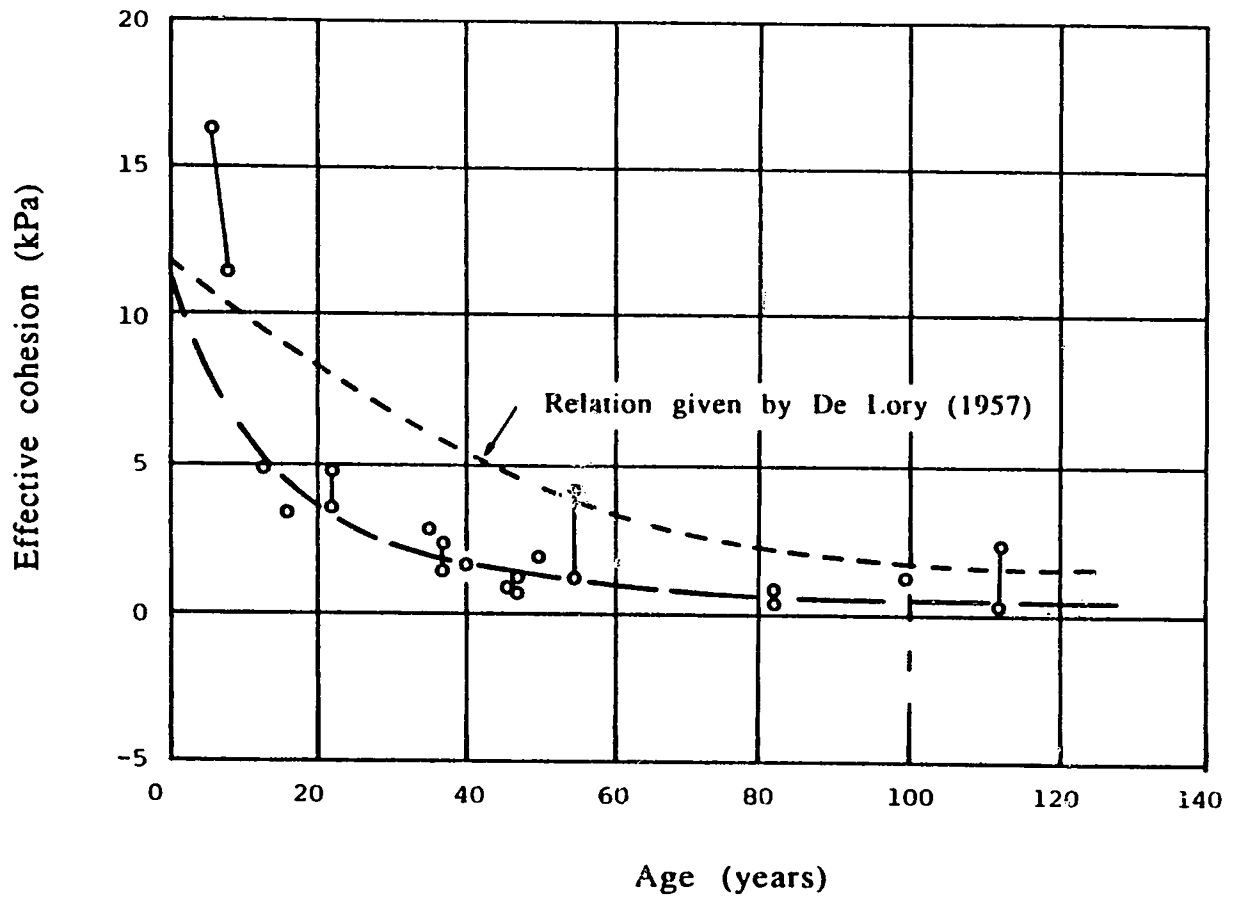

Figure 2.3 Strength reduction with time for London Clay (modified after James, 1970)

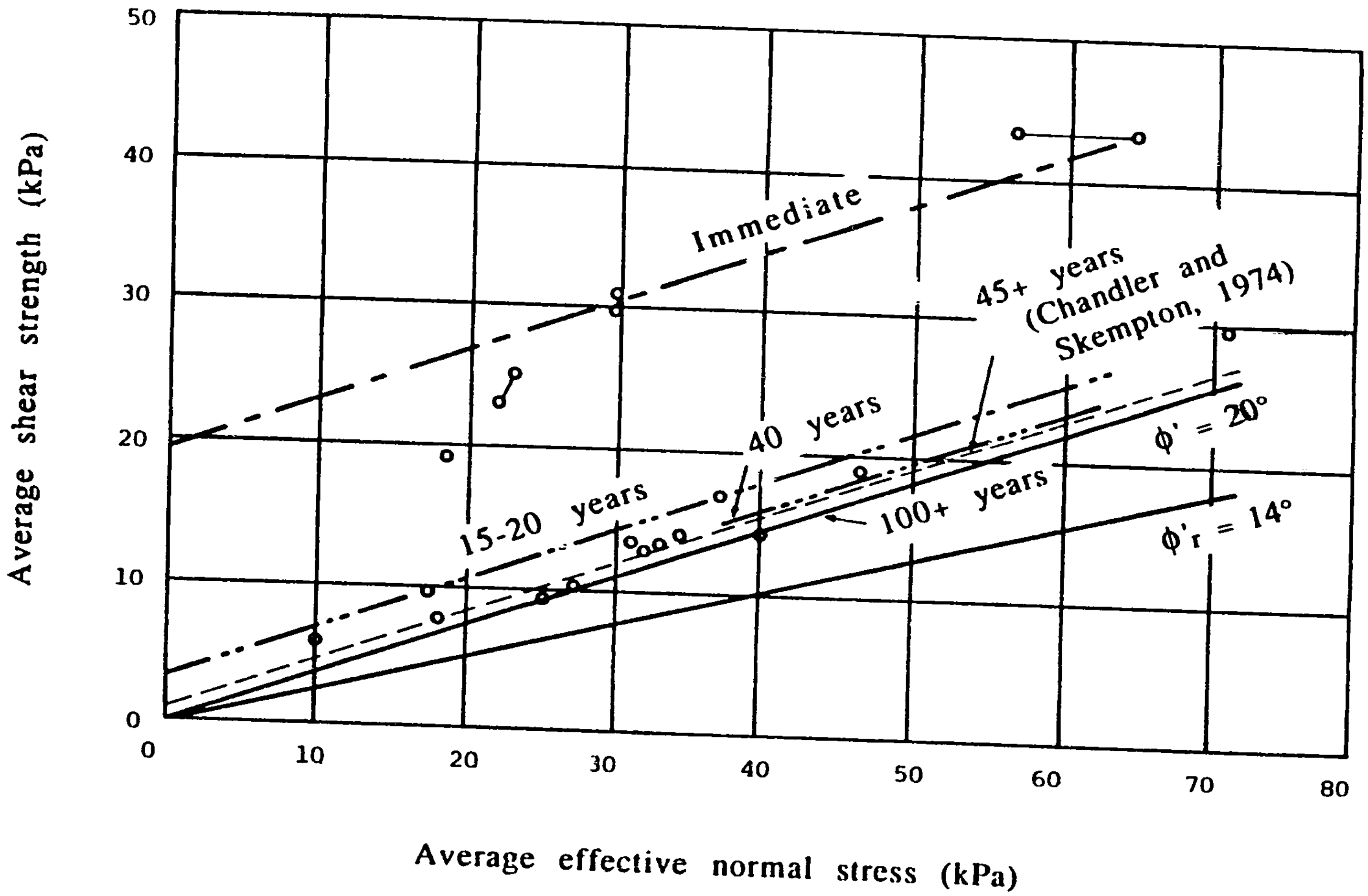

Figure 2.4 Relation between average shear strength and average effective normal stress (modified after James, 1970)

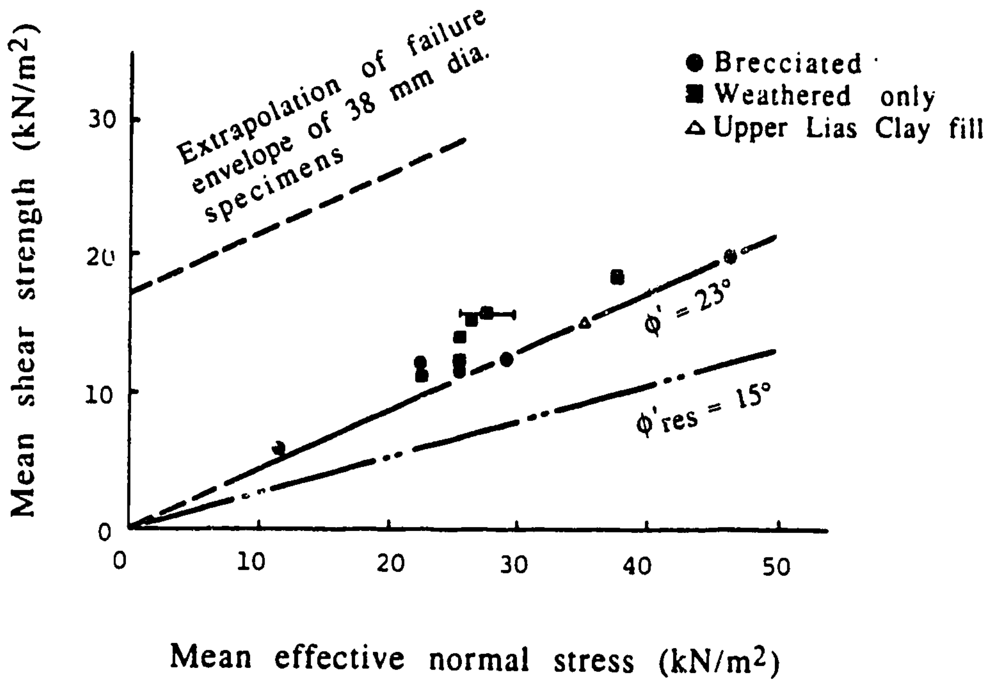

Figure 2.5 Relation between mean shear strength and mean effective normal stress for cutting slope failures in Upper Lias Clay (modified after Chandler, 1974)

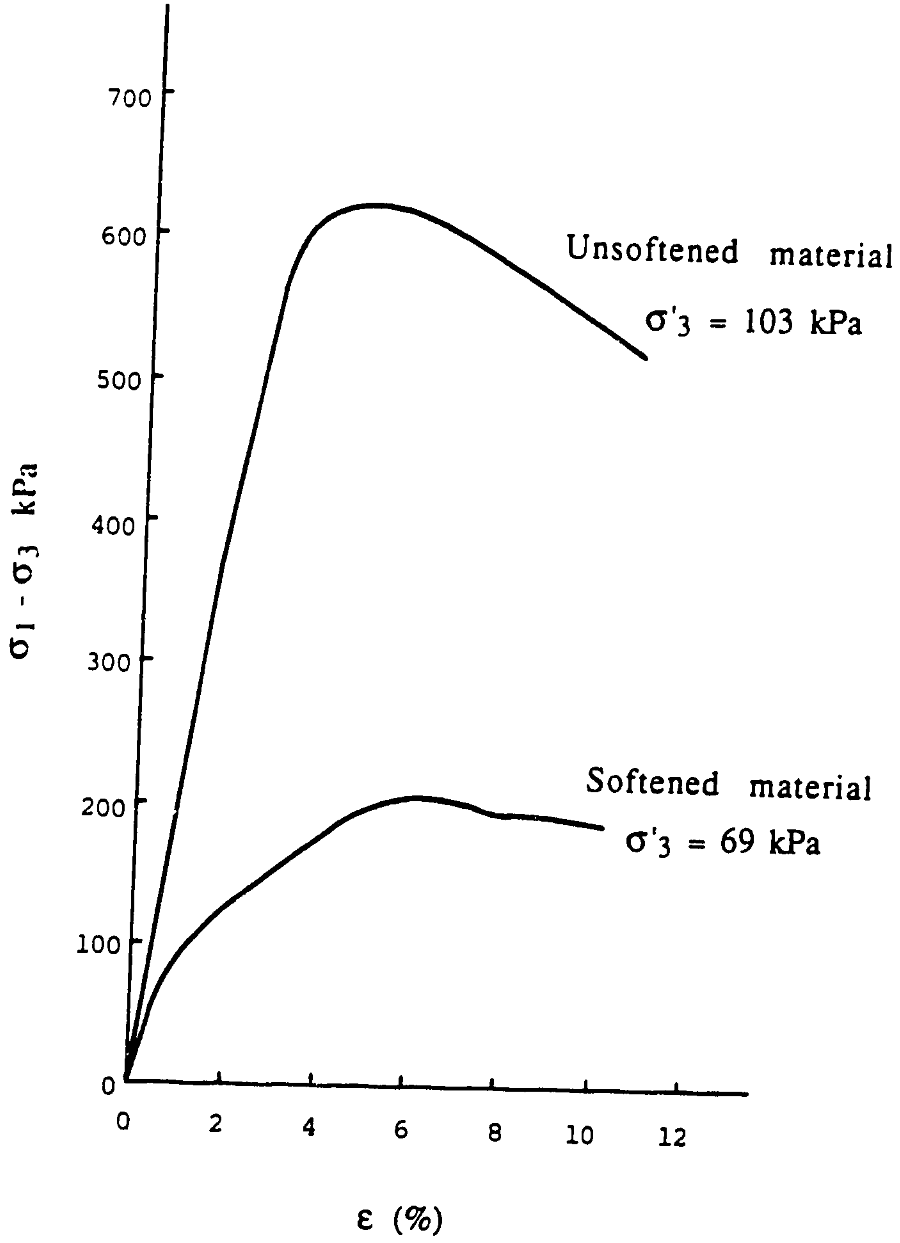

Figure 2.6 Typical stress-strain curves for softened and unsoftened back slope materials (modified after Eigenbrod and Morgenstern, 1971)

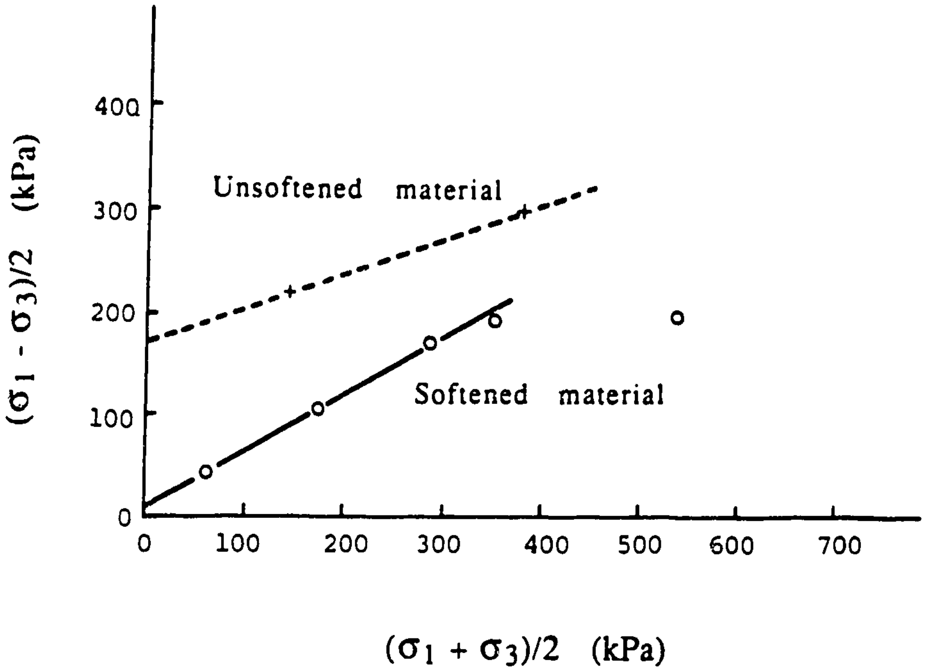

Figure 2.7 Results of triaxial tests on back slope materials (modified after Eigenbrod and Morgenstern, 1971)

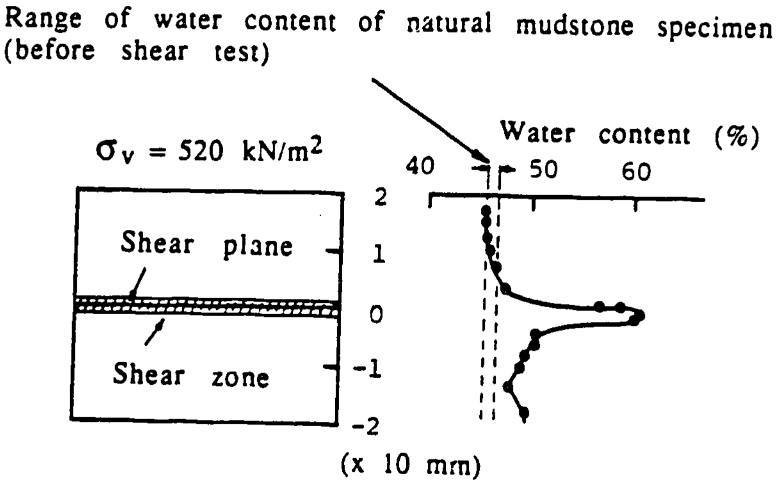

Figure 2.8 Water content distribution before and after drained direct shear tests on mudstone specimen taken from Noshiro Tunnel No. 4 (modified after Nakano, 1979)

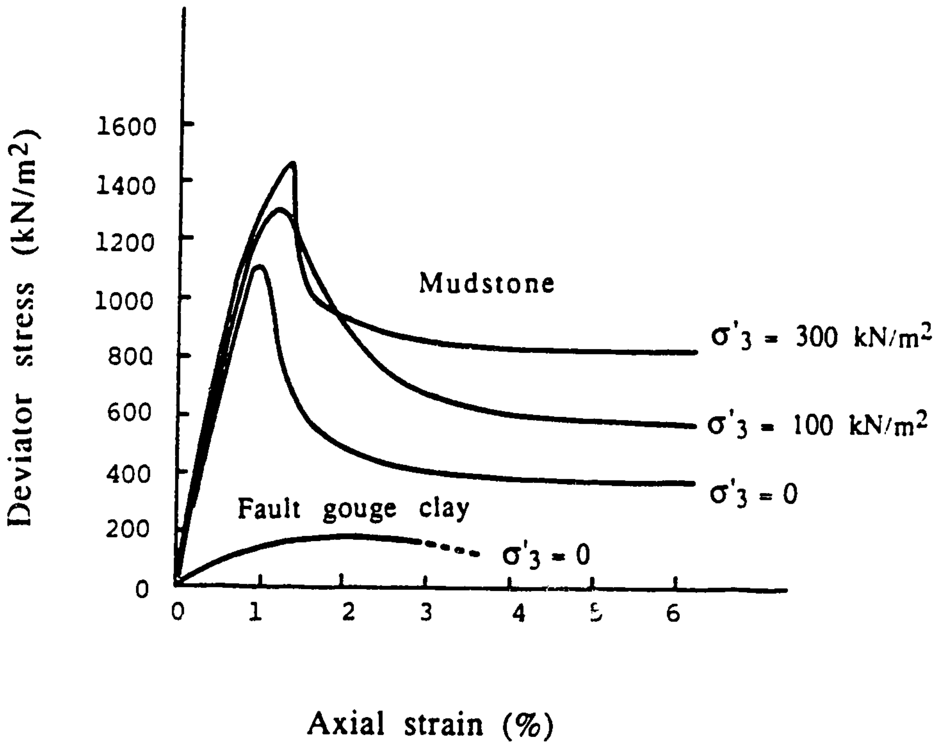

Figure 2.9 Typical stress-strain curves for mudstone and fault gouge clay taken from Noshiro Tunnel No. 4 (modified after Nakano, 1981)

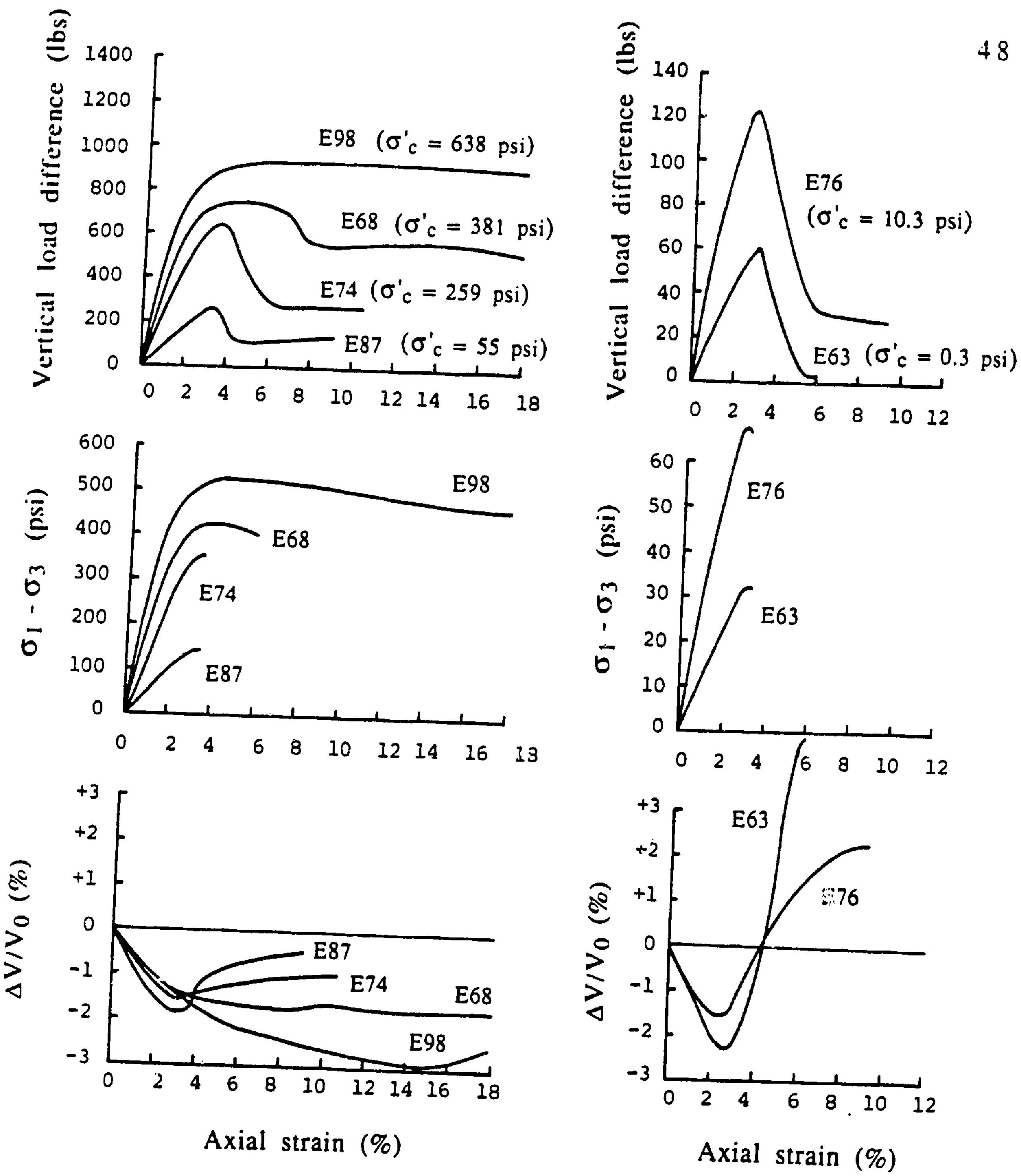

(a) Stress-strain curves

Figure 2.10 Typical results of drained triaxial compression tests on undisturbed Blue London Clay samples from Level E (modified after Bishop *et al.*, 1965)

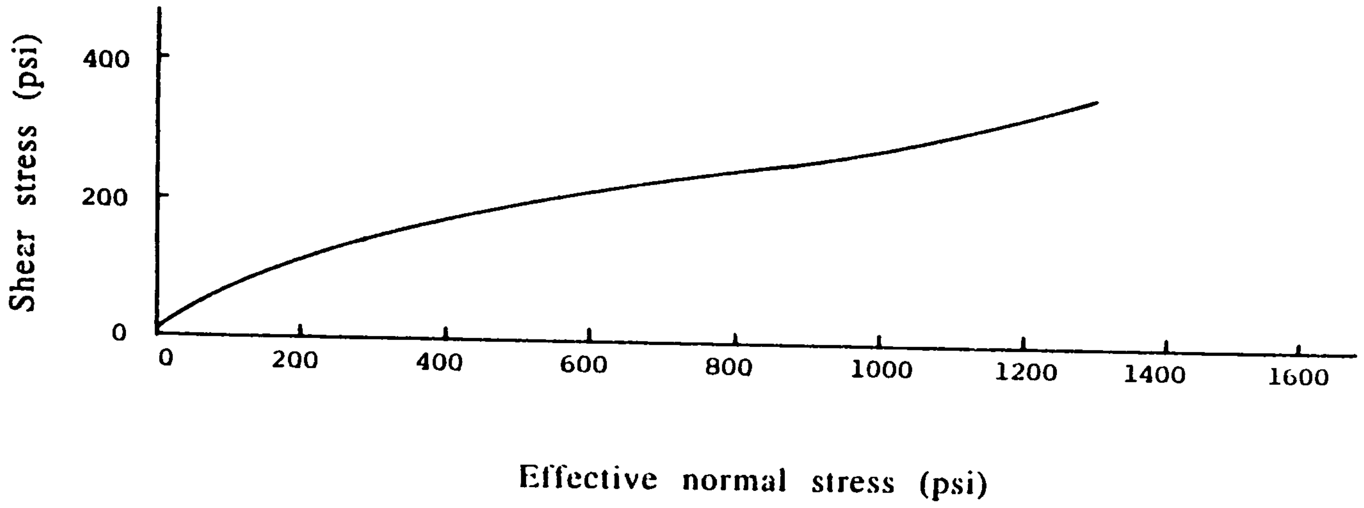

(b) Shear strength envelope

Figure 2.10 Typical results of drained triaxial compression tests on undisturbed Blue London Clay samples from Level E (modified after Bishop *et al.*, 1965) (Continued)

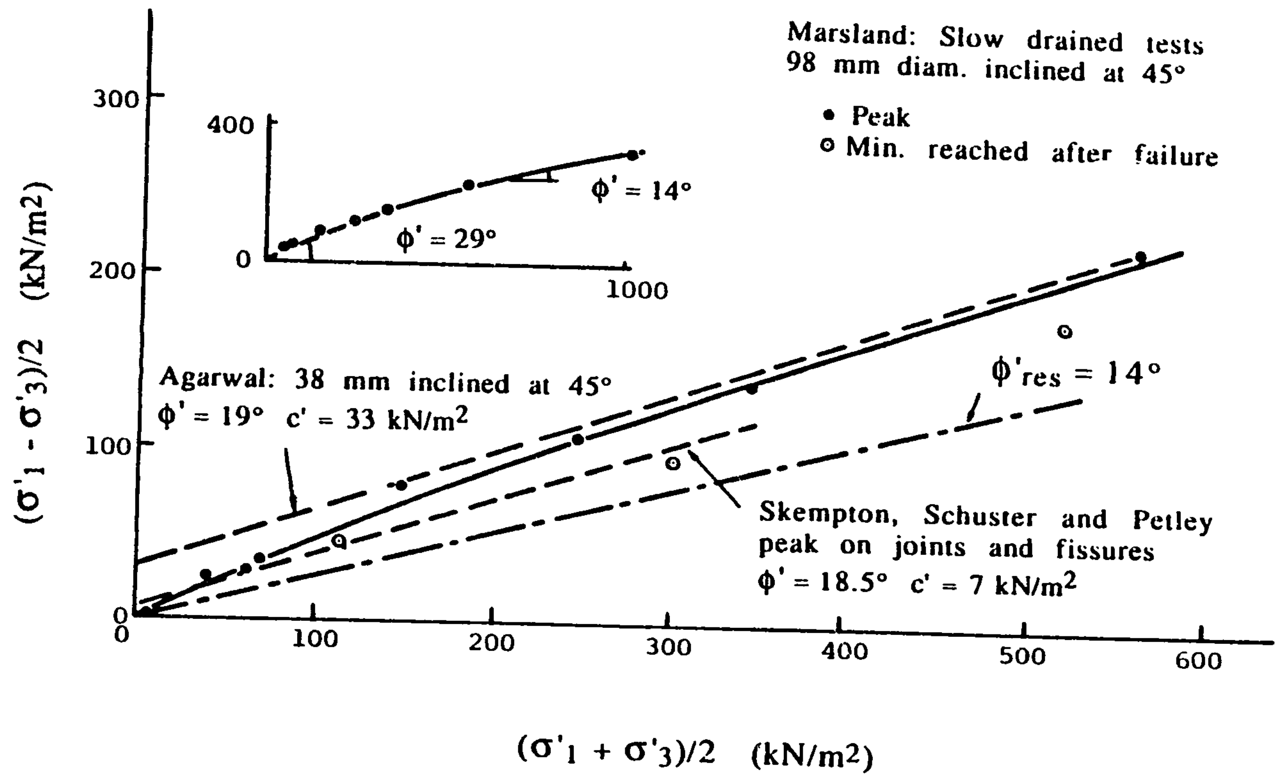

Figure 2.11 Shear strength of Blue London Clay taken from Wraysbury (modified after Marsland, 1971)

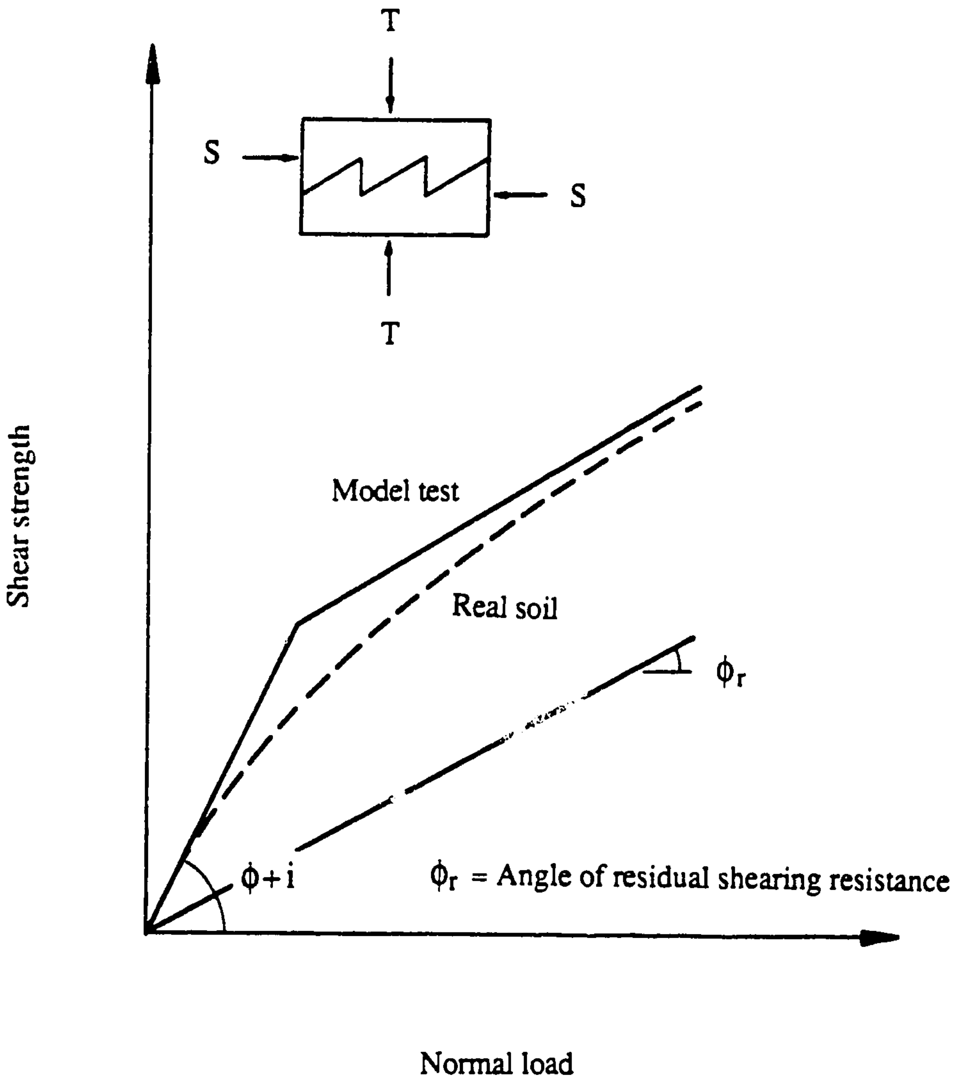
T
S
S
T
Shear strength
Model test
Real soil
ϕ_r
$\phi + i$
ϕ_r = Angle of residual shearing resistance
Normal load

Figure 2.12 Shear strength of model specimen having rough surfaces

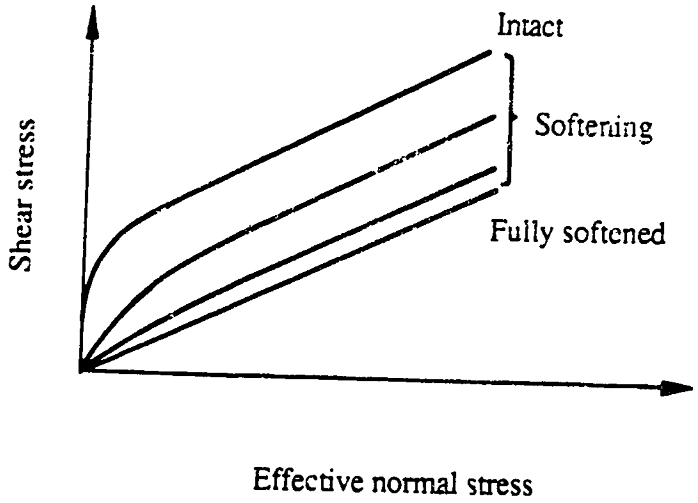

Figure 2.13 Shear strength reduction due to softening in stiff, fissured clay (modified after Morgenstern, 1977)

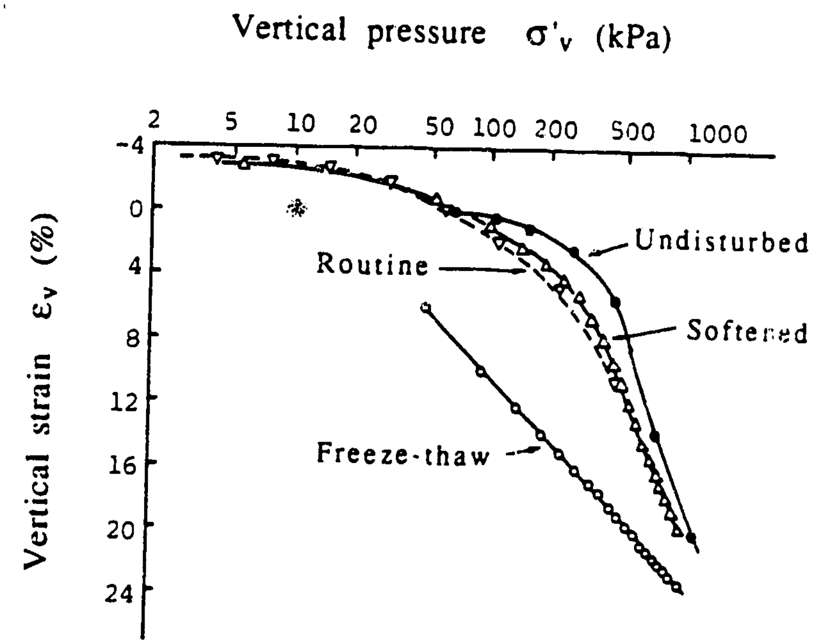

Figure 2.14 Results of oedometer tests using different procedures (modified after Graham and Au, 1985)

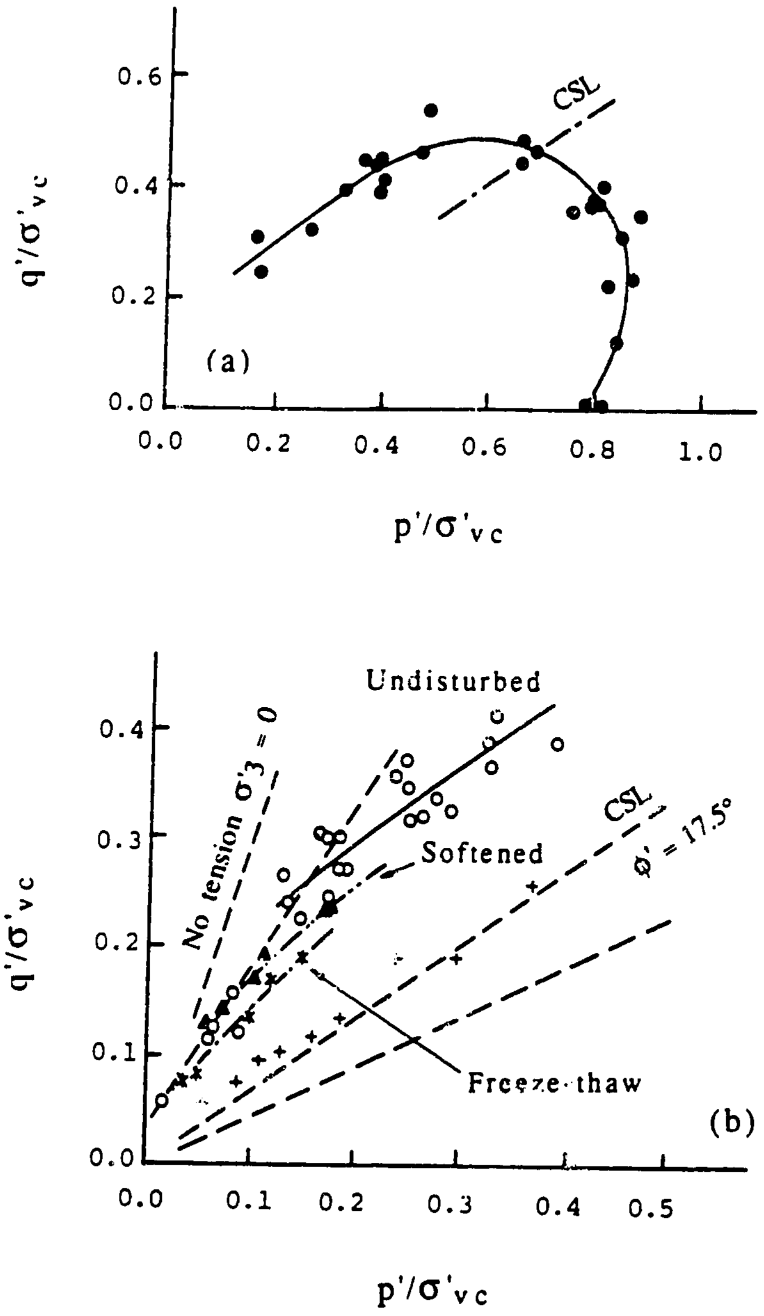

Figure 2.15 Results of triaxial tests on Lake Agssiz clays in normalized p'-q space (modified after Graham and Au, 1985)

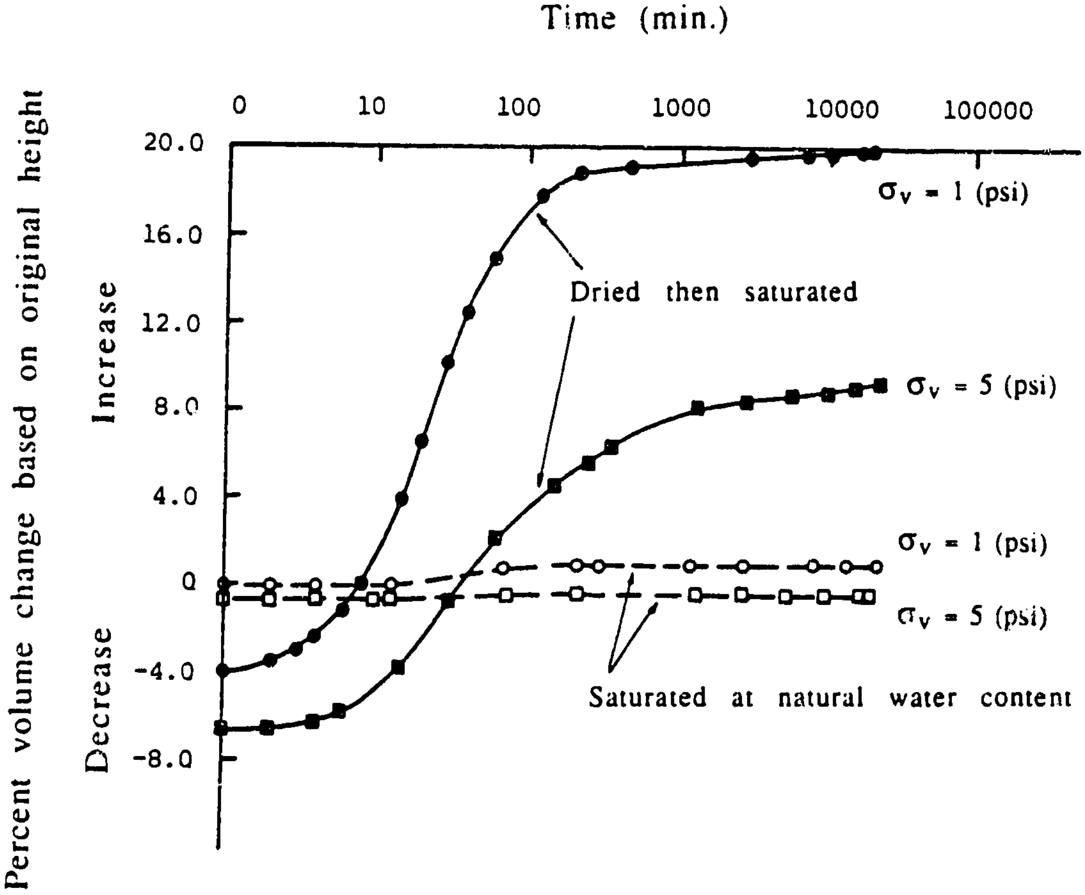

Figure 2.16 Results of swelling tests on shale samples (modified after Peterson and Peters, 1963)

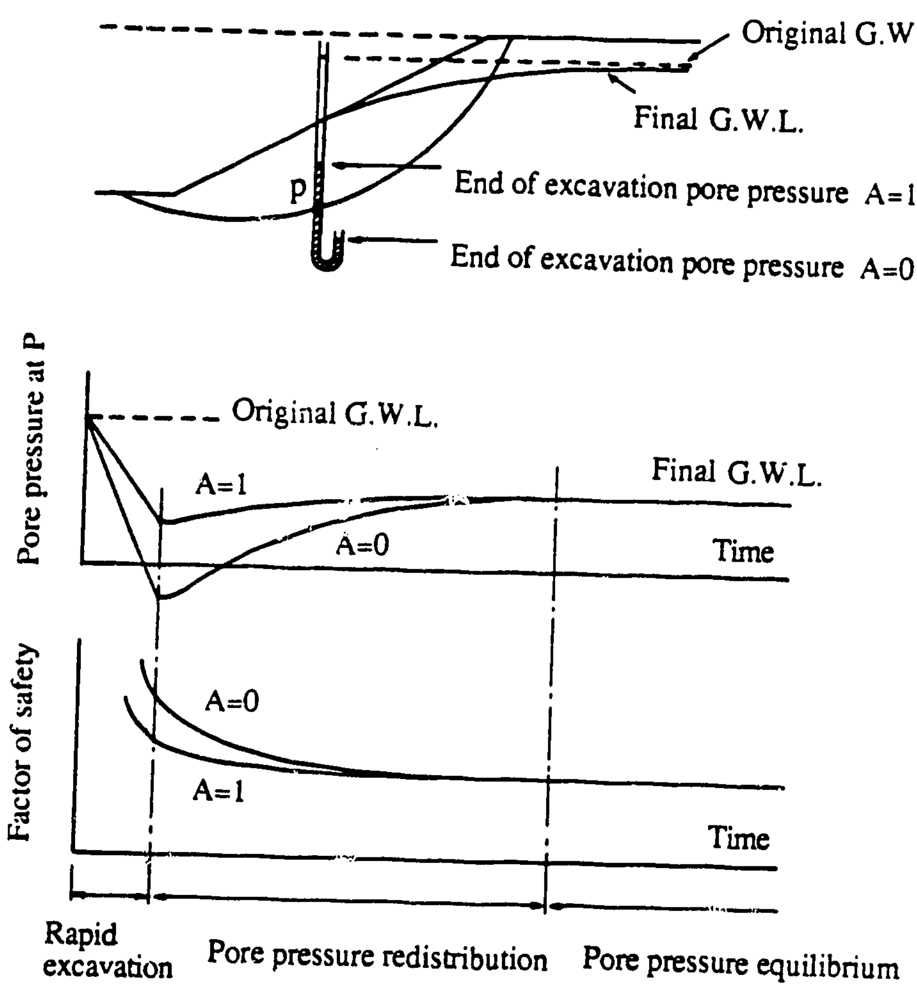
Original G.W.L.
Final G.W.L.
P
End of excavation pore pressure A=1
End of excavation pore pressure A=0
Pore pressure at P
Original G.W.L.
A=1
A=0
Final G.W.L.
Time
Factor of safety
A=0
A=1
Time
Rapid excavation
Pore pressure redistribution
Pore pressure equilibrium

Figure 2.17 Changes in pore water pressure and factor of safety during and after excavation in clay (modified after Bishop and Bjerrum, 1960)

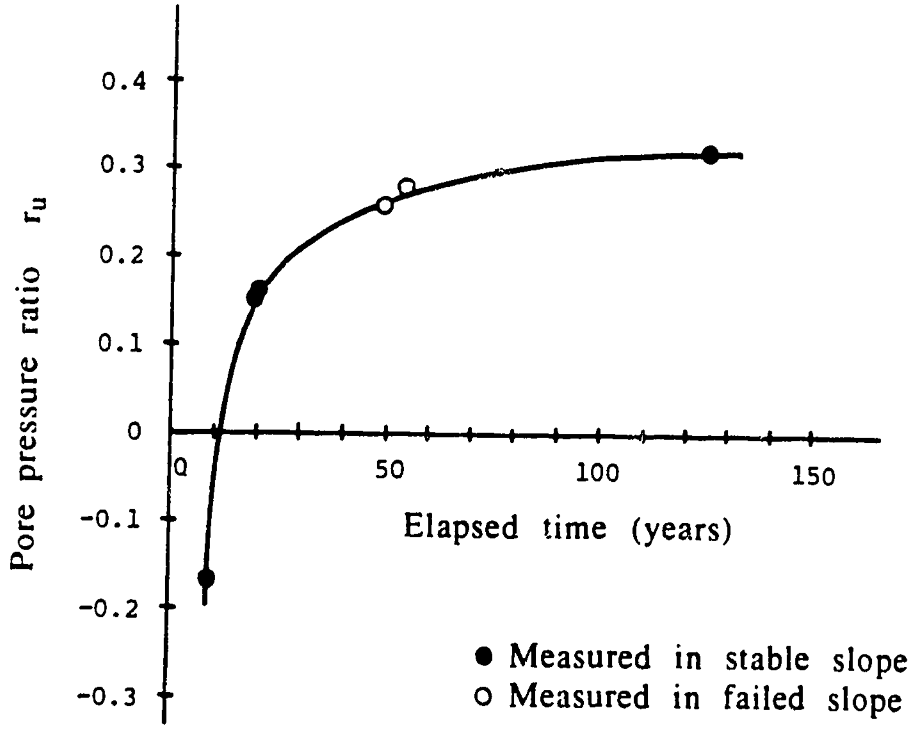

Figure 2.18 Relation between measured pore pressure ratio and elapsed time after excavation in Brown London Clay

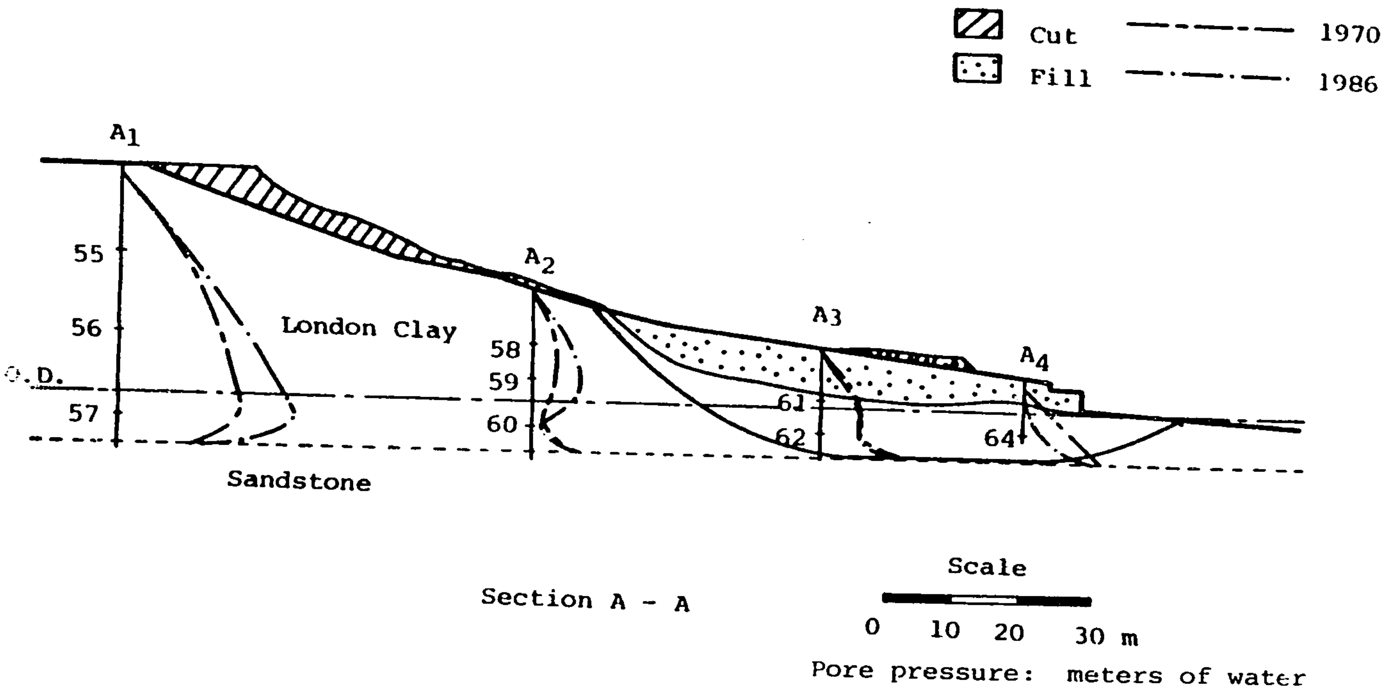
Cut
Fill
1970
1986
A1
A2
A3
A4
55
56
57
58
59
60
61
62
64
O.D.
London Clay
Sandstone
Section A - A
Scale
0 10 20 30 m
Pore pressure: meters of water

Figure 2.19 Pore water pressure measurements at Queens Avenue (modified after McGown *et al.*, 1987)

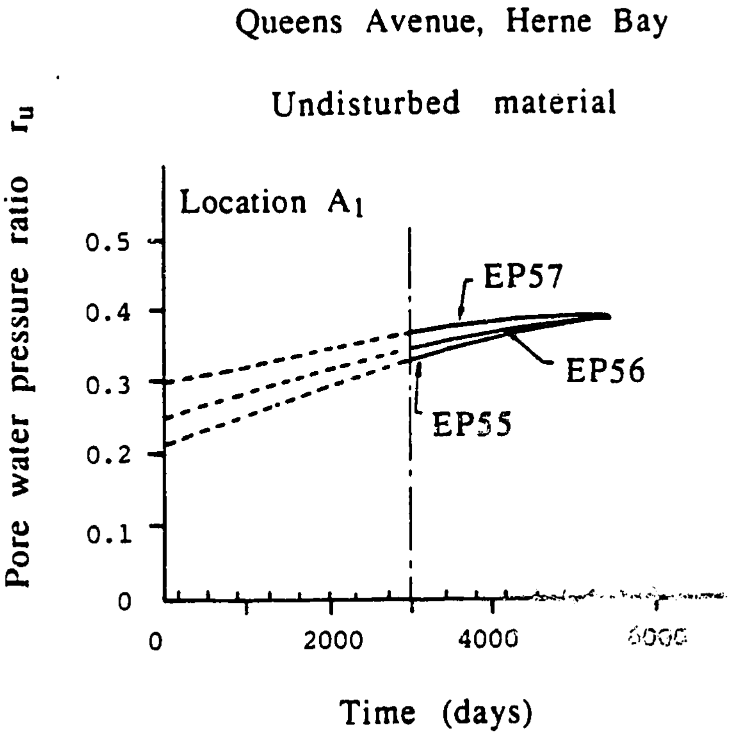

Figure 2.20 Pore water pressure equalization in undisturbed material at Queens Avenue (modified after McGown *et al.*, 1987)

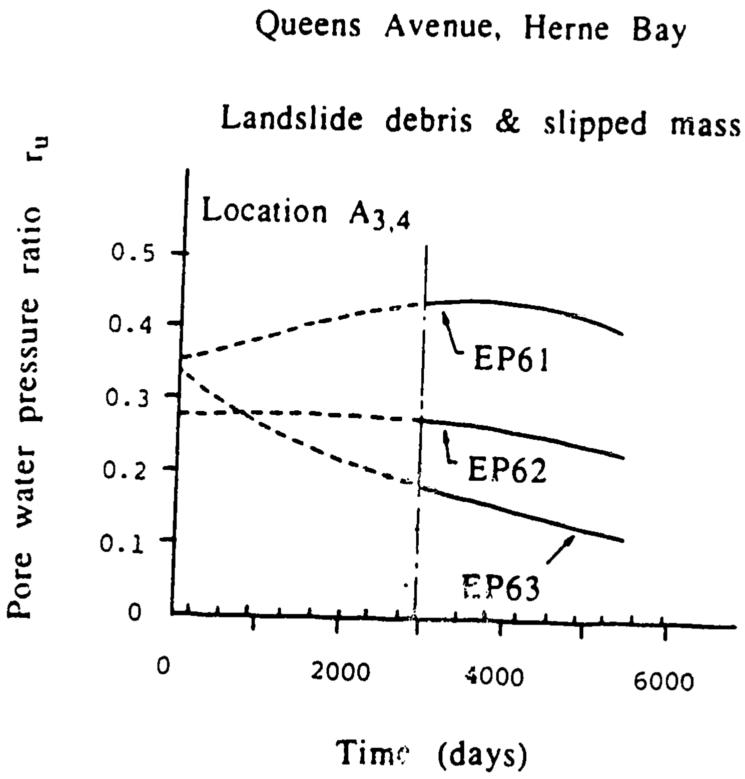

Figure 2.21 Pore water pressure equalization in disturbed material at Queens Avenue (modified after McGown *et al.*, 1987)

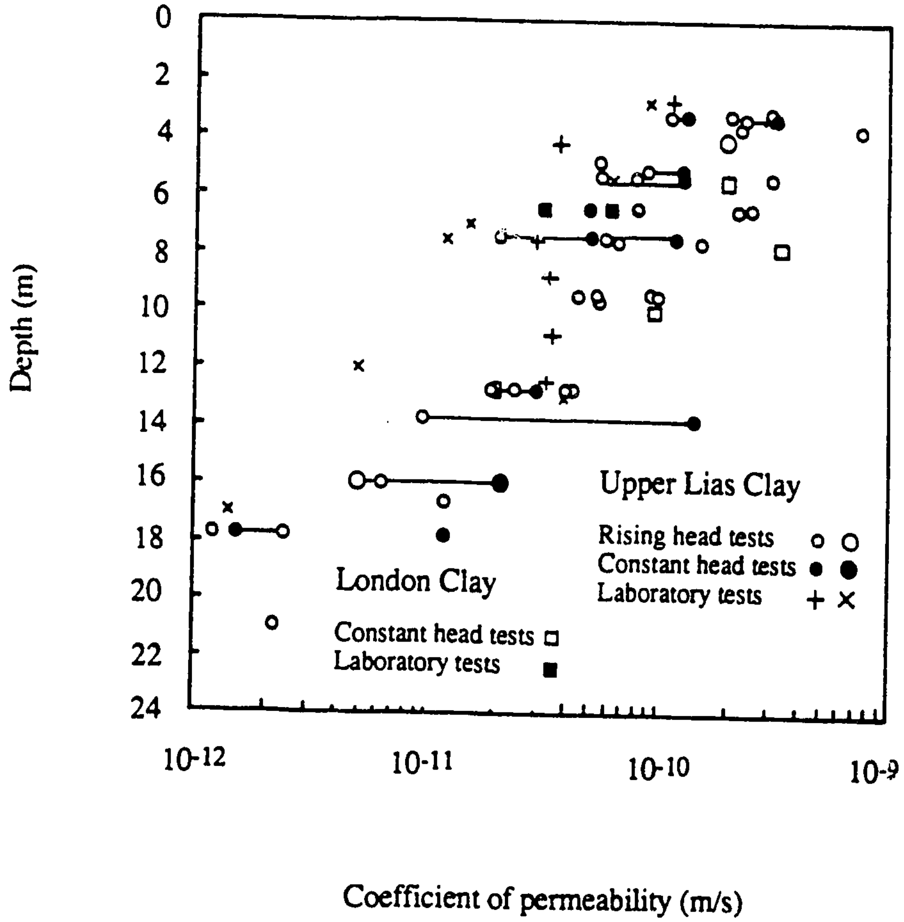

Figure 2.22 Relation between coefficient of permeability and depth for Blue London Clay and Upper Lias Clay (modified after Walbancke, 1975)

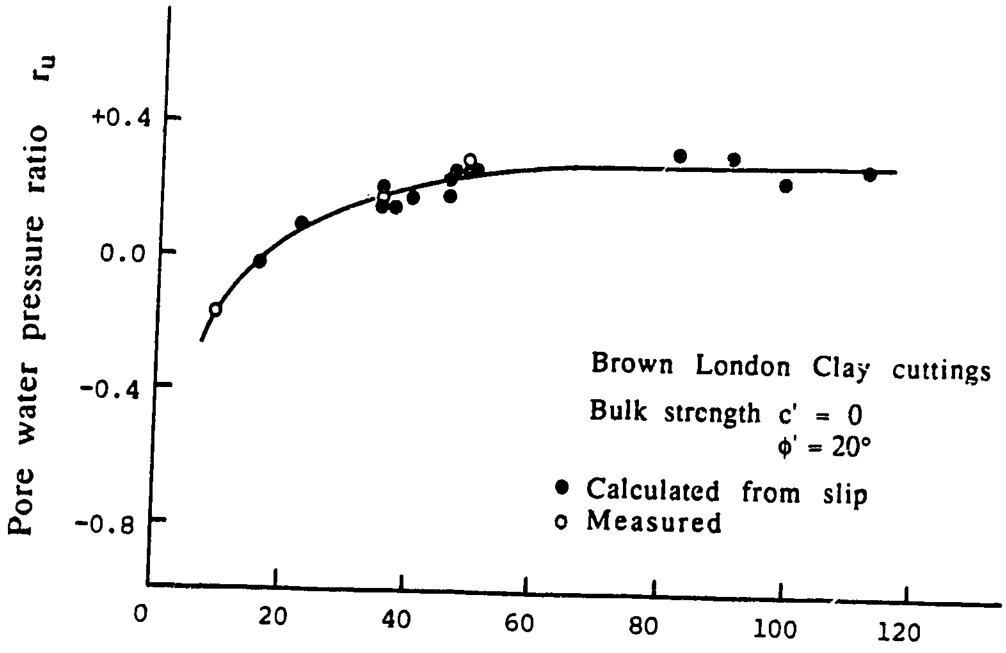

Time to failure (years)

Figure 2.23 Variation in pore pressure ratio with time (modified after Vaughan and Walbancke, 1973)

3. Failure criterion

3.1 Introduction

In Chapter 2, shear strength characteristics of fissured, overconsolidated clays and mudstones were reviewed in connection with the effect of softening. These materials exhibit non-linear failure envelopes. The softening effect was found to decrease the shear strength of a material with time and is accompanied by a reduction of the tendency to dilate.

This chapter introduces a simple non-linear failure criterion to represent the softening effect rationally. This failure criterion is applied to experimental data taken from the literature to show the effectiveness of this criterion. The variation in shear strength during softening is demonstrated using this criterion.

3.2 Failure criterion

3.2.1 Non-linear failure criterion

The Mohr-Coulomb failure criterion is no doubt the most widely used failure criterion in soil and rock mechanics. It is linear and very simple, containing only two parameters, c and ϕ. However, because of its linearity, it is often not appropriate to apply this failure criterion to materials exhibiting non-linear failure envelopes which are of interest in this study. It has been recognized important to model this non-linearity especially in slope stability problems.

Application of the Mohr-Coulomb failure criterion without caution could result in an over-estimate of the shear strength of a material.

Griffith (1921, 1924) proposed a non-linear criterion based upon a theoretical study of the physical process of [illegible] initiation in brittle materials such as glass. He approximated open flaws contained in a rock material as long, thin, elliptical openings. Assuming that there is no interaction between the openings and that there is no friction forces between the closed openings, a parabolic equation in terms of σ and τ was derived, paying special attention to tensile stresses developed at the boundary of these openings. McClintock and Walsh (1962) modified the Griffith criterion to take into account friction forces between closed cracks. Murrell (1965) expanded the original Griffith criterion to include triaxial stress conditions and hydrostatic pressure effects.

However, the difficulties in developing a mathematical model which adequately predicts fracture propagation and failure in rock materials has been recognized (Hoek, 1983). Consequently, many empirical failure criteria have been proposed (*e.g.*, Hobbs, 1966; Hoek, 1968; Bieniawski, 1974; Hoek and Brown, 1980; Yoshinaka and Yamabe, 1980; Adachi *et al.*, 1981). Among them, the failure criterion proposed by Hoek and Brown (1980) is worth noting because it has a simple form and is consistent with a large number of experimental data from intact rock to jointed rock masses. The criterion has a distorted parabolic shape in σ_1 and σ_3 space and is expressed as:

$$\sigma_1 = \sigma_3 + \sqrt{m\,\sigma_c\,\sigma_3 + s\,\sigma_c^2} \tag{3.1}$$

where σ_c is the uniaxial compression strength of intact rock and m and s are parameters which depend upon rock type and rock conditions. These parameters are determined from triaxial compression tests or direct shear tests using the least squares method. The parameter m always has a finite positive value ranging from the order of 10^{-3} for heavily jointed rock masses to the order of 10 for intact rock, and the value of s ranges from 0 to 1. For intact rock, the parameter s is unity. Results of the applications of this criterion to a wide range of rocks are tabulated by Hoek (1983). However, it can be seen from the form of the failure criterion that a failure envelope described by this criterion is always non-linear.

In developing a failure criterion, it is considered important here for a failure criterion to be simple and to contain only a small number of parameters which can be determined from conventional laboratory tests. Further, it should be able to express both non-linear and linear failure envelopes.

The proposed failure criterion consists of maximum and minimum principal stresses, σ_1 and σ_3, uniaxial compression strength, σ_c, and three parameters, A, B and S, and is expressed as follows:

$$\sigma_1 = \sigma_3 + A\,\sigma_c\left(\frac{\sigma_3}{\sigma_c} - S\right)^{\frac{1}{B}} \tag{3.2}$$

The parameters A, B and S can be determined from results of triaxial compression tests or direct shear tests using the least squares ethod. Details on the determination of these parameters are described in Appendix A. The failure criterion can be expressed in terms of total stress or effective stress, depending on the experimental data upon which the derivation of the parameters is based. Substituting $\sigma_3 = 0$ into the above equation gives

$$\frac{\sigma_1}{\sigma_c} = A(-S)^{\frac{1}{B}} \tag{3.3a}$$

Since the term in the left side is unity initially, the following condition should be satisfied:

$$A(-S)^{\frac{1}{B}} = 1 \tag{3.3b}$$

As described in Section 3.3, the softening effect is represented by a reduction in the values of strength parameters, A, B and S. In Equation (3.3a) σ_c is the initial strength and σ_1 is the strength at a given time. Thus, the above condition is not necessarily satisfied during softening. This can be considered similar to the condition imposed in the Hoek-Brown failure criterion when applied to intact rock materials, *i.e.*, the parameter s must be unity.

The Mohr-Coulomb and Hoek-Brown failure criteria can be derived from the proposed failure criterion. When the parameter B equals one, the criterion becomes Mohr-Coulomb. The strength parameters in the Mohr-Coulomb criterion, ϕ and c, are expressed as:

$$\sin \phi = \frac{A}{2 + A} \tag{3.4a}$$

$$c = -\frac{A\,S\,\sigma_c}{\sqrt{4 + 2A}} \tag{3.4b}$$

When the parameter B equals two, the Hoek-Brown criterion is obtained, whose strength parameters, m and s, are expressed as:

$$m = A^2 \tag{3.5a}$$

$$s = - A^2 S \tag{3.5b}$$

The proposed failure criterion does not take into account the effect of intermediate principal stress which has been observed in experimental studies on rocks and soils. Hoek and Brown (1980), following a review of many experimental studies on rock, concluded that it was admissible to neglect the intermediate principal stress effect in the interests of keeping the failure criterion as simple as possible. A review on shear strength of soils by Bishop (1966) seems to support this point of view. It was suggested that the Mohr-Coulomb failure criterion was accepted as the only simple criterion of reasonable generality.

From the above, it is felt that neglect of intermediate principal stress effects may be justified for practical purposes, considering the simplicity of the criterion.

3.2.2 Characteristics of proposed failure criterion

The proposed failure criterion contains three parameters A, B and S. These parameters influence the shape of a failure envelope. Figure 3.1 illustrates the effect of the parameter A. Similarly, the effects of the parameters B and S are shown in Figures 3.2 and 3.3, respectively. In order to produce these figures, the values of σ_c, A, B and S are kept constant as 1.0 MPa, 1.0, 1.5 and -1.0, respectively, except for the value concerned in each figure. It can be seen that the parameter A affects significantly both the slope and the intercept to the maximum principal stress axis. A larger value gives a more steeply inclined failure envelope. The smaller the value, the smaller is the curvature. The value of zero gives a linear relation. The parameter B influences mainly the inclination of the failure envelope. The larger the value, the greater is the inclination. The parameter S mainly influences the position of the intercept on the maximum principal stress axis.

The failure criterion can be plotted in terms of normal stress σ and shear stress τ. Referring to Figure 3.4, the relation between σ and τ on a critical plane is derived by Balmer (1952) as follows:

$$\sigma = \sigma_3 + \frac{\sigma_1 - \sigma_3}{1 + \frac{\partial\sigma_1}{\partial\sigma_3}} \qquad (3.6a)$$

$$\tau = \pm \frac{\sigma_1 - \sigma_3}{1 + \frac{\partial\sigma_1}{\partial\sigma_3}} \sqrt{\frac{\partial\sigma_1}{\partial\sigma_3}} \qquad (3.6b)$$

$$\tan \phi_i = \frac{\frac{\partial\sigma_1}{\partial\sigma_3} - 1}{2\sqrt{\frac{\partial\sigma_1}{\partial\sigma_3}}} \qquad (3.6c)$$

$$c_i = \tau - \sigma \tan \phi_i \qquad (3.6d)$$

where c_i and ϕ_i are the cohesion intercept and the angle of friction which are stress-dependent, and the subscript stands for 'instantaneous'. By substituting the values of σ_1 and σ_3 calculated by Equation (3.2) into these equations, one can draw a Mohr envelope corresponding to the proposed failure criterion. Figures 3.5, 3.6 and 3.7 are Mohr envelopes obtained in this manner and correspond to Figures 3.1, 3.2 and 3.3, respectively. Effects of the parameters A, B and S upon a Mohr envelope can be seen in these figures. As in the σ_1-σ_3 space, the parameter A influences both the slope and the intercept to the τ axis. The parameters B and S seem to play a similar role to the angle of friction and the cohesion intercept of the Mohr-Coulomb failure criterion, respectively. The stress-dependency of ϕ_i and c_i is illustrated in Figure 3.8. As the normal stress increases, the cohesion intercept increases and the angle of friction decreases.

The expression of a failure criterion in terms of principal stresses is very useful and convenient. It can easily be generalized in terms of stress invariants and be implemented in a finite element program. However, for cases such as slope stability calculations in which shear strength for a particular normal stress is required, it would be more convenient to have the mathematical expression of a failure criterion in terms of σ and τ. From an examination of the shape of a failure envelope in σ-τ space given by the proposed criterion, the following expression may be used for this approximation:

$$\tau = P\,\sigma_c \left(\frac{\sigma}{\sigma_c} - Q \right)^{\frac{1}{R}} \tag{3.7}$$

where P, Q and R are strength parameters. These parameters are determined using the least squares method, as described in Appendix A.

3.2.3 Applications

The proposed failure criterion has been applied to experimental data taken from the literature. A total of eighteen triaxial compression test results on clay and rock materials were collected. The results are tabulated in Table 3.1 and the corresponding plots are given in Figures 3.9 to 3.27. Although the number of test results collected is limited, the following observations can be made. The parameter A varies between 1.3 and 8.3, and the parameter B between 1.0 and 3.3 except Ohya-Ishi. The parameter S varies between -0.78 and -0.01. For the same rock type, each parameter lies in a narrow range. For mudstones, A ranges from 2.0 to 2.7, B from 1.5 to 2.8 and S from -0.36 to -0.06. For sandstones, A ranges from 3.4 to 5.3, B from 1.5 to 2.4 and S from -0.03 to -0.1. As illustrated in Figures 3.9 to 3.27, excellent agreement between the proposed failure criterion and the experimental results has been obtained.

3.3 Representation of softening

The effect of softening can be described by a reduction in the values of the strength parameters A, B and S in the proposed failure criterion. Further, the variation of shear strength during softening can be represented by a systematic reduction with time of these strength parameters. At the fully-softened condition, the values of B and S can be assumed as 1.0 and 0, respectively, to give a linear failure envelope with zero cohesion intercept.

Since only the initial and fully-softened shear strength can be determined with ease from experimental studies, an interpolation technique is required to derive shear strength during softening. According to the discussion on the rate of softening in Chapter 2, the following inverse-hyperbolic functions can be assumed for reducing the strength parameters with time:

$$A = A_0 \left\{ 1 - \frac{t}{a\,t + t_{fs}\left(\frac{A_0}{A_0 - A_{fs}} - a \right)} \right\} \tag{3.8a}$$

$$B = B_0 \left\{ 1 - \frac{t}{b\,t + t_{fs}\left(\frac{B_0}{B_0 - B_{fs}} - b \right)} \right\} \tag{3.8b}$$

$$S = S_0 \left\{ 1 - \frac{t}{c\,t + t_{fs}\left(\frac{S_0}{S_0 - S_{fs}} - c \right)} \right\} \tag{3.8c}$$

where A, B and S are strength parameters and the subscripts, 0 and fs, indicate the initial and fully-softened conditions, respectively. The a, b and c are strength reduction-rate parameters and t_{fs} is time to a fully-softened condition. As mentioned earlier, B_{fs} and S_{fs} are assumed as one and zero, respectively.

Figure 3.28 shows variations of A with time for different values of a in A/A_0 and t/t_{fs} coordinates. The range of variations of values in the ordinate depends upon the ratio of A_{fs}/A_0. The ratio of 1/3 was used for this figure. It can be seen that a larger value of a gives a more rapid reduction in A. A value of zero gives a linear reduction in A with time. Similarly, variations of B and S are shown in Figures 3.29 and 3.30, respectively. In these figures, the values of B_{fs}/B_0 and S_{fs}/S_0 are 1/2 and 0, respectively.

With these time-dependent strength parameters, the variation in the shape of a failure envelope during softening can be modelled. This is illustrated in Figure 3.31. The corresponding variations of the angle of friction and the cohesion intercept are shown in Figures 3.32 and 3.33, respectively. To plot these curves, the strength parameters A_0, A_{fs}, B_0 and S_0 are assumed as 3, 1, 2 and -0.1, respectively, and the strength reduction-rate parameters a, b and c are all zero. The fully-softened condition is assumed to be reached in 100 years. It can be seen from Figure 3.31 that the failure envelope changes from a non-linear envelope at the initial condition to a linear envelope at the fully-softened condition. The angle of friction and cohesion intercept decrease with time, and so does their stress-dependency. This can be considered to properly represent a reduction in shear strength due to softening.

3.4 Summary

A simple non-linear failure criterion is proposed which consists of maximum and minimum principal stresses, uniaxial compression strength and three strength parameters. The strength parameters can be determined from conventional triaxial compression tests or direct shear tests. The failure criterion neglects the effect of intermediate principal stress in the interest of the simplicity. Both the Mohr-Coulomb and the Hoek-Brown failure criteria can be derived from the proposed failure criterion. The failure criterion was applied to eighteen triaxial compression test results taken from the literature and excellent agreement between predicted and experimentally determined shear strengths was obtained.

Shear strength reduction due to softening can be described rationally by this failure criterion. Variation of shear strength during softening was demonstrated by interpolating the strength parameters, A, B and S, from the initial to fully-softened condition. For this interpolation, an inverse-hyperbolic relation with time of these parameters was assumed.

The proposed failure criterion is used as a yield function in elasto-plastic finite element analyses in subsequent chapters.

Table 3.1 Strength parameters (Continued)

Material	σ_c (MPa)	A	B	S	Notes	References
Devon Granite	179.6	5.498	1.848	-0.043	TS	Franklin and Hoek (1970)
Portland Limestone	42.3	3.954	1.423	-0.141	TS	ditto
Derbyshire Sandstone	52.7	4.564	1.538	-0.097	TS	ditto
Darley Dale Sandstone	80	4.147	1.720	-0.087	TS	ditto
Carrara Marble	92.4	2.707	2.546	-0.079	TS	ditto
Pennant Sandstone	197	3.385	2.442	-0.051	TS	ditto

Notes: ES and TS stand for effective stress and total stress parameters, respectively.

Table 3.1 Strength parameters

Material	σ_c (MPa)	A	B	S	Notes	References
Blue London Clay	0.206	3.525	1.763	-0.109	ES	Bishop *et al.* (1965)
Keuper Marl	0.409	4.504	2.080	-0.044	ES	Chandler (1967)
Kobe Mudstones	7.06, 2.63	2.572	1.528	-0.236	ES	Yoshinaka and Yamabe (1980)
Ohya-Ishi (Tuff)	5	1.743	7.246	-0.018	ES	Adachi *et al.* (1981)
Indiana Limestone	48.9	1.267	1.032	-0.783	TS	Schwartz (1964)
Georgia Marble	27.6	4.056	3.258	-0.011	TS	ditto
Pottsville Sandstone	62.1	5.333	2.143	-0.028	TS	ditto
Stone Mountain Granite	82.7	6.721	1.637	-0.042	TS	ditto
Tennessee Marble	132	2.432	2.150	-0.148	ES	Wawersik (1968)
Panguna Andesite	1.241	8.286	1.495	-0.042	TS	Jaeger (1970)
Shimajiri Mudstone	2.8	1.987	1.501	-0.357	ES	Shinjo (1976)
Tohoku Mudstone	2.17	2.684	2.801	-0.063	ES	Watanabe *et al.* (1988)

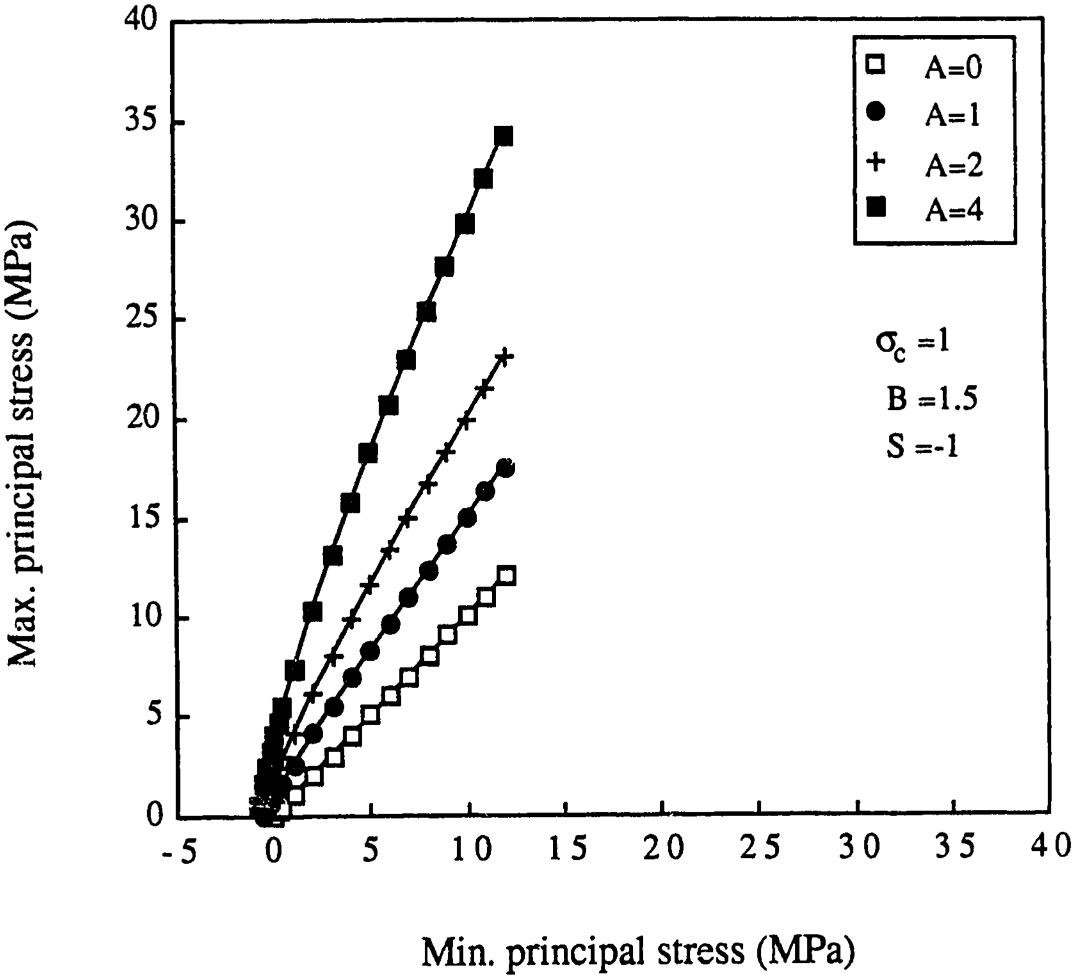

Figure 3.1 Influence of parameter A on failure envelope

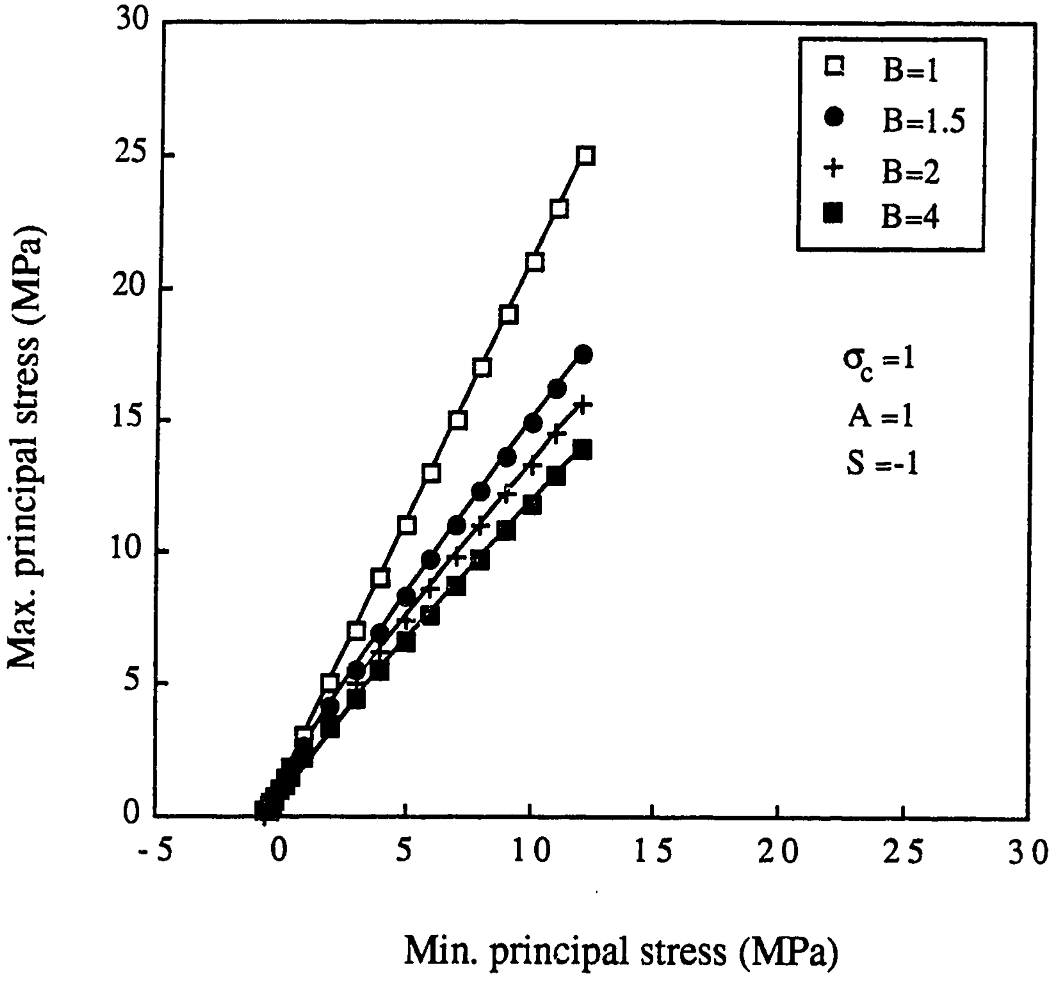

Figure 3.2 Influence of parameter B on failure envelope

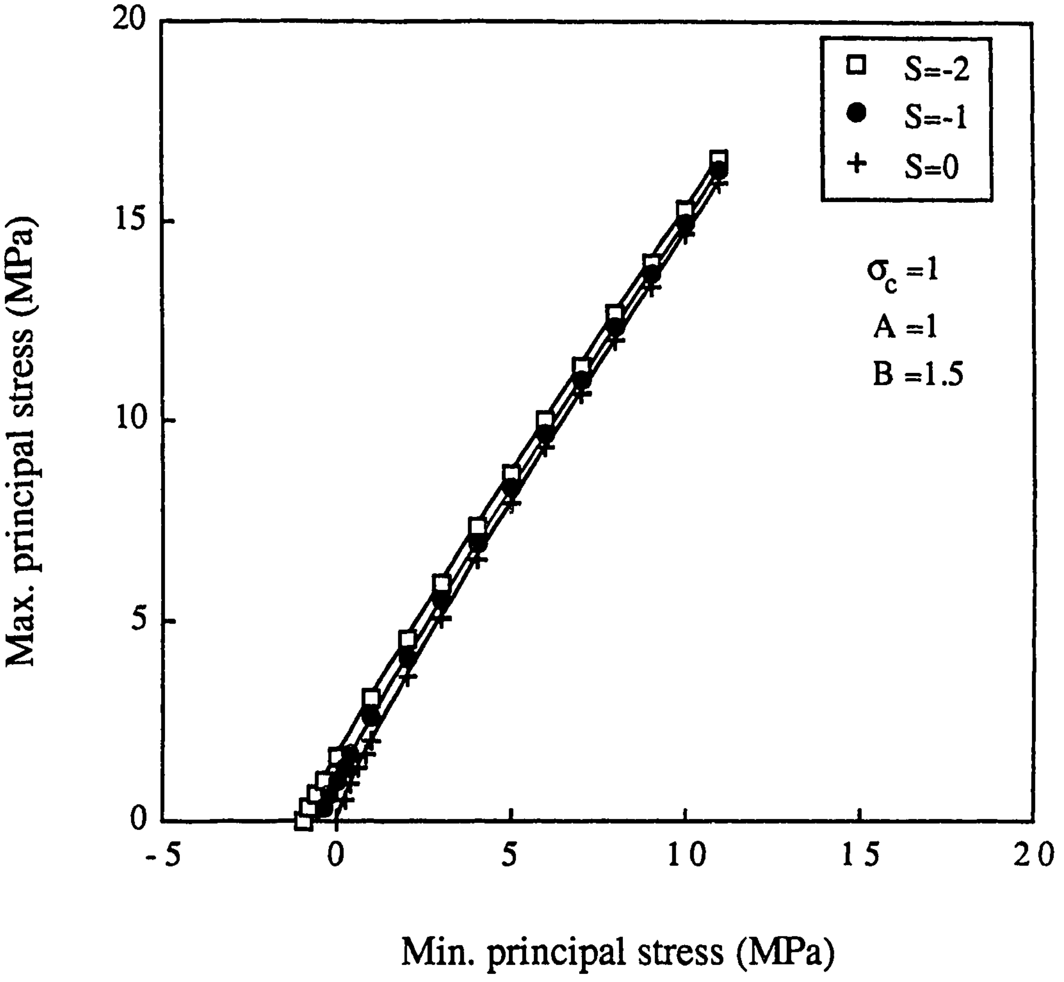

Figure 3.3 Influence of parameter S on failure envelope

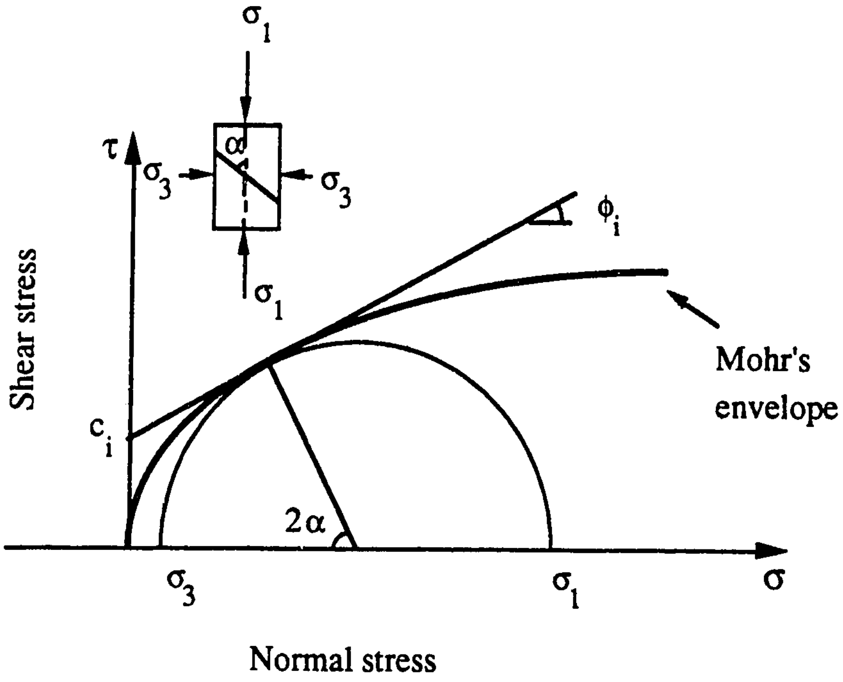
σ_1
τ
α
σ_3
σ_3
σ_1
ϕ_i
Shear stress
Mohr's envelope
c_i
2α
σ_3
σ_1
σ
Normal stress

Figure 3.4 Mohr's diagram (modified after Balmer, 1952)

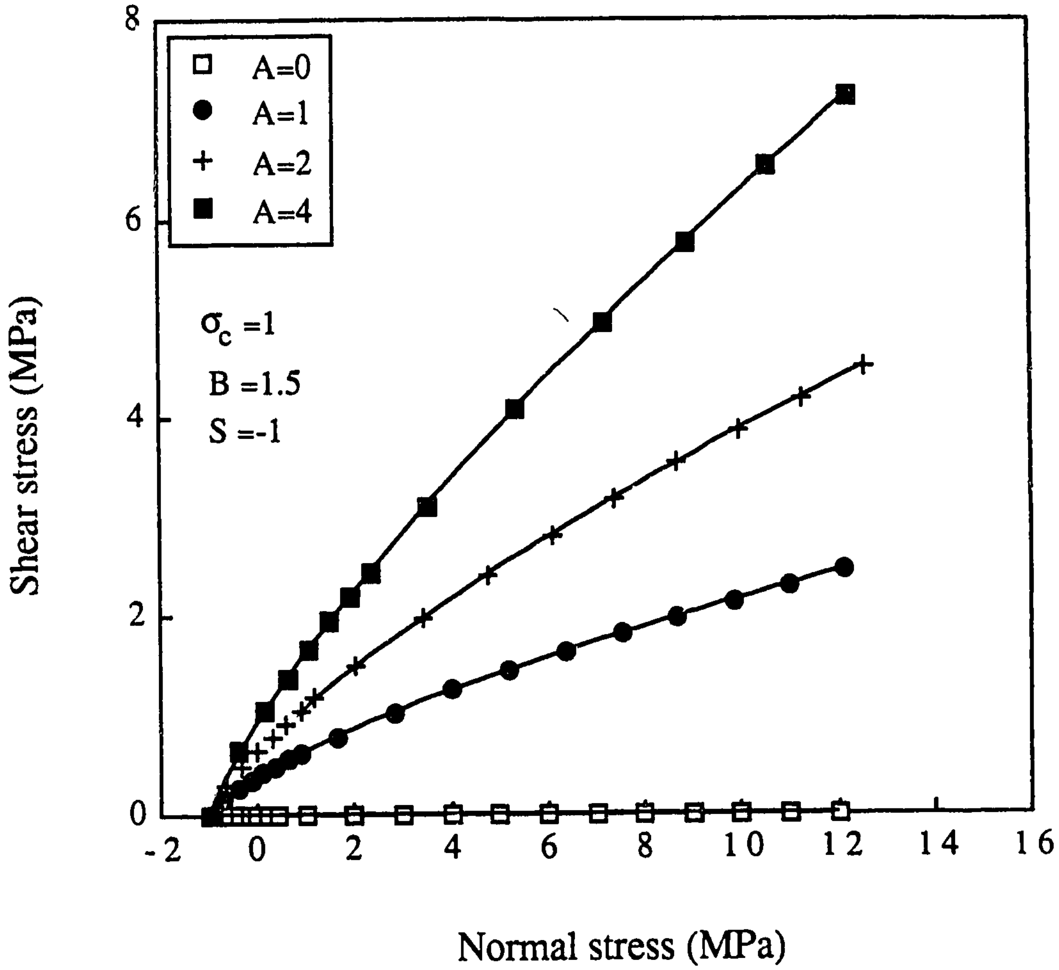

Figure 3.5 Influence of parameter A on Mohr failure envelope

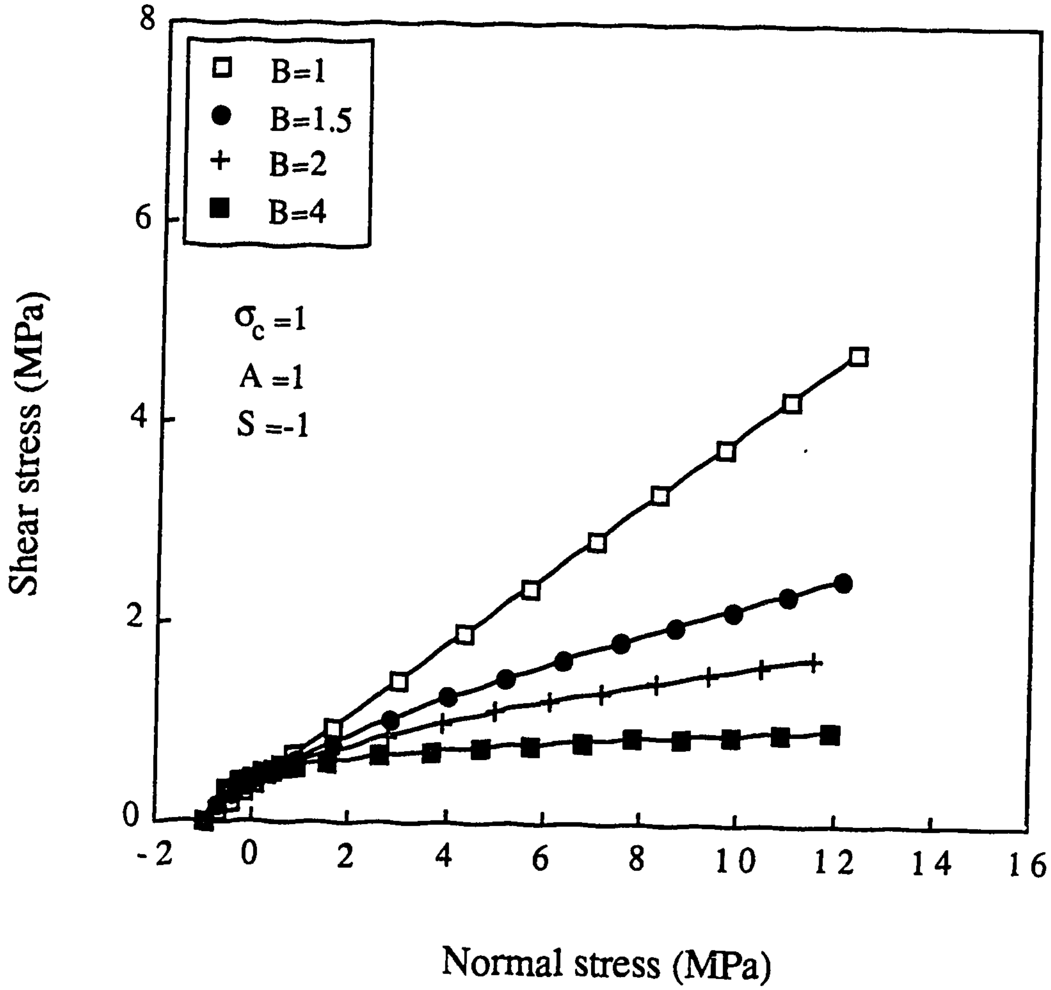

Figure 3.6 Influence of parameter B on Mohr failure envelope

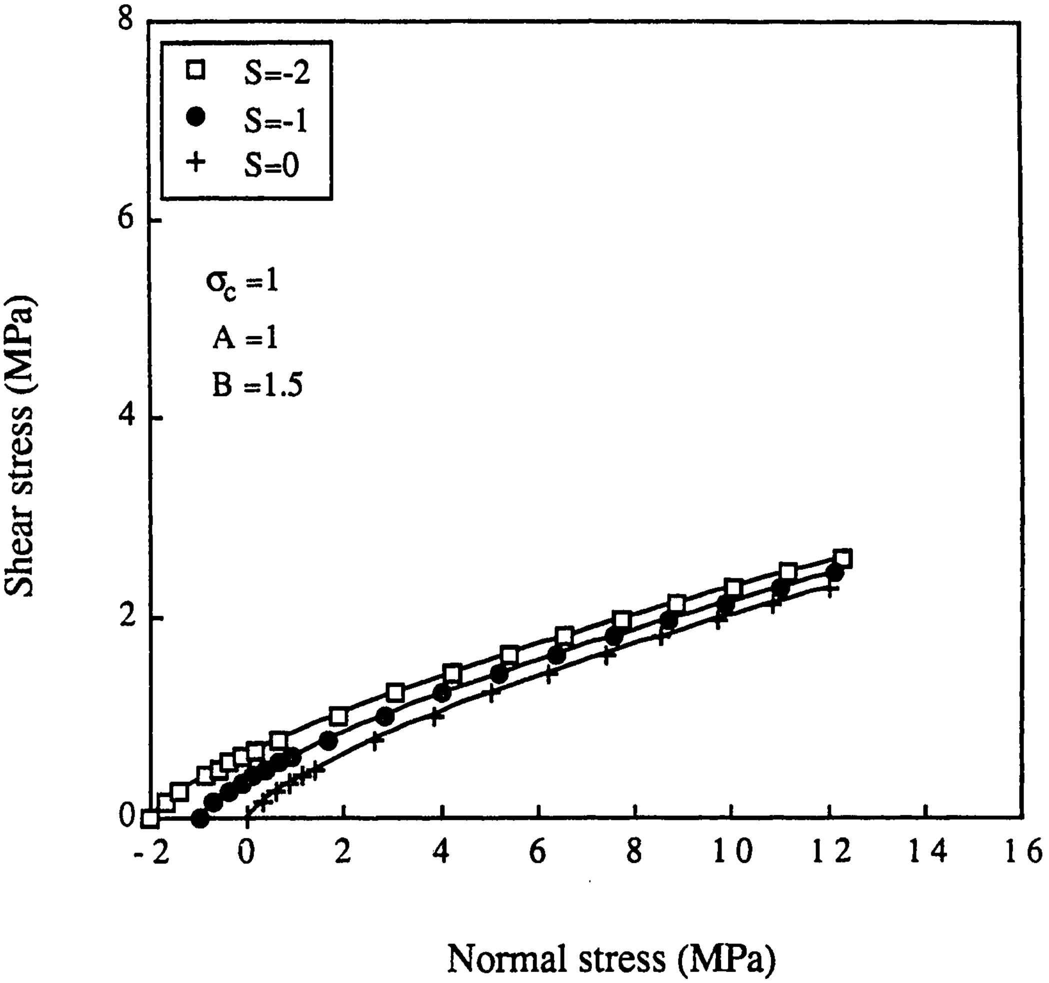

Figure 3.7 Influence of parameter S on Mohr failure envelope

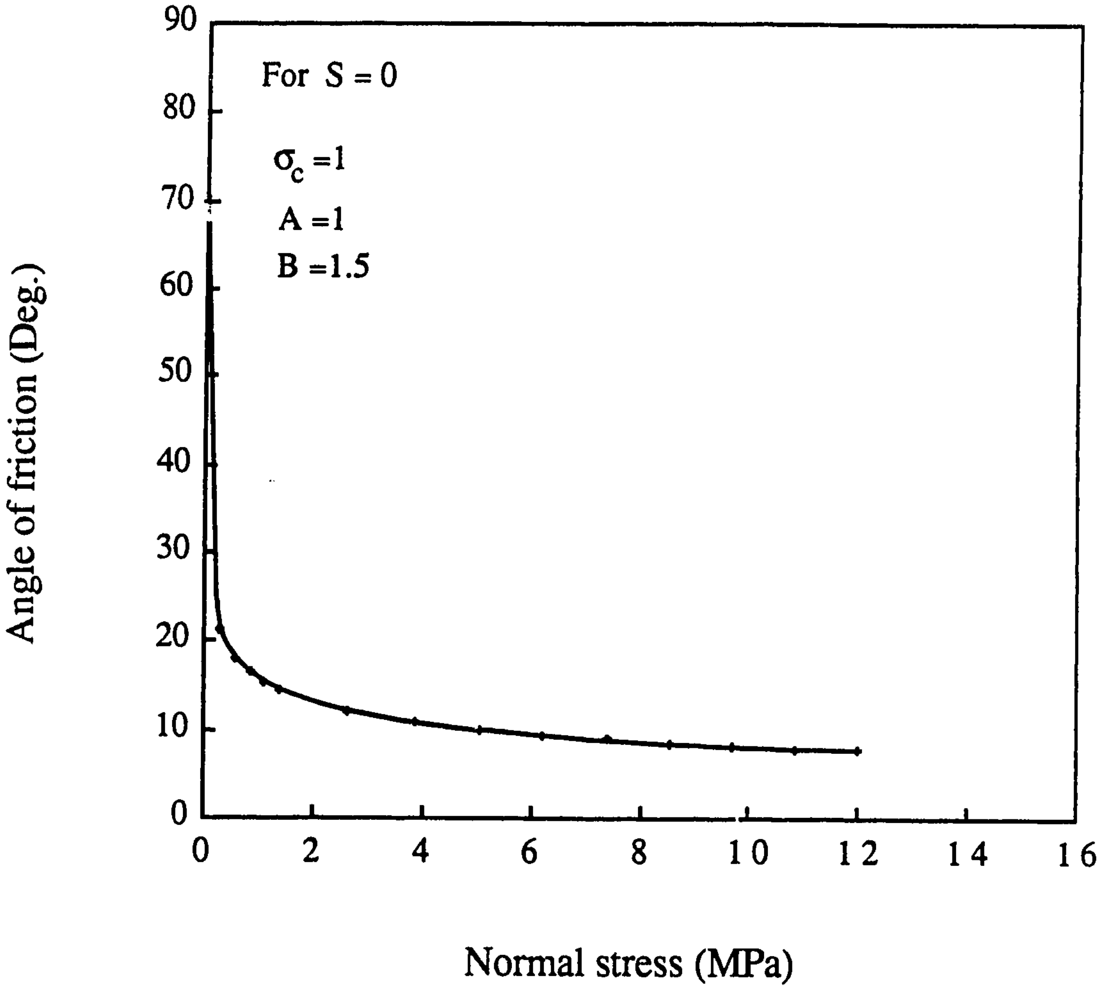

Figure 3.8(a) Influence of normal stress on angle of friction

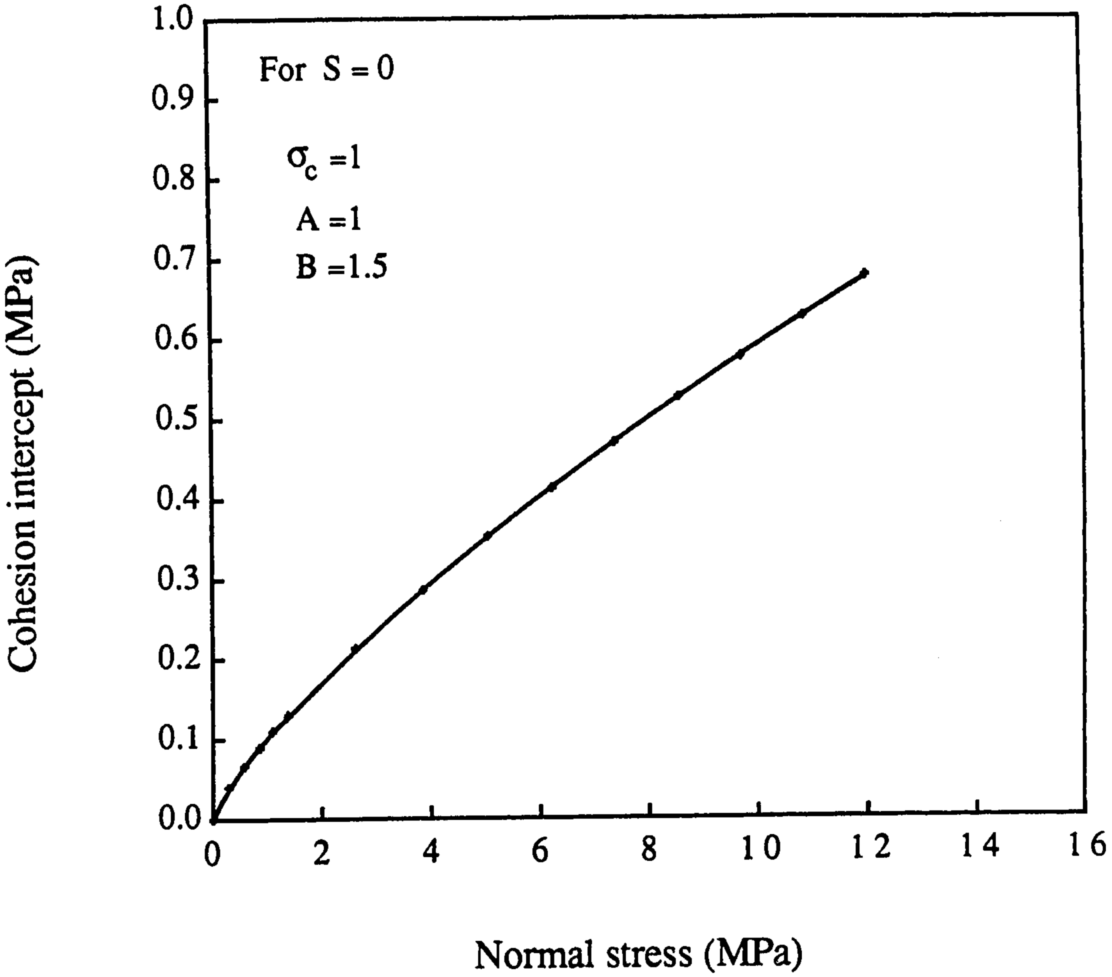

Figure 3.8(b) Influence of normal stress on cohesion intercept

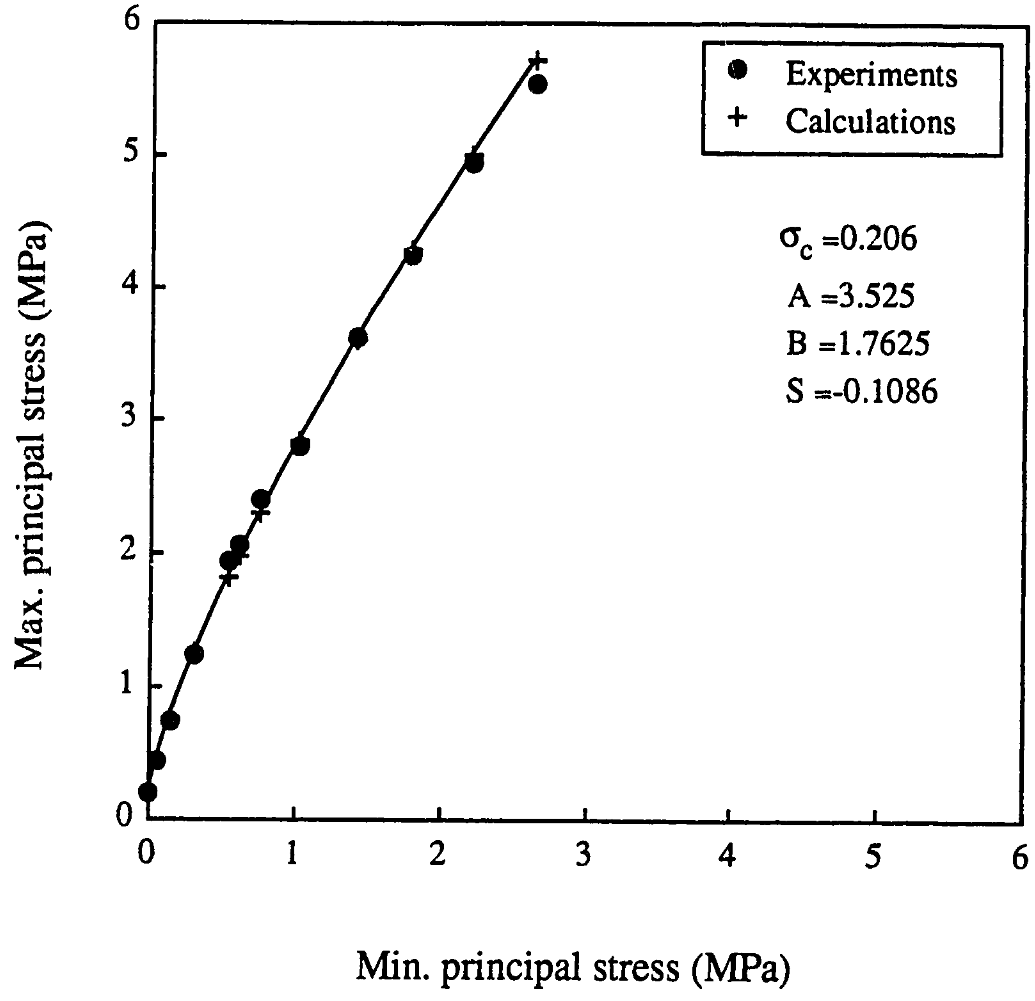

Figure 3.9 Comparison of failure criterion with triaxial test data for Blue London Clay (Bishop *et al.*, 1965)

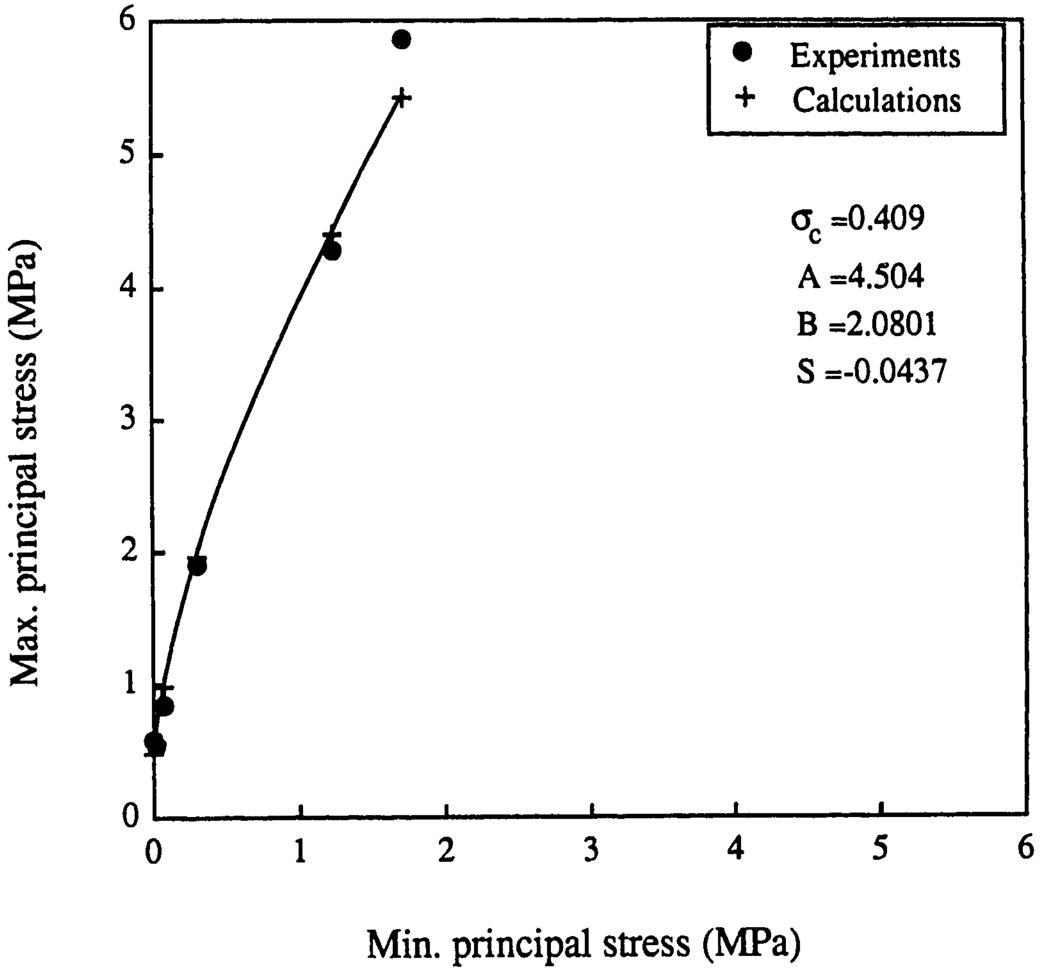

Figure 3.10 Comparison of failure criterion with triaxial test data for Keuper Marl (Chandler, 1967)

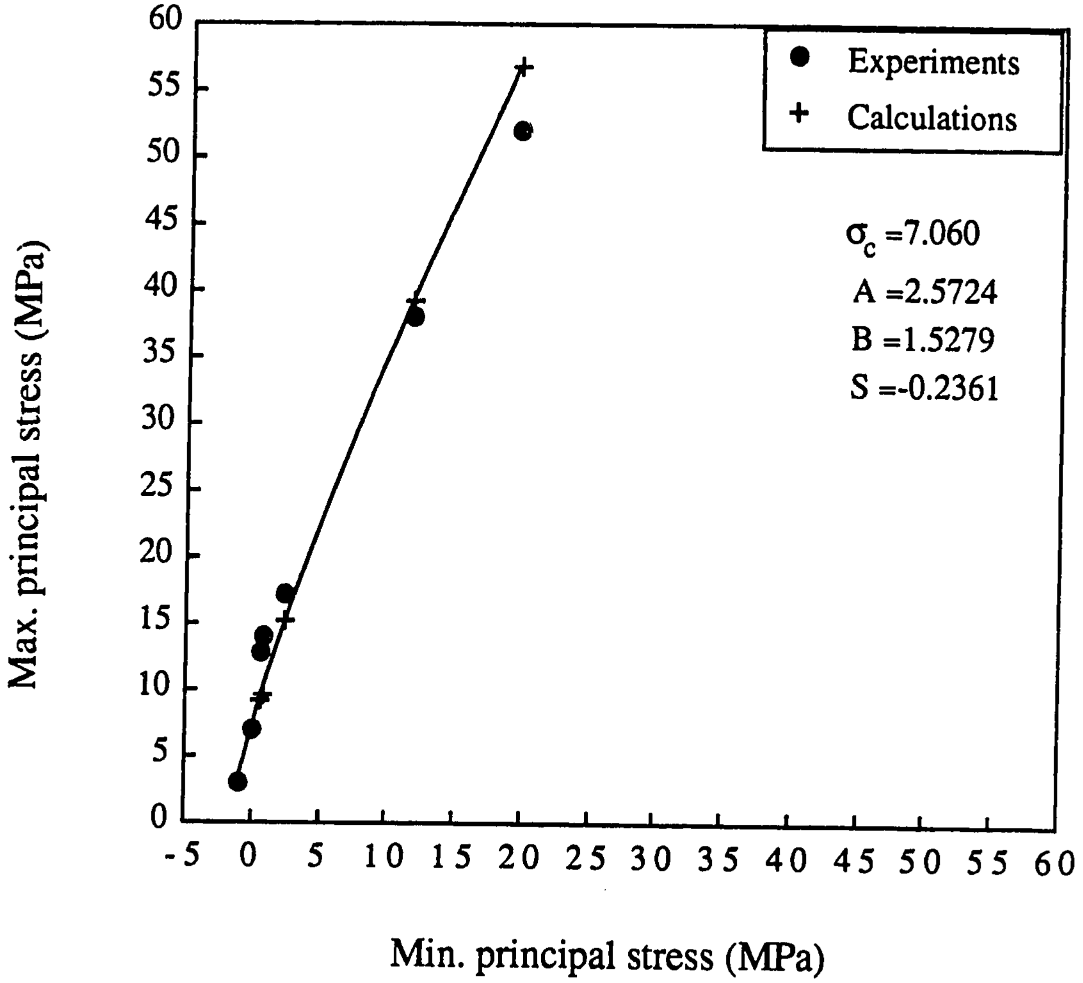

Figure 3.11 Comparison of failure criterion with triaxial test data for Kobe Mudstone 1 (Yoshinaka and Yamabe, 1980)

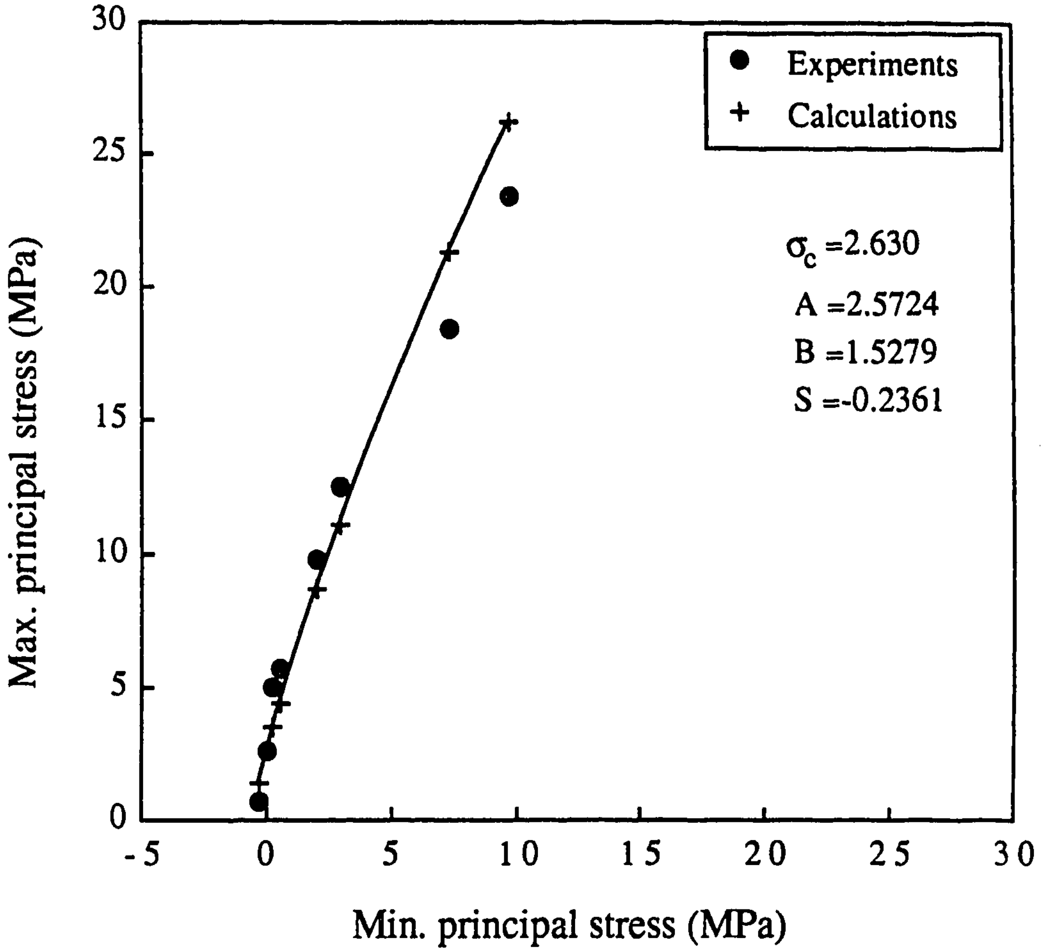

Figure 3.12 Comparison of failure criterion with triaxial test data for Kobe Mudstone 2 (Yoshinaka and Yamabe, 1980)

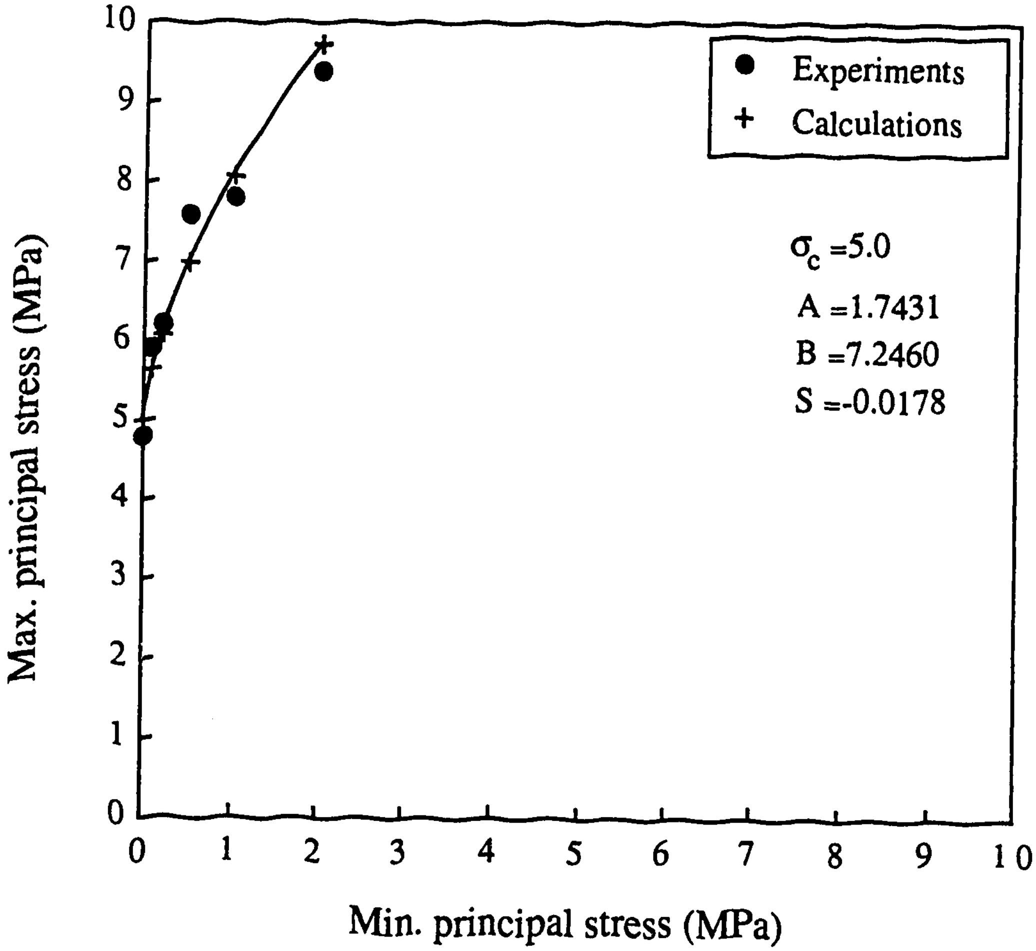

Figure 3.13 Comparison of failure criterion with triaxial test data for Ohya-Ishi (Tuff) (Adachi *et al.*, 1981)

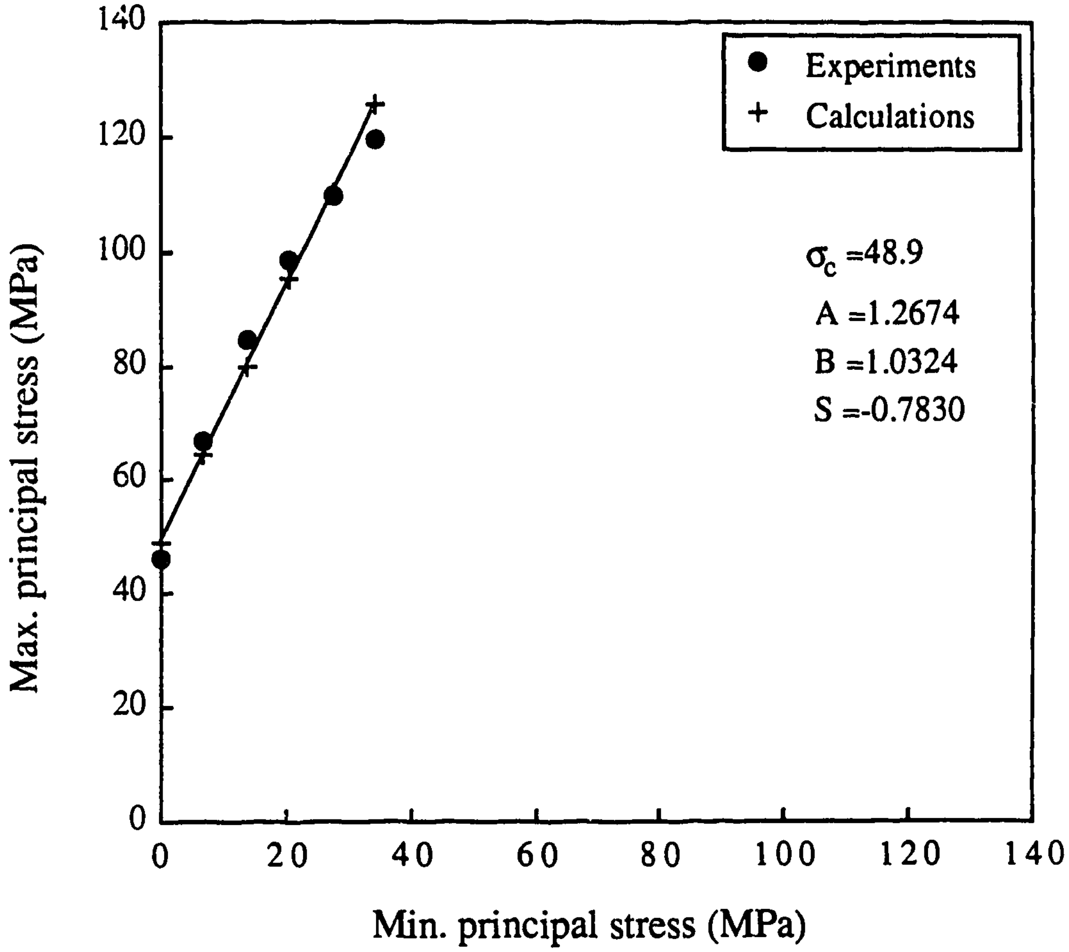

Figure 3.14 Comparison of failure criterion with triaxial test data for Indiana Limestone (Schwartz, 1964)

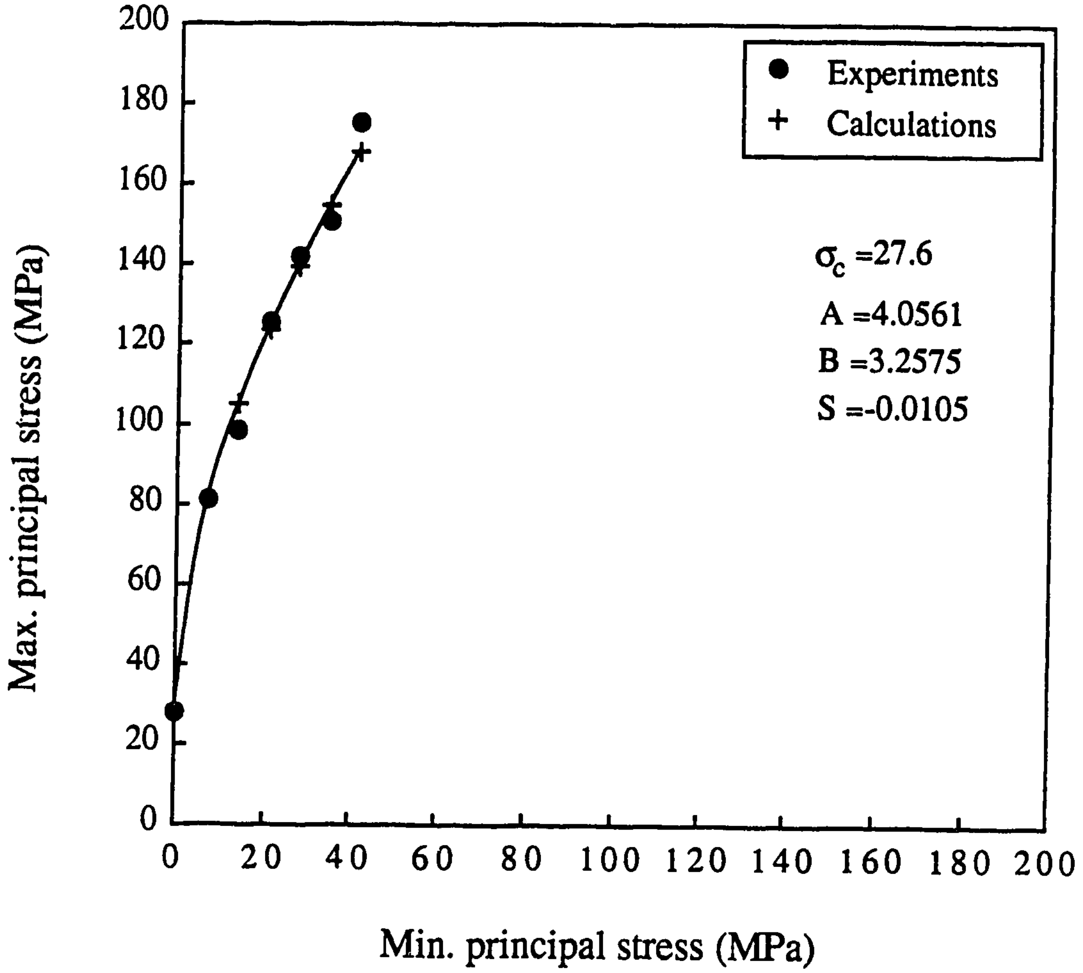

Figure 3.15 Comparison of failure criterion with triaxial test data for Georgia Marble (Schwartz, 1964)

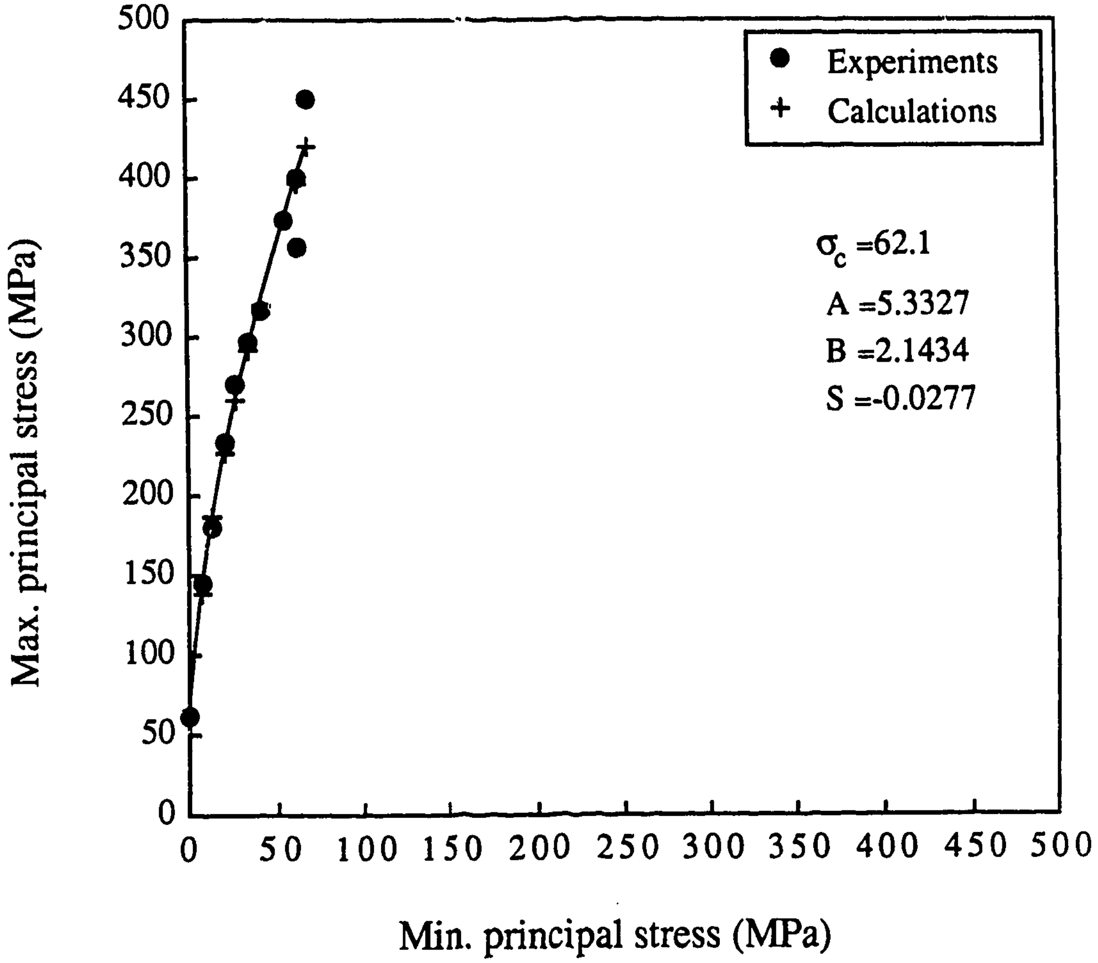

Figure 3.16 Comparison of failure criterion with triaxial test data for Pottsville Sandstone (Schwartz, 1964)

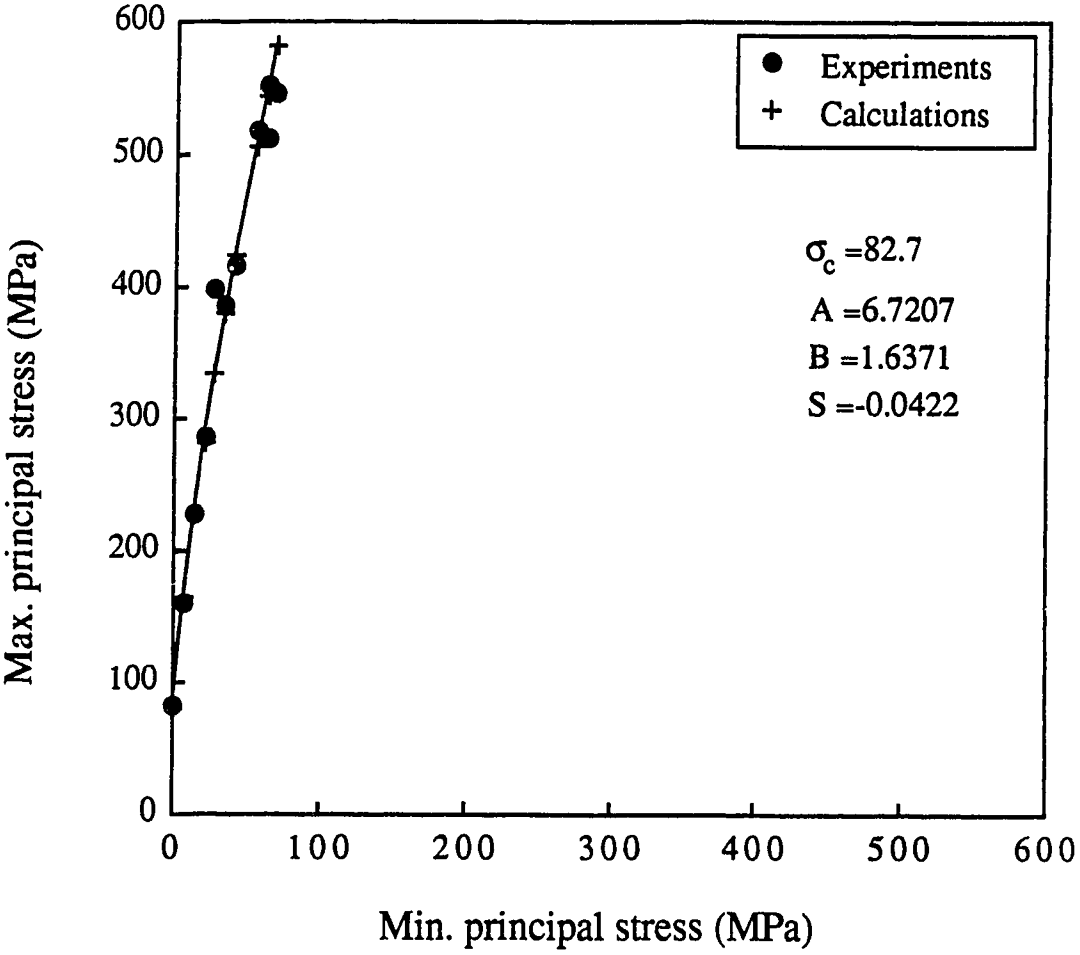

Figure 3.17 Comparison of failure criterion with triaxial test data for Stone Mountain Granite (Schwartz, 1964)

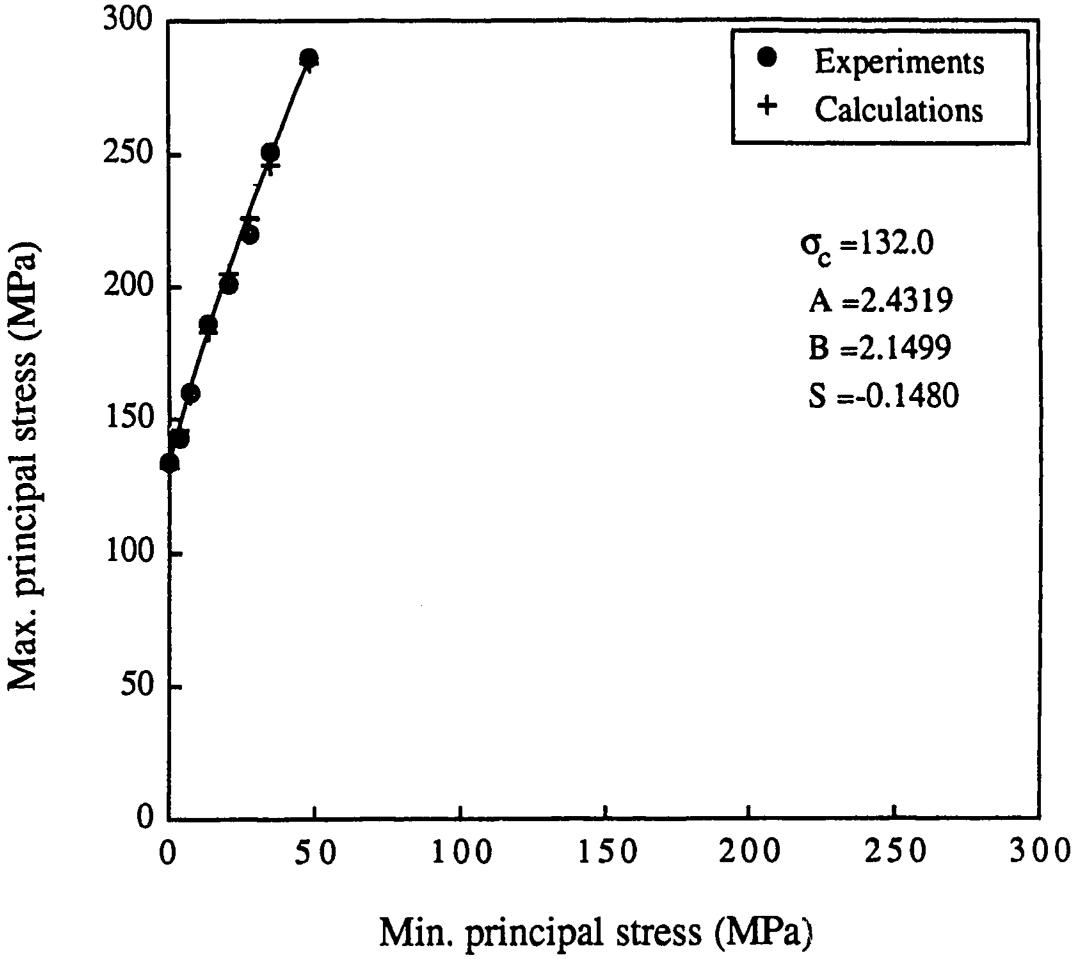

Figure 3.18 Comparison of failure criterion with triaxial test data for Tennessee Marble (Wawersik, 1968)

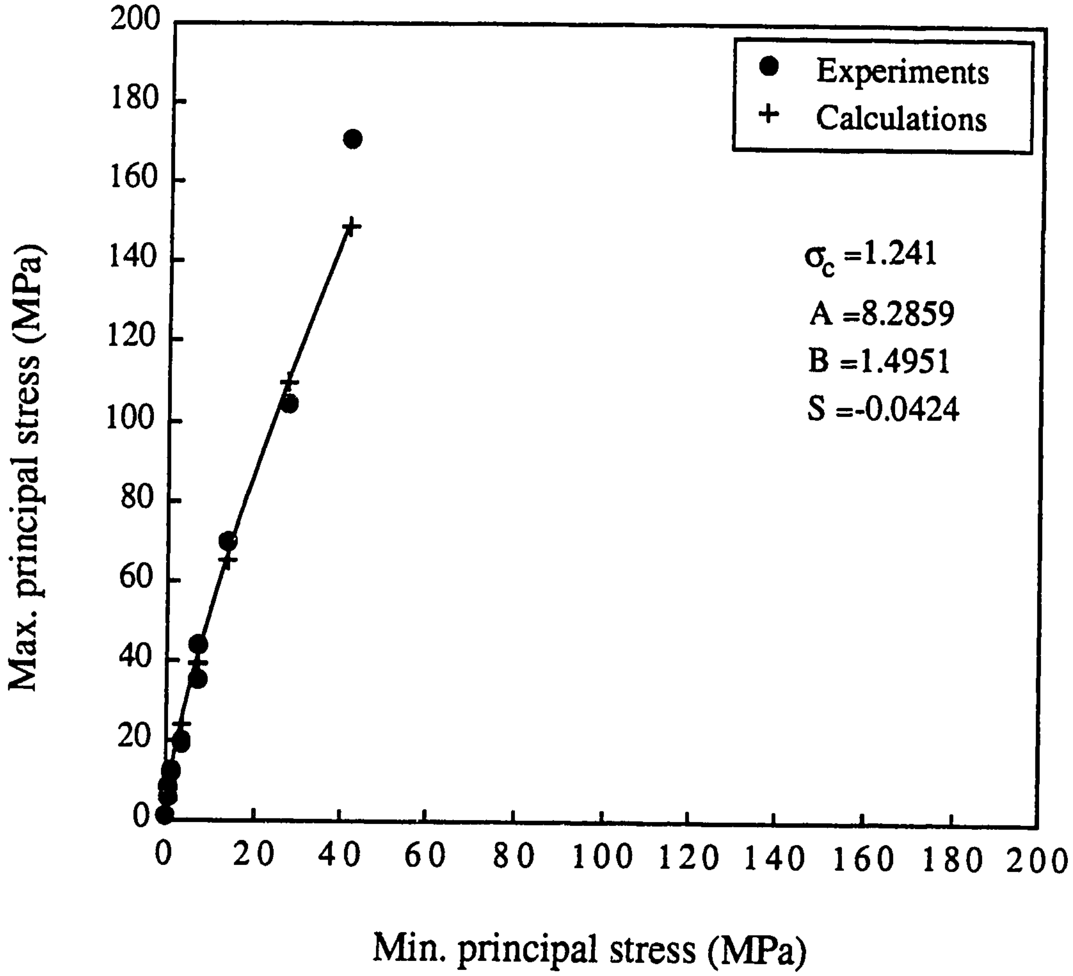

Figure 3.19 Comparison of failure criterion with triaxial test data for Panguna Andesite (Jaeger, 1970)

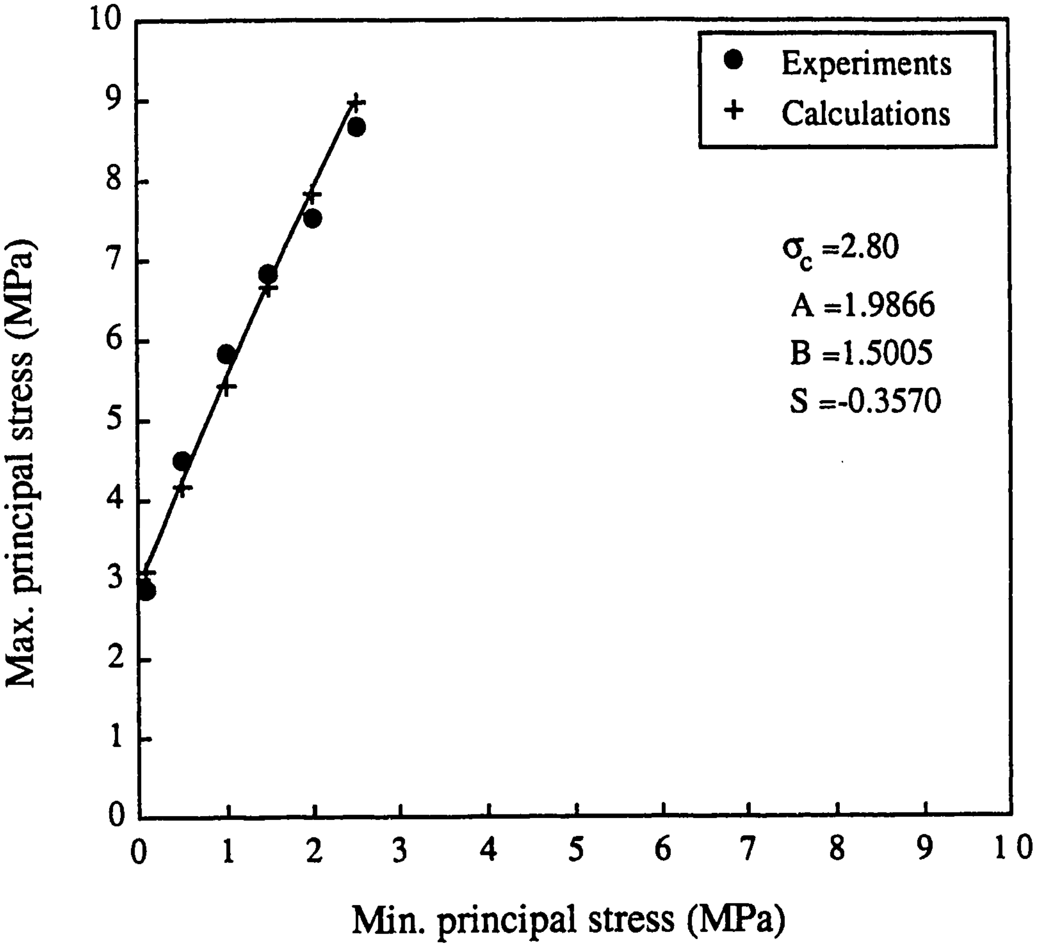

Figure 3.20 Comparison of failure criterion with triaxial test data for Shimajiri Mudstone (Shinjo, 1976)

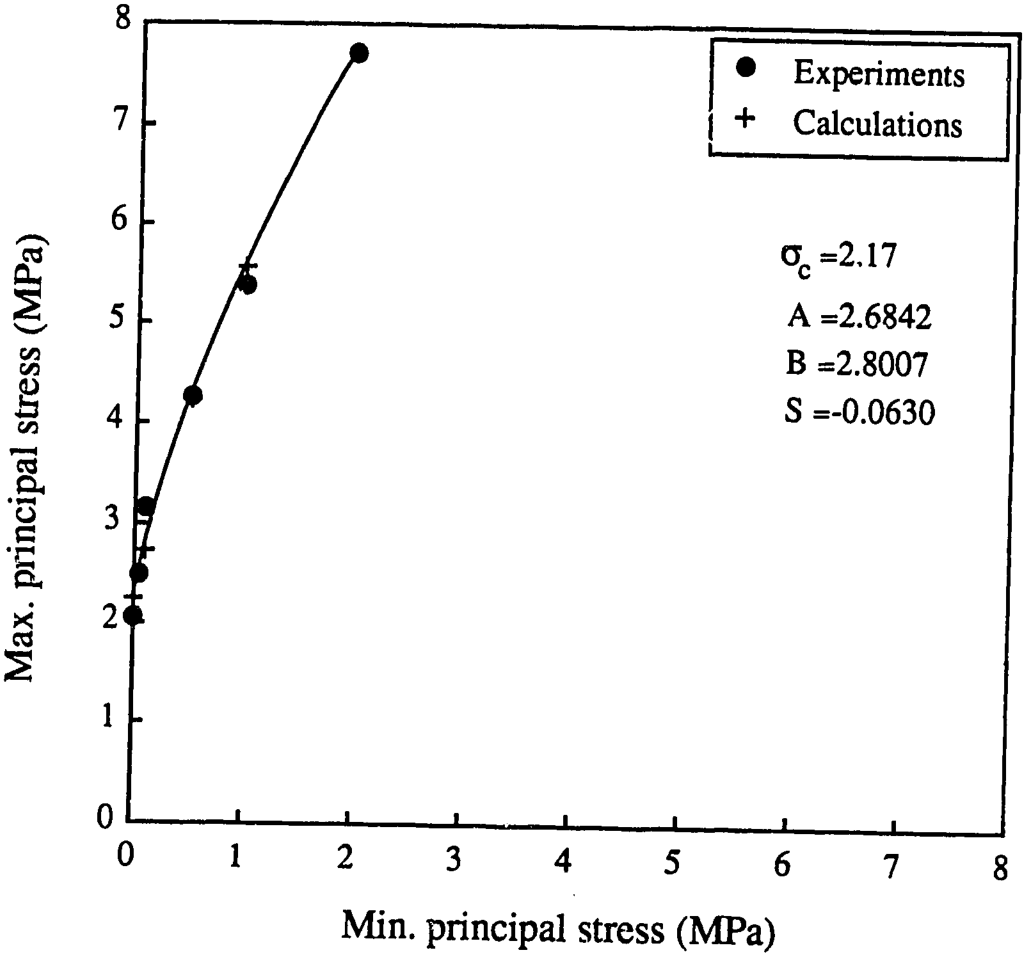

Figure 3.21 Comparison of failure criterion with triaxial test data for Tohoku Mudstone (Watanabe *et al.*, 1988)

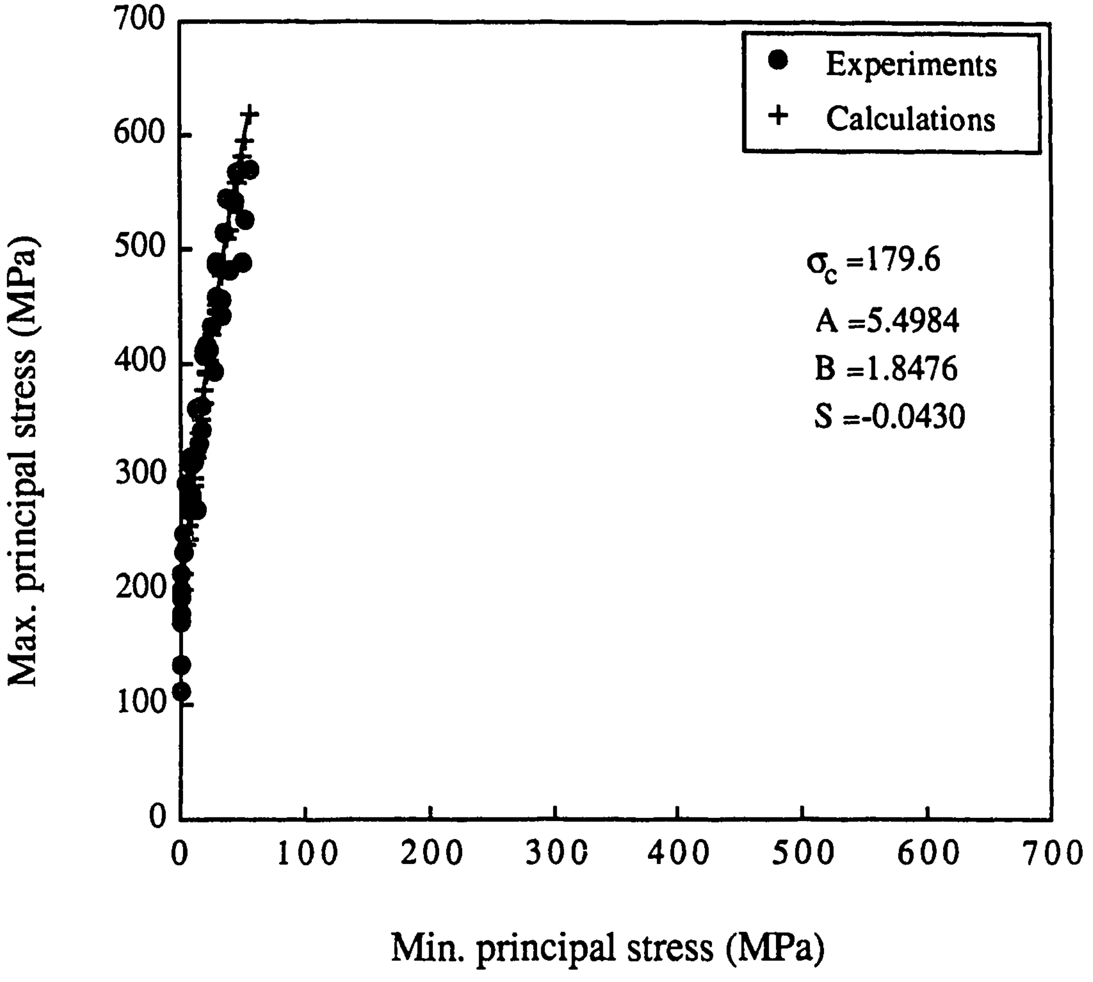

Figure 3.22 Comparison of failure criterion with triaxial test data for Devon Granite (Franklin and Hoek, 1970)

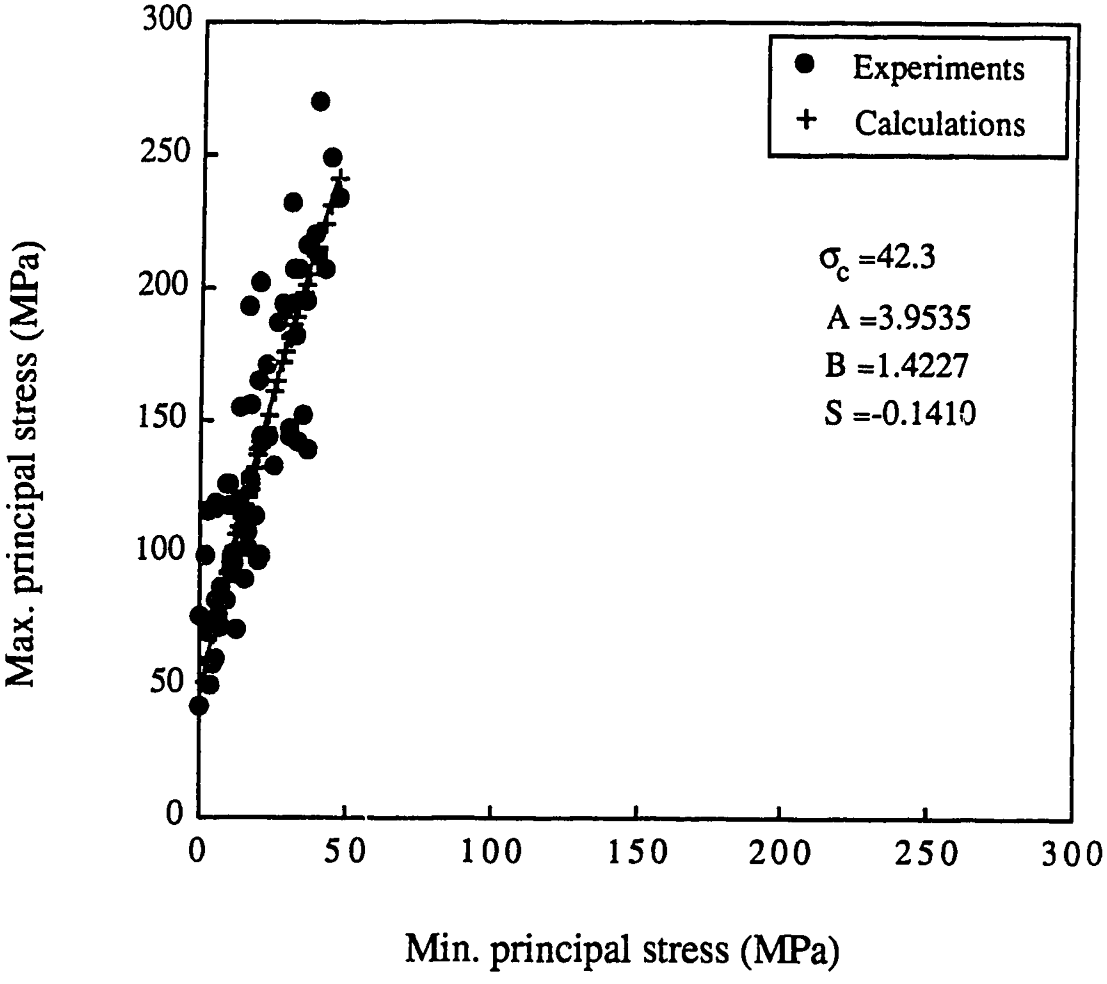

Figure 3.23 Comparison of failure criterion with triaxial test data for Portland Limestone (Franklin and Hoek, 1970)

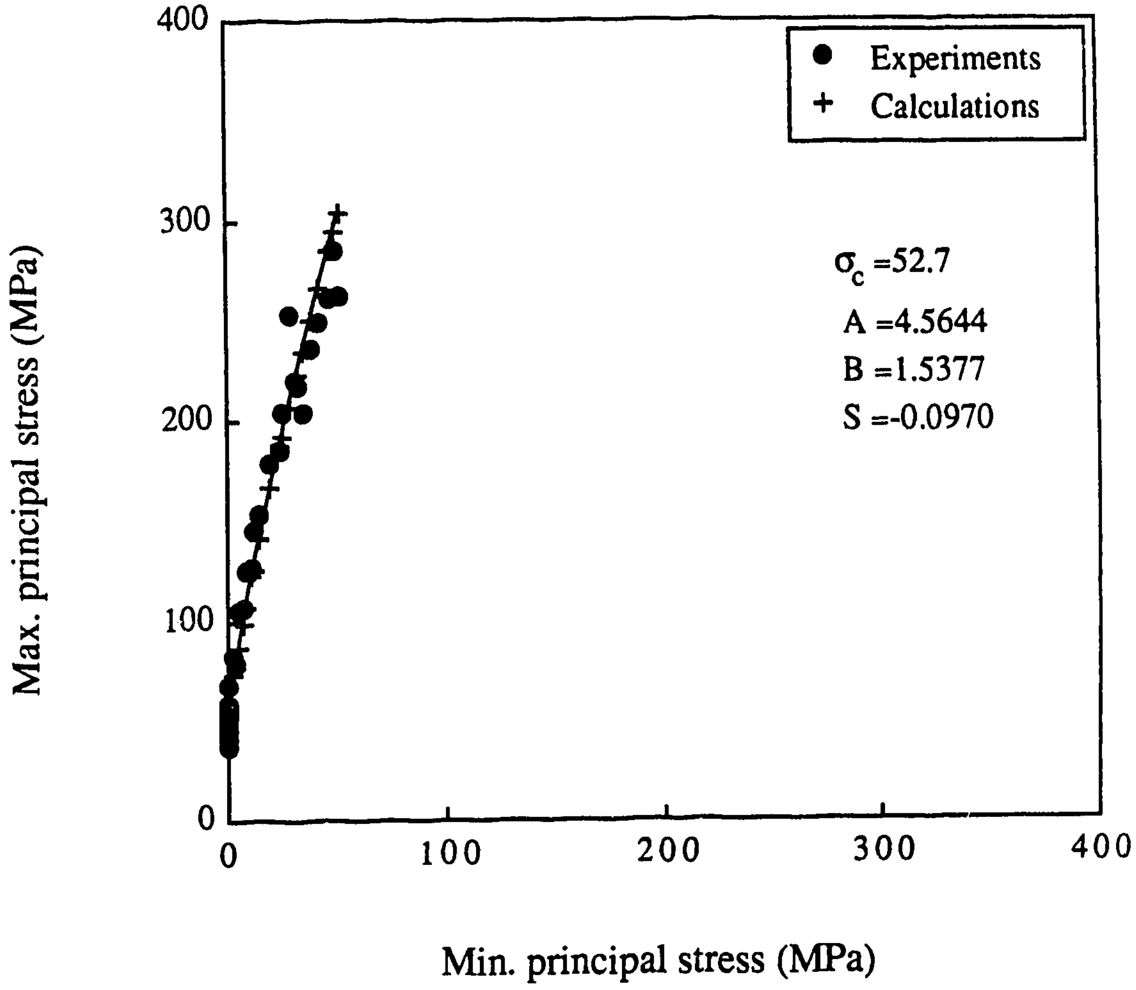

Figure 3.24 Comparison of failure criterion with triaxial test data for Derbyshire Sandstone (Franklin and Hoek, 1970)

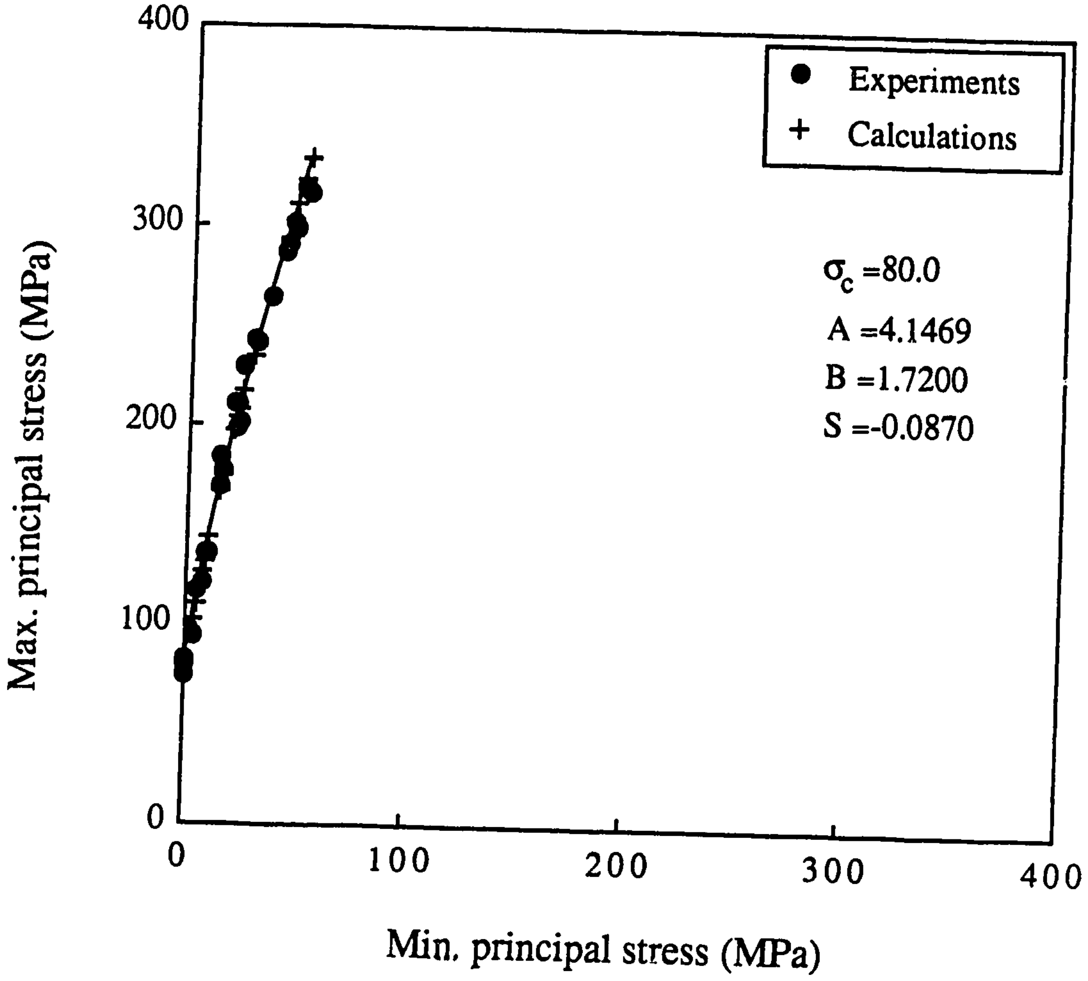

Figure 3.25 Comparison of failure criterion with triaxial test data for Darley Dale Sandstone (Franklin and Hoek, 1970)

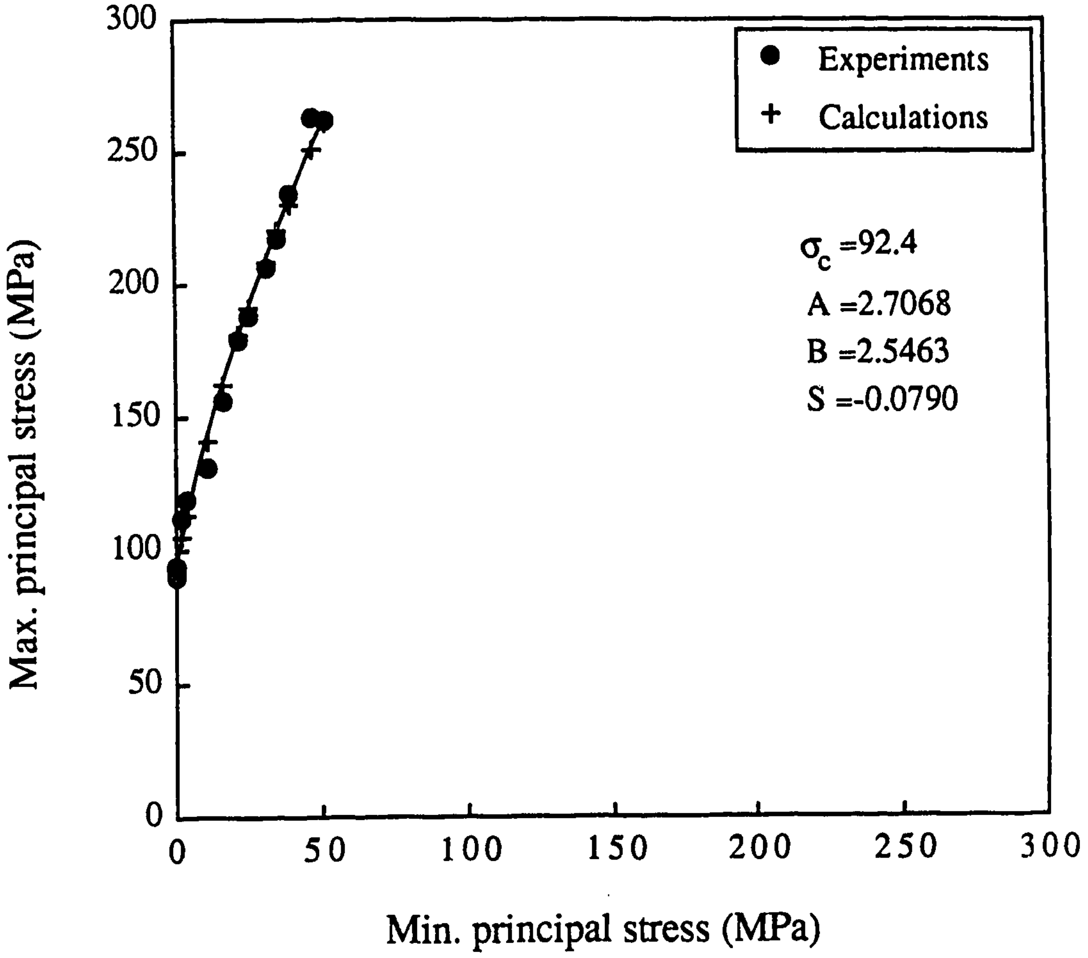

Figure 3.26 Comparison of failure criterion with triaxial test data for Carrara Marble (Franklin and Hoek, 1970)

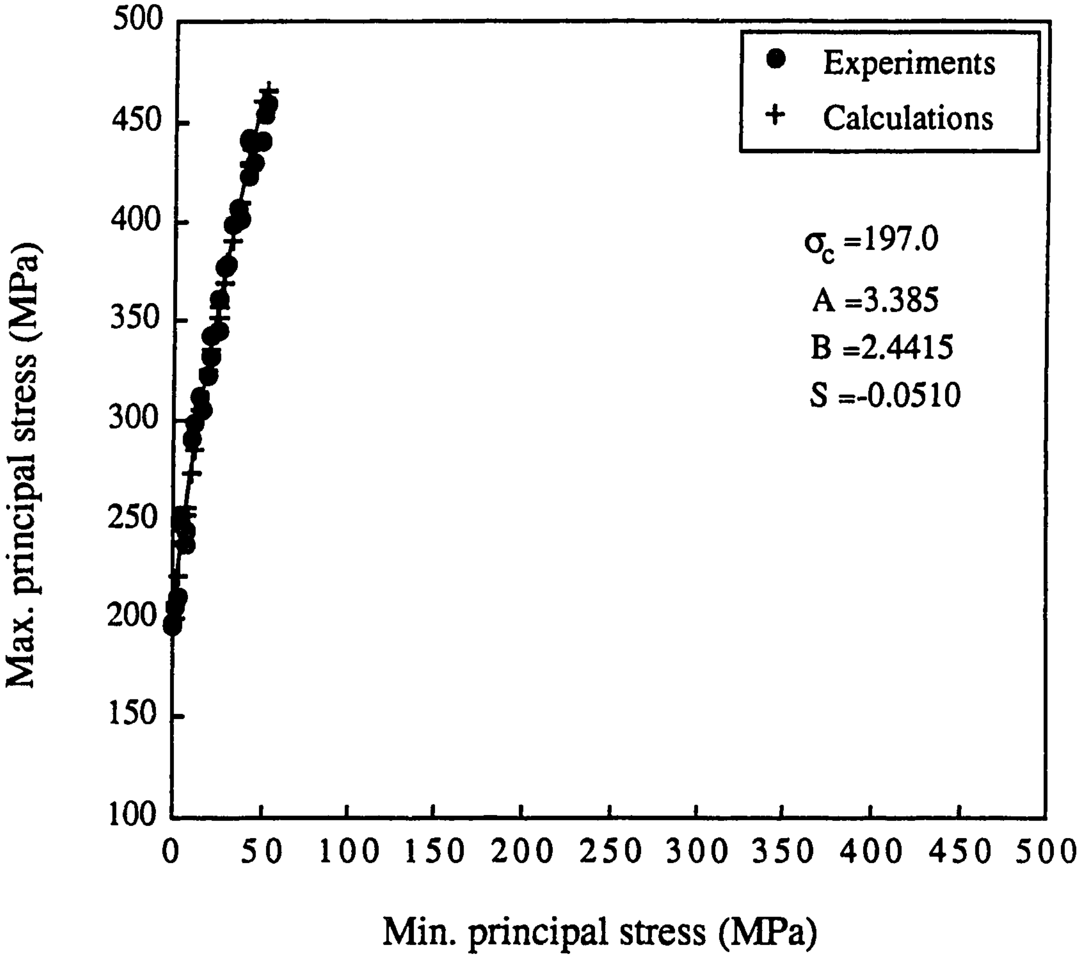

Figure 3.27 Comparison of failure criterion with triaxial test data for Pennant Sandstone (Franklin and Hoek, 1970)

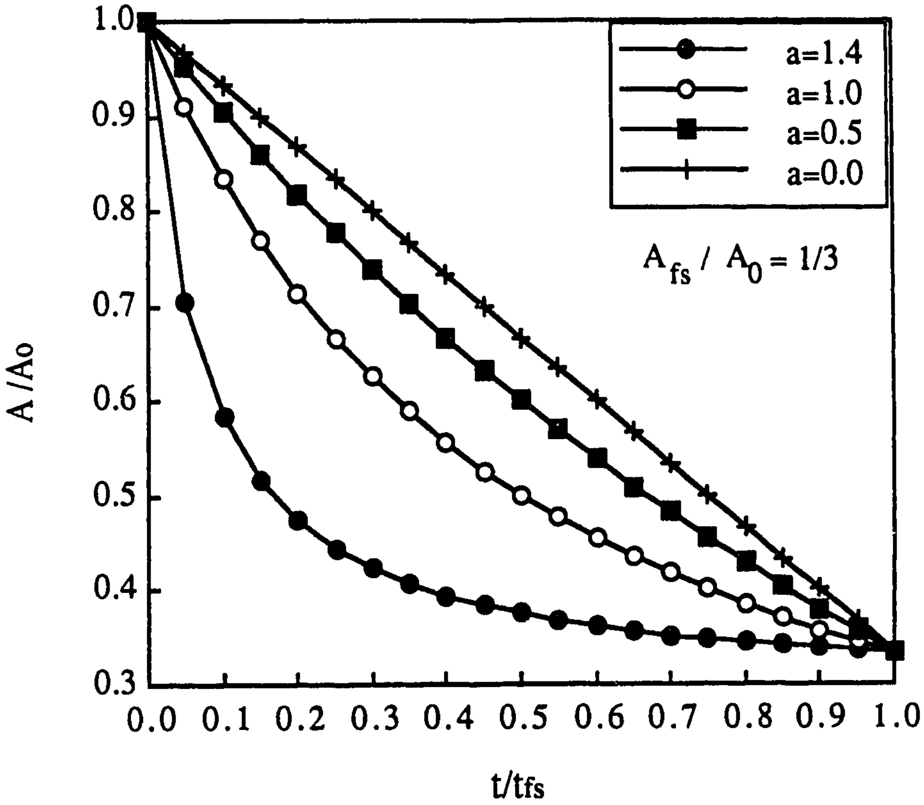

Figure 3.28 Variations of parameter A with time for different values of a

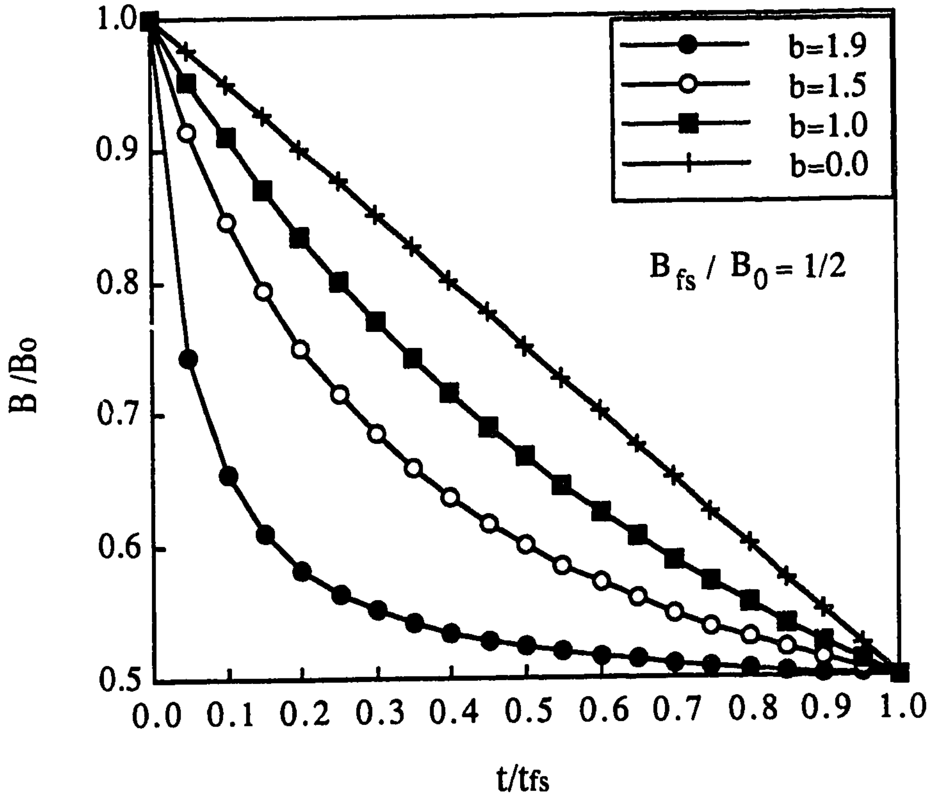

Figure 3.29 Variations of parameter B with time for different values of **b**

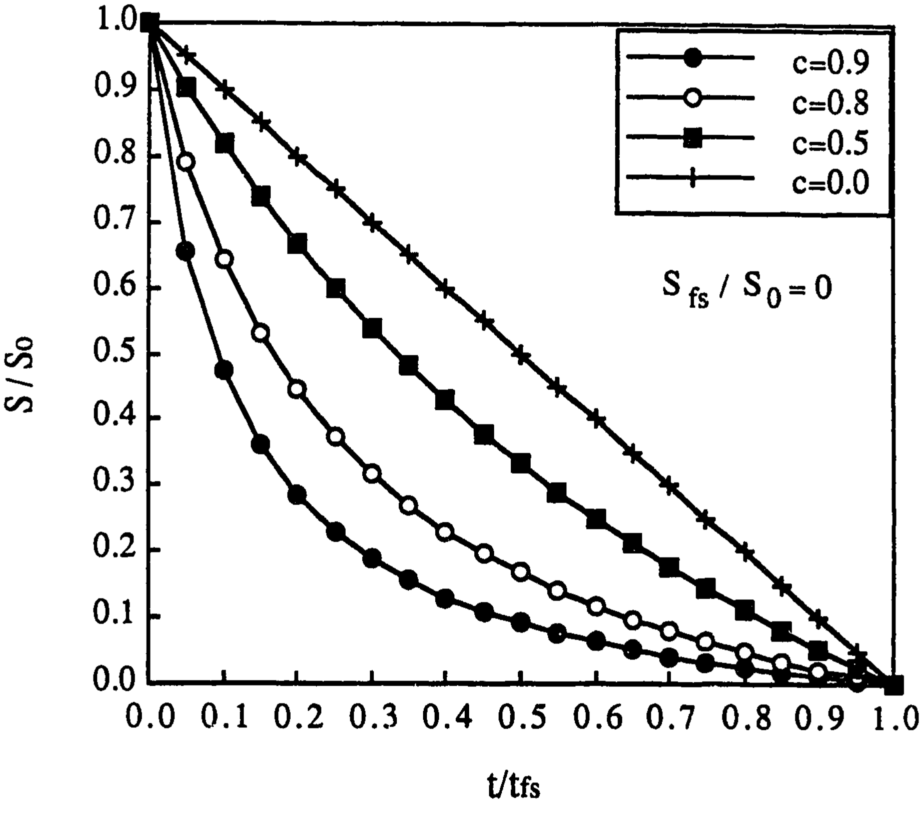

Figure 3.30 Variations of parameter S with time for different values of c

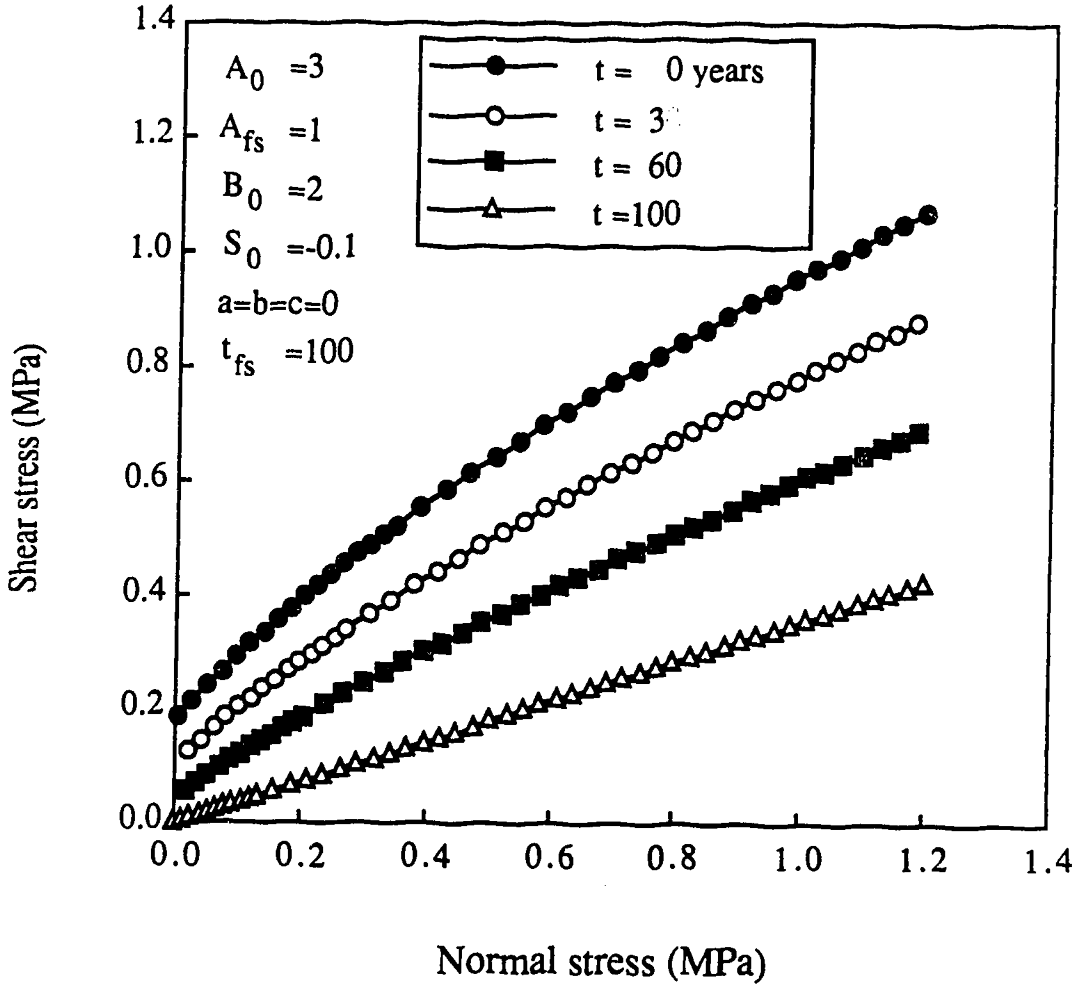

Figure 3.31 Variation in failure envelope during softening

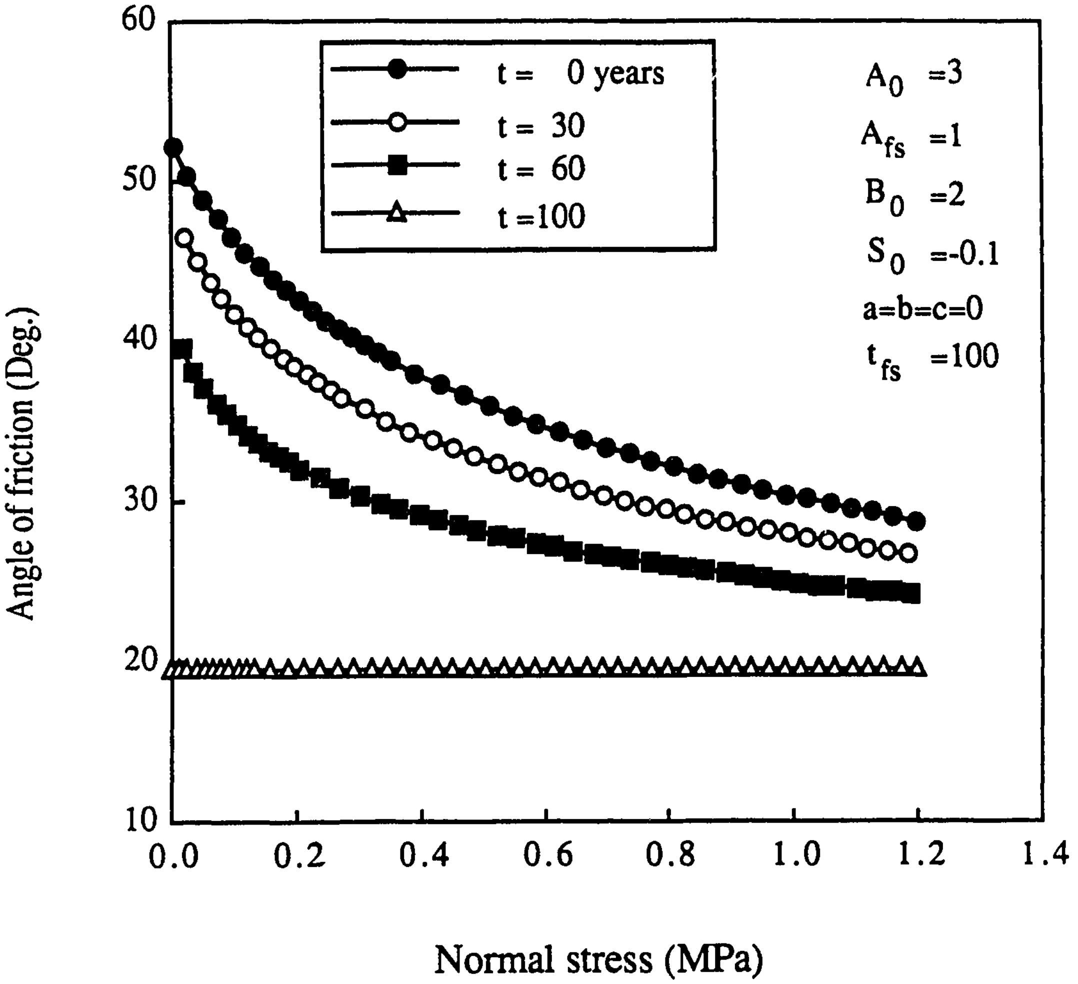

Figure 3.32 Variation of angle of friction during softening

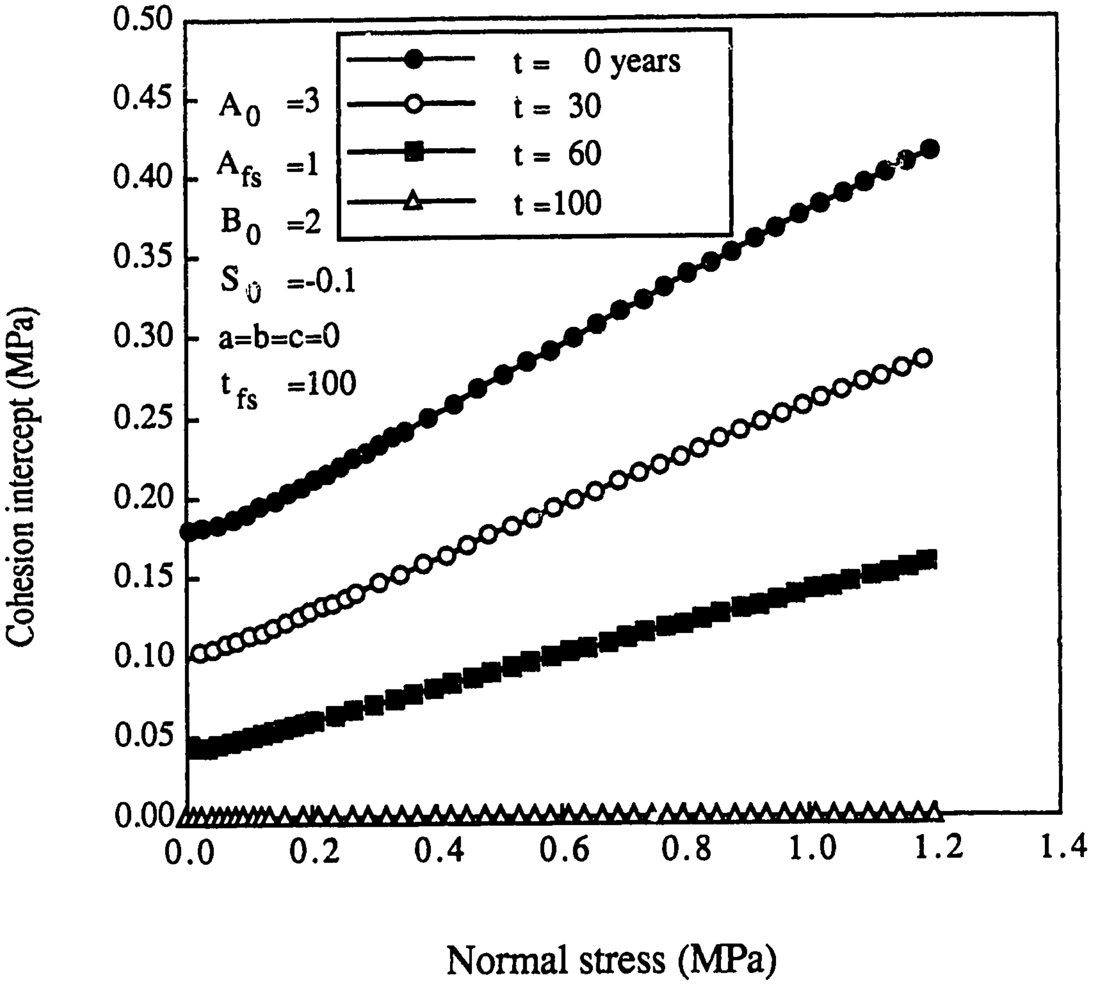

Figure 3.33 Variation of cohesion intercept during softening

4. Finite element analysis

4.1 Introduction

In Chapter 2, softening and its mechanism were discussed in detail. It was identified as a major cause of time-dependent instability of cut slopes and tunnels in fissured, over-consolidated clays and mudstones. The effect of softening is to reduce the strength by reducing dilatancy and it can be represented by a gradual reduction of curvature in a strength envelope at low stress levels. To describe this softening process in a simple but rational manner, a failure criterion was proposed in Chapter 3. Another cause of the time-dependent instability, long-term pore water pressure equalization, was discussed. This also results in an apparent strength reduction of the material through a decrease in effective stress.

A literature review revealed that there has been no finite element method to simulate the softening process rationally, although there are several finite element studies in which a rough approximation is made regarding the reduction of strength. This chapter presents a finite element method to model the above-mentioned softening effects. The effect of long-term excess pore water pressure dissipation is not taken into consideration in this study, but an attempt is made to include steady-state pore water pressure effects in an effective stress analysis.

The finite element formulation follows a conventional elastic-plastic formulation being based upon the principle of virtual work. The failure criterion proposed in Chapter 3 is used as a yield function. The formulation does not impose any restriction upon the type of constitutive law, thus any type of constitutive law can be introduced. Examples are presented in a later section.

4.2 Finite element method

4.2.1 Elastic-plastic constitutive relation

In order to derive an elastic-plastic constitutive equation, the following assumptions are generally made (Zienkiewicz, 1977).

(a) A total strain increment, $d\varepsilon_{ij}$, can be decomposed into the elastic and plastic components, $d\varepsilon^e_{ij}$ and $d\varepsilon^p_{ij}$;

$$d\varepsilon_{ij} = d\varepsilon^e_{ij} + d\varepsilon^p_{ij} \tag{4.1}$$

(b) A stress change, $d\sigma_{ij}$, is due solely to the elastic strain increment and is governed by a generalized Hooke's law:

$$d\sigma_{ij} = D^e_{ijkl} d\varepsilon^e_{kl} \tag{4.2}$$

where D^e_{ijkl} is the elastic constitutive tensor.

(c) A plastic potential function, G, exists and defines a plastic strain increment;

$$d\varepsilon^p_{ij} = \lambda \frac{\partial G}{\partial \sigma_{ij}} \tag{4.3}$$

where λ is a proportionality constant. When a potential function is the same as the yield function, Equation (4.3) is known as an associated flow rule.

The yield function used in this study is time-dependent as described in a later section, and it may be expressed as:

$$F = F\left(\sigma_{ij}, \varepsilon_{ij}^{p}, \kappa, t\right) \tag{4.4}$$

where κ is a hardening (softening) parameter, and t is time. During plastic deformation, the yield criterion must be satisfied (consistency condition), so:

$$dF = \frac{\partial F}{\partial \sigma_{ij}} d\sigma_{ij} + \frac{\partial F}{\partial \varepsilon_{ij}^{p}} d\varepsilon_{ij}^{p} + \frac{\partial F}{\partial \kappa} d\kappa + \frac{\partial F}{\partial t} dt = 0 \tag{4.5}$$

It should be noted that when isotropic hardening (softening) is assumed, the yield function, F, is independent of ε_{ij}^{p} since the shape and origin of the yield surface do not change.

A hardening (softening) parameter, k, controlling the size of the yield surface is expressed as some simple function of plastic strain. An accumulated plastic shear strain, for instance, was used by Simmons (1981) as an indicator of the post-peak softening in a strain softening model. Similarly, an equivalent plastic deviator strain was used by Vermeer and De Borst (1984) and Dounias (1987). A softening model described in Chapter 5 uses this equivalent plastic deviator strain to describe the post-peak softening. Thus, κ can be written as:

$$\kappa = \kappa\left(\bar{\varepsilon}^p\right) \tag{4.6}$$

where $\bar{\varepsilon}^p$ is an effective plastic strain and defined as:

$$\bar{\varepsilon}^p = \int_v d\bar{\varepsilon}^p \, dv \, ;$$

$$d\bar{\varepsilon}^p = \sqrt{\frac{2}{3}\left(d\varepsilon^p_{ij} - \frac{1}{3}\,\delta_{ij}\; d\varepsilon^p_{ll}\right)\left(d\varepsilon^p_{ij} - \frac{1}{3}\,\delta_{ij}\; d\varepsilon^p_{mm}\right)}$$

The flow rule may be modified as follows:

$$d\bar{\varepsilon}^p = \lambda\,\overline{\frac{\partial G}{\partial \sigma}} \tag{4.7}$$

where $\overline{\frac{\partial G}{\partial \sigma}}$ is defined as:

$$\overline{\frac{\partial G}{\partial \sigma}} = \sqrt{\frac{2}{3}\left(\frac{\partial G}{\partial \sigma_{ij}} - \frac{1}{3}\,\delta_{ij}\,\frac{\partial G}{\partial \sigma_{ll}}\right)\left(\frac{\partial G}{\partial \sigma_{ij}} - \frac{1}{3}\,\delta_{ij}\,\frac{\partial G}{\partial \sigma_{mm}}\right)}$$

Under these conditions, and with some algebraic manipulations, one can derive the following elastic-plastic constitutive relation:

$$d\sigma_{ij} = D^{ep}_{ij\alpha\beta}\, d\varepsilon_{\alpha\beta} - d\sigma^{t}_{ij} \tag{4.8}$$

where

$$D^{ep}_{ij\alpha\beta} = D^{e}_{ij\alpha\beta} - \frac{D^{e}_{ijkl}\,\frac{\partial G}{\partial \sigma_{kl}}\,\frac{\partial F}{\partial \sigma_{mn}}\,D^{e}_{mn\alpha\beta}}{-\,\frac{\partial F}{\partial \kappa}\,\frac{\partial \kappa}{\partial \bar{\varepsilon}^p}\,\overline{\frac{\partial G}{\partial \sigma}} + \frac{\partial F}{\partial \sigma_{mn}}\,D^{e}_{mn\alpha\beta}\,\frac{\partial G}{\partial \sigma_{\alpha\beta}}}$$

$$d\sigma_{ij}^{t} = \frac{D_{ijkl}^{e} \frac{\partial G}{\partial \sigma_{kl}} \frac{\partial F}{\partial t} dt}{- \frac{\partial F}{\partial \kappa} \frac{\partial \kappa}{\partial \bar{\varepsilon}^{p}} \frac{\overline{\partial G}}{\partial \sigma} + \frac{\partial F}{\partial \sigma_{mn}} D_{mn\alpha\beta}^{e} \frac{\partial G}{\partial \sigma_{\alpha\beta}}}$$

It is noted that the first term of the denominator in the above equations is related to an isotropic hardening (softening), and that this term is zero for a perfectly plastic model.

Equation (4.8) is rewritten, in the matrix form, as:

$$\{d\sigma\} = [D]^{ep} \{d\varepsilon\} - \{d\sigma^{t}\} \tag{4.9}$$

where

$$[D]^{ep} = [D]^{e} - \frac{[D]^{e} \left\{\frac{\partial G}{\partial \sigma}\right\} \left\{\frac{\partial F}{\partial \sigma}\right\}^{T} [D]^{e}}{A + \left\{\frac{\partial F}{\partial \sigma}\right\}^{T} [D]^{e} \left\{\frac{\partial G}{\partial \sigma}\right\}}$$

$$\{d\sigma^{t}\} = \frac{[D]^{e} \left\{\frac{\partial G}{\partial \sigma}\right\} \frac{\partial F}{\partial t} dt}{A + \left\{\frac{\partial F}{\partial \sigma}\right\}^{T} [D]^{e} \left\{\frac{\partial G}{\partial \sigma}\right\}}$$

$$A = - \frac{\partial F}{\partial \kappa} \frac{\partial \kappa}{\partial \bar{\varepsilon}^{p}} \frac{\overline{\partial G}}{\partial \sigma}$$

4.2.2 Finite element formulation

The basic incremental equilibrium equation in finite element displacement discretization is derived based on the principle of virtual displacement and is expressed, in a global system, as (Bathe, 1982):

$$\sum_{m=1}^{nel} \int_{v_m} [B]^T \{d\sigma\}\, dv_m = \sum_{m=1}^{nel} \int_{v_m} [N]^T \{d\bar{f}\}\, dv_m + \sum_{m=1}^{nel} \int_{s_m} [N]^T \{d\bar{t}\}\, ds_m \tag{4.10}$$

where nel is the total number of elements, $[B]$ is the strain-displacement transformation matrix, $\{d\sigma\}$ is the total stress increment vector, $[N]$ is the displacement interpolation matrix, $\{d\bar{f}\}$ is the body force vector and $\{d\bar{t}\}$ is the surface traction vector. It should be noted that all traction and body forces above are in terms of total stress and that stress vectors $\{d\sigma\}$ are also in terms of total stress. Since the behaviour of soils and rocks is controlled by effective stress, it would be better to rewrite the above equation in terms of effective stress.

An effective stress is written, in the incremental form, as:

$$\{d\sigma'\} = \{d\sigma\} - \{d\,p\} \tag{4.11}$$

where $\{d\sigma'\}$ is the effective stress increment vector, $\{d\sigma\}$ is the total stress increment vector and $\{d\,p\}$ is the pore water pressure increment vector.

From Equations (4.9), (4.10) and (4.11), the equilibrium equation becomes

$$[K]\{dU\} = \{dR\} + dt\,\{dR^t\} - \{dR^p\} \tag{4.12}$$

where

$$[K] = \sum_{m=1}^{nel} \int_{v_m} [B]^T [D']^{ep} [B]\, dv_m$$

$$\{dR^t\} = \sum_{m=1}^{nel} \int_{v_m} \frac{[B]^T [D']^e \left\{\frac{\partial G}{\partial \sigma}\right\} \frac{\partial F}{\partial t}}{A + \left\{\frac{\partial F}{\partial \sigma}\right\}^T [D']^e \left\{\frac{\partial G}{\partial \sigma}\right\}}\, dv_m$$

$$\{dR^p\} = \sum_{m=1}^{nel} \int_{v_m} [B]^T \{dp\}\, dv_m$$

$$\{dR\} = \sum_{m=1}^{nel} \int_{v_m} [N]^T \{d\bar{f}\}\, dv_m + \sum_{m=1}^{nel} \int_{s_m} [N]^T \{d\bar{t}\}\, ds_m$$

$\{dU\}$ = displacement increment vector

dt = time increment

It should be noted that the constitutive relations in the above equation are now in terms of effective stress.

In this study, the pore water pressure is assumed to be known. It can be obtained independently from field measurements or a seepage analysis. In this way, an effective stress analysis can be carried out easily and inexpensively. Desai and Christian (1977) discussed this technique in some detail. The method has been used by Kawamoto and Tanaka (1988) who conducted a seepage analysis for pore water pressure calculations and by Alencar (1988) who incorporated field-measured pore water pressures.

4.2.3 Computational procedure

The solution scheme starts from a known initial condition at time t=0. For each time step, the yield condition is updated and an elastic-plastic analysis is carried out. At the beginning of each time step, load vectors are computed which result from external load increments and body force increments. If existing stresses in an element violate the new yield condition, load vectors due to this overshooting are also evaluated based upon the stresses projected to the new yield surface (the second term in the right hand side of Equation (4.12)). During subsequent equilibrium iterations, it is checked whether or not the total equilibrium condition, not the incremental equilibrium condition, is satisfied. When convergence cannot be reached within a pre-specified number of iterations for a given time increment, the time increment is subdivided and the solution scheme is repeated with the smaller time increment. Otherwise, a new time step is started. The solution scheme will continue until the total time reaches the time to fully-softened conditions. However, if a pre-specified minimum time increment is reached or convergence cannot be achieved during computation, the solution scheme will be terminated.

It is seen that the role of the time increment is similar to that of load increment in an elastic-plastic analysis.

4.3 Yield function

4.3.1 Generalization of yield function

A failure criterion was proposed in Chapter 3 to describe the effect of softening upon shear strength. This failure criterion is used as a yield function here and is rewritten as:

$$F = \sigma_1 - \sigma_3 - A\,\sigma_c \left(\frac{\sigma_3}{\sigma_c} - S \right)^{\frac{1}{B}} = 0 \qquad (4.13)$$

where σ_1 is the maximum principal stress, σ_3 is the minimum principal stress, σ_c is the initial uniaxial compression strength, and A, B and S are strength parameters. These stress and strength parameters are expressed in terms of either total stress or effective stress depending upon the situation upon which the yield function is based.

From the viewpoint of finite element programming, it is convenient to generalize a yield function in terms of stress invariants, I_1, J_2 and J_3.

Following the technique used by Nayak and Zienkiewicz (1972), one can derive a generalized form of the above yield function as:

$$F = \left(\frac{2\sqrt{J_2}\cos\theta}{A\,\sigma_c} \right)^B + \frac{\sqrt{J_2}}{\sigma_c}\left(\frac{\sin\theta}{\sqrt{3}} + \cos\theta \right) - \frac{I_1}{3\sigma_c} + S = 0 \tag{4.14}$$

where

$$I_1 = \sigma_{ii}$$

$$J_2 = \frac{1}{2}\, s_{ij}\, s_{ij}$$

$$J_3 = \frac{1}{3}\, s_{ij}\, s_{jk}\, s_{ki}$$

$$\theta = \frac{1}{3}\sin^{-1}\left(-\frac{3\sqrt{3}}{2}\,\frac{J_3}{J_2\sqrt{J_2}} \right) \;;\; -\frac{\pi}{6} \leq \theta \leq \frac{\pi}{6}$$

$$s_{ij} = \sigma_{ij} - \frac{1}{3}\,\delta_{ij}\,\sigma_{ll}$$

$\delta_{ij} =$ Kronecker delta

The corresponding gradient vector is expressed as:

$$\frac{\partial F}{\partial \sigma_{ij}} = C_1 \frac{\partial I_1}{\partial \sigma_{ij}} + C_2 \frac{\partial \sqrt{J_2}}{\partial \sigma_{ij}} + C_3 \frac{J_3}{\partial \sigma_{ij}} \tag{4.15}$$

where

$$C_1 = -\frac{1}{3\,\sigma_c}$$

$$\begin{aligned} C_2 = &\left\{ 2\cos\theta\left(\frac{A}{B}\right) M + \left(\frac{\sin\theta}{\sqrt{3}} + \cos\theta \right) \right\} \frac{1}{\sigma_c} \\ &+ \left\{ 2\sin\theta\left(\frac{A}{B}\right) M - \left(\frac{\cos\theta}{\sqrt{3}} - \sin\theta \right) \right\} \frac{\tan 3\theta}{\sigma_c} \end{aligned}$$

$$C_3 = \frac{\sqrt{3}}{2\, J_2\, \sigma_c \cos 3\theta} \left\{ 2 \sin\theta \left(\frac{A}{B} \right) M - \left(\frac{\cos\theta}{\sqrt{3}} - \sin\theta \right) \right\}$$

$$M = \left(\frac{2 \sqrt{J_2} \cos\theta}{A\, \sigma_c} \right)^{B-1}$$

Table 4.1 summarizes various yield functions used in the finite element analysis and the corresponding gradient vectors are given in Table 4.2. Figure 4.1 shows a geometrical representation of the proposed yield criterion. The yield surface is defined by an irregular pyramid with curved faces in principal stress space, and it is an irregular hexagon in the octahedral plane. Figure 4.2 shows the variation of a yield surface during the softening process. The yield surface contracts from the initial condition to the fully softened condition. The contraction of the yield surface, due to strength reduction, is assumed to follow the inverse-hyperbolic function of time as discussed in Chapter 3.

4.3.2 Singular points treatment

A yield surface defined by the proposed yield function has corners located at $\theta = \pm 30°$ where the gradient vectors, $dF/d\sigma_{ij}$, cannot be defined uniquely. A numerical difficulty arises when θ approaches ± 30°, as can be seen from Table 4.2. Both C2 and C3 become indeterminate for these values of θ. To overcome this difficulty, a 'round-off' technique (Owen and Hinton, 1980) is used. When a stress state enters within the pre-specified "vicinity" of a corner, the flow vector is evaluated from expressions derived directly from the yield function for the explicit value of θ of + 30° or - 30°. In the actual computation, this approximation is applied when θ meets the condition, $|\theta| \geq 29.5°$.

4.4 Computer program

The time-dependent elastic-plastic finite element formulation presented in this chapter was programmed using the FORTRAN 66 language and implemented into a geotechnical engineering-oriented general purpose finite element program, SAGE (Stress Analysis in Geotechnical Engineering). This program was initially developed by Chan (1986) and has been modified at the Geotechnical Division of the Department of Civil Engineering of the University of Alberta.

The implemented constitutive relations are an elastic, perfectly-plastic type and an elastic-plastic, strain-softening type. Both associated and non-associated flow rules are taken into consideration.

4.5 Examples

For the purpose of demonstrating the finite element analysis for softening proposed in this chapter, three examples are presented here. The first example deals with the ground behaviour under a flexible strip footing. Considering the discussion on softening given in Chapter 2, this example may not be suitable since no unloading stress path is imposed. Nevertheless this problem is chosen as an example because it is a classic problem in geotechnical engineering. The second and third examples are more realistic, dealing with a cut slope and a tunnel.

4.5.1 Elastic perfectly plastic model

Due to its simplicity, an elastic, perfectly-plastic constitutive relation is adapted in all subsequent examples. Both associated and non-associated flow rules are employed, and in the non-associated flow rule case the plastic volumetric strain during yielding is set equal to zero.

Figure 4.3 shows the variation of stress, strain and strength during softening. The solid line and curve refer to the case of a non-associated flow rule, and the broken ones refer to the case of an associated flow rule. Curve A indicates an initial strength envelope for a given confining pressure and the corresponding deviator stress, axial strain and volumetric strain relations are depicted by Curves A' and A", respectively. Softening progresses with time. After a certain time has elapsed, say, Δt, the strength envelope is lowered to Curve B, and the stress and strain relations are changed to those given by Curve B' and Curve B". In this way, the strength envelope and stress-strain relations are modified as time goes by. In the end, the fully softened strength condition (Curves D, D' and D") is reached. The time required to reach that condition is assumed to be 100 years in all subsequent examples.

4.5.2 Strip footing analysis

This example considers a plane-strain uniformly loaded flexible strip footing on a fissured, over-consolidated clay. The finite element mesh for this analysis is shown in Figure 4.4 together with the geometry and boundary conditions. The ground is discretized by nine eight-node quadratic isoparametric elements with a total of forty nodes. The material properties are given in Table 4.3. The reduction-rate parameters of shear strength, a, b and c, are 1.0, 1.5 and 0.5, respectively.

The analysis starts with generation of initial stresses in the ground. This is done simply by the application of a gravity force. Next, a constant pressure of 0.1 MPa is applied uniformly to the ground surface as shown in Figure 4.4. Then, the softening process starts from t=0.

Figure 4.5 shows the relations between elapsed time and displacement at the center line, computed with both associated and non-associated flow rules. The displacement increases gradually at the beginning, and as the ground approaches its collapse the displacement increases rapidly. It can seen that little difference in the time to collapse is predicted using these two flow rules. This suggests the shear strength at collapse would be almost identical in both cases. Figure 4.6 confirms this point, showing the strength envelopes for these two cases at their final time increments. On the other hand, significant differences are noticed in the computed displacements using these two rules: the non-associated flow rule produces greater displacements at a given time.

The developments of plastic zones are shown in Figure 4.7 for the associated flow rule and in Figure 4.8 for the non-associated flow rule. The propagation of plastic zones is very similar in both these cases. The plastic zone starts below the footing and extends, in the shape of a bulb, vertically and laterally.

4.5.3 Cut slope analysis

The second example deals with a cut slope behaviour in a fissured, over-consolidated clay. Suppose that a cutting of a depth of 8 m is made, with a 45° slope. The excavation is assumed to be done instantaneously, thus softening does not begin during this time. A plane-strain condition is assumed. The finite element mesh for this analysis is shown in Figure 4.9 together with the geometry and boundary conditions. Three hundred and sixty four-node isoparametric elements are used in this discretization, with three hundred and seventy-nine nodes. The same material properties are used as in the previous example (Table 4.3). The reduction rate parameters of strength are all zero.

As a first step of the analysis, a gravity force is imposed to the ground. Then, the excavation simulation is performed, step by step, by removing the pre-specified elements. The softening process starts after excavation.

Figure 4.10 shows the relations between elapsed time and vertical displacement at the crest of the cut slope. As in the previous example, both associated and non-associated flow rules are considered. The corresponding horizontal displacement variations with time are shown in Figure 4.11. These results indicate that the cut slope deforms gradually as time goes by, but that as the slope approaches its collapse the deformation rate becomes significant. Very little difference is observed in the calculated time to collapse using the associated and non-associated flow rules. The strength envelopes just before the collapse of the slope are shown in Figure 4.12. The final strengths for these two cases are seen as almost identical. Regarding the amount of displacement, the non-associated flow rule develops greater displacements at a given time.

The propagation of plastic zones with time is shown in Figure 4.13 for the associated flow rule and in Figure 4.14 for the non-associated flow rule. It is seen that the plastic zone initiates from the surface of the slope and extends inward. No significant differences are observed between the two figures.

The analysis was also carried out with a different reduction rate of strength. The reduction-rate parameters of strength, a,b and c, used are 1.3, 2.0 and 0.9, respectively. Figures 4.15 and 4.16 show the resulting displacement-time curves. The corresponding spread of plastic zones is given in Figures 4.17 and 4.18. It is noticed that the shape of the displacement-time curves is very similar to the previous ones, but that the time to collapse is much less since the reduction rate is higher in this case. Regarding the spread of plastic zones, the total plastic zone seems not to be affected by the reduction rate of strength, but the propagation rate of the plastic zone is much higher in this case.

The displacement-time relations presented in this section (Figures 4.10, 4.11, 4.15 and 4.16) might be interpreted as creep curves since the slope was under a constant load - gravity force. There is a trend to analyze time-dependent problems in slopes and tunnels from the viewpoint of creep, since a creep analysis can easily account for time-dependency. Considering the fact that the displacement-time relations presented in this section are the results not of creep but of softening, the importance of a proper understanding of the mechanism causing such time-dependent instability should be emphasized.

4.5.4 Tunnel analysis

The final example deals with an unlined tunnel. Suppose that an unlined circular opening of 4 m diameter is excavated at a depth of 32 m in a mudstone bedrock. The tunnelling work is assumed to be done simultaneously, so that softening does not take place during this time. A plane-strain condition is assumed.

The ground is discretized by seventy-eight eight-node isoparametric elements with two hundred and seventy-three nodes (Figure 4.19). The material properties of the bedrock are given in Table 4.4. The reduction-rate parameters of strength, a, b and c, are 1.0, 1.5 and 0.5, respectively. After the application of a gravity force, the excavation is simulated through removals of core elements. Then, softening of the bedrock material starts at time t=0.

Figure 4.20 shows the tunnel wall convergence-time relations computed at the springline. It is seen that the tunnel convergence increases gradually and that the increase becomes rapid as the tunnel approaches its collapse. The propagation of plastic zones is shown in Figure 4.21. Yielding initiates at the springline and propagates obliquely upward and downward creating so-called 'ears'. In this example, a lined tunnel was not considered, but it is expected that the variation with time of rock pressure exerted upon the lining can be traced in the same way.

4.6 Summary

This chapter presented a finite element method for analyzing time-dependent problems due to softening. The finite element formulation follows the principle of virtual work and imposes no restriction on the constitutive relation of a material used in the analysis. A time-dependent yield function is introduced to model the softening process and its generalized form is derived in terms of stress invariants. The computational procedure is very similar to a conventional elastic-plastic analysis.

Three examples are presented for demonstration purposes, illustrating that time-dependent instability can be traced with this finite element method. Further, the importance of a proper understanding of the dominant mechanism of a time-dependent problem is noted. An elastic, perfectly-plastic constitutive relation has been considered due to its simplicity. The next chapter introduces a strain softening model for more realistic analysis.

Table 4.1 Various yield functions

Name	Yield function
Tresca	$F = 2\sqrt{J_2}\cos\theta - Y = 0$
Von-Mises	$F = \sqrt{3}\,\sqrt{J_2} - Y = 0$
Mohr-Coulomb	$F = \frac{I_1}{3}\sin\phi + \sqrt{J_2}\cos\theta - \frac{\sqrt{J_2}}{\sqrt{3}}\sin\phi\sin\theta - c\cos\phi = 0$
Drucker-Prager	$F = \alpha I_1 + \sqrt{J_2} - \kappa = 0$
This study	$F = \left(\frac{2\sqrt{J_2}\cos\theta}{A\sigma_c}\right)^B + \frac{\sqrt{J_2}}{\sigma_c}\left(\frac{\sin\theta}{\sqrt{3}} + \cos\theta\right) - \frac{I_1}{3\sigma_c} + S = 0$

Table 4.2 Gradient vectors for various yield functions

Yield function	C_1	C_2	C_3
Tresca	0	$2\cos\theta\,(1+\tan\theta\tan 3\theta)$	$\dfrac{\sqrt{3}\sin\theta}{J_2\cos 3\theta}$
Von-Mises	0	$\sqrt{3}$	0
Mohr-Coulomb	$\frac{1}{3}\sin\phi$	$\cos\theta\left\{1+\tan\theta\tan 3\theta+\dfrac{\sin\phi\,(\tan 3\theta-\tan\theta)}{\sqrt{3}}\right\}$	$\dfrac{\sqrt{3}\sin\theta+\sin\phi\cos\theta}{2J_2\cos 3\theta}$
Drucker-Prager	α	1.0	0
This study	$-\dfrac{1}{3\sigma_c}$	$\dfrac{1}{\sigma_c}\left\{2\cos\theta\left(\dfrac{B}{A}\right)M+\left(\dfrac{\sin\theta}{\sqrt{3}}+\cos\theta\right)\right\}$ $+\dfrac{\tan 3\theta}{\sigma_c}\left\{2\sin\theta\left(\dfrac{B}{A}\right)M-\left(\dfrac{\cos\theta}{\sqrt{3}}-\sin\theta\right)\right\}$	$\dfrac{\sqrt{3}}{2\sigma_c J_2\cos 3\theta}\left\{2\sin\theta\left(\dfrac{B}{A}\right)M-\left(\dfrac{\cos\theta}{\sqrt{3}}-\sin\theta\right)\right\}$

$$M=\left(\frac{2\sqrt{J_2}\cos\theta}{A\,\sigma_c}\right)^{B-1}$$

Table 4.3 Material properties for strip footing and cut slope analyses

E (MPa)	ν	γ (MN/m^3)	σ_c (MPa)	A_0	A_f	A_r	B_0	S_0
13.79	0.35	0.018	0.206	3.7734	1.0396	0.5805	1.8731	-0.0831

Table 4.4 Material properties for tunnel analysis

E (MPa)	ν	γ (MN/m^3)	σ_c (MPa)	A_0	A_f	A_r	B_0	S_0
150	0.25	0.02	2.9	2.8997	1.0396	0.6984	1.7272	-0.159

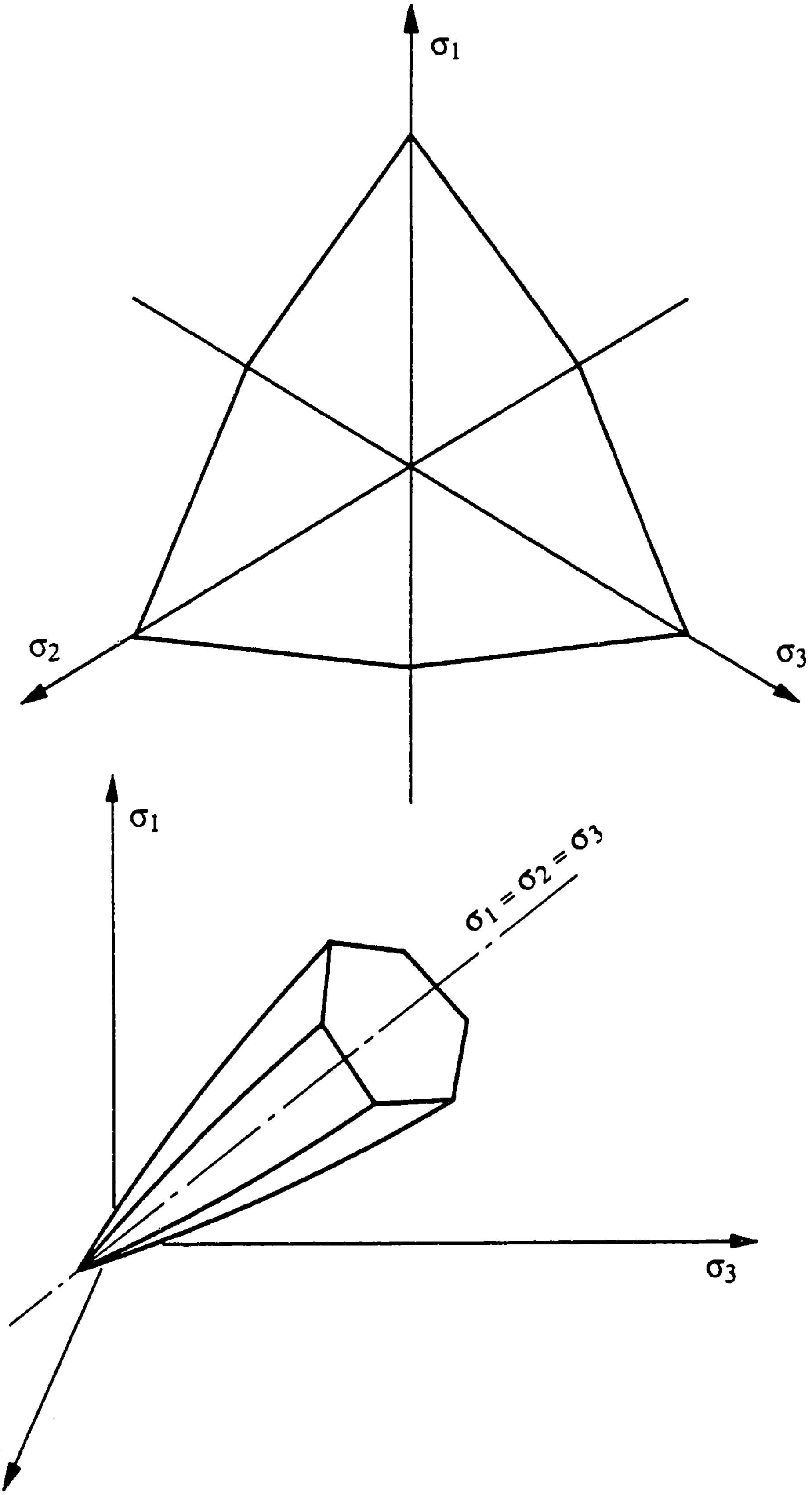
σ_1
σ_2
σ_3
σ_1
$\sigma_1 = \sigma_2 = \sigma_3$
σ_3
σ_2

Figure 4.1 Proposed yield criterion in principal stress space

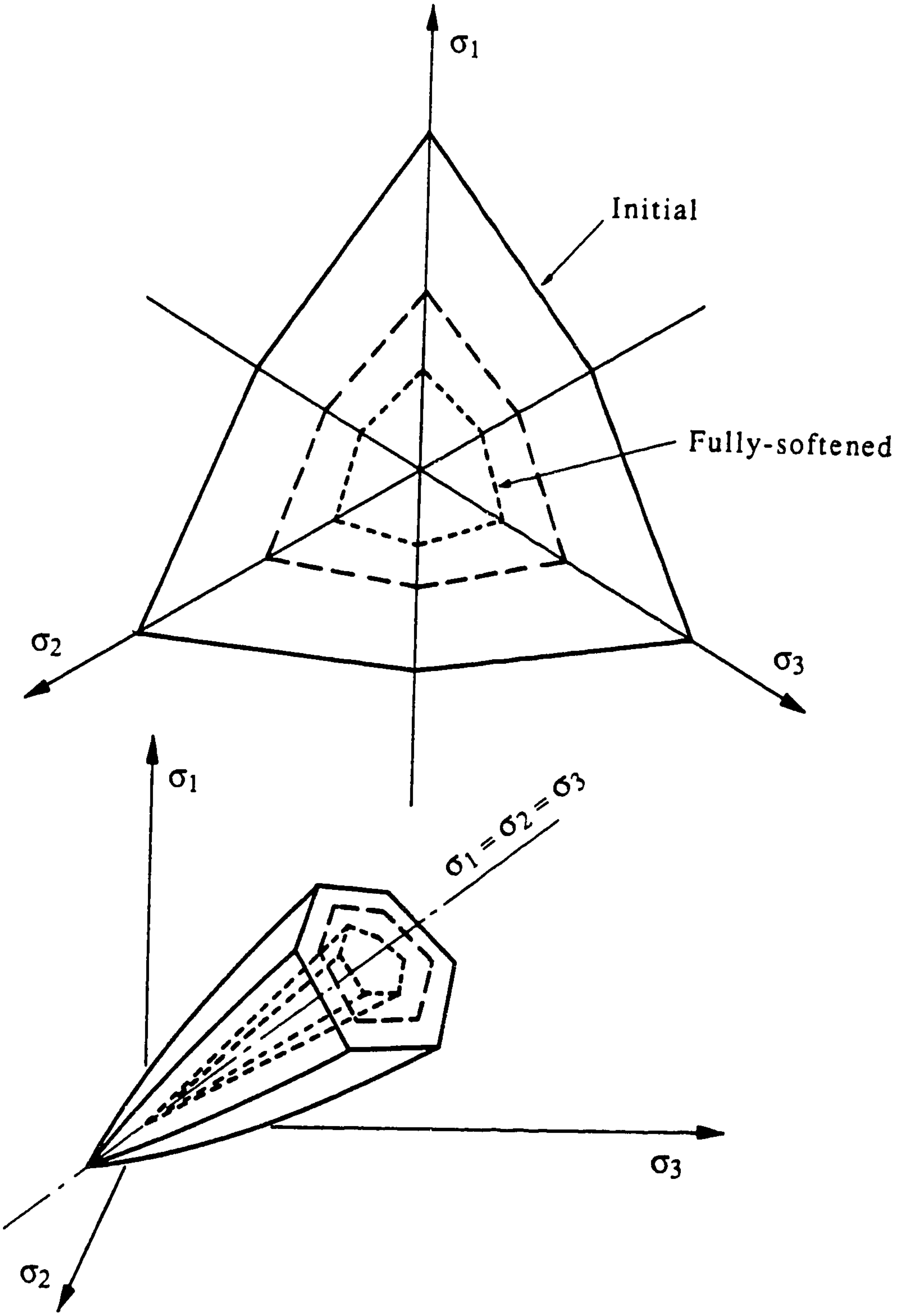
σ_1
Initial
Fully-softened
σ_2
σ_3
σ_1
$\sigma_1 = \sigma_2 = \sigma_3$
σ_3
σ_2

Figure 4.2 Variation of yield surface during softening

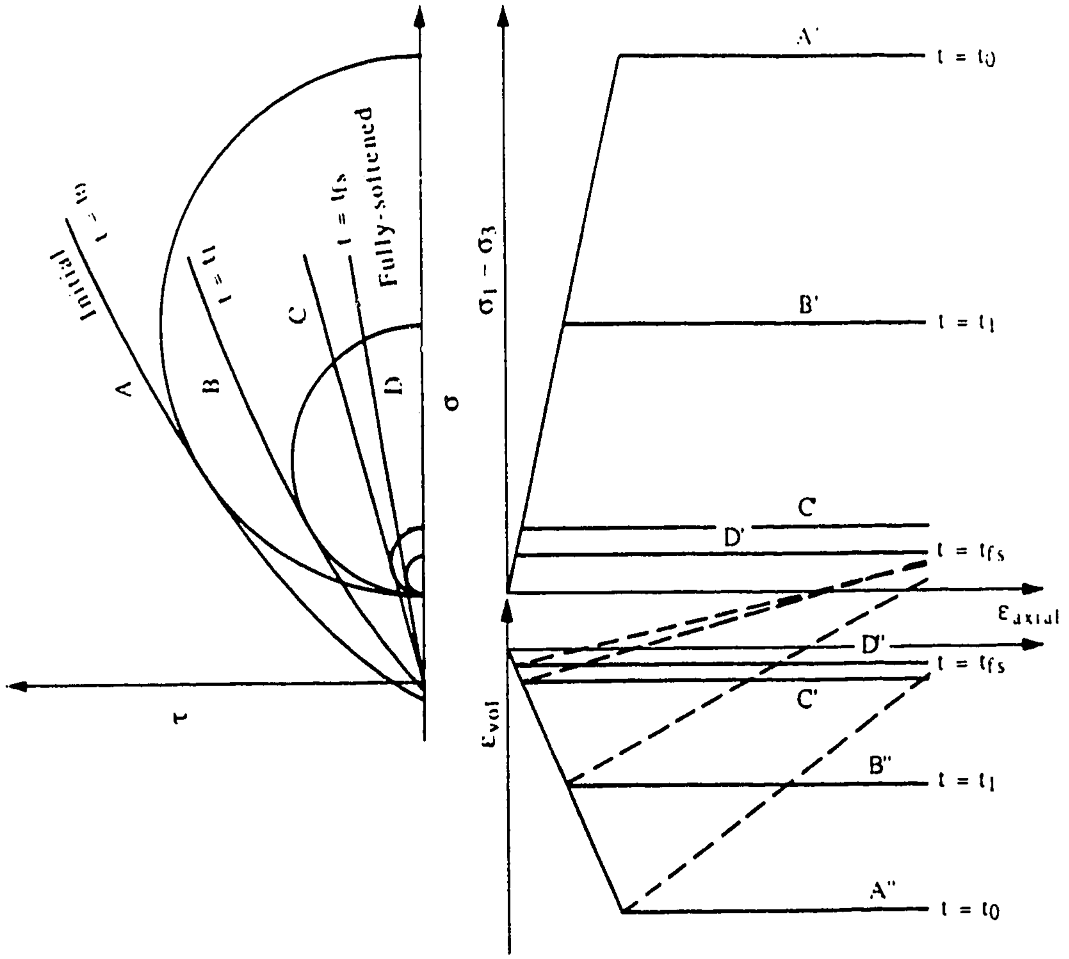
Initial
t = t0
t = t1
t = tfs
Fully-softened
A
B
C
D
σ
τ
σ1 - σ3
A'
t = t0
B'
t = t1
C
D'
t = tfs
ε axial
ε vol
D'
t = tfs
C'
B''
t = t1
A''
t = t0

Figure 4.3 Variations of stress, strain and shear strength during softening

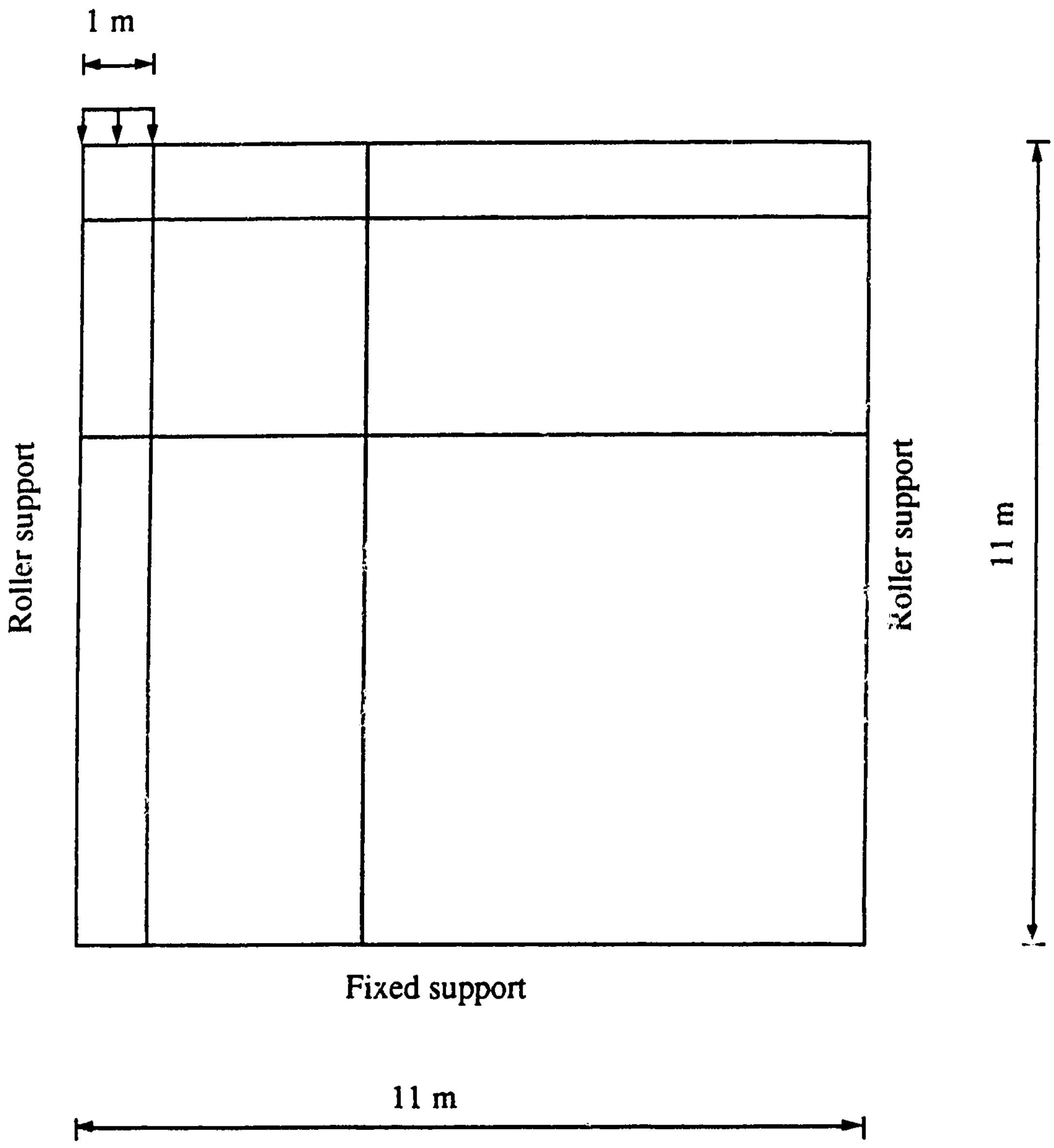
1 m
Roller support
Roller support
11 m
Fixed support
11 m

Figure 4.4 Finite element mesh for strip footing analysis

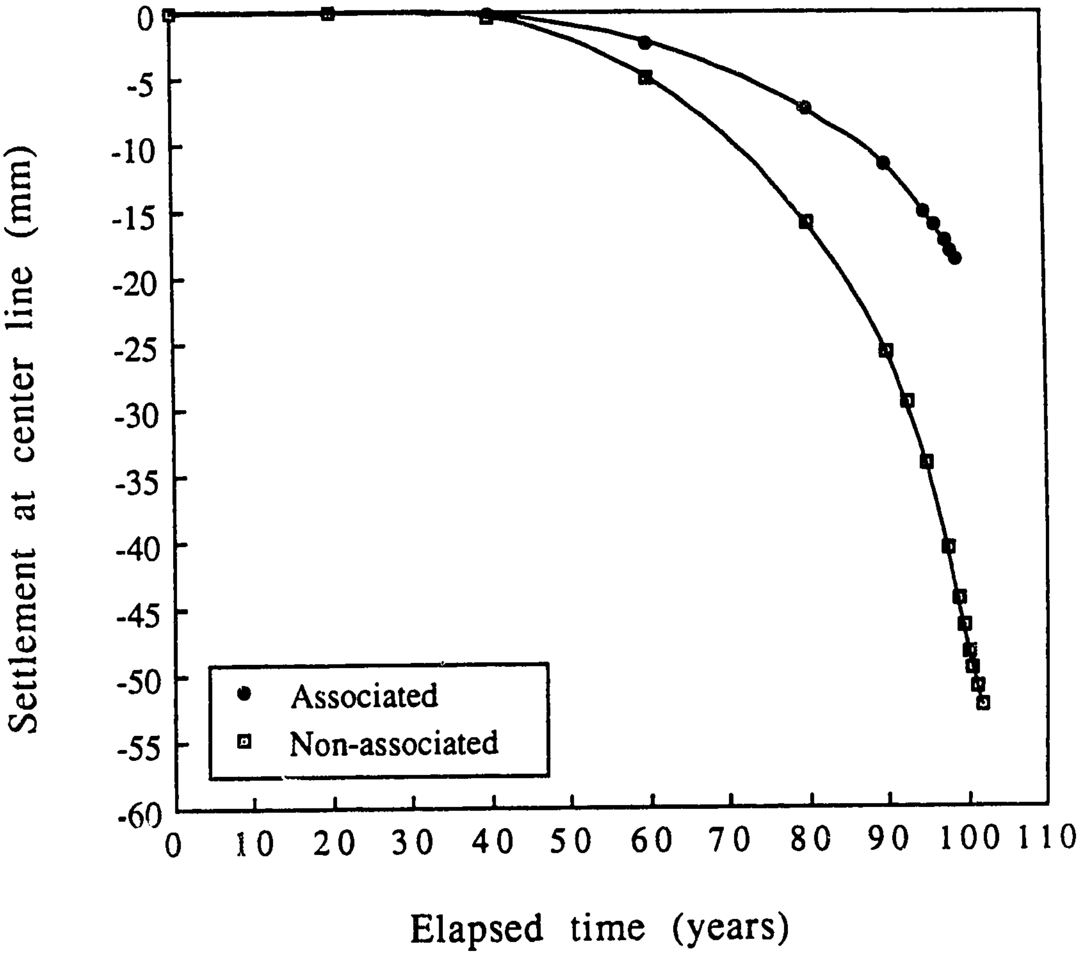

Figure 4.5 Variation of settlement at center line with time

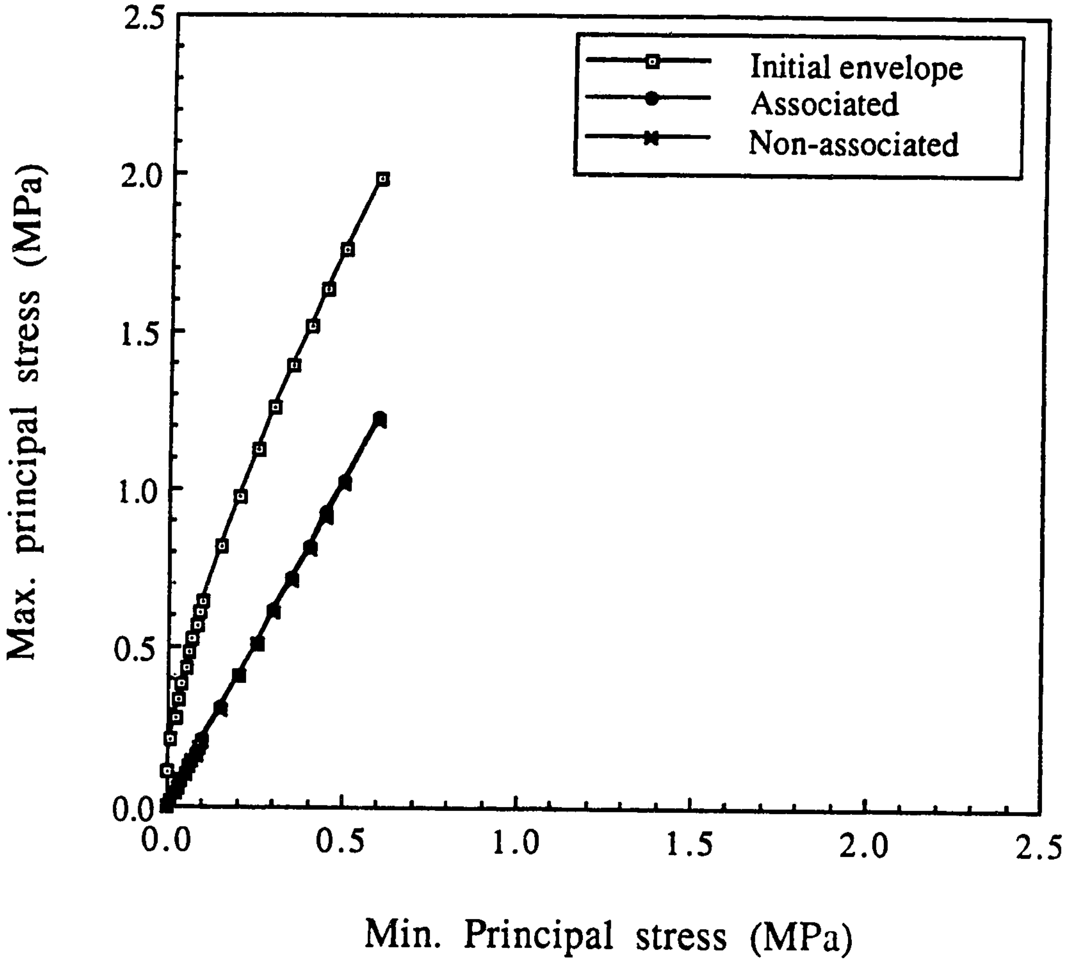

Figure 4.6 Strength envelopes just before collapse of ground

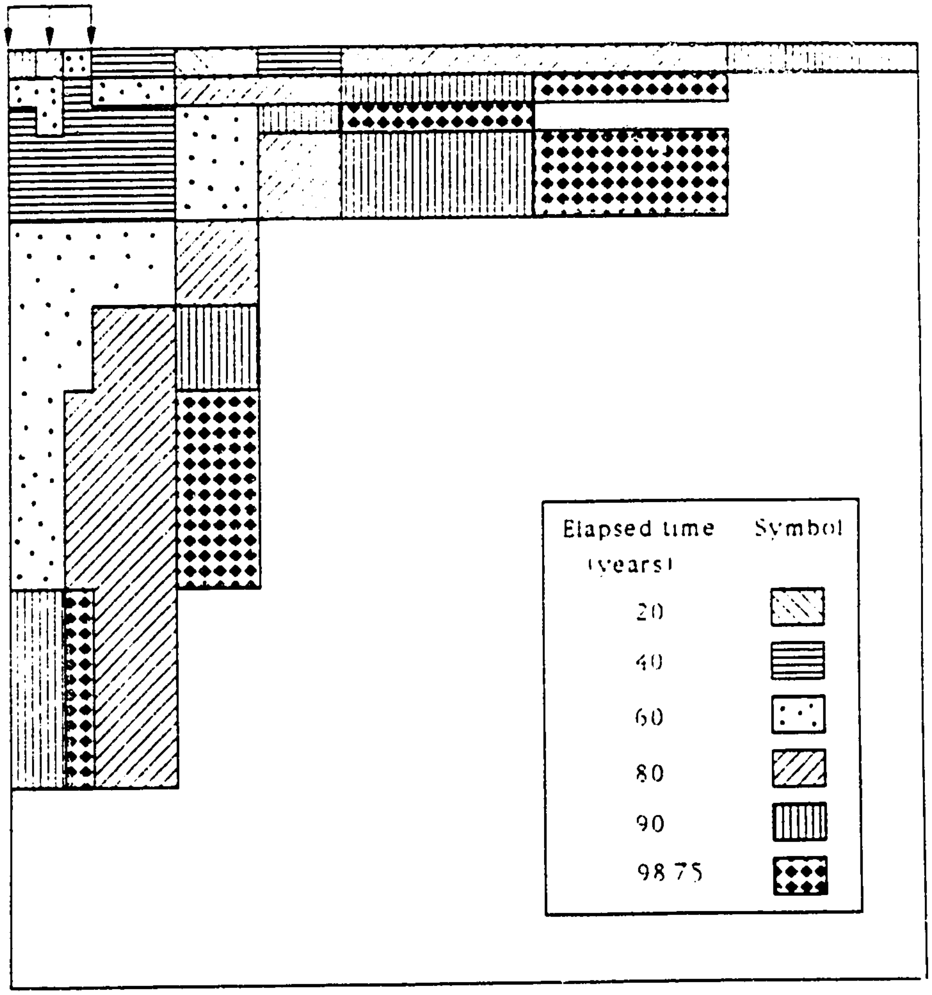
Elapsed time (years)
Symbol
20
40
60
80
90
98.75

Figure 4.7 Development of plastic zones under footing (associated flow rule)

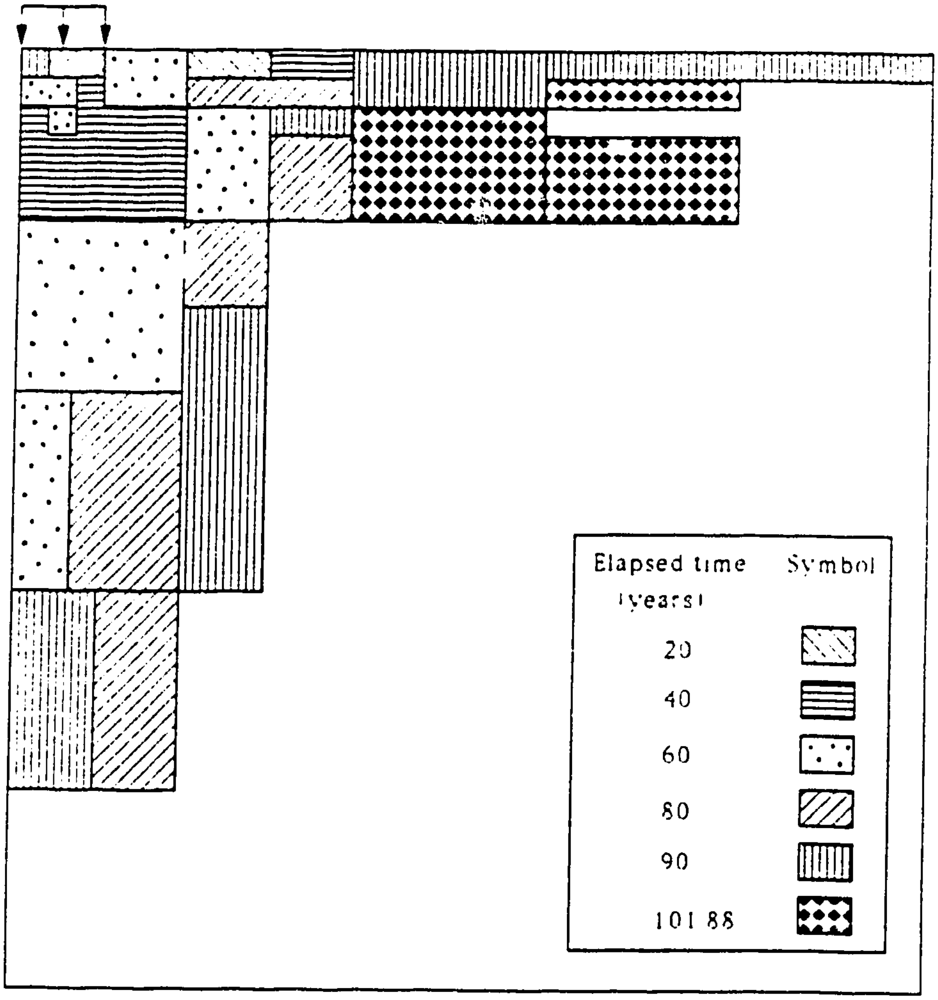
Elapsed time
(years)
Symbol
20
40
60
80
90
101.88

Figure 4.8 Develepment of plastic zones under footing (non-associated flow rule)

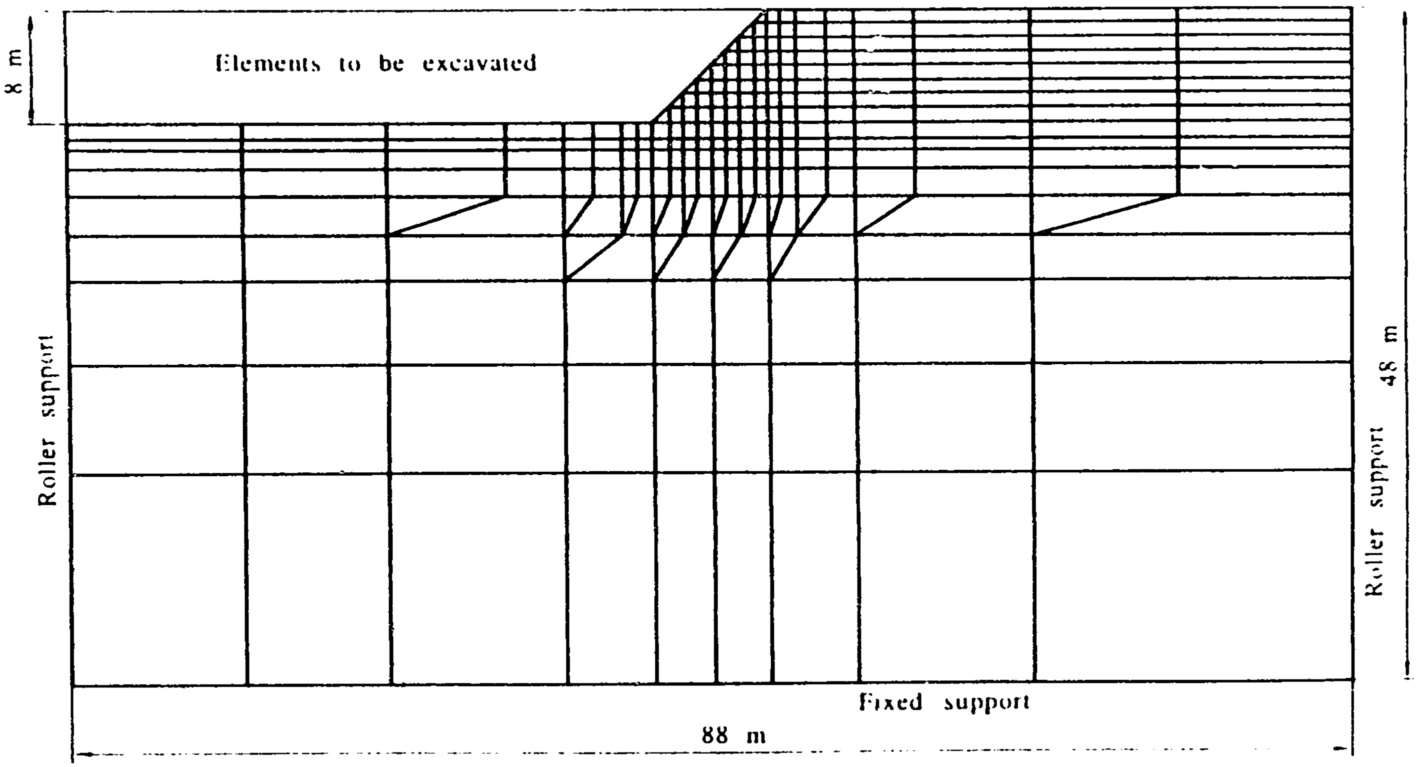
8 m
Elements to be excavated
Roller support
Roller support
48 m
Fixed support
88 m

Figure 4.9 Finite element mesh for cut slope analysis

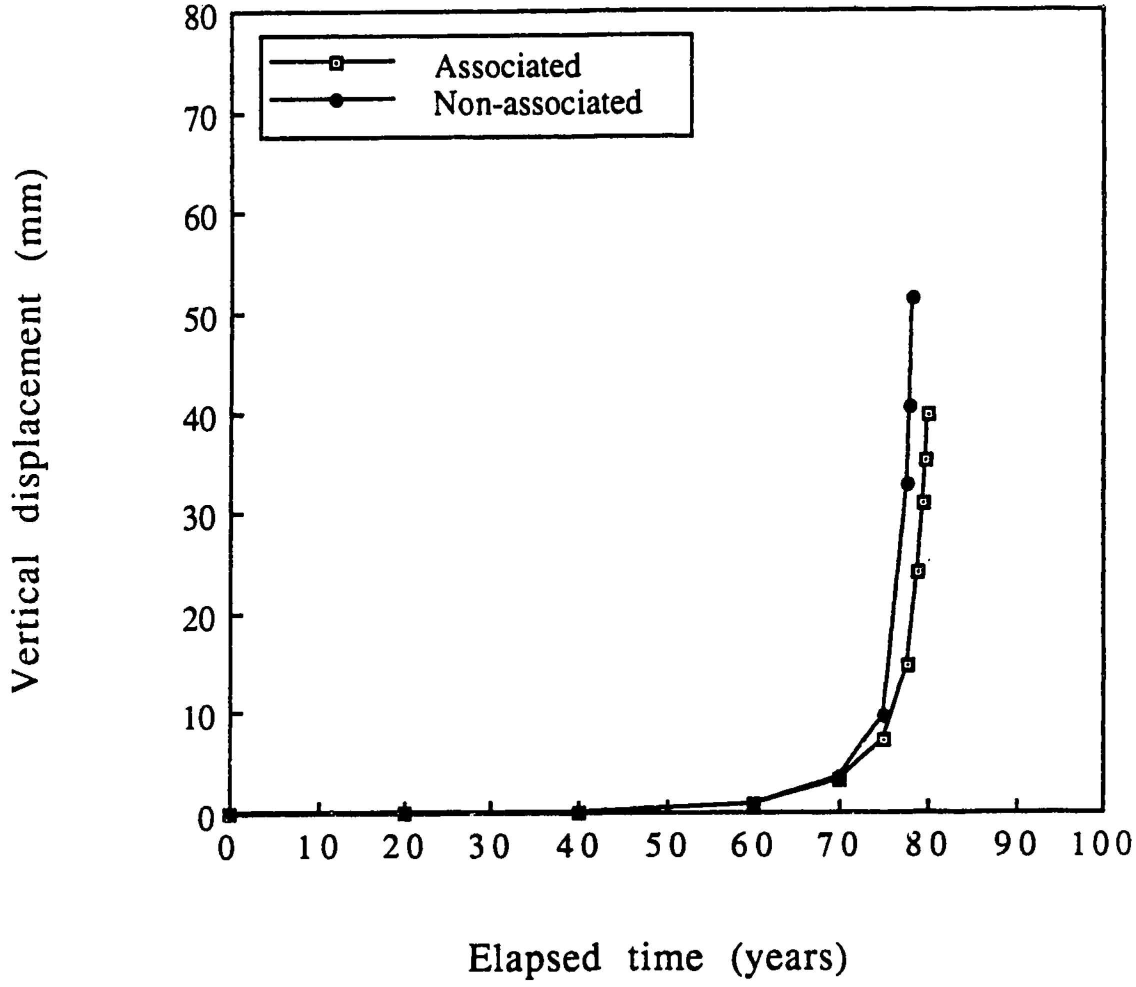

Figure 4.10 Variation of vertical displacement at crest of slope with time

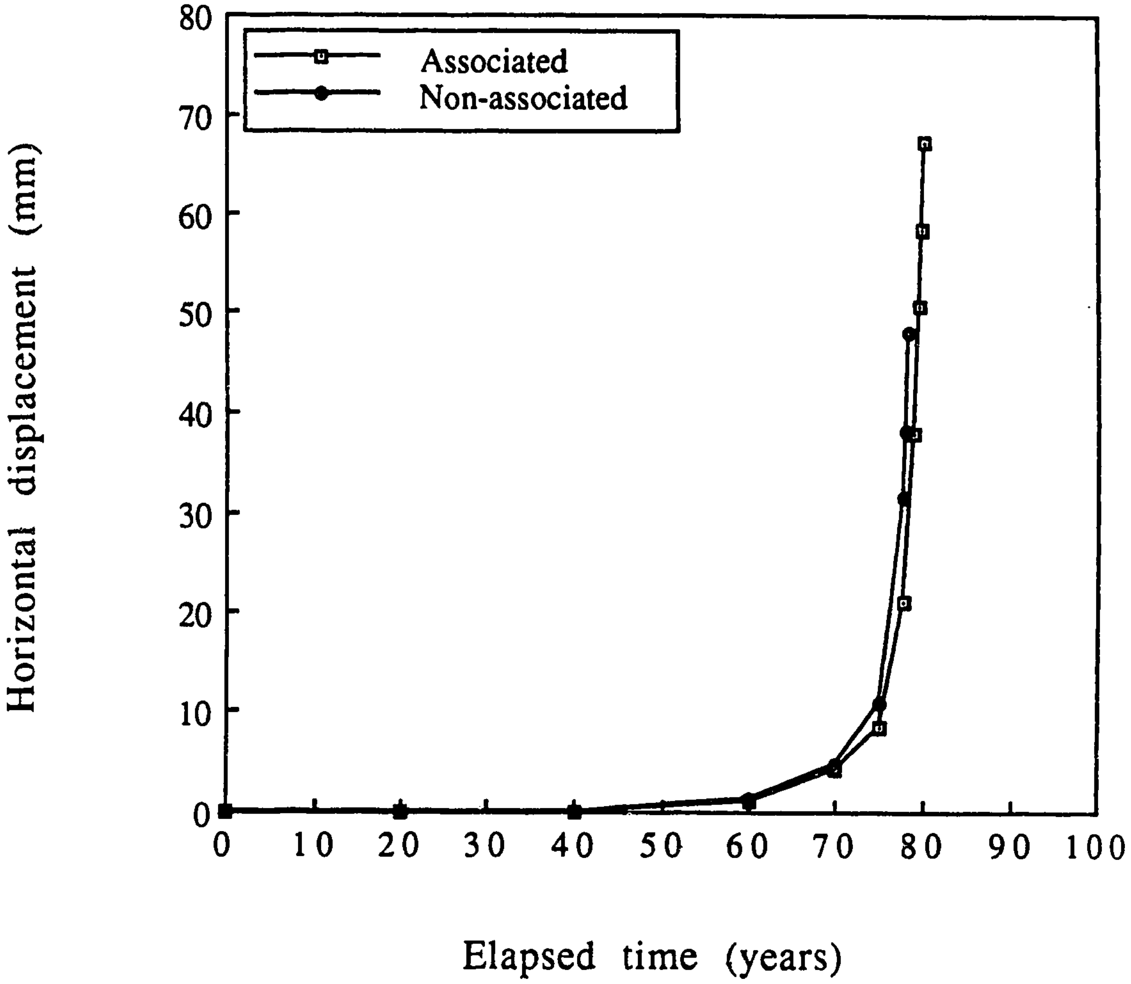

Figure 4.11 Variation of horizontal displacement at crest of slope with time

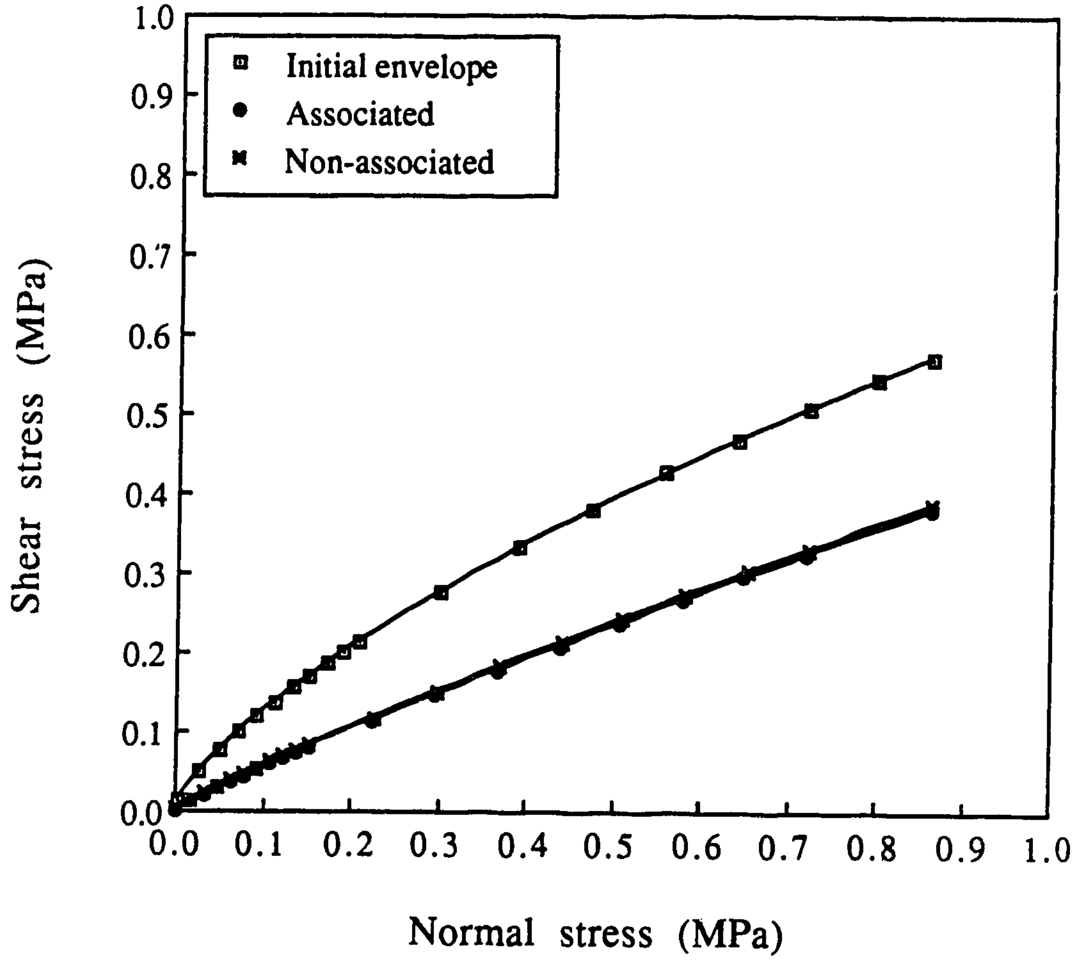

Figure 4.12 Strength envelopes just before collapse of slope

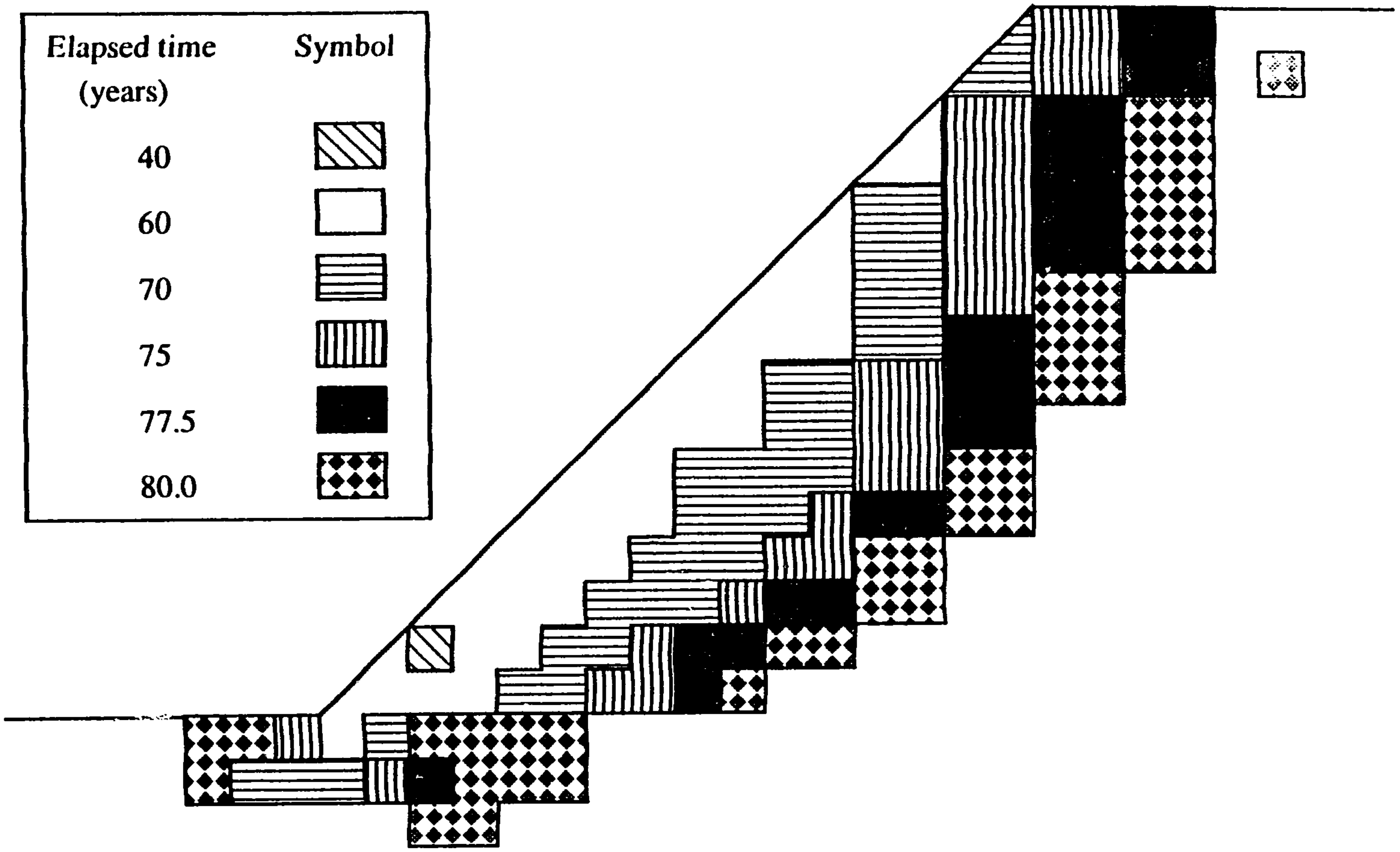
Elapsed time (years)
Symbol
40
60
70
75
77.5
80.0

Figure 4.13 Development of plastic zones in slope (associated flow rule)

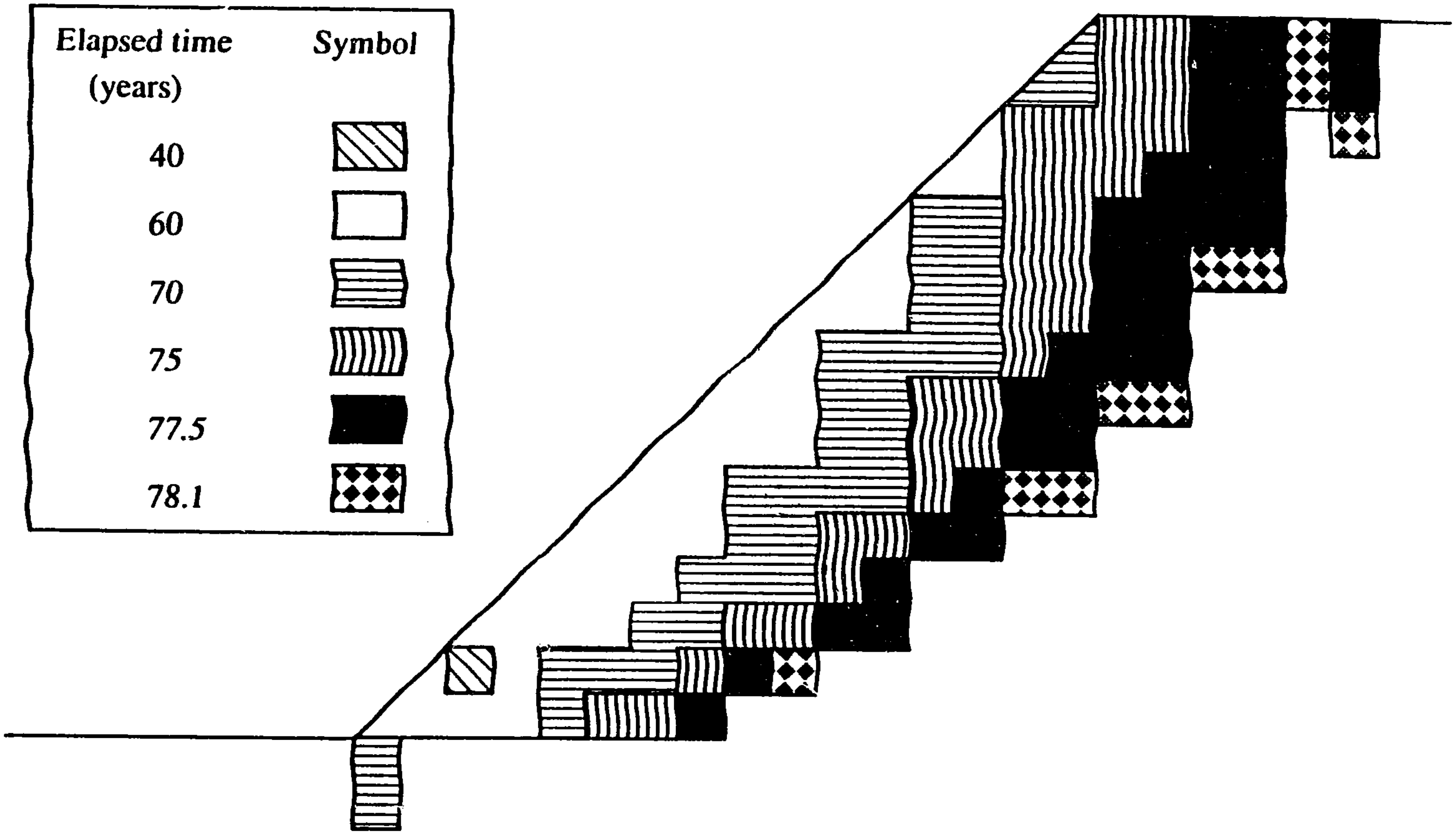
Elapsed time (years)
Symbol
40
60
70
75
77.5
78.1

Figure 4.14 Development of plastic zones in slope (non-associated flow rule)

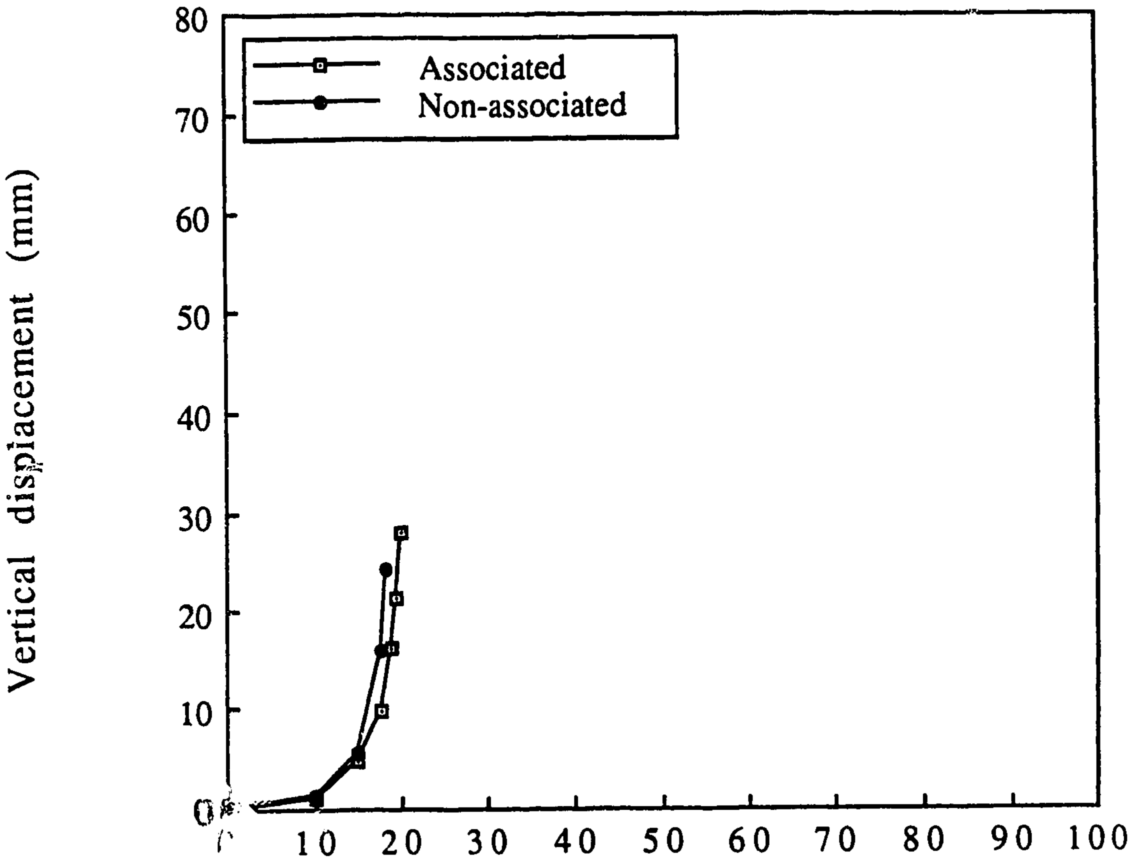

Figure 4.15 Variation of vertical displacement at crest of slope with time

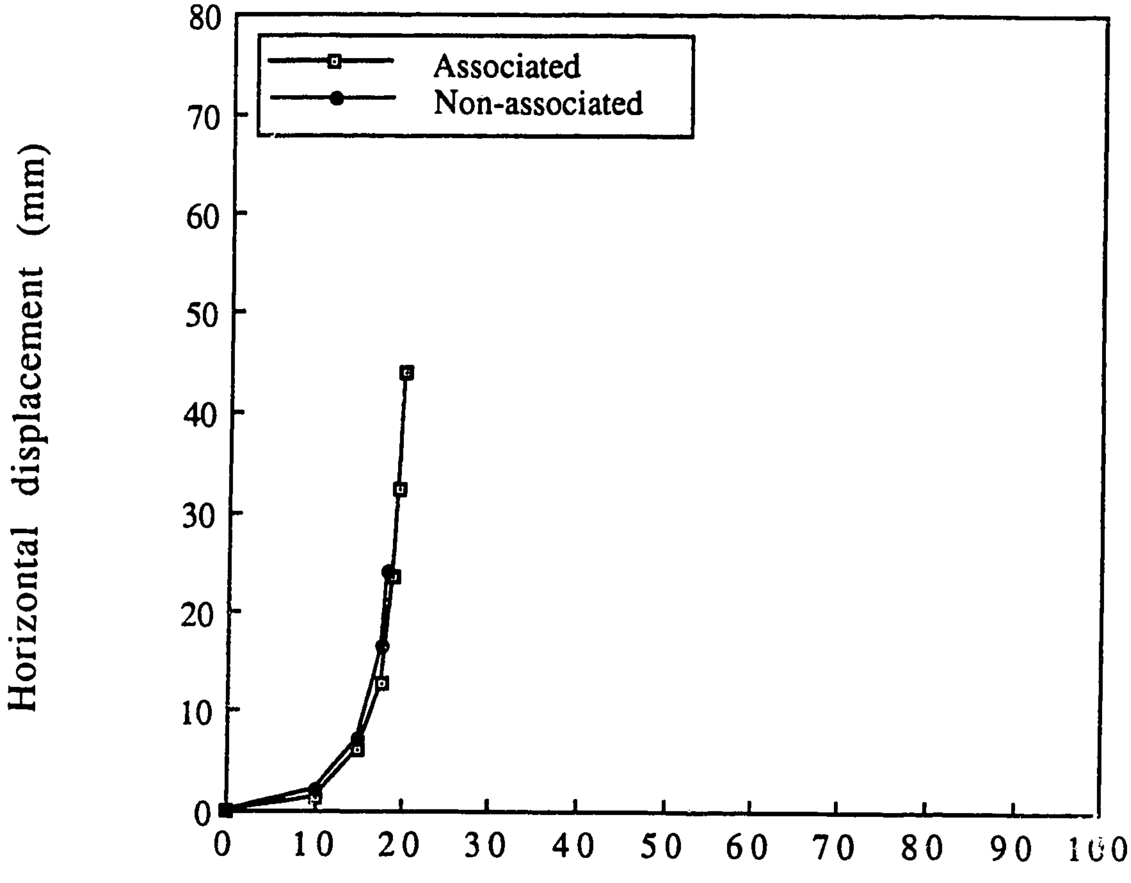

Figure 4.16 Variation of horizontal displacement at crest of slope with time

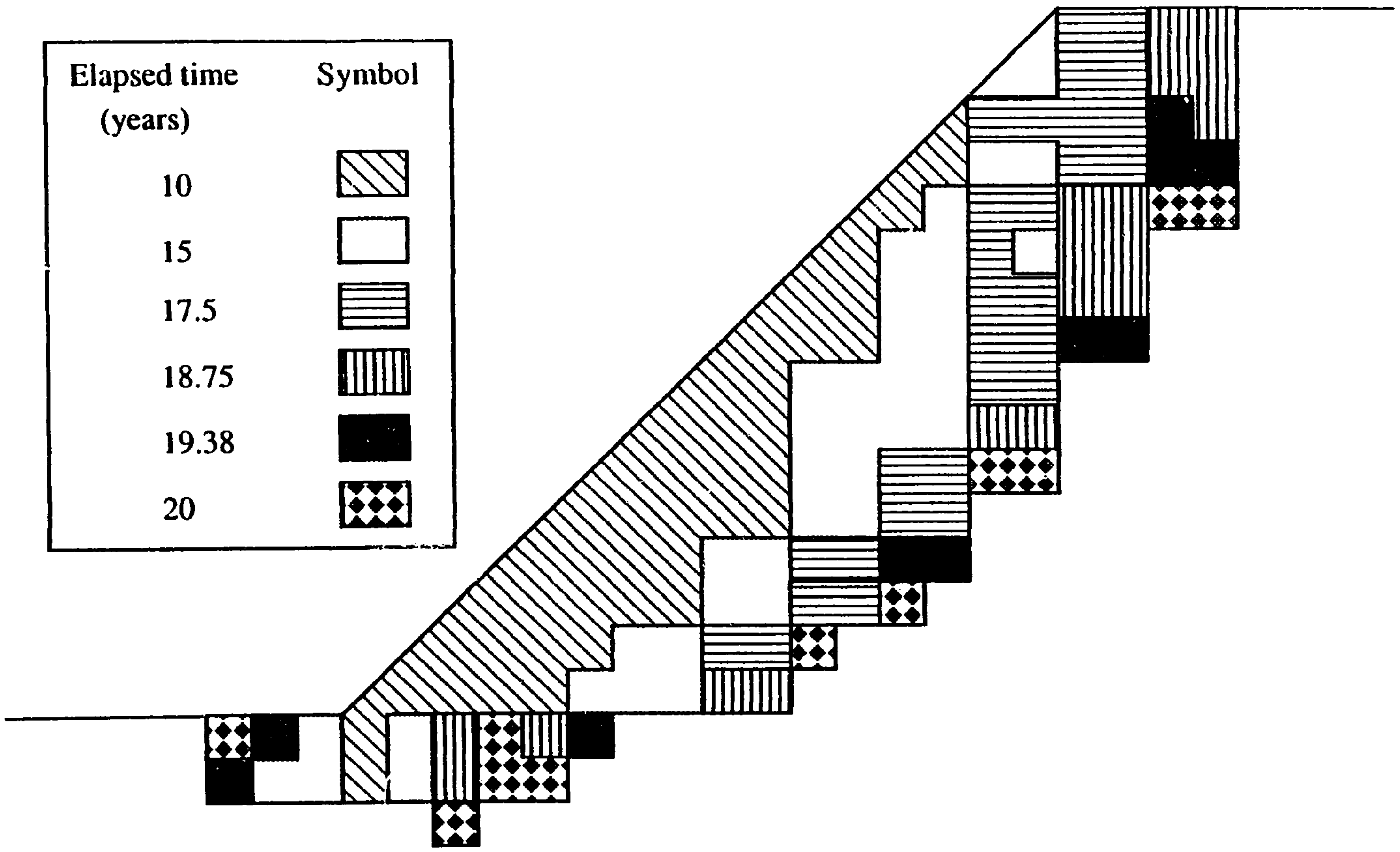
Elapsed time (years)
Symbol
10
15
17.5
18.75
19.38
20

Figure 4.17 Development of plastic zones in slope (associated flow rule)

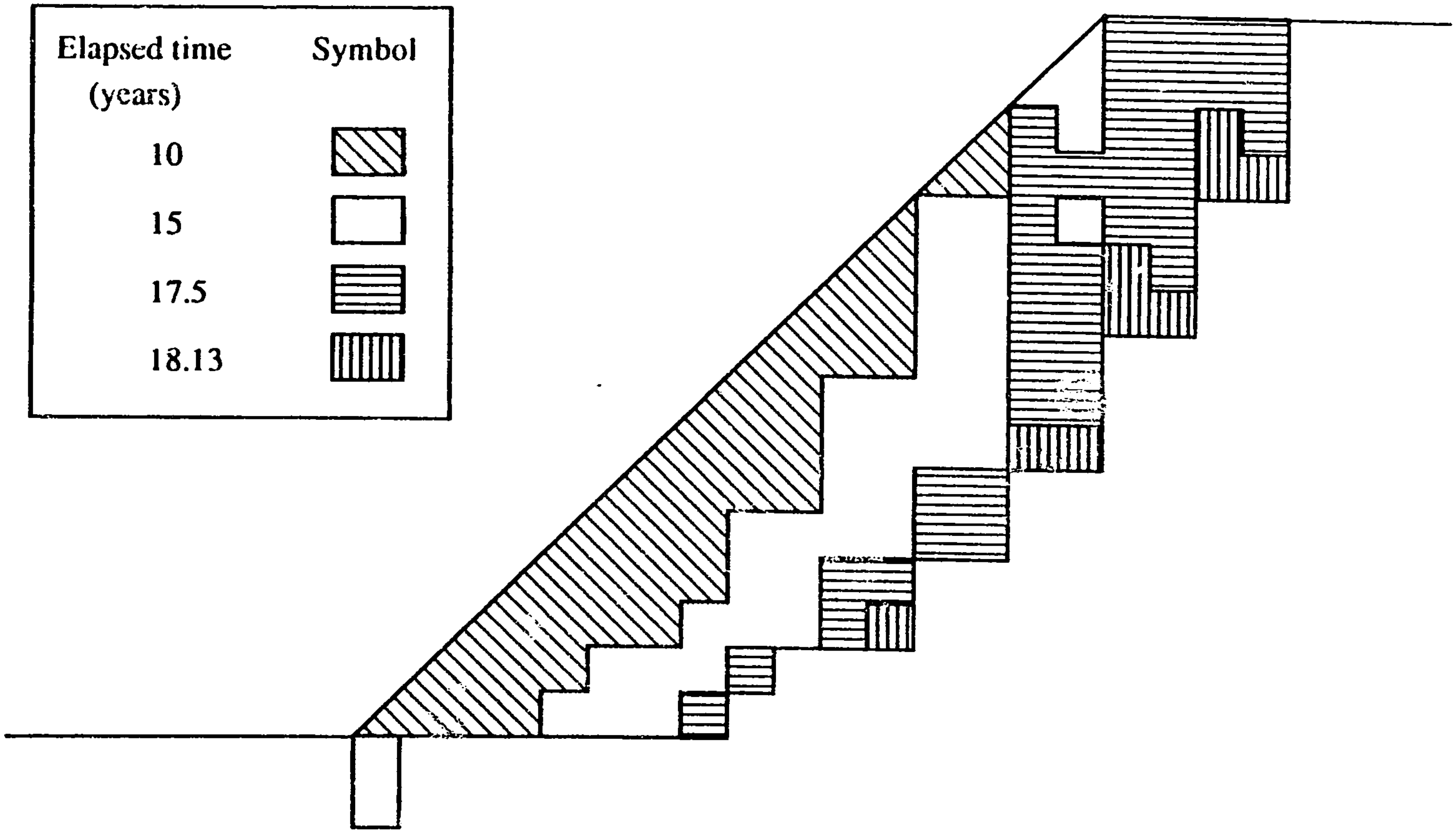
Elapsed time (years)
Symbol
10
15
17.5
18.13

Figure 4.18 Development of plastic zones in slope (non-associated flow rule)

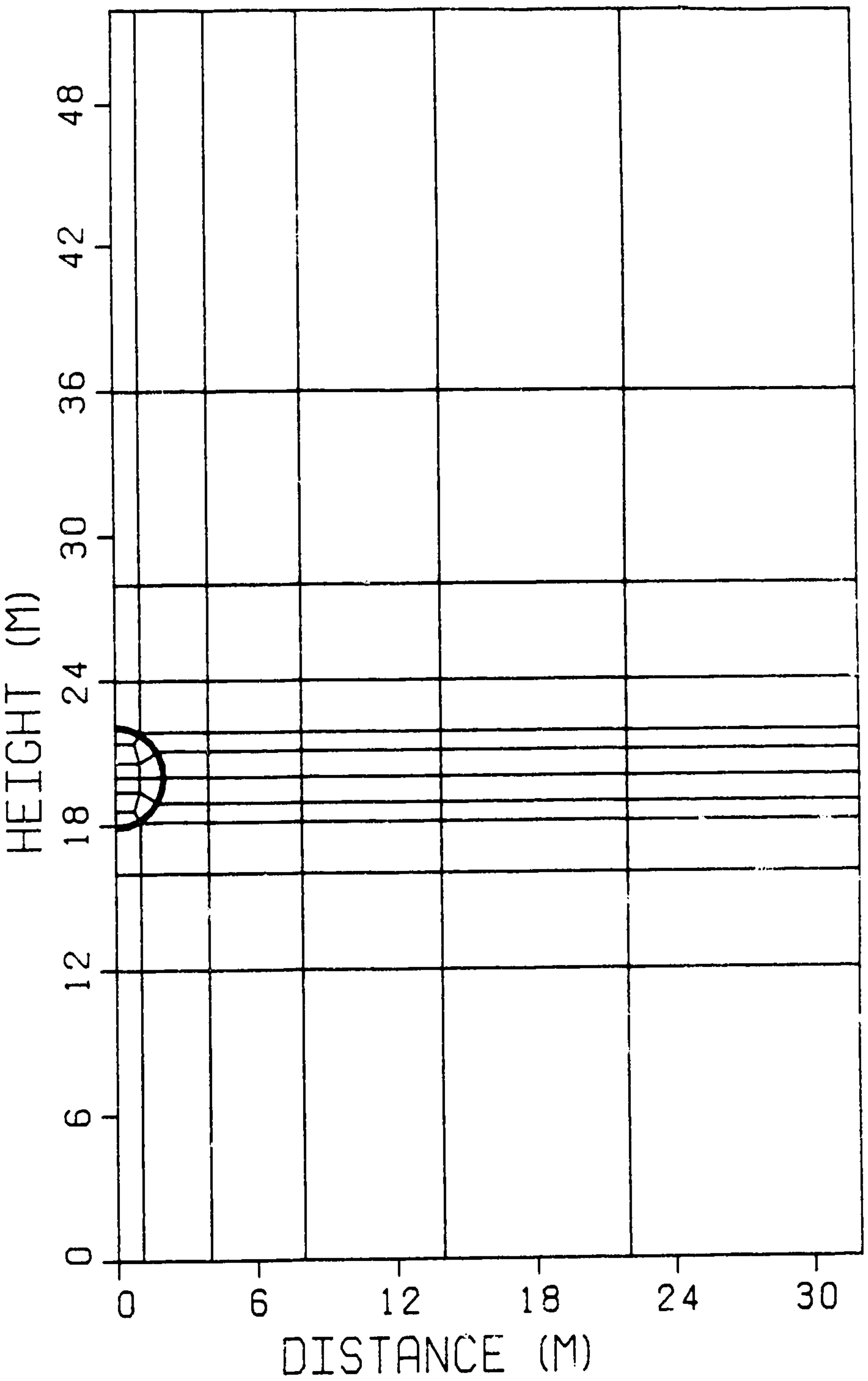
48
42
36
30
24
18
12
6
0
HEIGHT (M)
0
6
12
18
24
30
DISTANCE (M)

Figure 4.19 Finite element mesh for tunnel analysis

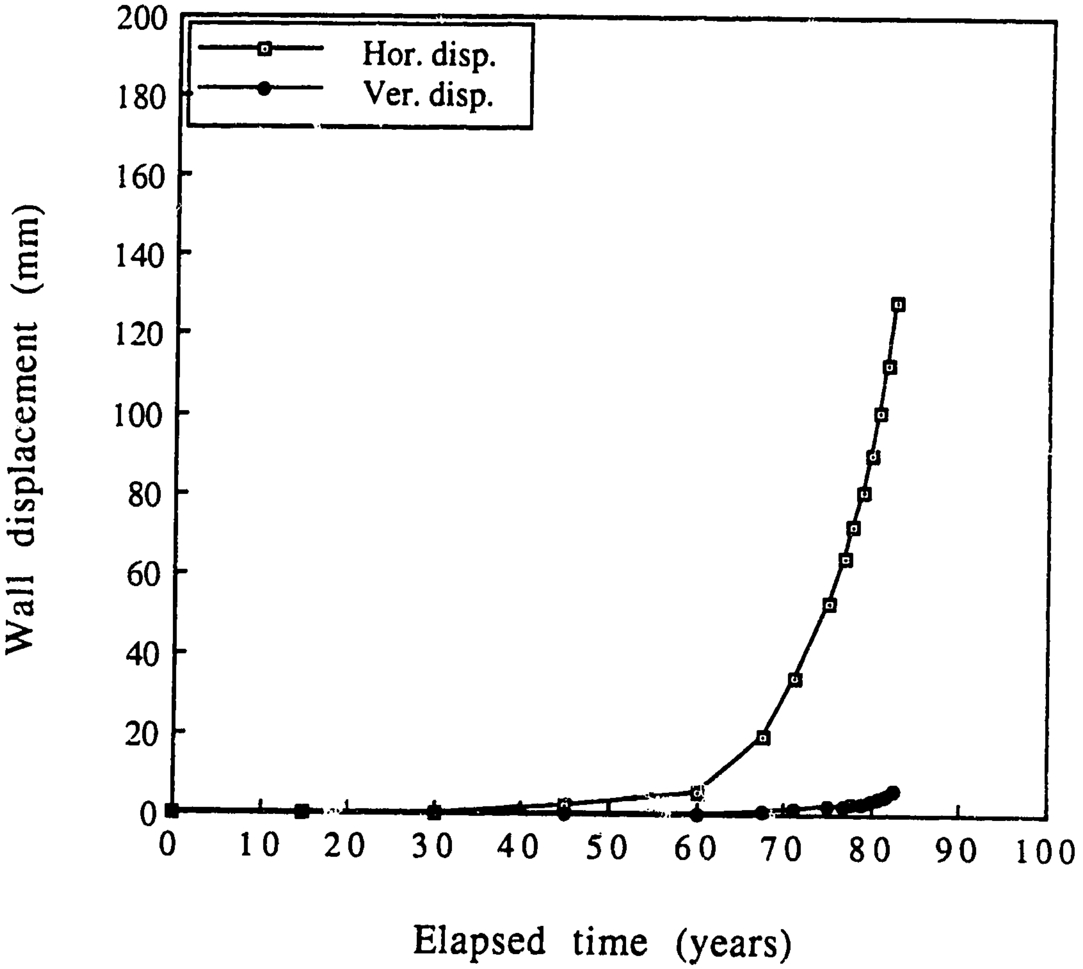

Figure 4.20 Variation of tunnel wall displacement with time

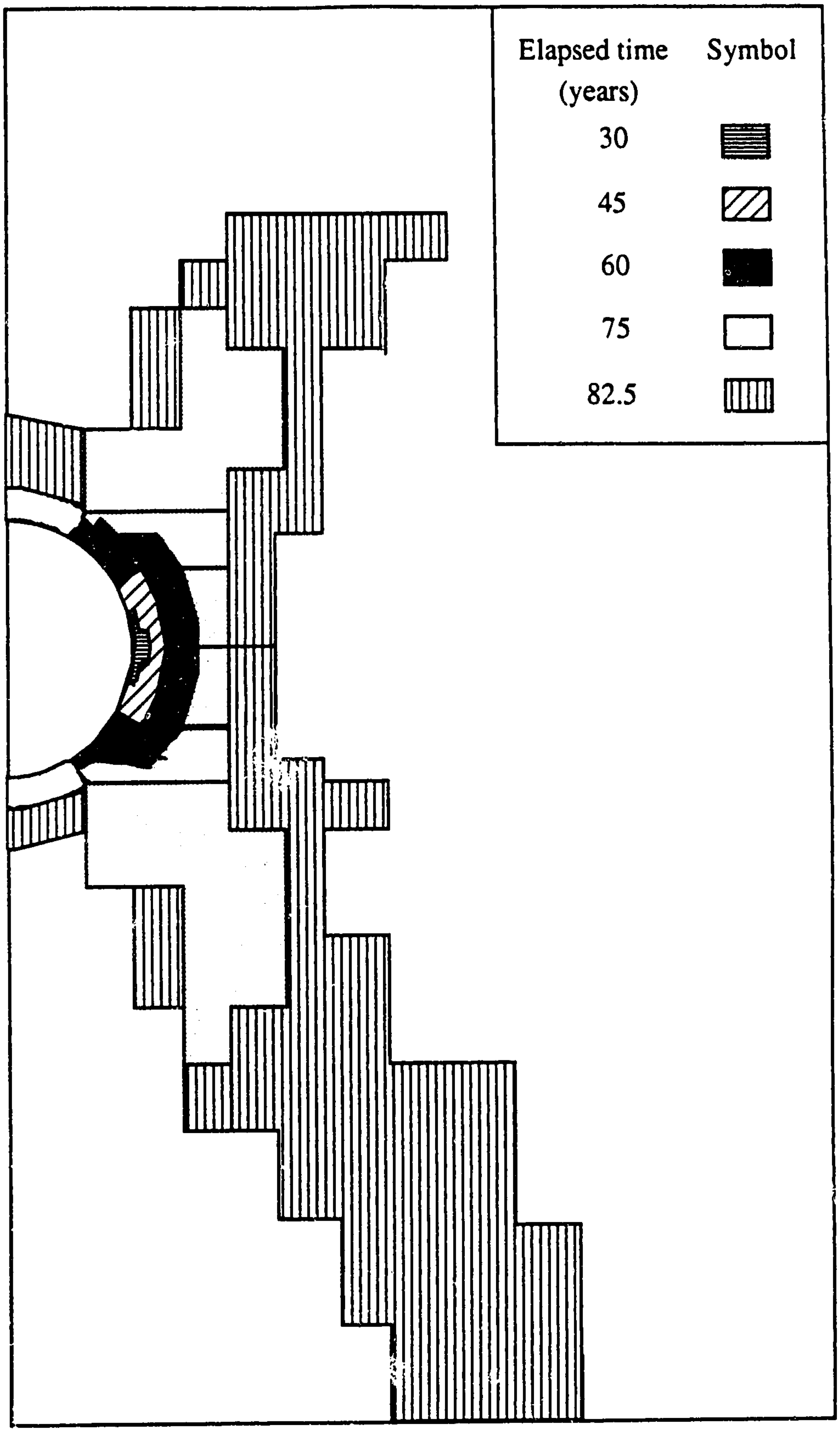
Elapsed time (years)
Symbol
30
45
60
75
82.5

Figure 4.21 Development of plastic zones around tunnel

5. Softening analysis with strain-softening model

5.1 Introduction

Experimental studies on fissured, over-consolidated clays and mudstones have indicated that these materials exhibit strain-softening characteristics. Bishop (1967) presented a detailed discussion of the effect of strain-softening on the stability of slopes. Bjerrum (1967) emphasized the importance of recognizing this strain-softening in considering stability problems in heavily over-consolidated clays and clayshales.

A number of constitutive models have been proposed to describe strain-softening behaviour. A brief review of strain-softening models used in soil mechanics is presented in the following paragraphs. Comprehensive reviews can be found in the theses by Simmons (1981) and Chan (1986) and in the research paper by Moore and Rowe (1988).

Lo and Lee (1973) introduced a brittle model which is based on elasticity theory and uses the stress transfer method to treat post-peak deformations in the analyses of slopes. Gates (1972) and Hoeg (1972) described several simple constitutive models for brittle behaviour using elasto-plasticity theory. Prevost and Hoeg (1975) introduced a strain-softening model for undrained conditions in which the expansion and contraction of the yield surface is assumed to be controlled by an equivalent plastic strain. Prevost (1974) proposed an undrained strain-softening model based upon the critical state concept in which the volumetric yield surface and shear yield surface vary with plastic volumetric strain and shear strain, respectively. This model was extended by Matsumoto and Ko (1982) to handle strain-softening behaviour under drained conditions. Pietruszczak and Mroz (1981) assumed a pre-existing shearband of finite thickness to exist in an element and, further, that plastic deformation occurred only in this shearband. To describe strain-softening behaviour, the cohesion component in the Coulomb yield function was assumed to decrease with the plastic strain. This so-called smeared shearband approach was further extended by Pietruszczak and Stolle (1985) who applied the critical state concept and assumed that the contraction of the yield surface was controlled by a change in plastic void ratio during shearing.

A simple strain-softening model is introduced in this chapter for a more realistic analysis of the softening process in fissured, over-consolidated clays and mudstones. It is a linear-elastic, post-peak plastic, strain-softening model and contains only two extra parameters in addition to conventional strength and deformation parameters. This model is incorporated into the finite element model of the softening process, presented in the previous chapter. An example analysis is then presented.

5.2 Strain-softening model

5.2.1 Description

A linear elastic, post-peak plastic, strain-softening model is described as a simple strain-softening model. The yield function is the same as used in the previous chapter,

$$F = \sigma_1 - \sigma_3 - A\,\sigma_c \left(\frac{\sigma_3}{\sigma_c} - S \right)^{\frac{1}{B}} = 0 \tag{5.1}$$

The shear strength reduction from peak to residual is represented by the reduction in the strength parameters A, B and S from their peak to residual values. The law controlling this transition of shear strength from peak to residual can be specified by some functions. For instance, Prevost and Hoeg (1975) used a rational function of an equivalent plastic strain for a softening parameter. Simmons (1981) applied a power function of plastic shear strain to the variation in c' and ϕ' in the Mohr-Coulomb yield criterion and dilatancy rate. A hyperbolic function of an equivalent plastic strain was used by Chan (1986). Dounias *et al.* (1988) used a simple linear function of an equivalent plastic strain for c' and ϕ' in the Mohr-Coulomb yield criterion. In this study, the following linear functions are assumed for the strength parameters:

$$A = A_0 - (A_0 - A_r) \frac{\overline{\varepsilon^p}}{\varepsilon^p_{ps}} \tag{5.2a}$$

$$B = B_0 - (B_0 - B_r) \frac{\overline{\varepsilon^p}}{\varepsilon^p_{ps}} \tag{5.2b}$$

$$S = S_0 - (S_0 - S_r) \frac{\overline{\varepsilon^p}}{\varepsilon^p_{ps}} \tag{5.2c}$$

where the subscripts, 0 and r, in the strength parameters, indicate the peak and residual values, respectively, $\overline{\varepsilon^p}$ is the equivalent plastic strain (see Equation 4.7 in Chapter 4) and $\overline{\varepsilon^{p}_{ps}}$ is a parameter which is $\overline{\varepsilon^p}$ / $\overline{\varepsilon^{p}_{ps}}$ = 1 when $\overline{\varepsilon^p} \geq \overline{\varepsilon^{p}_{ps}}$. Figure 5.1 shows a schematic variation of the strength parameters.

The plastic potential function is assumed to be of the same form as the yield function:

$$G = \sigma_1 - \sigma_3 - A^* \sigma_c \left(\frac{\sigma_3}{\sigma_c} - S^* \right)^{\frac{1}{B^*}} = 0 \tag{5.3}$$

If the values of A*, B* and S* were equal to those in the yield function, the associated flow rule would result.

Consider an isotropic, homogeneous plane-strain condition. Under this condition, the relation between stress and strain increment can be easily visualized since the principal axes of stress and strain increment coincide. Using Equations (5.3) and (4.3), one can derive the following expression:

$$\sin \psi = - \frac{d\varepsilon_1^p + d\varepsilon_3^p}{d\varepsilon_1^p - d\varepsilon_3^p} = \frac{\frac{A^*}{B^*}\left(\frac{\sigma_3}{\sigma_c} - S^* \right)^{\frac{1}{B^*} - 1}}{2 + \frac{A^*}{B^*}\left(\frac{\sigma_3}{\sigma_c} - S^* \right)^{\frac{1}{B^*} - 1}} \tag{5.4}$$

where ψ is the dilatancy angle proposed and defined by Davis (1968). This expression indicates that the dilatancy angle with this plastic potential function is stress-dependent. As the stress level increases the dilatancy angle decreases. For this reason, the term instantaneous dilatancy angle, ψ_i, is used here. Similarly, the ratio of principal plastic strain increments is expressed as follows:

$$\frac{d\varepsilon_3^p}{d\varepsilon_1^p} = -1 - \frac{A^*}{B^*}\left(\frac{\sigma_3}{\sigma_c} - S^*\right)^{\frac{1}{B^*} - 1} = -N_{\psi_i} \tag{5.5}$$

where

$$N_{\psi_i} = \frac{1 + \sin \psi_i}{1 - \sin \psi_i}$$

Figure 5.2 shows this relation schematically. When B takes a value of unity, the plastic potential function becomes a Mohr-Coulomb function and the dilatancy angle is stress-independent. Equation (5.4) can be simplified to:

$$\sin \psi = \frac{A^*}{2 + A^*} \tag{5.6}$$

When the associated flow rule is applied, *i. e.*, A* = A, the right hand side of the above equation equal to sin ϕ, where ϕ is the angle of internal friction. It is well known that the application of the associated flow rule to geologic materials predicts excessive dilatancy compared with the experimental observations, and it is usual to assume a much smaller angle for ψ in an empirical manner. Further, the dilatancy rate of real soil decreases once the peak strength has been reached and becomes zero when the residual condition is reached. In order to take these observations into account, the following assumption is made. The parameters, A*, B* and S*, decrease with the increase of equivalent plastic strain from the peak to residual values in the same manner as the strength parameters, A, B and S do. A* decreases from an initial value, smaller than the peak value of A, to zero, which makes dilatancy rate be zero. A* may be determined intuitively like the determination of dilatancy angle.

5.2.2 Triaxial compression test simulation

In order to examine the behaviour of the proposed strain-softening model, a triaxial compression test simulation was conducted. The experimental results were from drained triaxial compression tests on a Tertiary mudstone from the Tohoku district of Japan reported by Watanabe *et al.* (1987), Denda *et al.* (1987) and Watanabe *et al.* (1988). Physical properties of the Tohoku mudstone are given in Table 5.1. Input data for the simulation are summarized in Table 5.2. The peak and residual strength parameters were determined by the application of the least squares method to the experimentally determined strength data, in terms of effective stress. The deformation parameters were estimated from the shear modulus, G, and bulk modulus, K, given in the references. Parameters, $\overline{\epsilon^{p}_{ps}}$ and A*, were determined based upon the shape of the experimentally obtained stress-strain curves.

Isotropic, homogeneous deformation is assumed in the computation, thus a single axisymmetric element with unit size can be used. The triaxial compression test was simulated by applying a variable number of axial deformation increments, step by step, following the application of isotropic confining pressure.

The simulation results are shown in Figure 5.3 together with the experimental results. Good agreement can be seen between the computed and experimental stress-strain curves. Differences can be noticed in the volume change behaviour at the confining pressure of 0.05 MPa. The test sample does not reach the residual condition and exhibits a continuing dilatancy, while the model reaches its residual condition at about 3 % axial strain.

Effects of parameters, $\overline{\varepsilon^{p}_{ps}}$ and A*, upon a stress-strain curve are illustrated for the confining pressure of 0.5 MPa in Figures 5.4 and 5.5. In Figure 5.4 stress-strain curves are computed for $\overline{\varepsilon^{p}_{ps}}$ of 5, 10 and 20 % with A* of A/8 where A is the strength parameter. It is seen that $\overline{\varepsilon^{p}_{ps}}$ influences both the post-peak stress-strain curve and the volume change curve, and that the larger the value the lower the post-peak strain-softening rate and the lower the dilatancy rate. In Figure 5.5 stress-strain curves are computed for A* of A/8 and A with $\overline{\varepsilon^{p}_{ps}}$ of 5 %. It is seen that A* affects mainly the rate and amount of dilatancy.

From the above, it can be said that by selecting proper values for these parameters, one can model strain-softening behaviour, for practical purposes.

5.3 Softening analysis

The strain-softening model proposed in this chapter is incorporated into the finite element model of the softening process described in the previous chapter. In order to illustrate the model behaviour, it is assumed that an excavation is made in a fissured, over-consolidated clay and that softening starts just after the completion of the excavation. Figure 5.6 shows the relations among stress, strain, strength and time during softening schematically. At time t = 0, at the completion of excavation, the clay is assumed to exhibit strength and deformation behaviour as denoted by A in the figure. As softening progresses, the clay deteriorates, indicating by a reduction in brittleness and dilatancy (Curve B). At the end of softening, the fully-softened condition, Curve C, is reached. For instance, the stress state at a point in the ground just after excavation is assumed to be at Point P in the figure. The soil element does not fail at this time. When some time elapses, say Δt, the strength envelope of the soil contracts from Curve A to Curve B, accompanied by a change in the stress-strain relation. The soil element yields and the stress state is brought to Point P', accompanied by further contraction of the strength envelope to Curve P" due to plastic deformations. As softening progresses further, the soil element continues to yield and it will reach the residual condition if it experiences sufficiently large plastic deformation. In this way, softening advances toward the fully-softened condition (Curve C). As in the previous chapter, deformation moduli are assumed not to vary during softening.

5.4 Example

For the purpose of demonstration, softening in a cut slope is considered. The same cut slope as the one analyzed in the previous chapter is used here. The cut was made to a depth of 8 m with a 45° slope. The finite element mesh is shown in Figure 5.7 together with the geometry and boundary conditions. The ground is assumed to consist of a fissured, over-consolidated clay whose material properties are summarized in Table 5.3. The values of $\overline{\varepsilon^{p}_{ps}}$ and A* are 30 % and A/8, respectively, where A is the peak shear strength parameter. The strength reduction parameters, a, b and c, are all zero. Figures 5.8 and 5.9 show the input strength envelopes and stress-strain relations at different elapsed times, respectively. The fully-softened condition is assumed to be reached in 10 years after excavation. The same analysis procedure as in the previous chapter is used in this analysis.

Figure 5.10 shows the displacement-time relation computed at the crest of the slope. The displacement increases gradually with time in the early stages, then rapidly as the slope approaches collapse. The time to collapse is about 75 years from the completion of the excavation. Propagation of plastic zones in the slope is shown in Figure 5.11. Yielding starts at the lower part of the slope surface and propagates along the slope, then inwards. Figure 5.12 shows the distribution of accumulated equivalent plastic strain just before collapse, along a horizontal plane at an elevation of 1.8 m from the excavation base. The maximum plastic deformation is seen to occur near the slope surface at this particular elevation, and the plastic deformation decreases with distance from the slope surface. Since plastic deformation is related to shear strength, a similar variation in the shear strength mobilized is expected. This is illustrated in Figure 5.13 which shows shear strength envelopes mobilized at the locations given in Figure 5.12. The strength envelopes are magnified for low stresses in Figure 5.13(b) and for high stresses in Figure 5.13(c). As expected, the lowest shear strength is mobilized near the slope surface.

It is of interest to compare these results with those analyzed using an elastic, perfectly-plastic model in the previous chapter. The time to collapse is a little shorter in the case of the strain-softening ground than in the elastic, perfectly-plastic case. Further, the computed displacements at the crest of the slope at a given elapsed time are greater in the strain-softening ground than in the elastic, perfectly-plastic ground. Regarding the plastic zones, propagation seems to be similar in these two cases. However, the analyses were conducted imposing the gravity force, while initial K_0 stresses were not imposed. Since K_0 is known to affect the magnitude of the shear stresses significantly, the plastic zone would be different between in the two cases.

5.5 Summary

This chapter extended a finite element method described in the previous chapter, for a more realistic analysis of softening. For this purpose, a simple strain-softening model was introduced. The model is very simple and contains, in addition to conventional strength and deformation parameters, only two extra-parameters controlling strain-softening.

An example analysis was presented which deals with softening in a cut slope excavated in strain-softening ground. The deformation pattern and yielding in the slope were traced up to collapse. The influence of strain-softening behaviour was noted in the results. The results were compared with the previous results for the elastic, perfectly-plastic case, which indicates the detrimental effect of strain-softening.

Table 5.1 Index properties of Tohoku Mudstone

w_n (%)	LL (%)	PL (%)	PI (%)	G_s	γ_t (MN/m^3)	Clay %
29.3	130.1	34.1	96.0	2.66	0.019	68.3

Table 5.2 Input data for triaxial test simulation

Strength properties

	Peak			Residual		
A_p	B_p	S_p	A_r	B_r	S_r	σ_c (MPa)
2.6842	2.8007	-0.0630	1.3409	2.4772	0.0	2.17

Deformation properties and others

0.05 MPa(1)		0.5 MPa(1)		$\overline{\varepsilon^{p}_{ps}}$ (%)	A*
E' (MPa)	ν'	E' (MPa)	ν'		
136.7	0.08	176.6	0.08	5.0	0.336 (= $A_p/8$)

(1) : confining pressure

Table 5.3 Input data for cut slope analysis

E' (MPa)	ν'	γ (MN/m^3)	σ_c (MPa)	A_0	A_{fs}	A_r	B_0	S_0
13.79	0.35	0.018	0.206	3.7734	1.0396	0.5805	1.8731	-0.0831

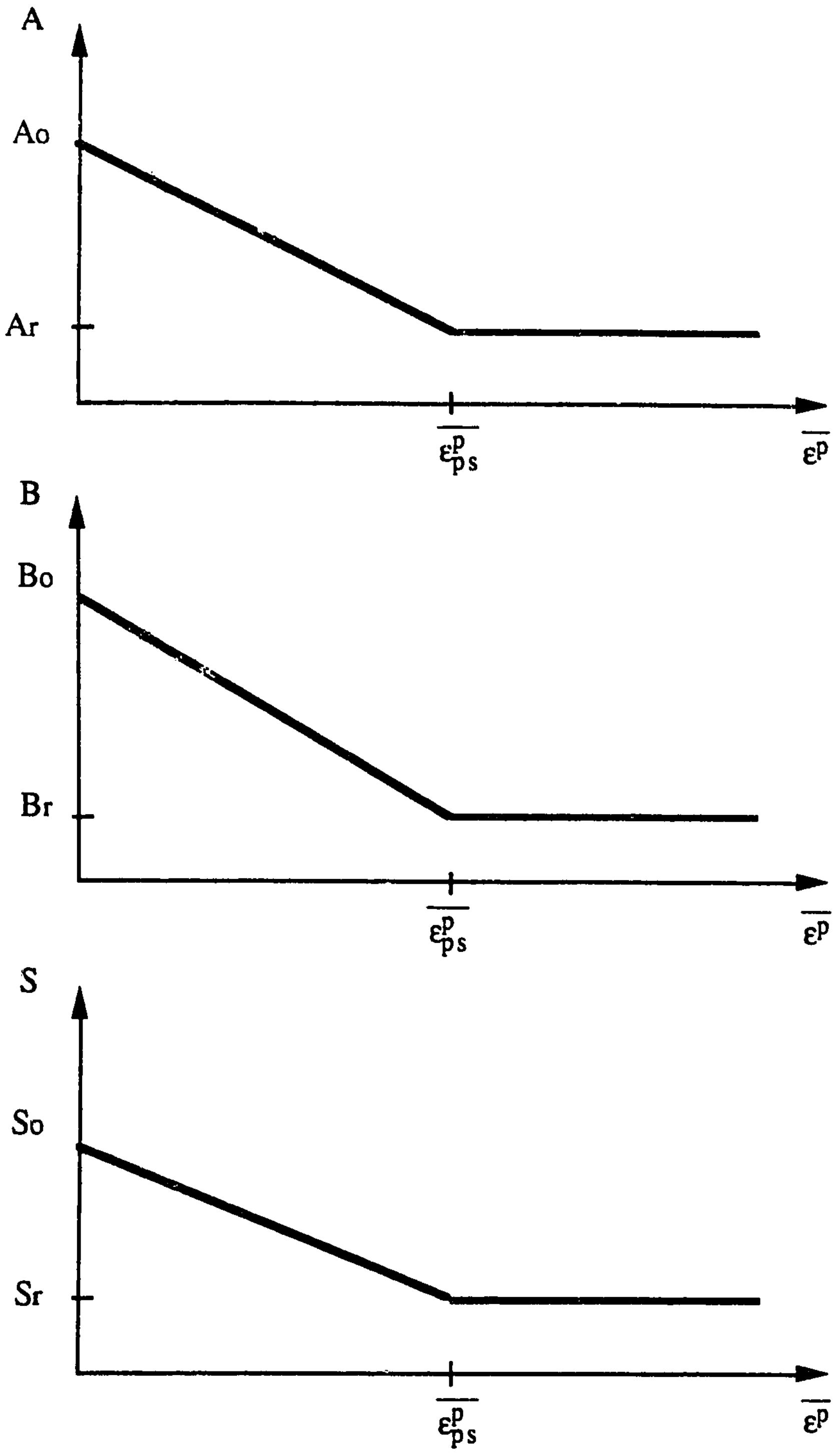

Figure 5.1 Assumed variations of strength parameters for post-peak behaviour

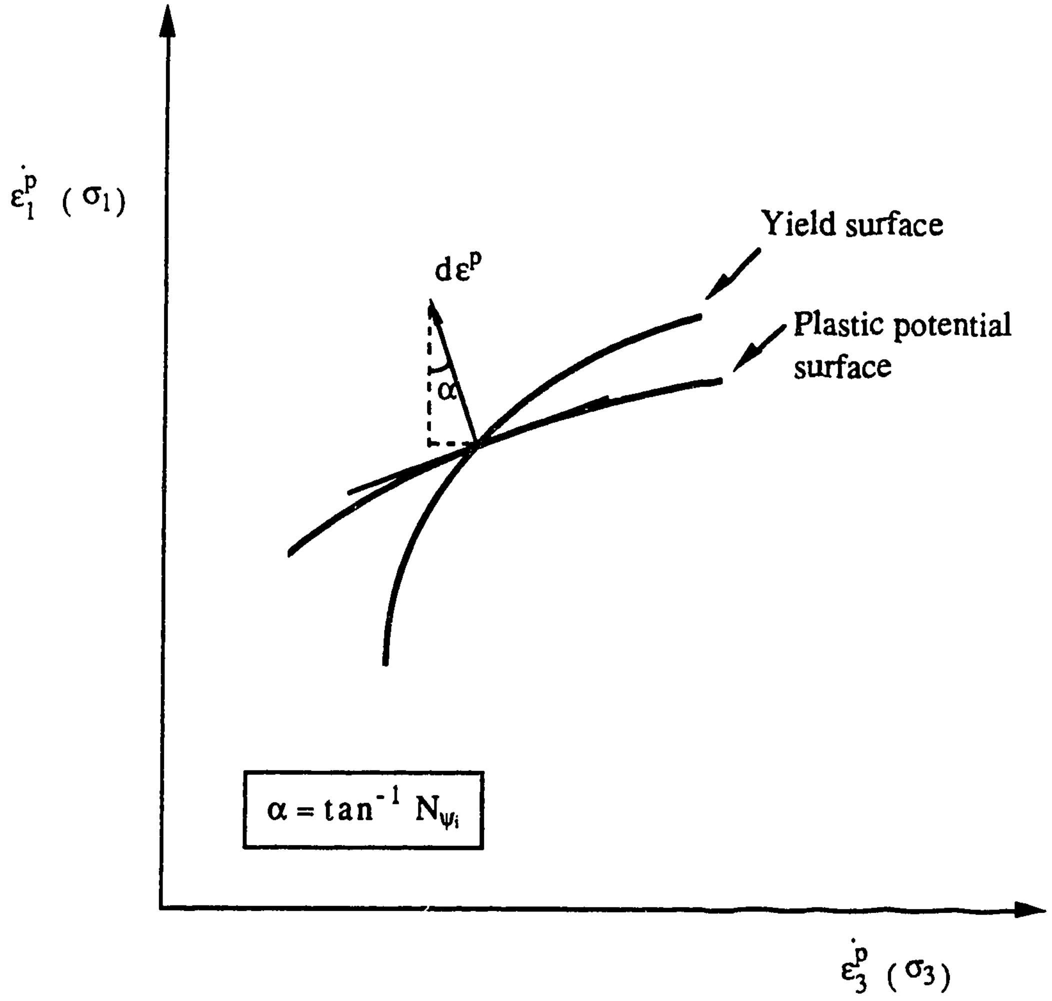
$\dot{\varepsilon}_1^p$ (σ_1)
Yield surface
$d\varepsilon^p$
Plastic potential surface
α
$\alpha = \tan^{-1} N_{\psi_i}$
$\dot{\varepsilon}_3^p$ (σ_3)

Figure 5.2 Yield surface and plastic potential surface

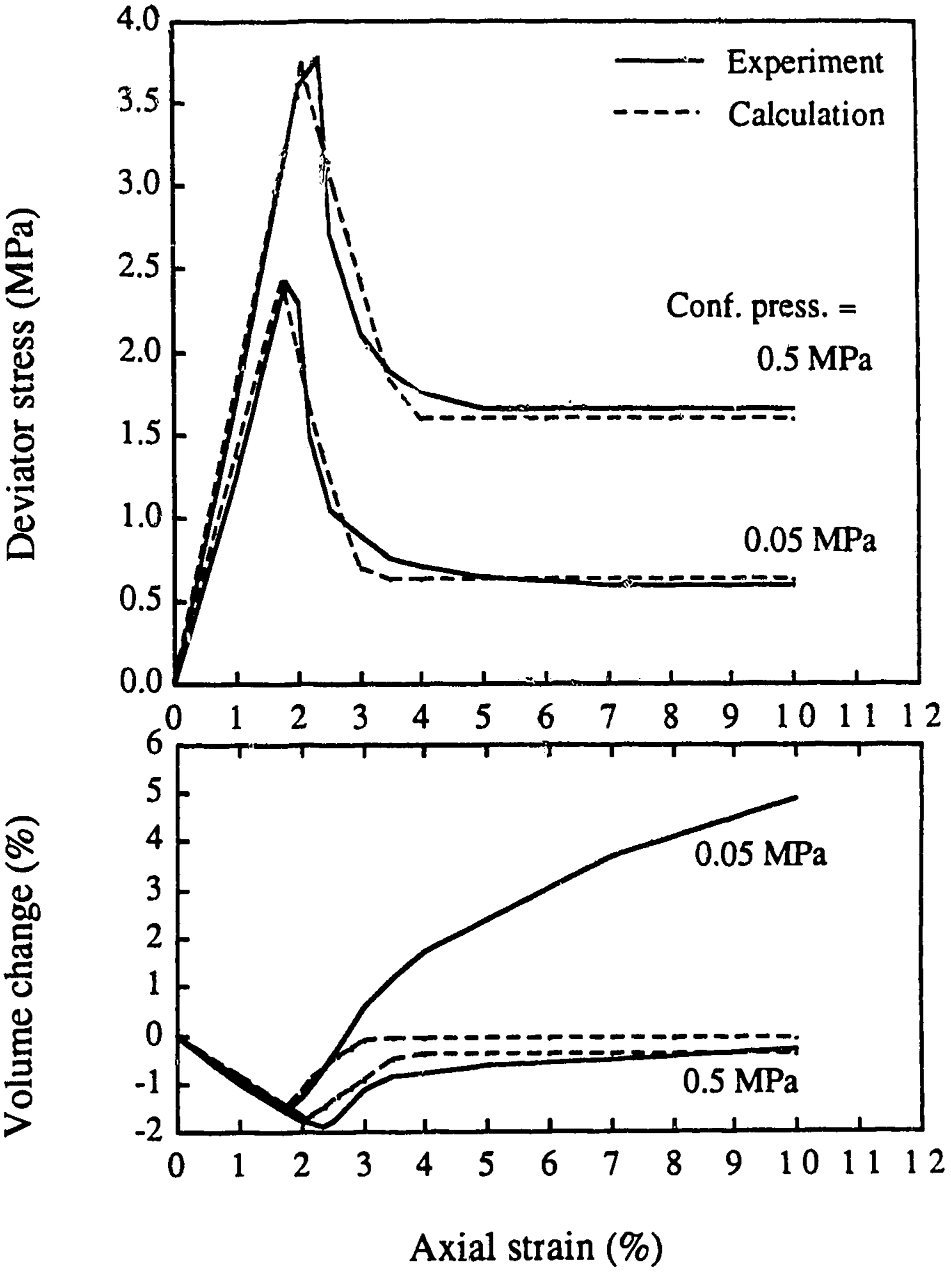

Figure 5.3 Comparison of computation with experimental results for Tohoku Mudstone

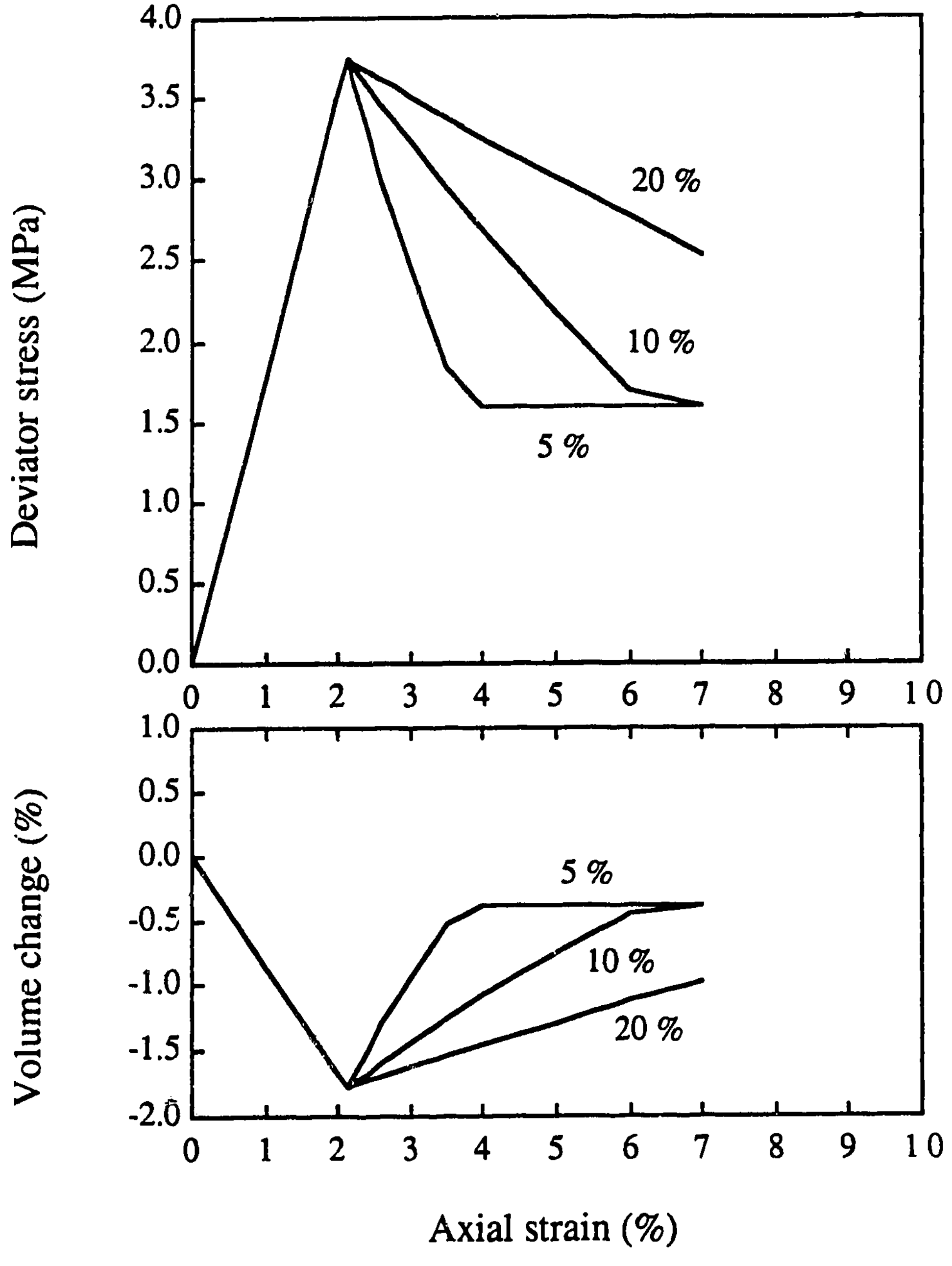

Figure 5.4 Effect of $\overline{\varepsilon^p_{ps}}$ on computed stress-strain relation

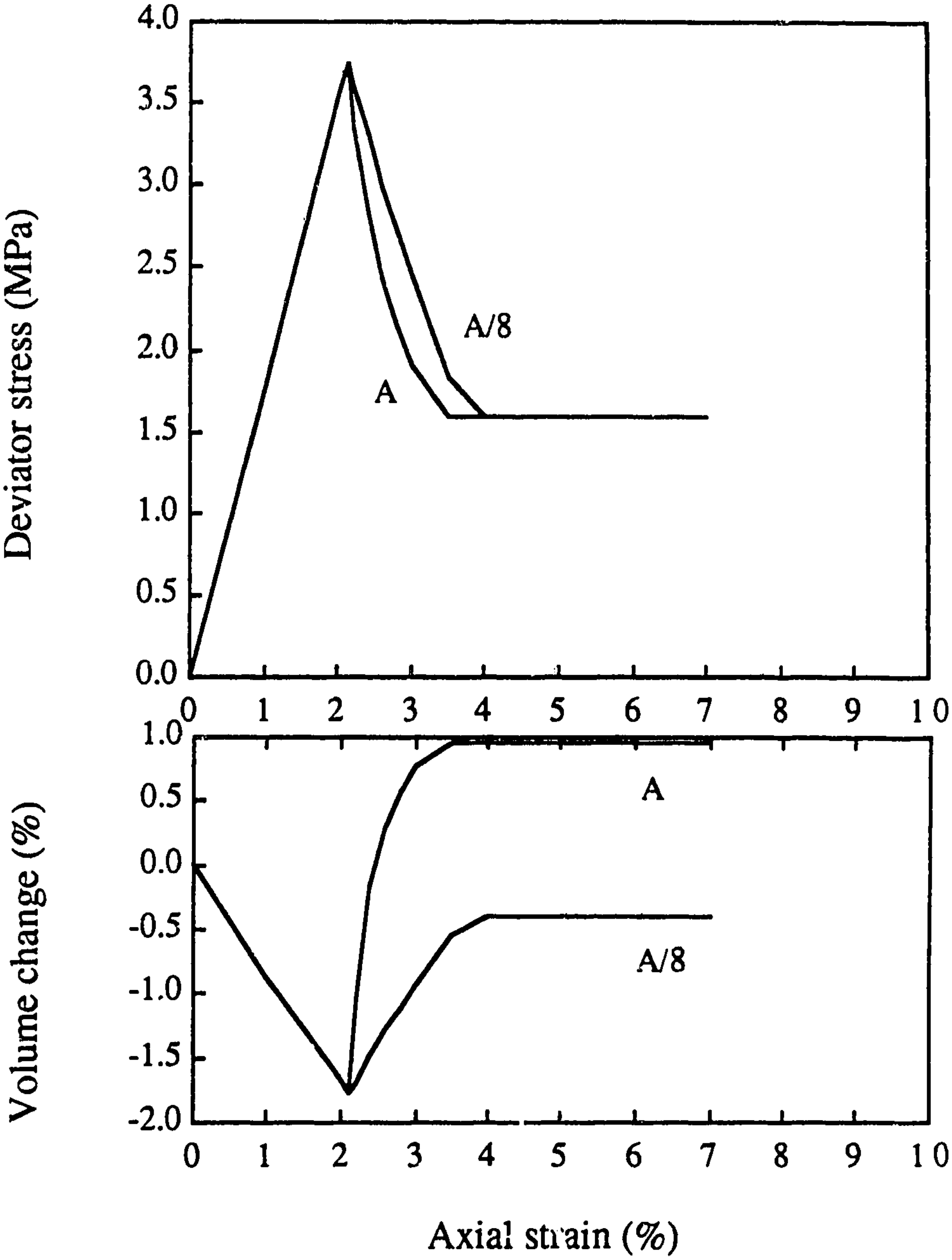

Figure 5.5 Effect of A* on computed stress-strain relation

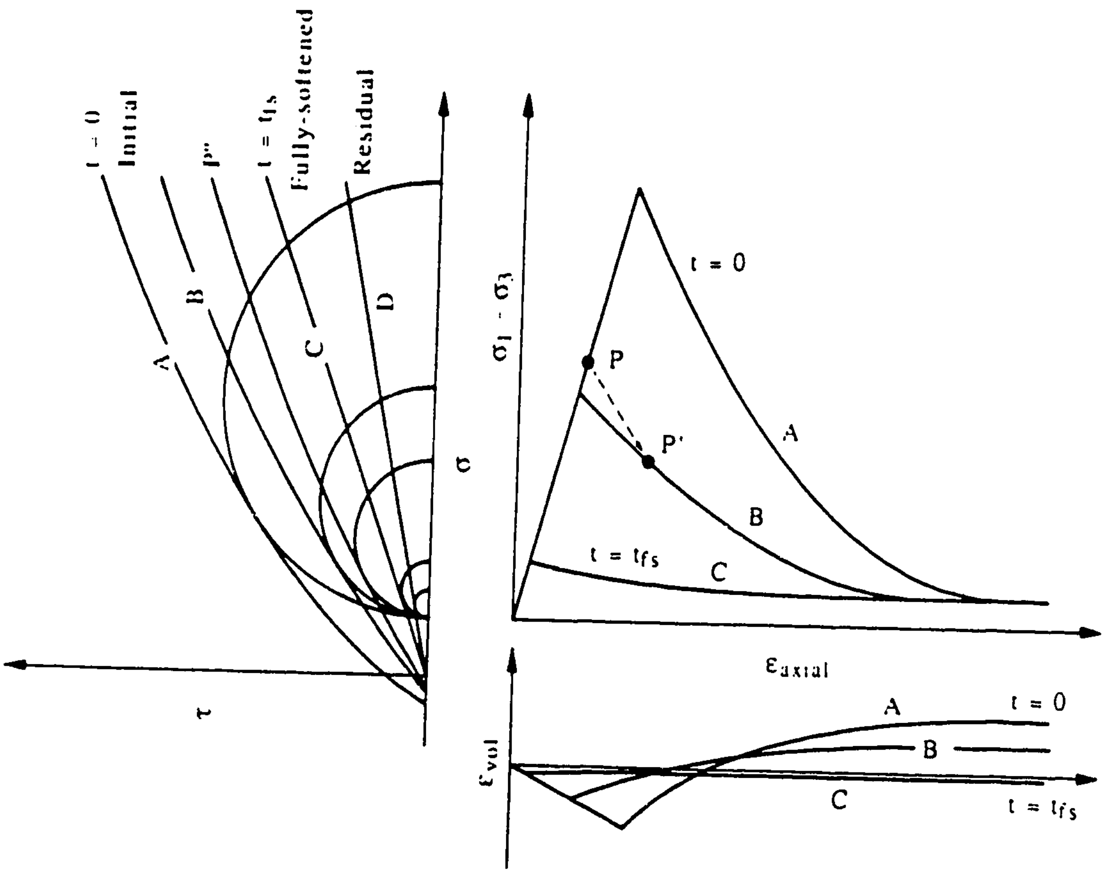
t = 0
Initial
P''
t = t_fs
Fully-softened
Residual
A
B
C
D
σ
τ
σ1 - σ3
t = 0
P
P'
A
B
t = tfs
C
εaxial
A
t = 0
B
εvol
C
t = tfs

Figure 5.6 Variation of stress, strain and strength during softening

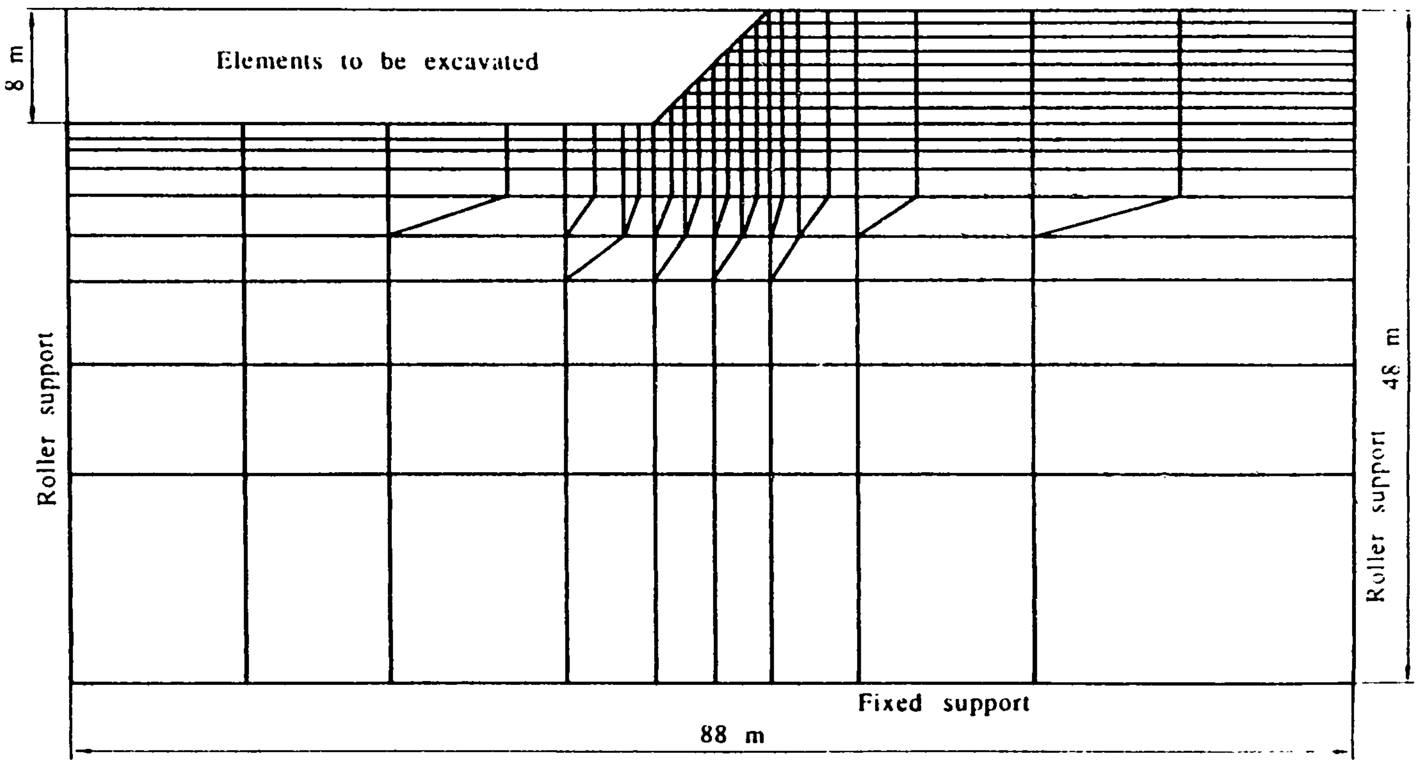
8 m
Elements to be excavated
Roller support
Roller support
48 m
Fixed support
88 m

Figure 5.7 Finite element mesh for cut slope analysis

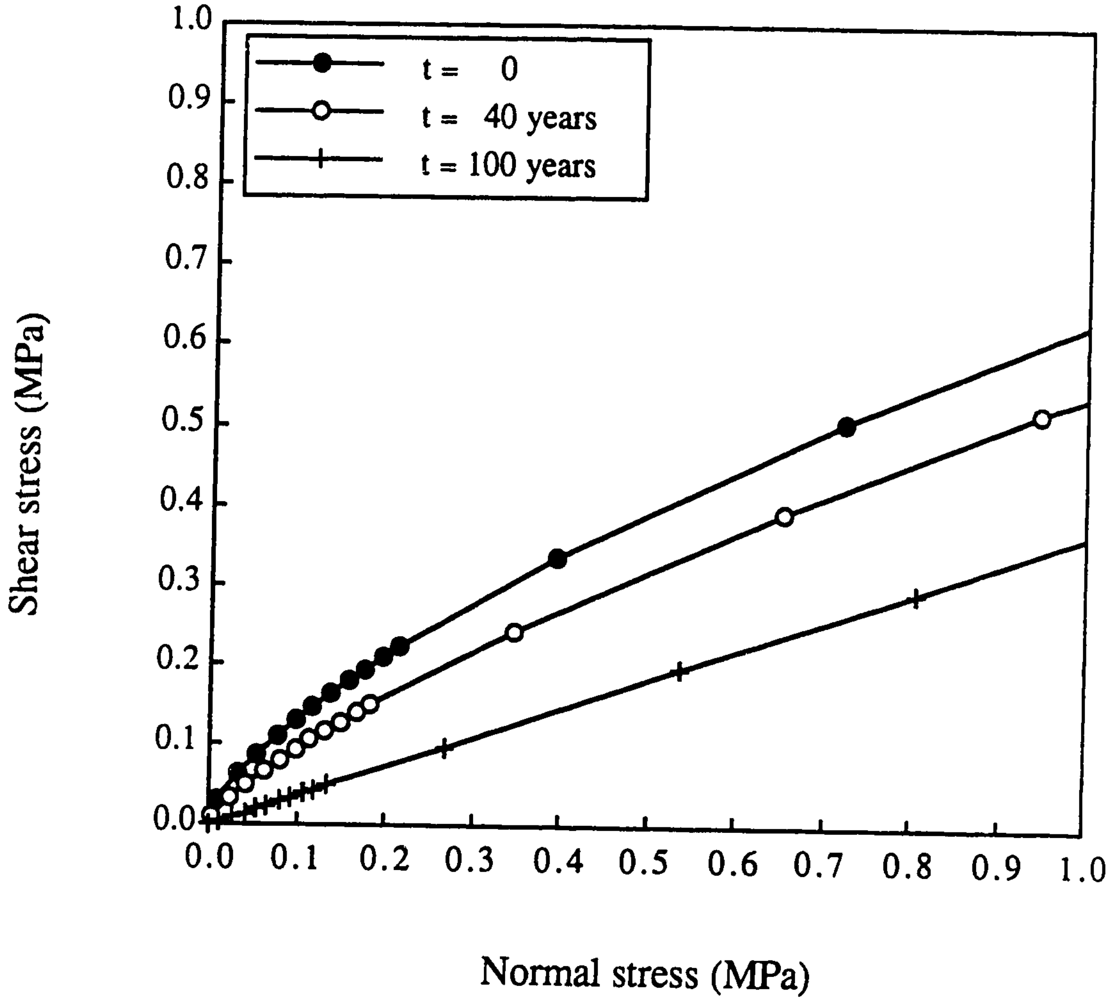

Figure 5.8 Strength envelopes at 0, 40 and 100 years

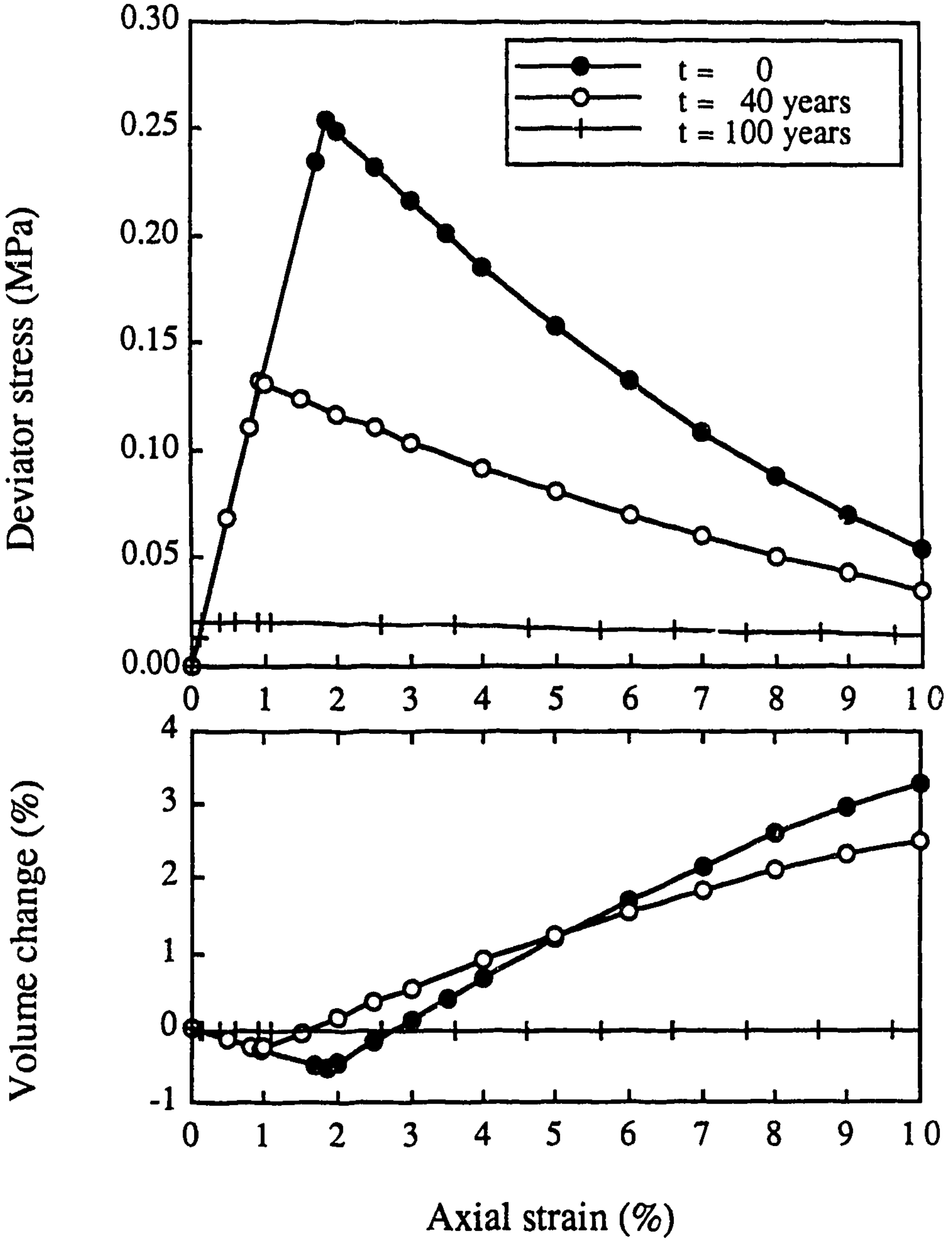

Figure 5.9 Stress and strain relations at 0, 40 and 100 years

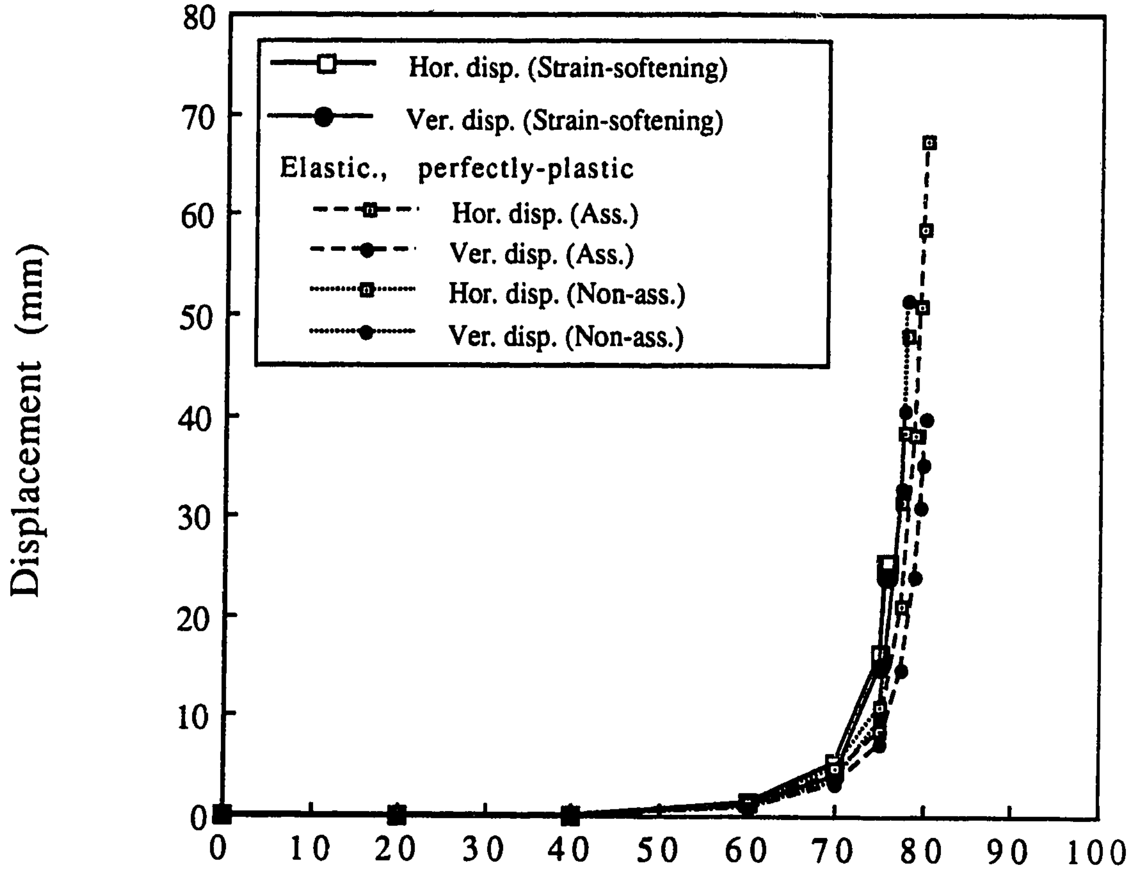

Figure 5.10 Variation of displacements at crest of slope with time

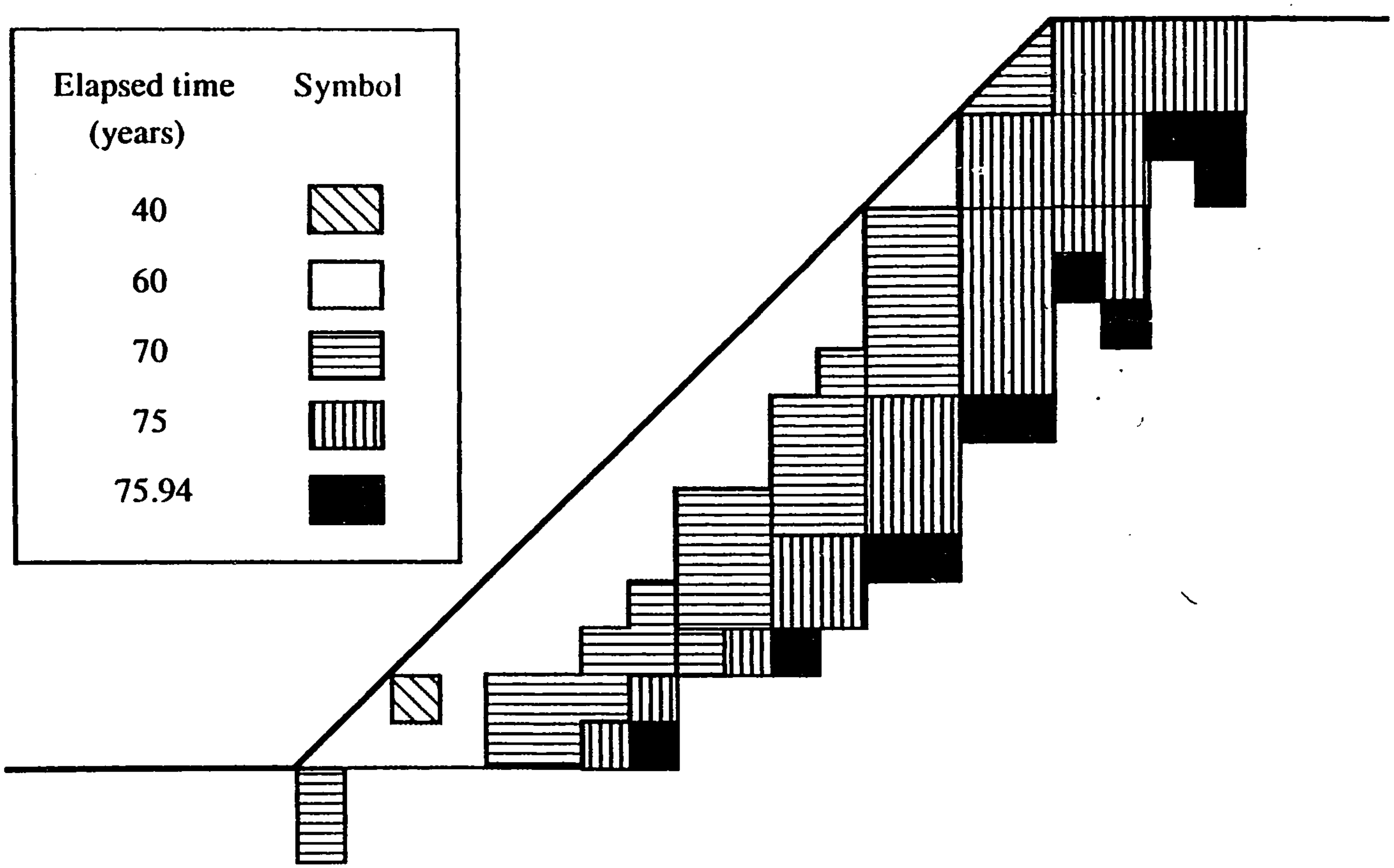
Elapsed time (years)
Symbol
40
60
70
75
75.94

Figure 5.11 Development of plastic zones in slope

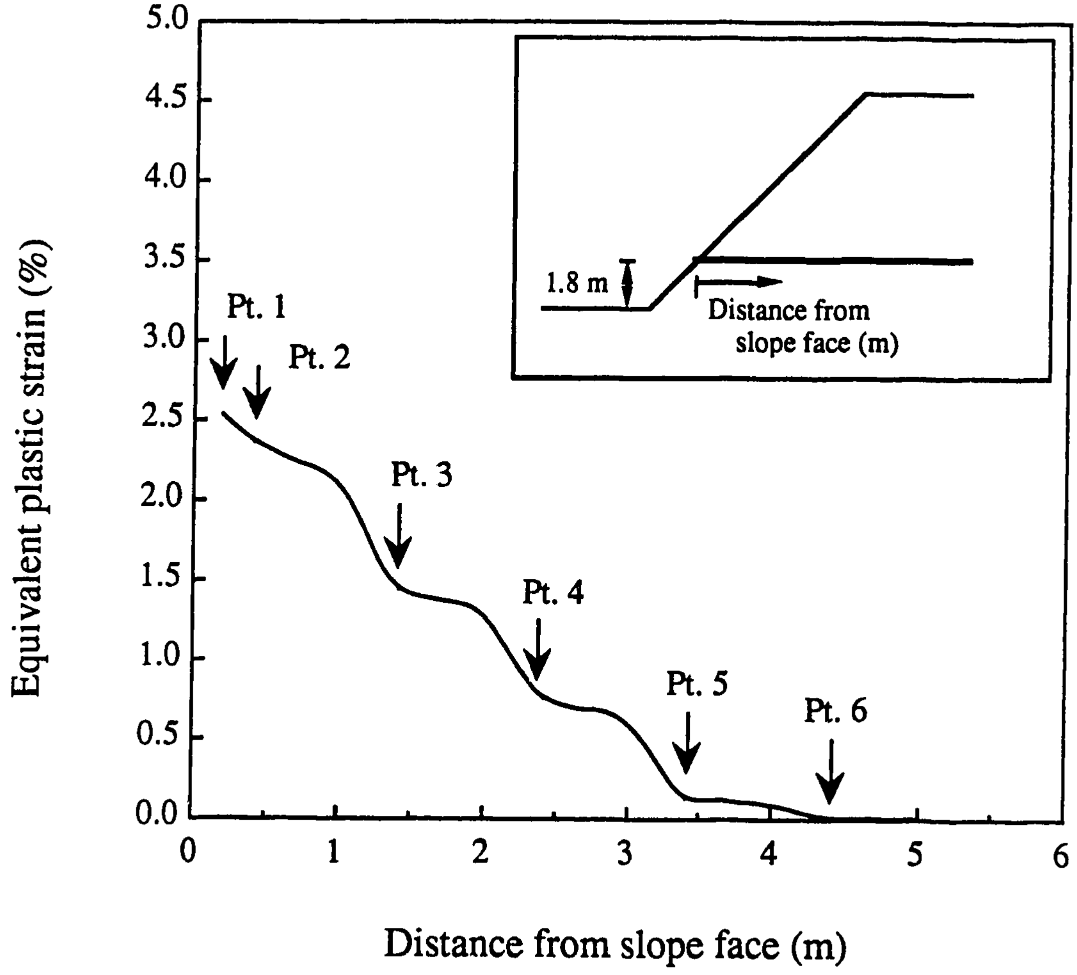

Figure 5.12 Distribution of accumulated equivalent plastic strains along horizontal plane

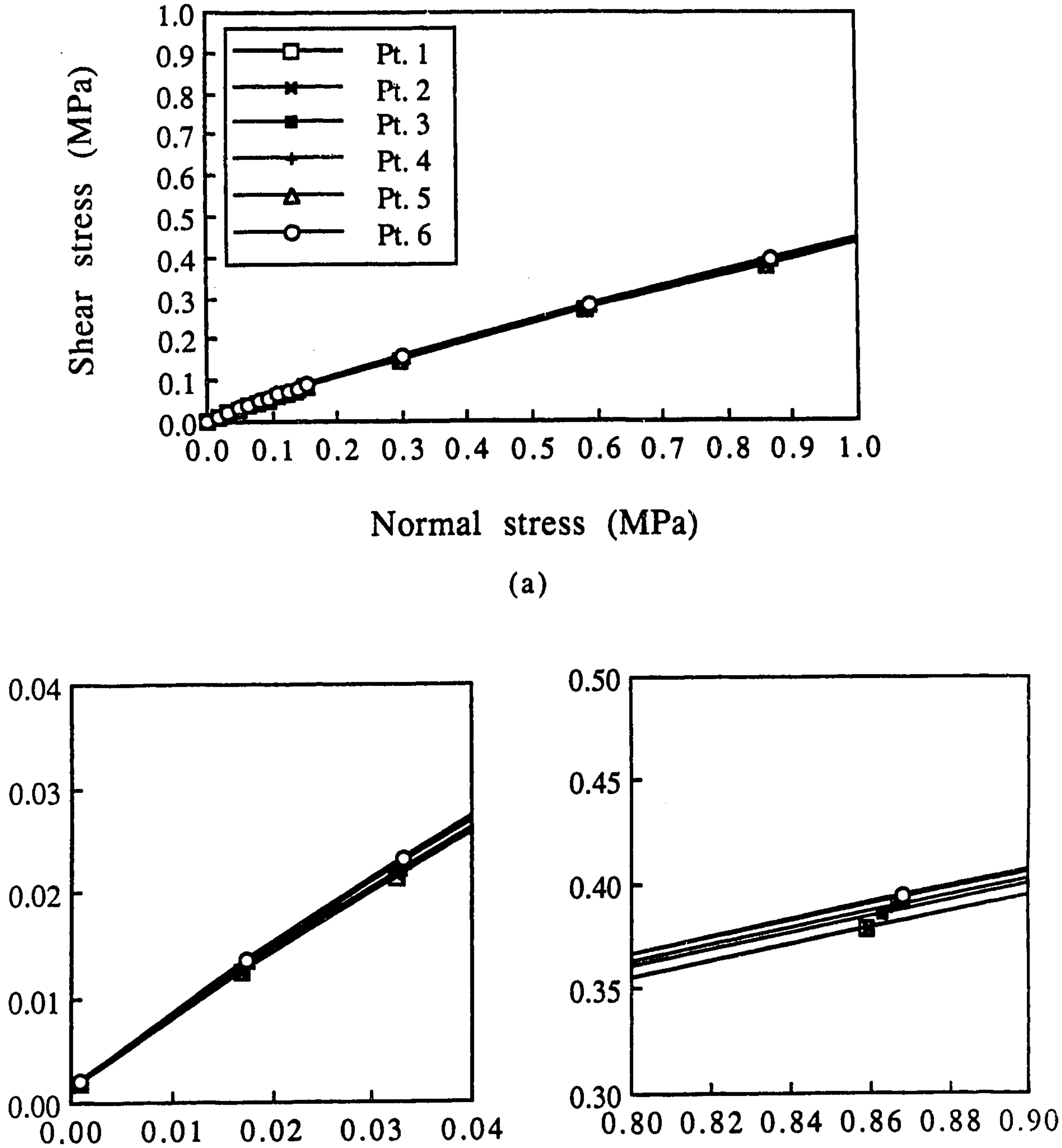

(a)

(b)

(c)

Figure 5.13 Variation of mobilized shear strength envelopes along horizontal plane

6. Analysis of high rock pressure in tunnelling

6.1 Introduction

High rock pressure has been encountered in many tunnelling works in the Tertiary mudstone bedrocks of Japan. In Chapter 2, this high rock pressure encountered during and after the construction of a tunnel in mudstone bedrock was discussed in relation to the mechanism of softening and Noshiro Tunnel No. 4 was described as a case history illustrating this problem. Thus, it was considered that it would be of interest to deal with this problem here, and further, that this case study could serve as an example of how rock pressure is developed in the lining of a tunnel if it is constructed in a similar geologic condition.

The main purpose of this chapter is to demonstrate the development of rock pressure on the lining of a tunnel with time due to the softening of rock surrounding the tunnel. For this purpose, finite element analyses are carried out using the elastic, perfectly plastic model and strain-softening model introduced in the previous chapters. The geotechnical data related to a tunnel analyzed are based on the case history of Noshiro Tunnel No. 4.

6.2 Noshiro Tunnel No. 4

6.2.1 Brief description of tunnel

Noshiro Tunnel No. 4 is briefly described in the following paragraphs. A detailed description of the tunnel can be found in the literature (Nakano, 1974, 1979 and 1981).

Noshiro Tunnel No. 4 is one of the main waterway tunnels constructed as part of the irrigation and reclamation projects in the Akita prefecture located in northern Japan. The tunnel has a horse-shoe shape, 3.6 m wide and 3.5 m high and was driven at a depth of 25 to 30 m in the Neogene mudstone bedrock of the Fujikotogawa formation. The geologic condition and tunnel location are shown in Figure 6.1. The excavation was carried out by conventional drilling and blasting techniques with steel ribs and concrete lining. During the tunnelling, very high rock pressure was encountered. Figure 6.2 shows typical measurements of the stresses induced in steel supports at Test Section (II) during construction. These are fibre stresses computed from strains measured by means of strain gauges installed on steel supports. The stresses increased gradually with time due to softening. A significant increase in the stresses observed about two weeks after the installation of supports, however, could be also due to the change in the stress conditions around the tunnel from three dimensional to two dimensional response as a results of the advance of the excavation face. The rock pressure finally exerted on the supports is estimated to be 120-160 kPa vertically and 90 kPa horizontally.

6.2.2 Geotechnical properties of bedrock material

The bedrock material at the tunnel site is the typical Petroliferous Neogene Tertiary mudstone and its index properties are summarized in Table 6.1. For the purpose of reference, data on other mudstones are also listed in the table.

Triaxial compression tests and direct shear tests were carried out on intact samples of the bedrock material (Nakano, 1979). The results of the direct shear tests are plotted in Figure 6.3. The stress-strain curves obtained from the triaxial tests are given in Figure 2.9 in Chapter 2. The corresponding volume change curves were not reported.

The mudstone has been known to disintegrate upon immersion when mechanical disturbance is applied. Figure 6.4 shows the swelling curves of remoulded mudstone samples under different vertical pressures. From the results of swelling tests and uniaxial compression tests, relationships among applied vertical pressure, water content and uniaxial compression strength are established as shown in Figure 6.5.

6.3 Finite element analysis

6.3.1 Determination of input data

The peak shear strength parameters are determined based on the results of drained direct shear tests on mudstone samples taken from the tunnel site. The fully-softened strength parameters are determined from the test results on the remoulded samples and are expressed, in terms of Mohr-Coulomb strength parameters, as:

$$c' = 0 \qquad \phi' = 25°$$

Since the residual strength of this mudstone is not reported in the literature, the following values are assumed, referring to residual strengths of other Japanese Tertiary mudstones:

$$c' = 0 \qquad \phi' = 15°$$

The strength parameters used in subsequent analyses are summarized in Table 6.2 and the corresponding strength envelopes are shown in Figure 6.3.

Deformation moduli, namely Young's modulus and Poisson's ratio, for the mudstone are taken from the literature and given in Table 6.2.

In the subsequent analyses, ground is assumed to have either elastic, perfectly plastic or strain-softening characteristics. In the elastic, perfectly plastic case, no plastic volume change is assumed to occur. For the strain-softening case, the parameters controlling the degree of strain-softening, $\overline{\varepsilon^{p}_{ps}}$ and A*, are assumed as 15% and 0.5, respectively. The computed stress-strain and volume change curves are shown in Figure 6.6.

Figure 6.7 illustrates softening of the mudstone in terms of normalized uniaxial compression strength. This figure is constructed from the swelling curves and relation among vertical stress, water content and uniaxial compression strength (Figures 6.4 and 6.5). From Figure 6.7, the strength reduction-rate parameters, **a**, **b** and **c**, are determined, by trial and error, as 1.0, 2.5 and 0.8, respectively. As can be seen in Figure 6.7, the fully-softened condition is reached in about 27 days. It is of interest to note that Hirano *et al.* (1983)

provided a very close estimate of 25 days for the time to reach a fully-softened condition for Tertiary mudstone at a different tunnel site which was obtained from finite element back-analyses of tunnel deformations. With these parameters, the variation in shear strength is calculated. Figure 6.8 shows the variation in strength envelopes with time.

The concrete lining is assumed to be linear elastic. The deformation properties are given in Table 6.2.

6.3.2 Analysis procedure

The ground is discretized by three hundred and fifteen four-node isoparametric elements with a total of three hundred and forty-four nodes, as shown in Figure 6.9. The Noshiro Tunnel is approximated as a D-shaped tunnel with a height and width of 3.6 m and located 28 m below ground surface.

The finite element analysis starts with the application of an initial stress to the ground. Two initial stress conditions are considered: $K_0 = 1$ and $K_0 = 1.5$. Then, tunnelling is simulated by a gradual removal of elements within tunnel cross section. After this excavation step, a concrete lining is installed by re-activating relevant elements which have been killed during excavation. Then, softening of the ground starts. Since the lining is installed after the completion of excavation in this analysis, no stress will exist in the lining elements at this time, as noted by Katzenbach (1981). Thus, subsequently developed stress is due solely to softening. No attempt was made to model three dimensional effects resulting from the advance of excavation face. This analysis procedure certainly departs from reality, but since the main interest of this analysis concerns the stresses developed during softening and the variation of those stresses with time, it is felt that this analysis procedure can be adopted.

6.4 Results of analysis and discussion

All the calculations conducted have been terminated at an elapsed time of 25 days instead of 27 days to reduce computing costs. The preliminary study showed that even if the analyses had been continued to 27 days collapse of the tunnel-bedrock system would not have occurred.

The variations with time in normal stresses developed at the floor, spring line and roof within a lining are shown in Figures 6.10, 6.11 and 6.12, respectively. These stresses are evaluated at Gaussian integration points near the outer edge in a lining element. The ground is assumed elastic, perfectly plastic. At the floor, negligible stress is developed at early stages for $K_0 = 1$, then the stress increases gradually with time and reaches about 750 kPa in 25 days. For $K_0 = 1.5$, stress increases rapidly from the beginning and reaches as high as 1650 kPa. At the roof, stress is very small for $K_0 = 1$ and the magnitude of stress increases as the K_0 value increases. At the spring line, stress increases gradually for both initial stress conditions. The stresses of 400 kPa and 250 kPa are developed for $K_0 = 1$ and 1.5, respectively. It appears that an increase in K_0 results in an increase in stresses developed at roof and floor and a decrease at spring line. Figures 6.13, 6.14 and 6.15 show the tangential stress variation with time evaluated at the same locations as above. The variation of these stresses is quite similar to that of the normal stresses. These stress variations seem to be consistent with field measurements shown in Figure 6.2, although the magnitude of stress is quite different. This discrepancy in the stresses is attributed to ignoring the effect of swelling in the analysis. It is important to note that very small rock pressure is reported to have been measured in the supports at Noshiro Tunnel No. 3 and No. 6 which was constructed in the same geological condition as Tunnel No. 4 but whose mudstone has higher uniaxial compression strength and considerably lower swelling capacity upon mechanical disturbance compared with the mudstone at Tunnel No. 4.

Normal stress distributions along the lining are shown in Figures 6.16 and 6.17 for $K_0 = 1$ and 1.5, respectively. Large inward stresses are developed at the floor and spring line. On the other hand, much smaller stresses are induced in the roof area. An increase in K_0 induces larger stresses at the floor and roof and smaller stresses at the spring line. In both cases, a significant stress concentration is created at the lower right corner of the opening.

Plastic zones developed during softening are shown in Figures 6.18 and 6.19 for $K_0 =1$ and 1.5, respectively. Yielding starts near the lower right corner of tunnel and propagates around the tunnel. Relatively large plastic zones are developed at the floor and spring line for $K_0 = 1$. The shape of this plastic zone is quite similar to that obtained from a conventional elasto-plastic finite element analysis.

For $K_0 = 1.5$, a much larger plastic zone is formed around the roof and spring line.

The normal stress variations with time computed using the strain-softening model are shown in Figures 6.20, 6.21 and 6.22. The corresponding tangential stress variations are given in Figures 6.23, 6.24 and 6.25. The development of these stresses are almost the same as that in elastic, perfectly plastic analyses. In comparison with the results of elastic, perfectly plastic analyses, the magnitude of stress developed is slightly larger at the floor and spring line and smaller at the roof. Figures 6.26 and 6.27 show the plastic zones developed for $K_0 = 1$ and 1.5, respectively. Again, these results are very similar to those of elastic, perfectly plastic analyses. A detailed examination of equivalent plastic strains developed in the ground for $K_0 = 1.5$ reveals a maximum value of 1.5% and that most equivalent plastic strains are smaller than 1%. Since the equivalent plastic strain controls the degree of strength reduction, it can be considered that for most zones in the ground, the mobilized shear strengths are close to those in the elastic, perfectly plastic case.

The analysis results presented above show that large inward stresses develop with time at the floor and spring line. The stresses are particularly large at the floor. This suggests that if this tunnel was unlined, significant heaving of the floor would result.

6.5 Summary

A rock pressure problem encountered in tunnelling was dealt with in this chapter, referring to an actual case history: the Noshiro

Tunnel No. 4 in Japan. The main emphasis of the analysis was placed on stresses developed in the lining due to softening of the ground.

The parameters controlling the degree of softening were determined from results of swelling tests and uniaxial compression tests on the bedrock material. The fully-softened condition was estimated to be reached in 27 days.

Two dimensional finite element analyses were carried out using an elastic, perfectly plastic model and a strain-softening model. The K_0 values considered were 1 and 1.5. The results illustrate the variation in stresses developed in the lining with time, which seem to be consistent with field observations. Since stresses considered in these analyses are due solely to softening of the ground and do not include stress components which would be induced during excavation in reality, the magnitude of stress may not be realistic. Nevertheless, it can be concluded that relatively large stresses are developed at floor and spring line due to softening. This indicates that if an unlined tunnel was constructed in a similar geologic condition, heaving of the floor would likely occur. The analysis presented here placed its main interest on softening and the effect of swelling was neglected. The results, however, indicate that this case history is dominated by swelling and not softening.

Table 6.1 Index properties of Japanese Tertiary mudstones

Material	LL(%)	PL(%)	PI(%)	References
Noshiro Tunnel No. 4	96	48	48	Nakano (1979)
Tohoku	130	34	96	Watanabe *et al.* *(1988)*
Shimajiri	73	29	45	Komiya and Shinjo (1984)

Table 6.2 Material properties for analysis of Noshiro Tunnel No. 4

Ao	Bo	So	A_{fs}	A_r	σ_c (MPa)	γ_t (kN/m^3)
3.8608	1.4819	-0.1351	1.4639	0.6984	1.7	0.018

		Concrete	
E' (MPa)	ν'	E' (MPa)	ν'
150.0	0.10	21000.0	0.25

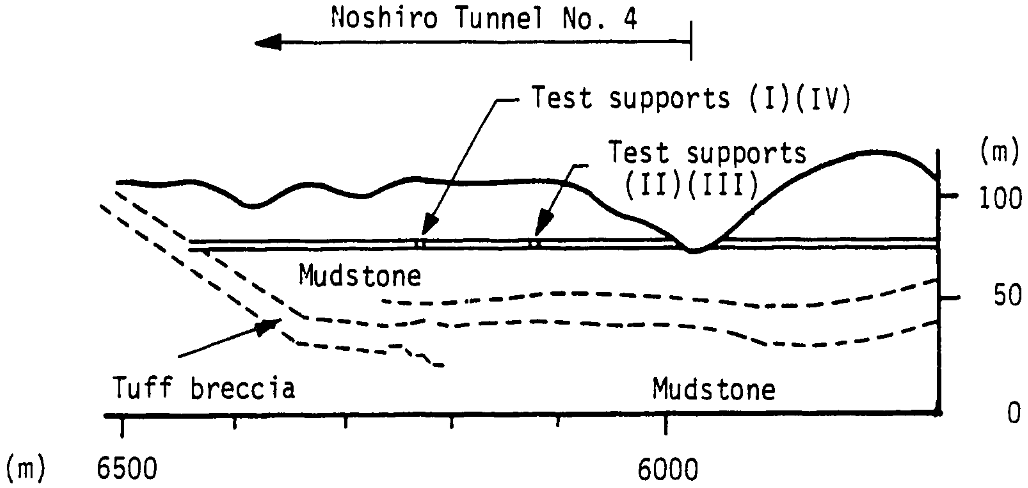
Noshiro Tunnel No. 4
Test supports (I)(IV)
Test supports
(II)(III)
Mudstone
Tuff breccia
Mudstone
(m)
100
50
0
(m)
6500
6000

Figure 6.1 Geology and location of Noshiro Tunnel No. 4 (modified after Nakano, 1979)

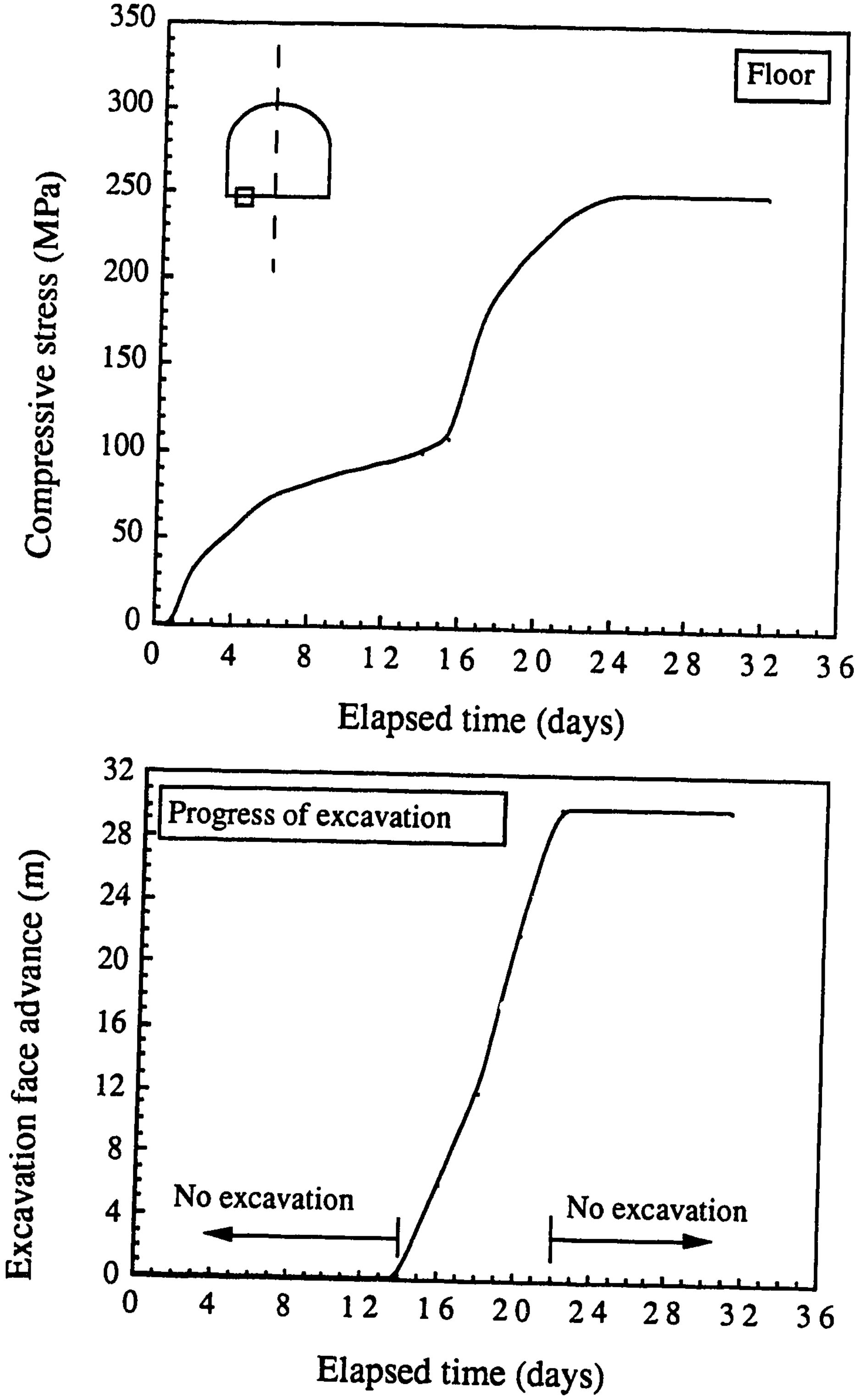

Figure 6.2 Measured fibre stresses at floor, spring line and roof in steel supports (modified after Nakano, 1974)

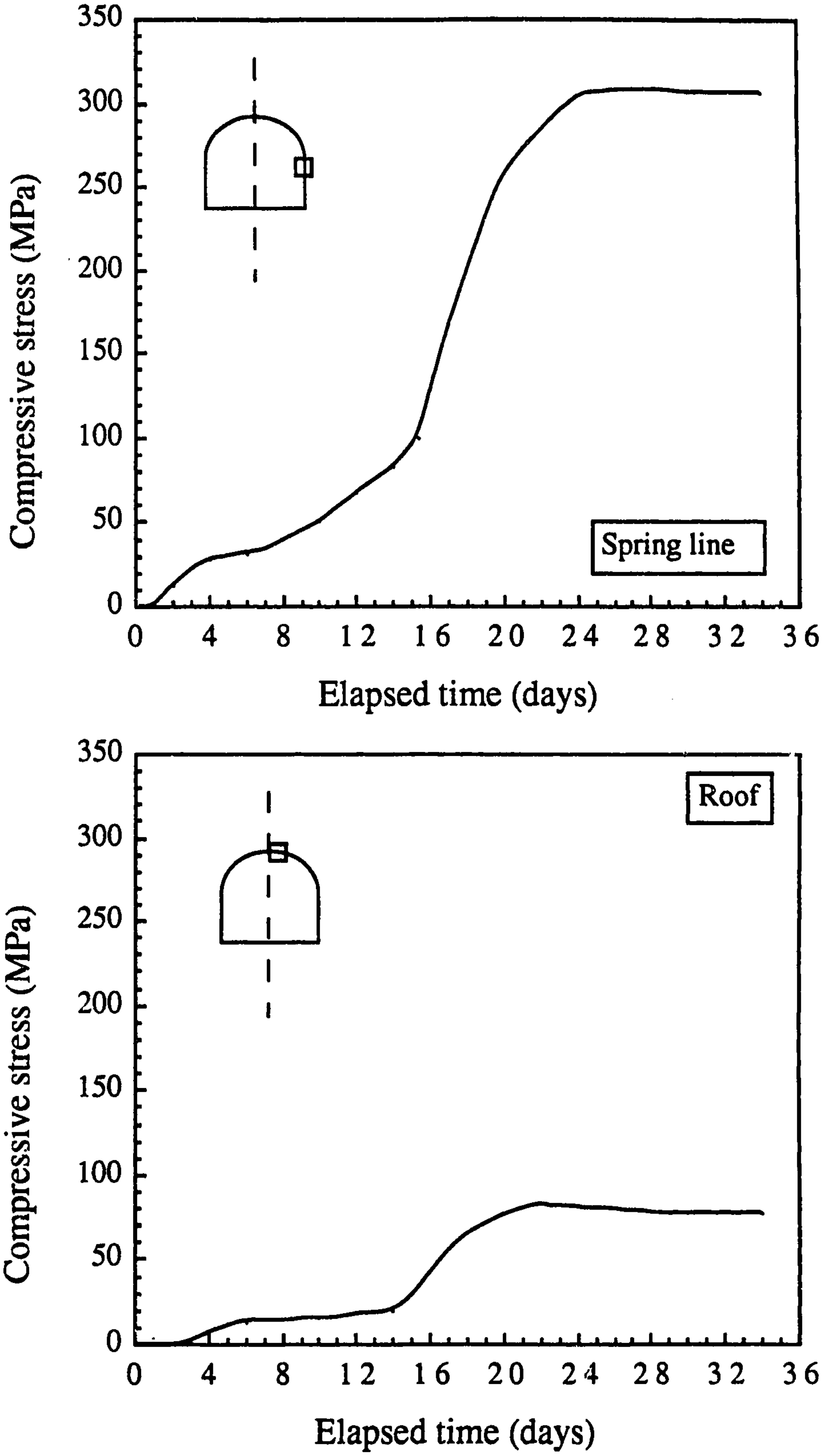

Figure 6.2 Measured fibre stresses at floor, spring line and roof in steel supports (modified after Nakano, 1974) (Continued)

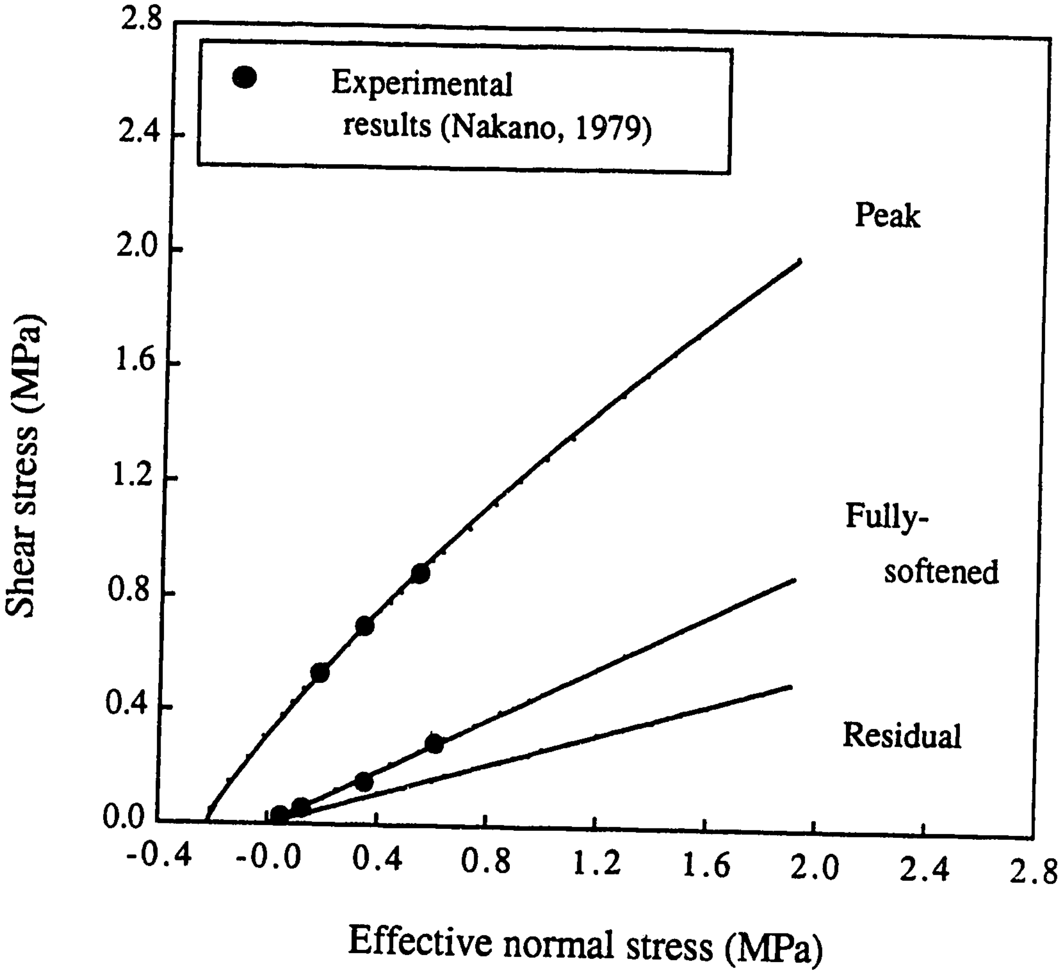

Figure 6.3 Shear strength of mudstone of Noshiro Tunnel No. 4

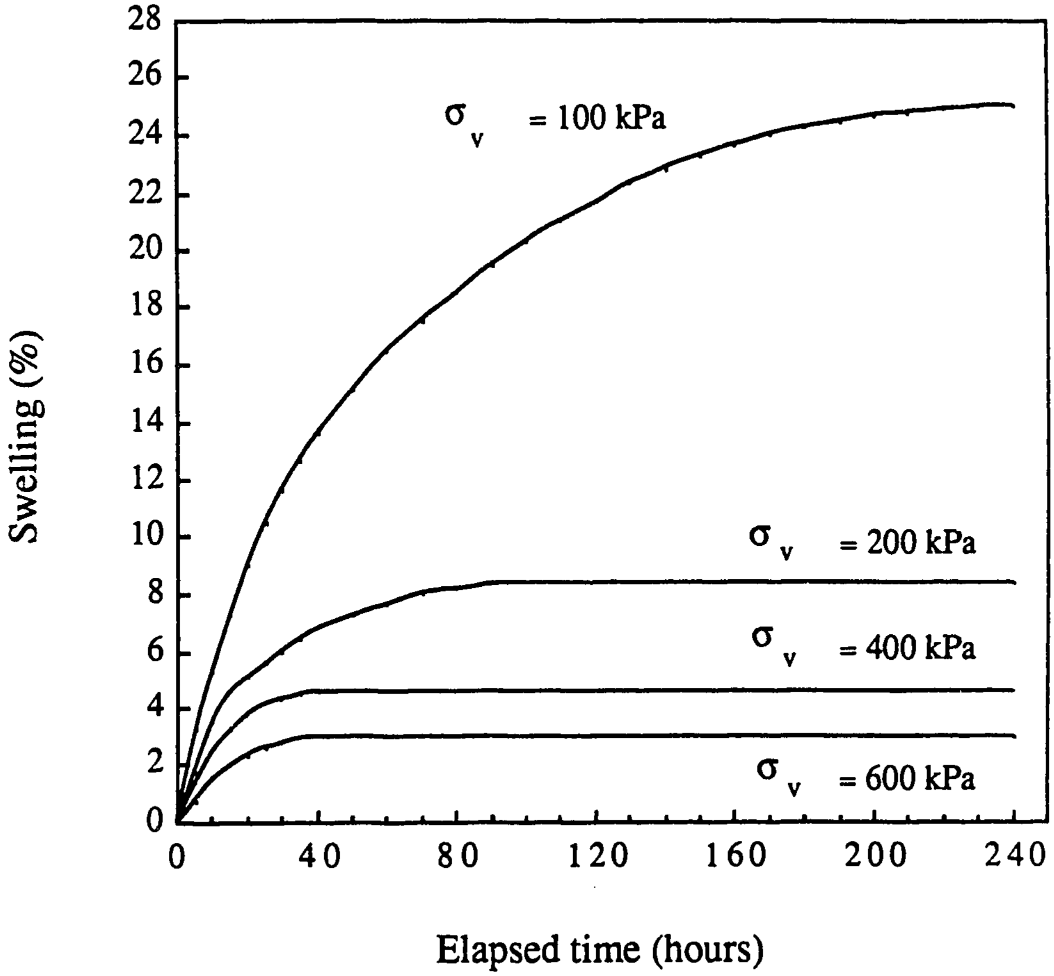

Figure 6.4 Swelling of remoulded mudstone under various vertical pressures (modified after Nakano, 1979)

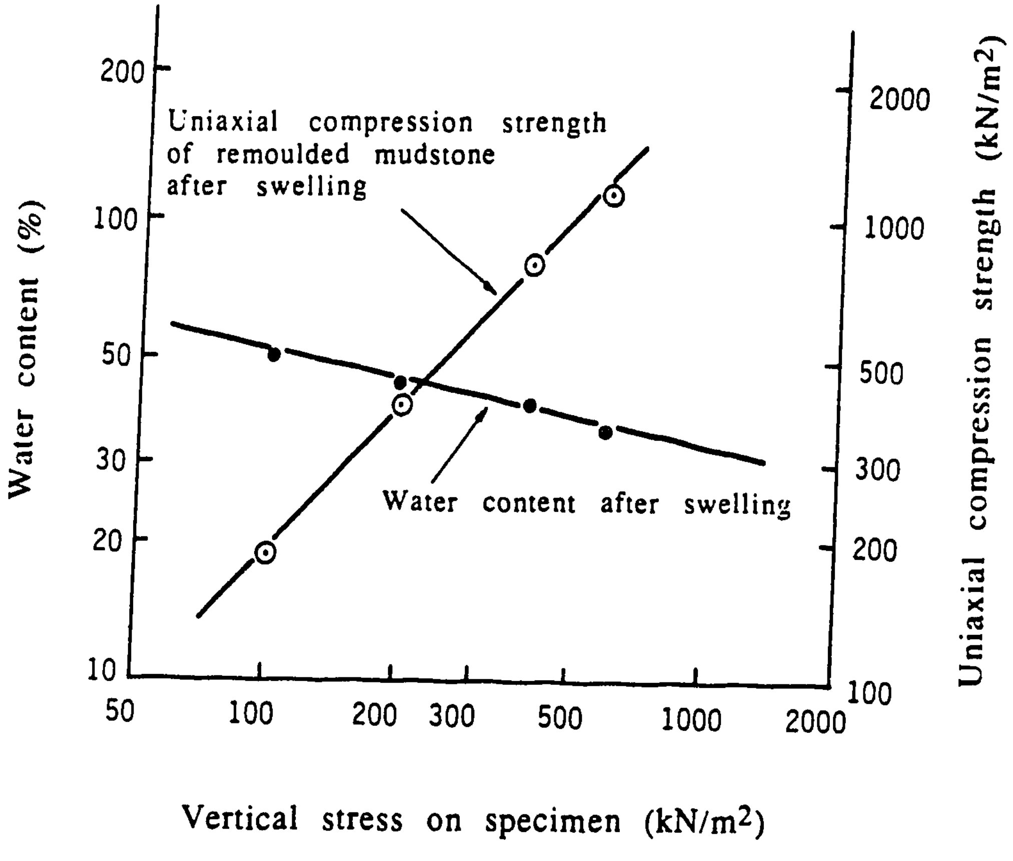

Figure 6.5 Relation among vertical pressure, water content and uniaxial compression strength of mudstone (modified after Nakano, 1979)

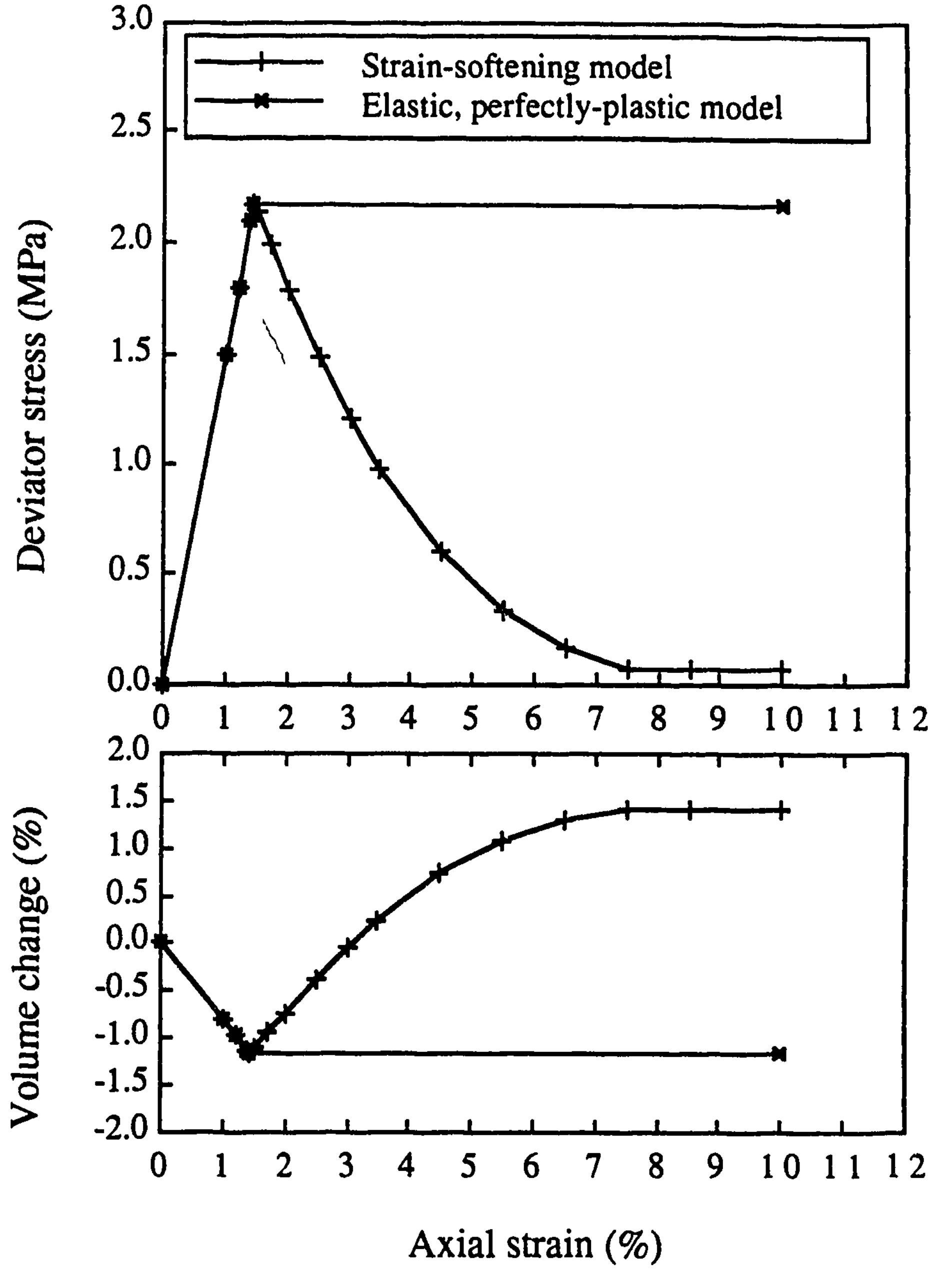

Figure 6.6 Input stress-strain relations

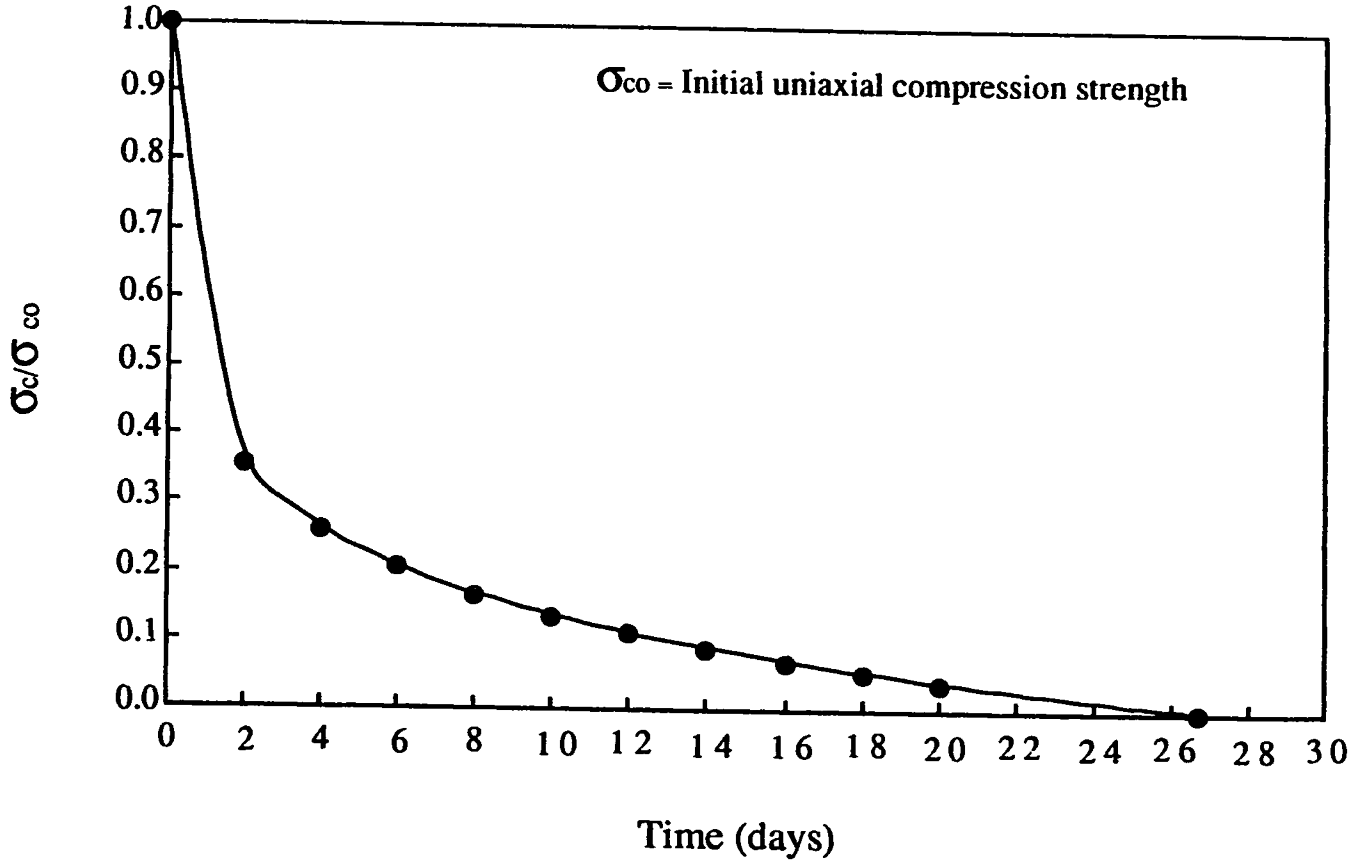

Figure 6.7 Softening of mudstone in terms of normalized uniaxial compression strength

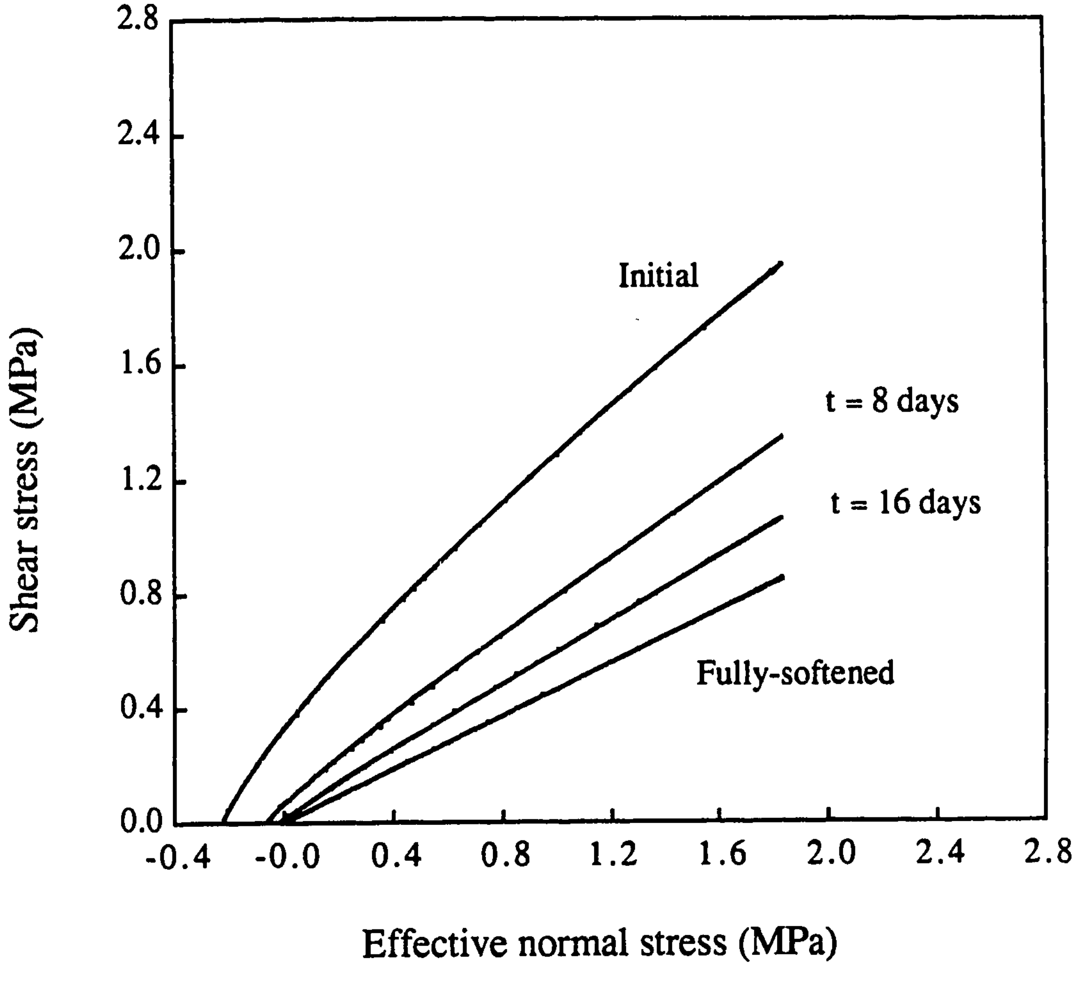

Figure 6.8 Input variation of shear strength with time

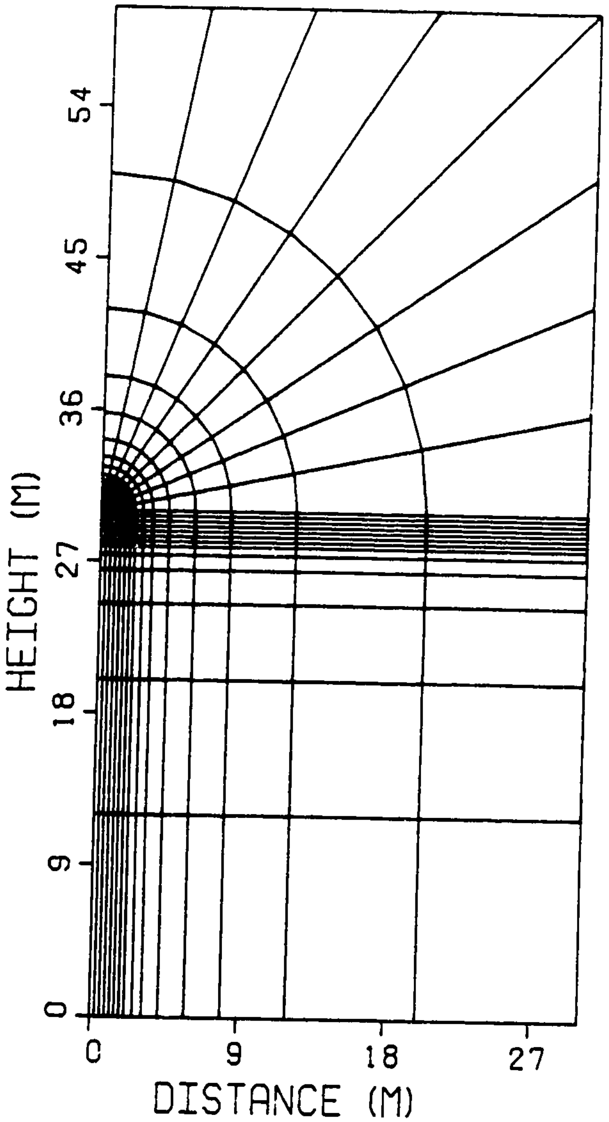
HEIGHT (M)
0
9
18
27
36
45
54
DISTANCE (M)
0
9
18
27

Figure 6.9 Finite element mesh for analysis of Noshiro Tunnel No. 4

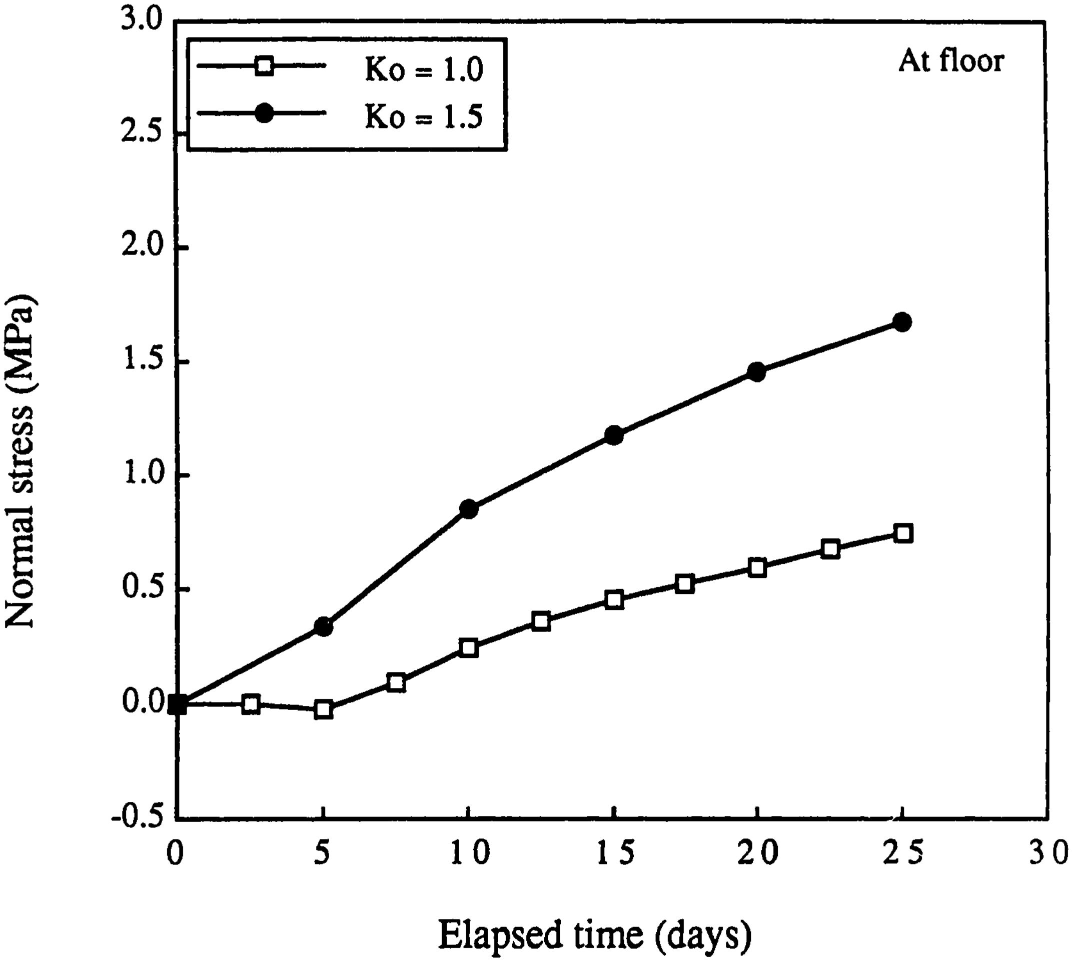

Figure 6.10 Variation of normal stress at floor with time (elastic, perfectly-plastic model)

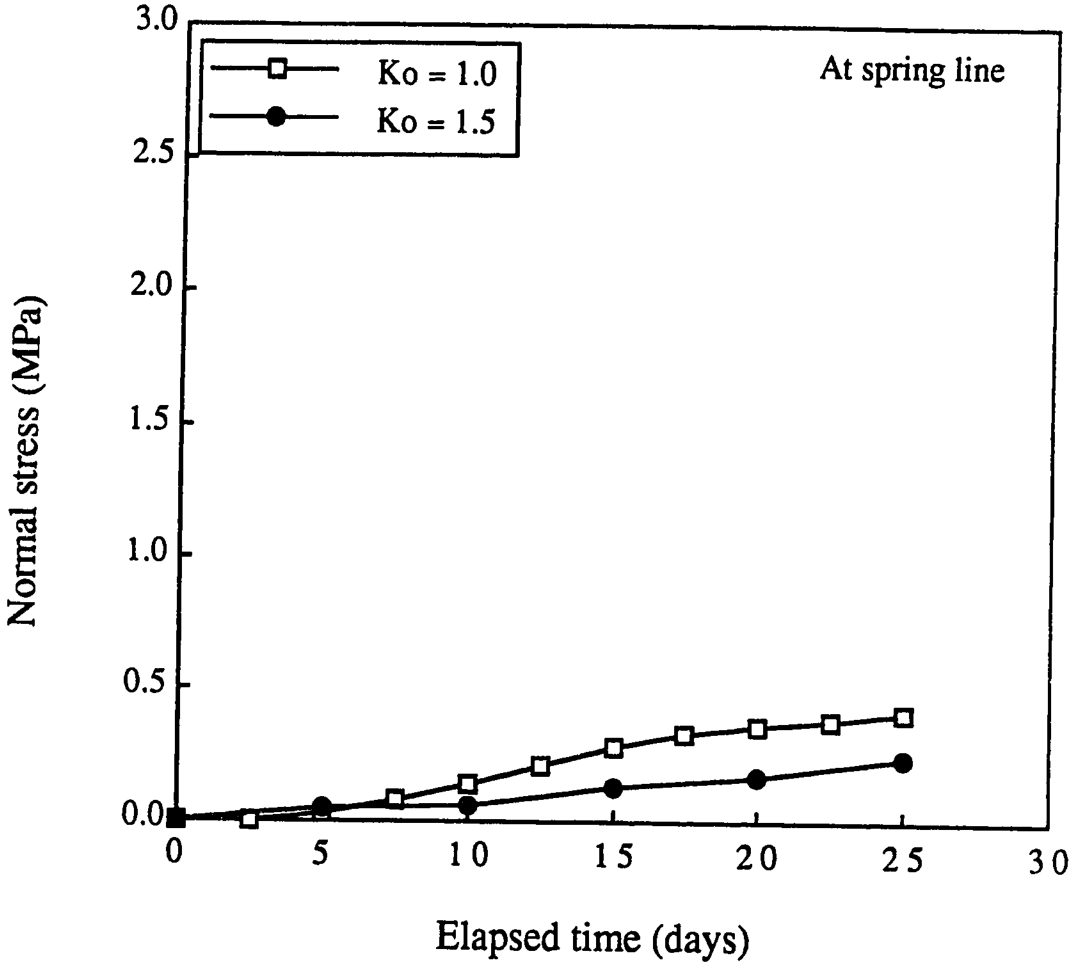

Figure 6.11 Variation of normal stress at spring line with time (elastic, perfectly-plastic model)

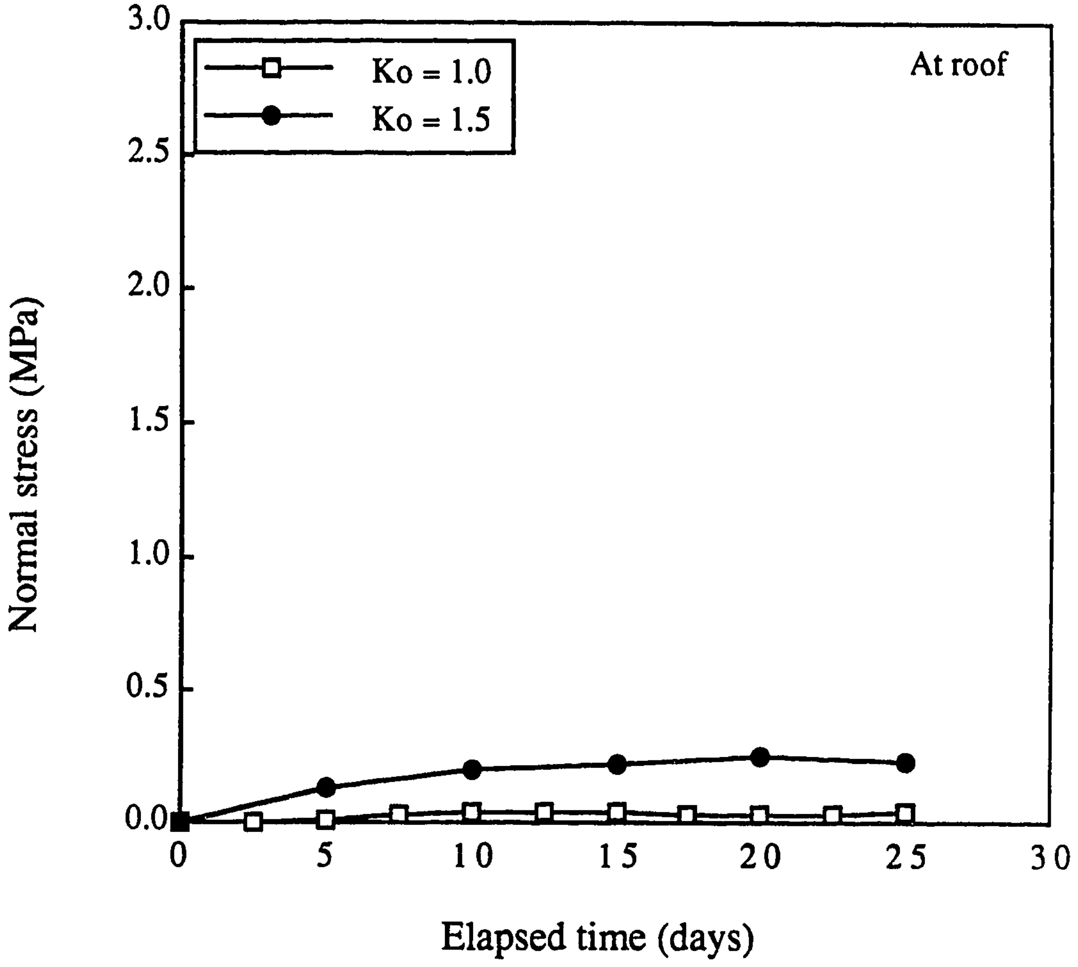

Figure 6.12 Variation of normal stress at roof with time (elastic, perfectly-plastic model)

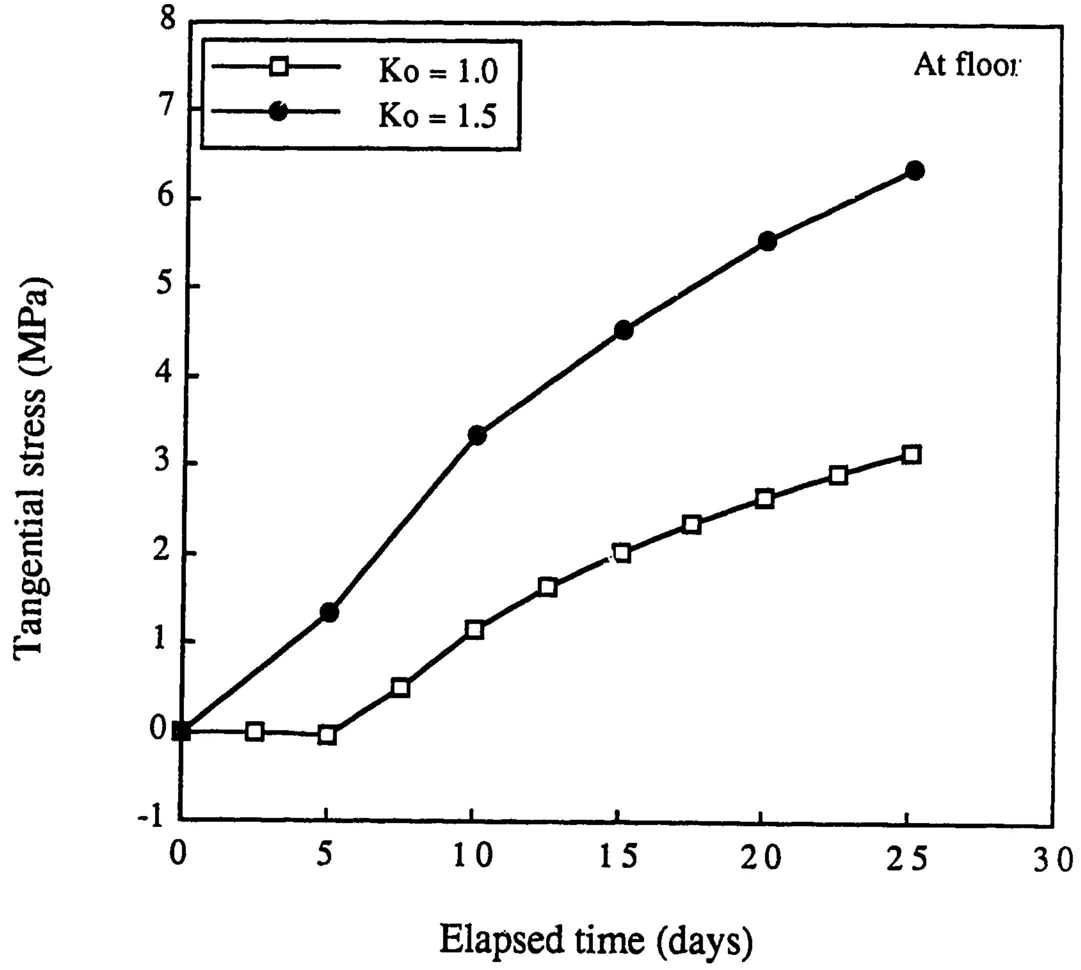

Figure 6.13 Variation of tangential stress at floor with time (elastic, perfectly-plastic model)

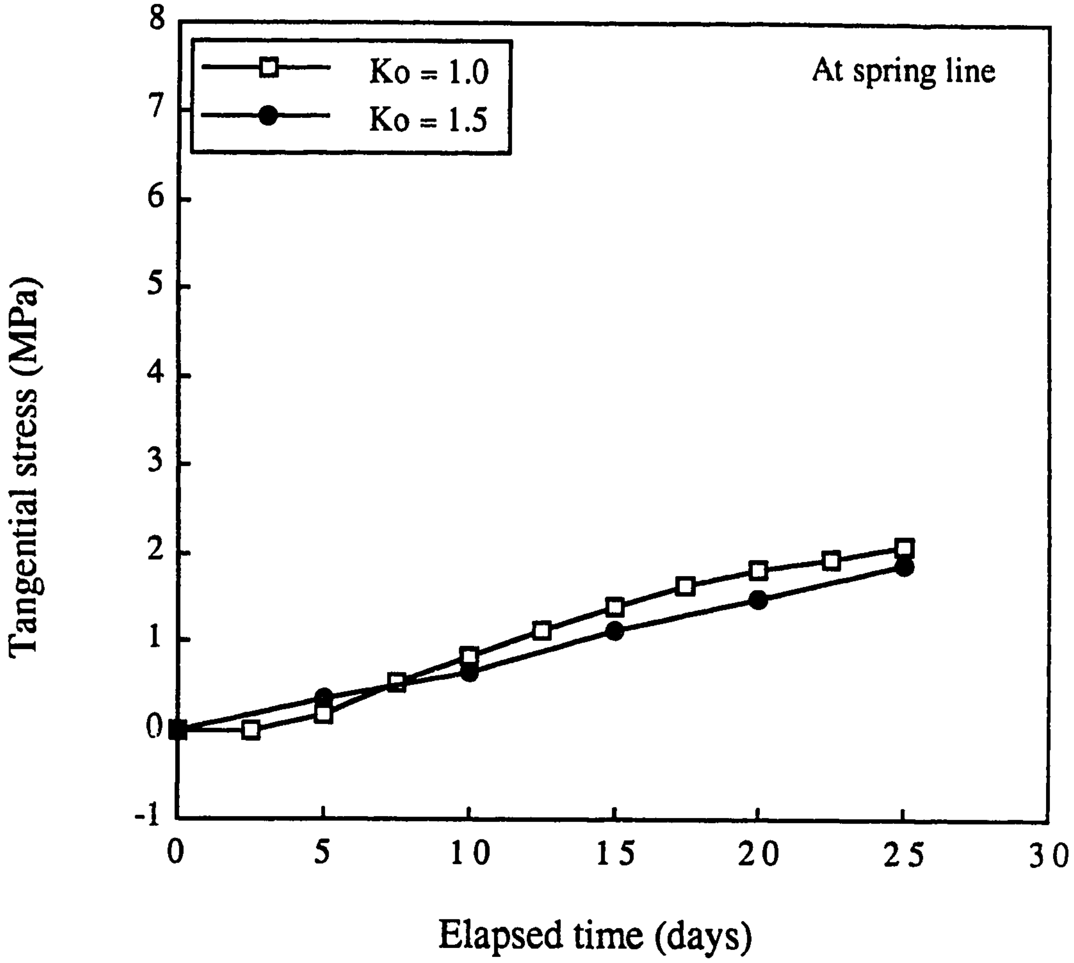

Figure 6.14 Variation of tangential stress at spring line with time (elastic, perfectly-plastic model)

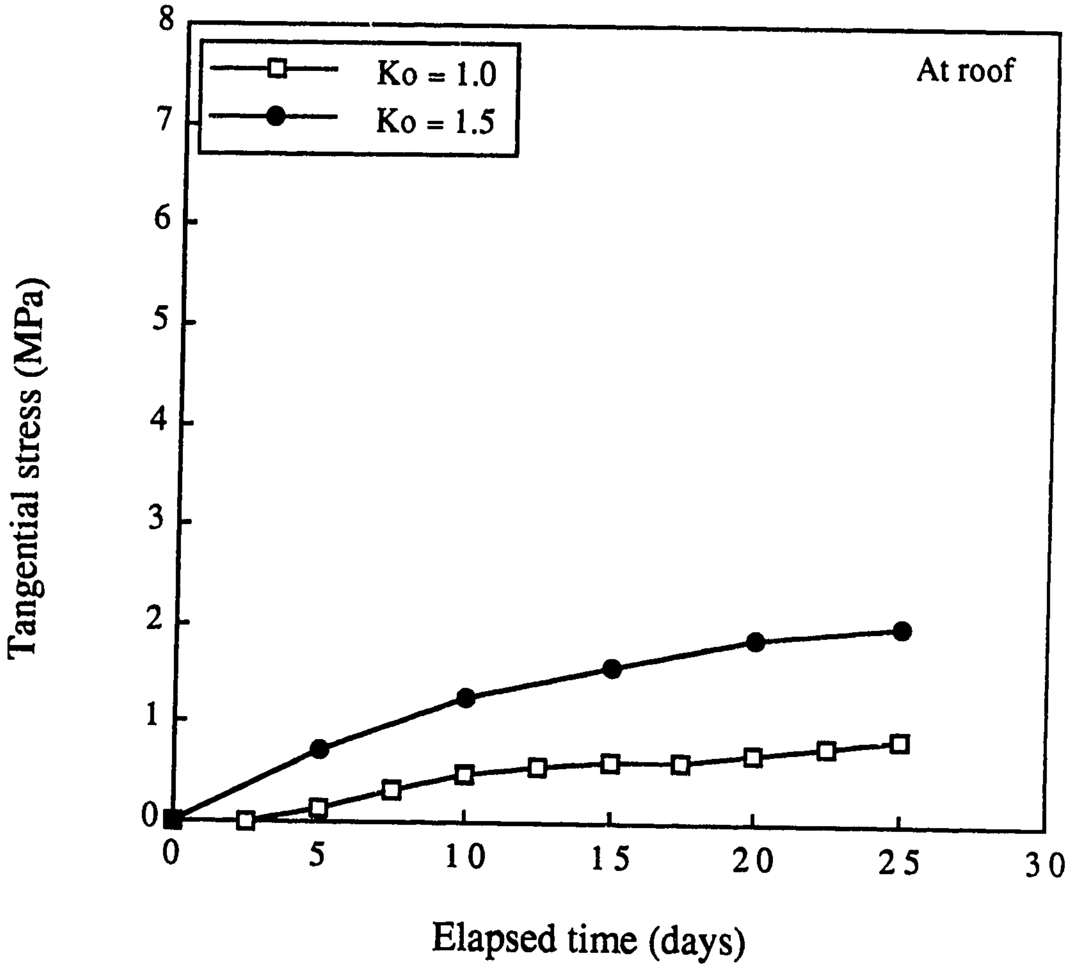

Figure 6.15 Variation of tangential stress at roof with time (elastic, perfectly-plastic model)

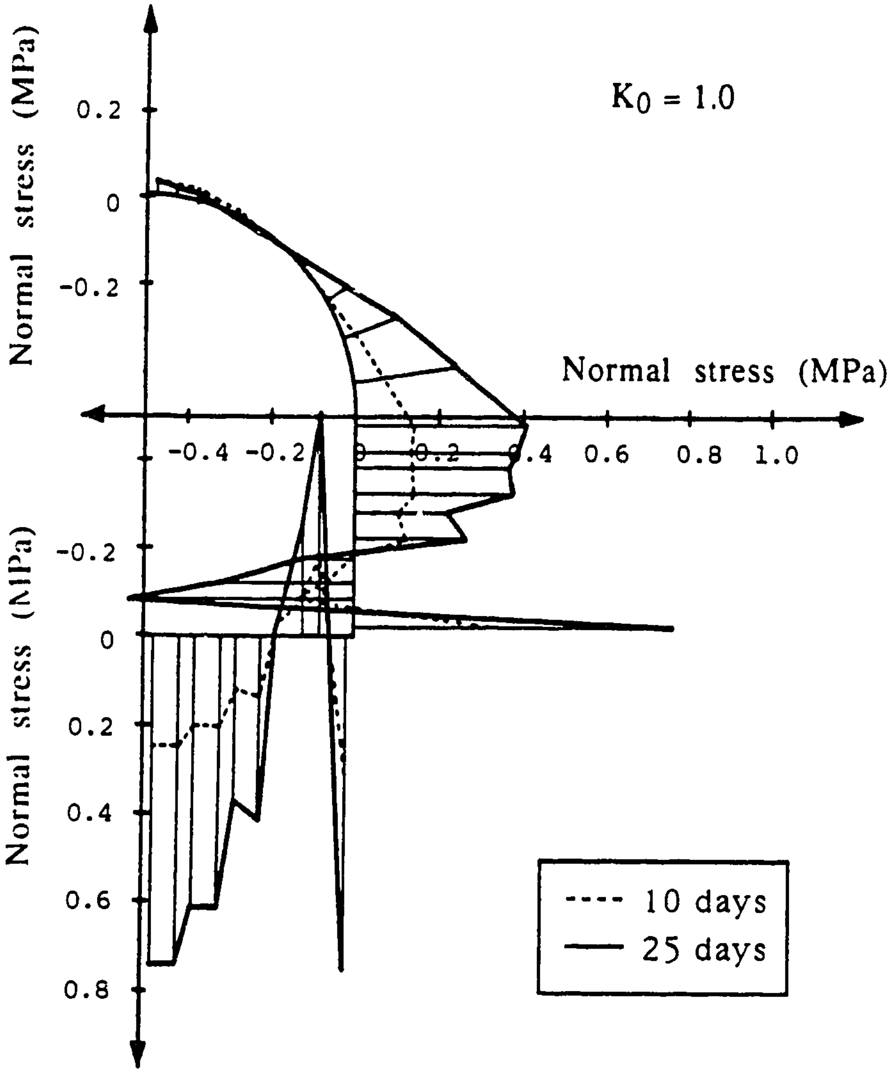

Figure 6.16 Normal stress distribution along lining (K_0 = 1.0)

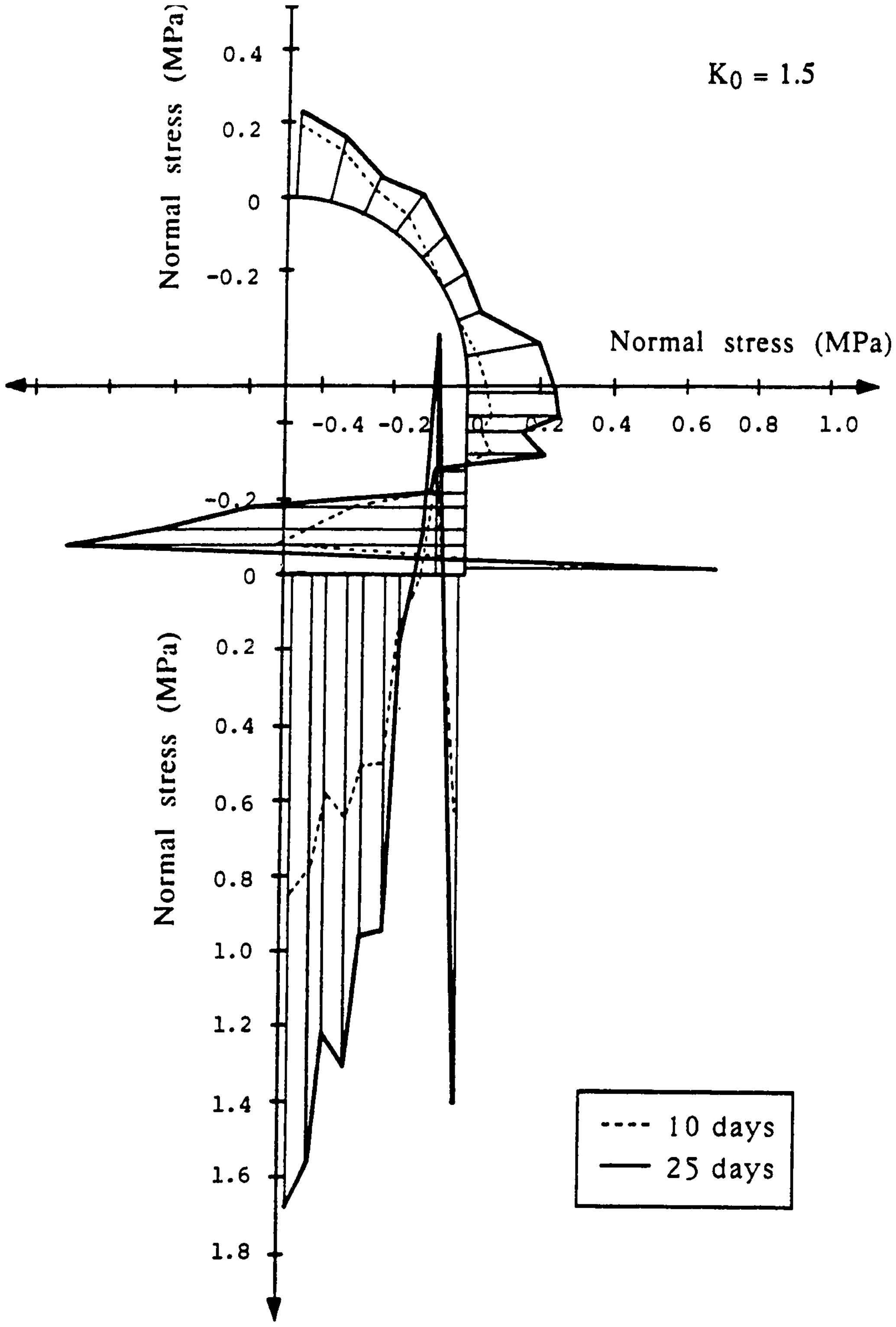

Figure 6.17 Normal stress distribution along lining (K_0 = 1.5)

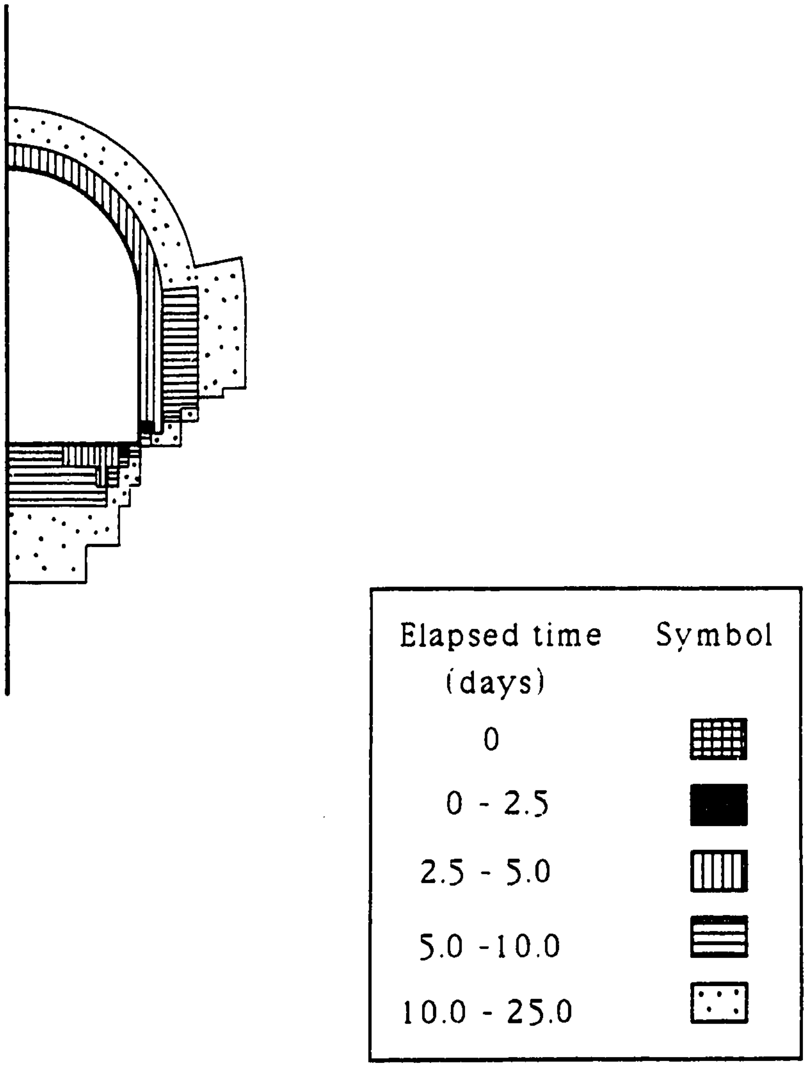
Elapsed time (days)
Symbol
0 ▦
0 - 2.5 ■
2.5 - 5.0 ▥
5.0 -10.0 ▤
10.0 - 25.0 ⁘

Figure 6.18 Development of plastic zones around tunnel (K_0 = 1.0)

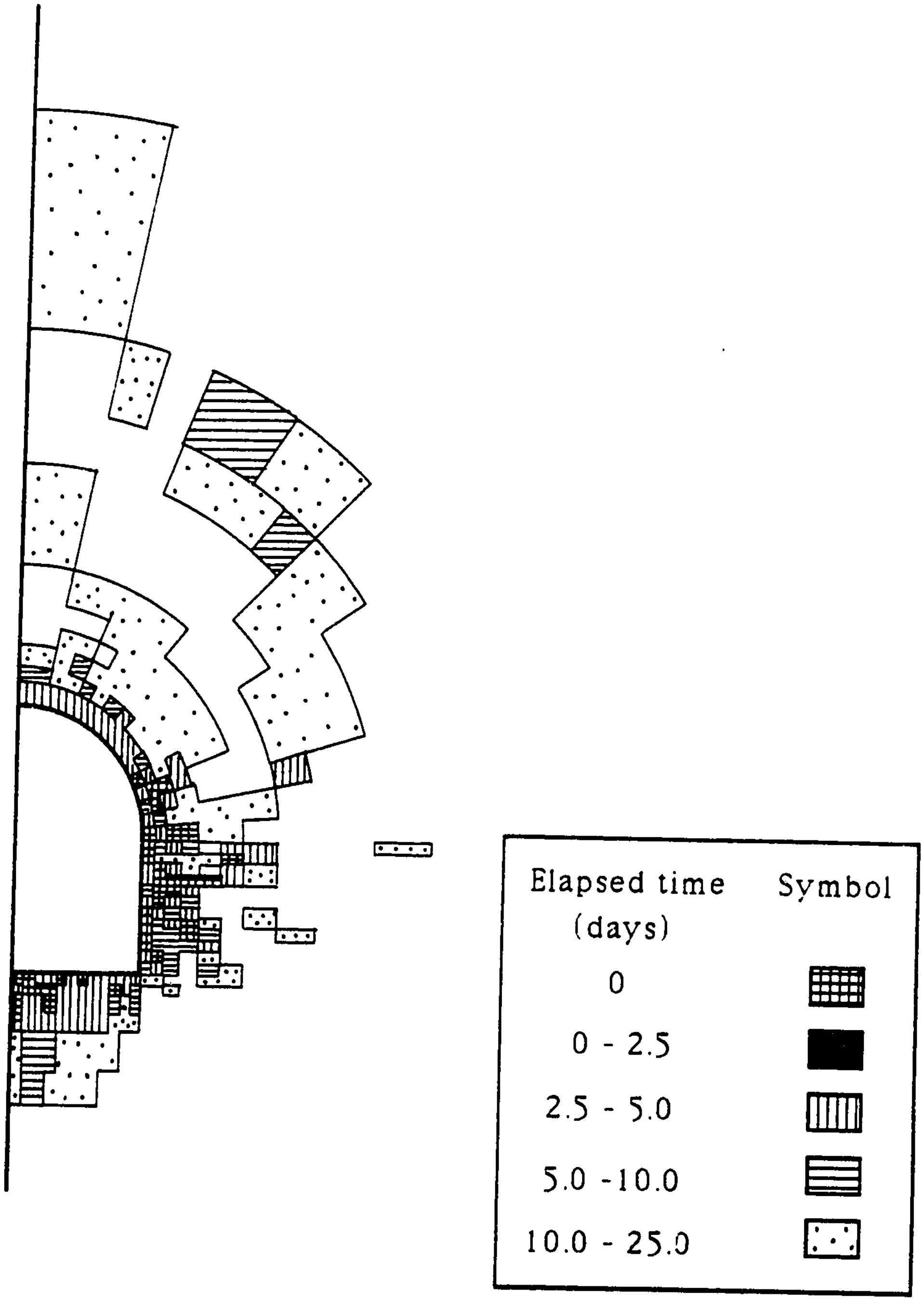
Elapsed time (days)
Symbol
0
0 - 2.5
2.5 - 5.0
5.0 -10.0
10.0 - 25.0

Figure 6.19 Development of plastic zones around tunnel (K_0 = 1.5)

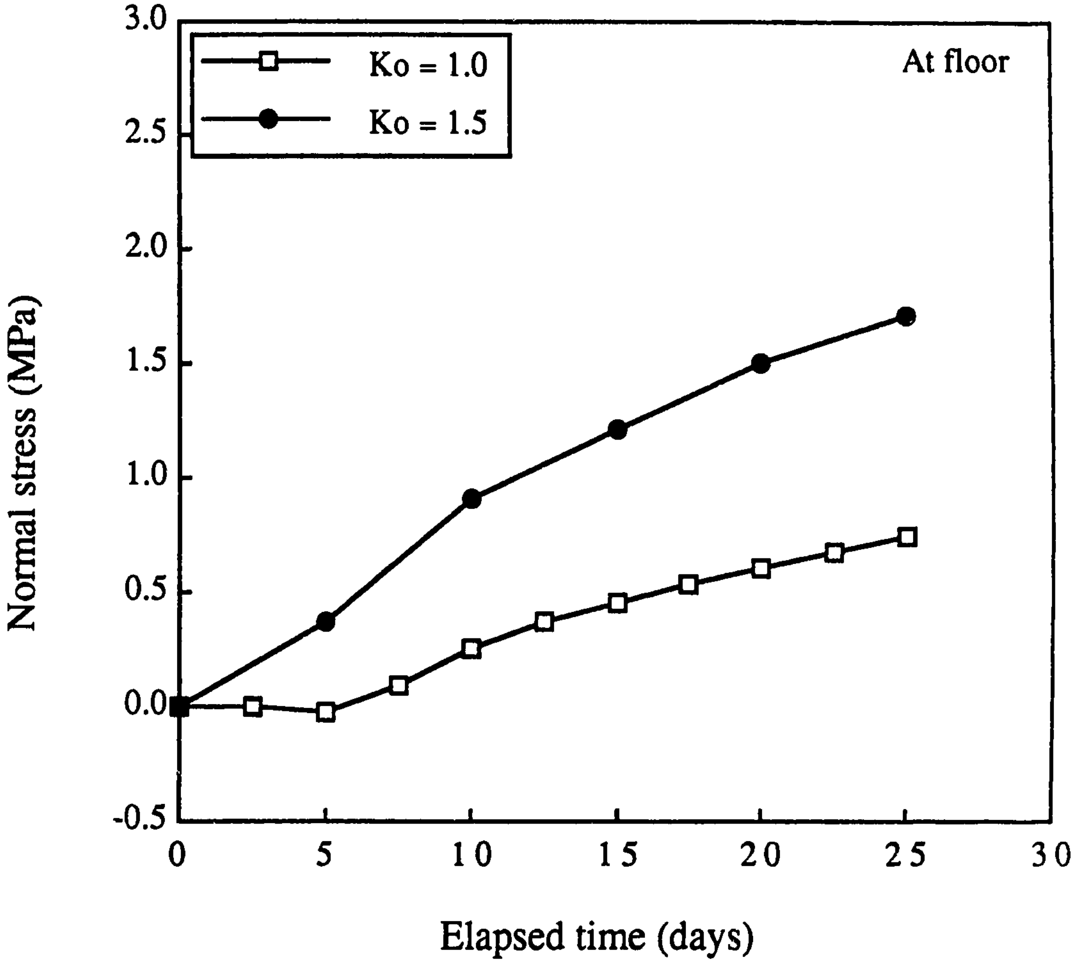

Figure 6.20 Variation of normal stress at floor with time (strain-softening model)

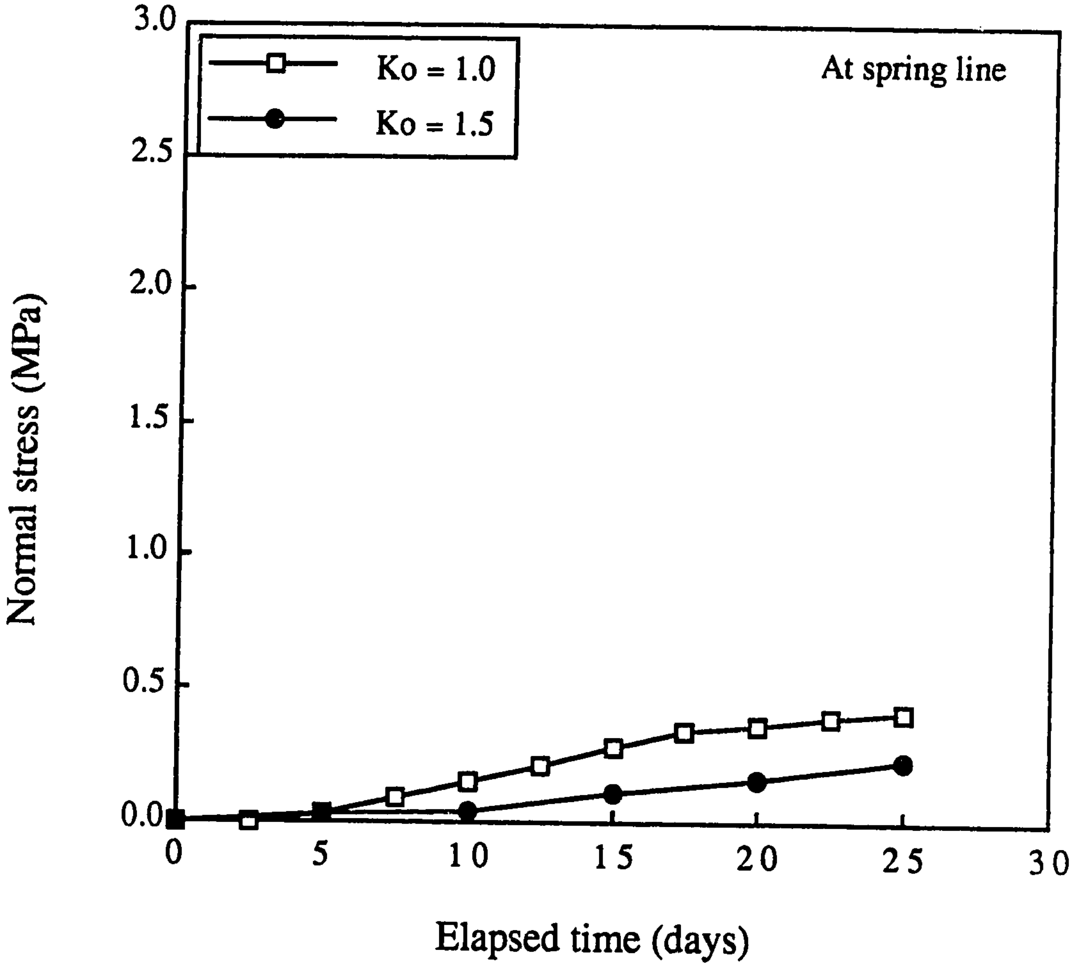

Figure 6.21 Variation of normal stress at spring line with time (strain-softening model)

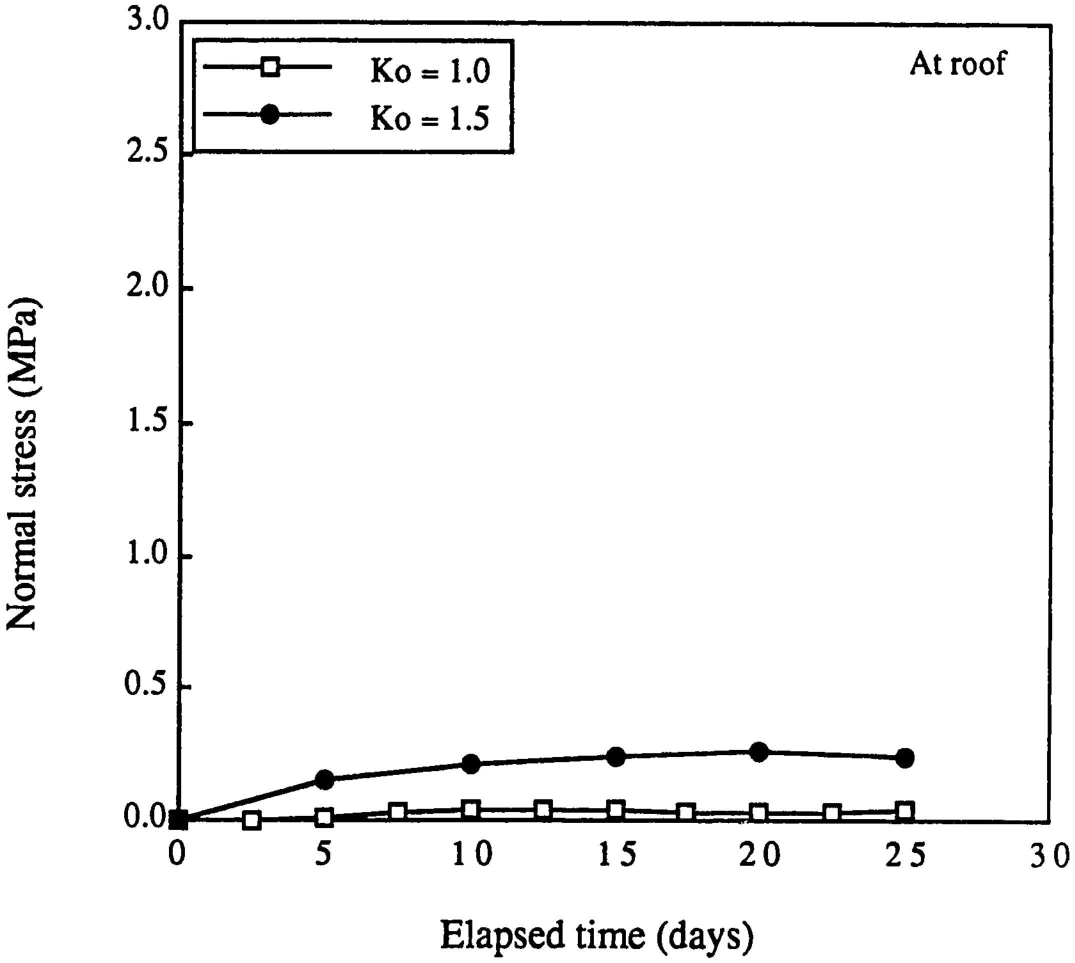

Figure 6.22 Variation of normal stress at roof with time (strain-softening model)

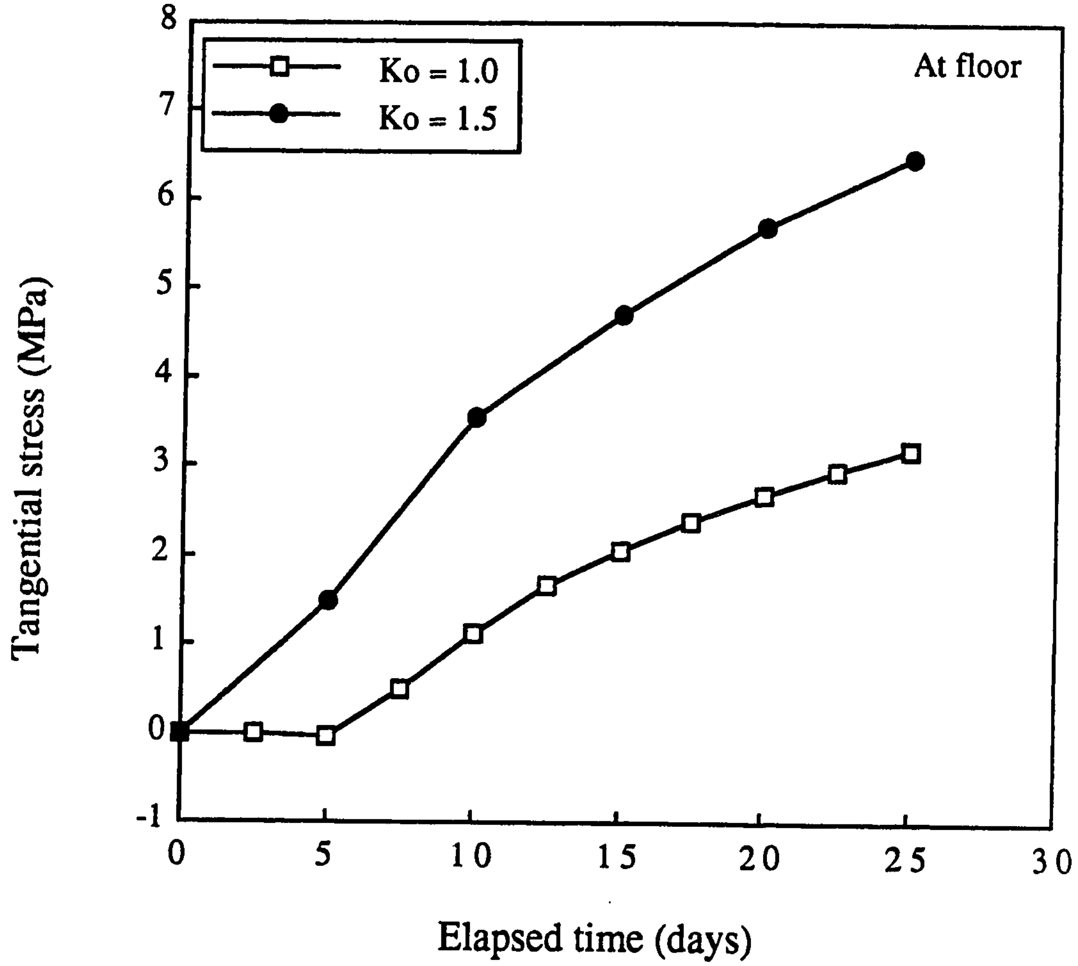

Figure 6.23 Variation of tangential stress at floor with time (strain-softening model)

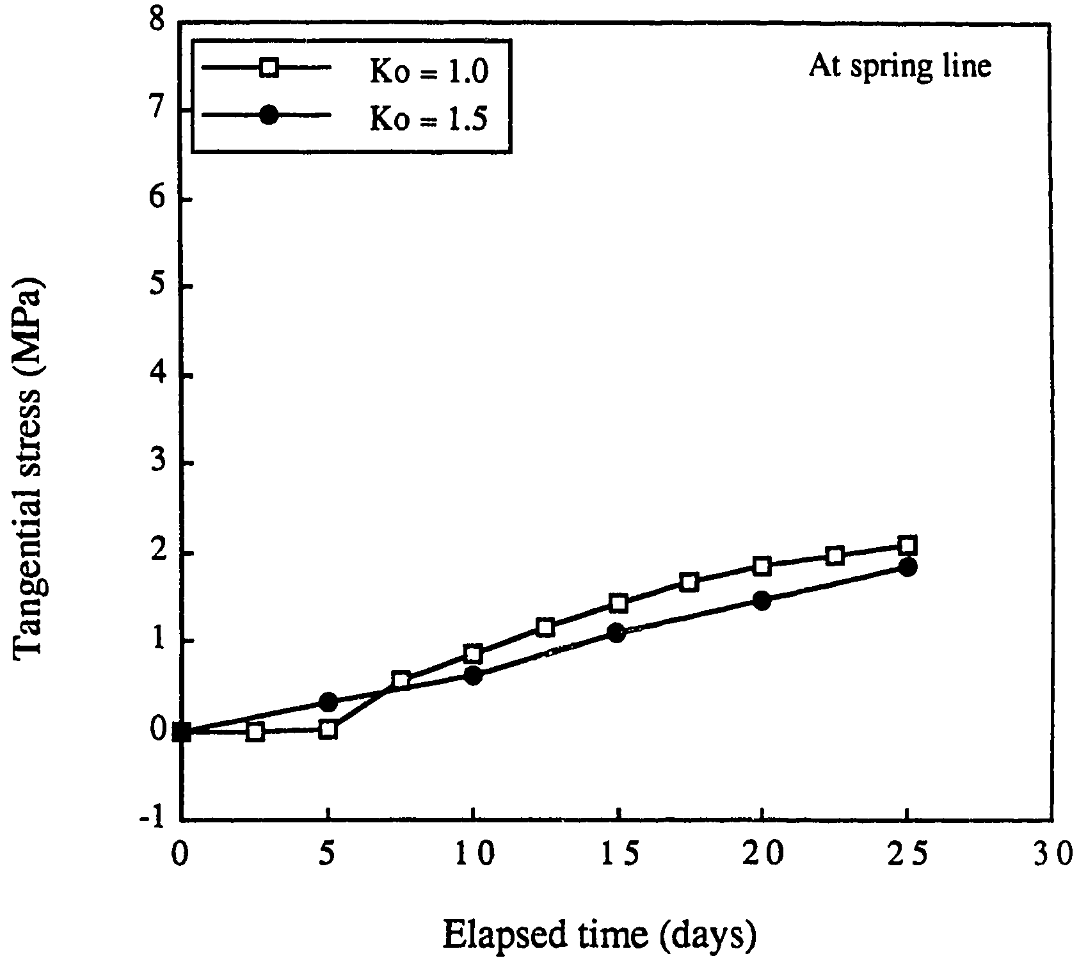

Figure 6.24 Variation of tangential stress at spring line with time (strain-softening model)

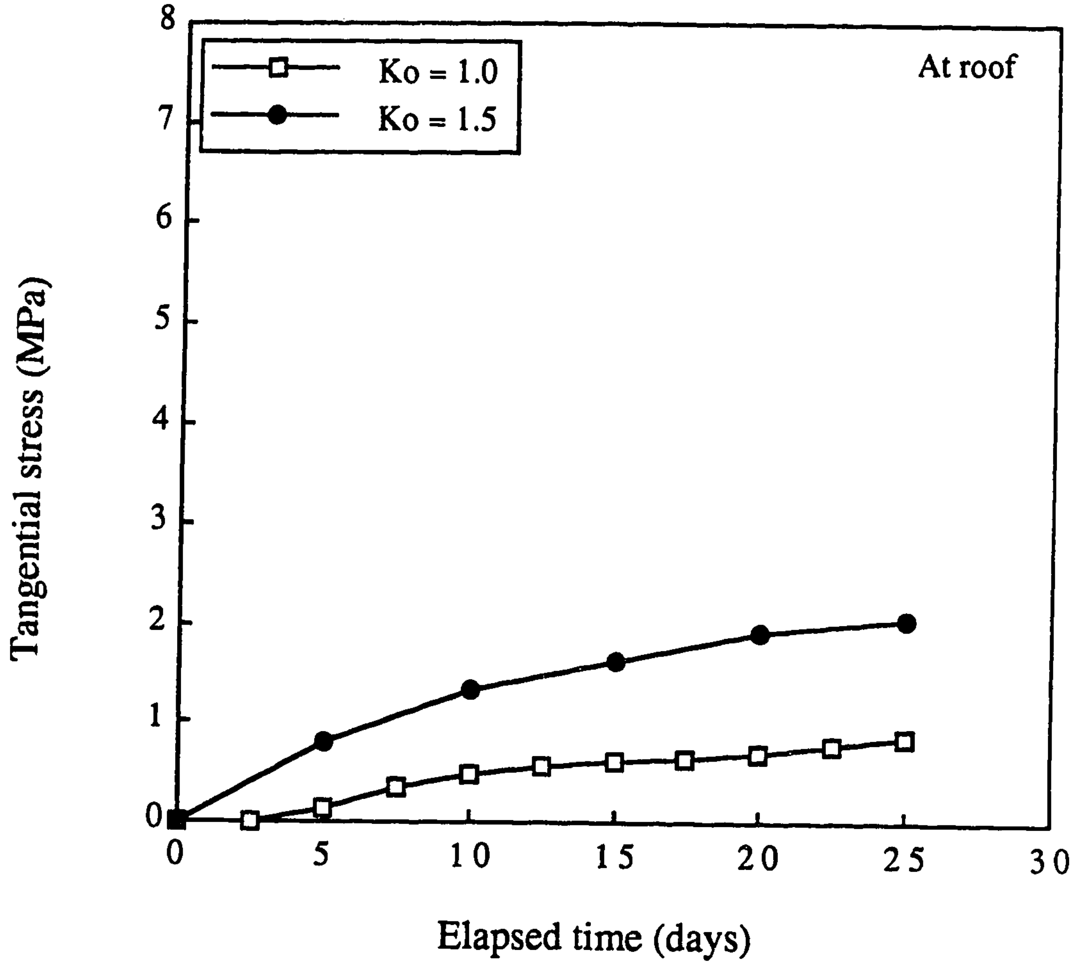

Figure 6.25 Variation of tangential stress at roof with time (strain-softening model)

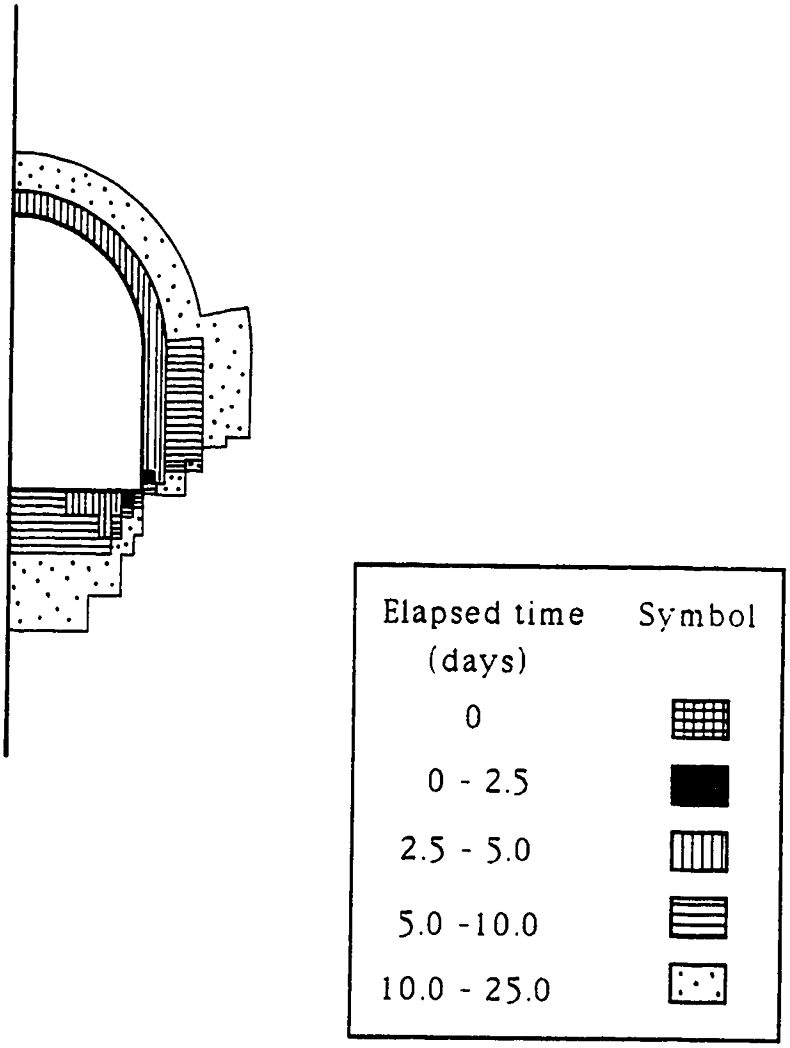
Elapsed time (days)
Symbol
0
0 - 2.5
2.5 - 5.0
5.0 -10.0
10.0 - 25.0

Figure 6.26 Development of plastic zones around tunnel (K_0 = 1.0)

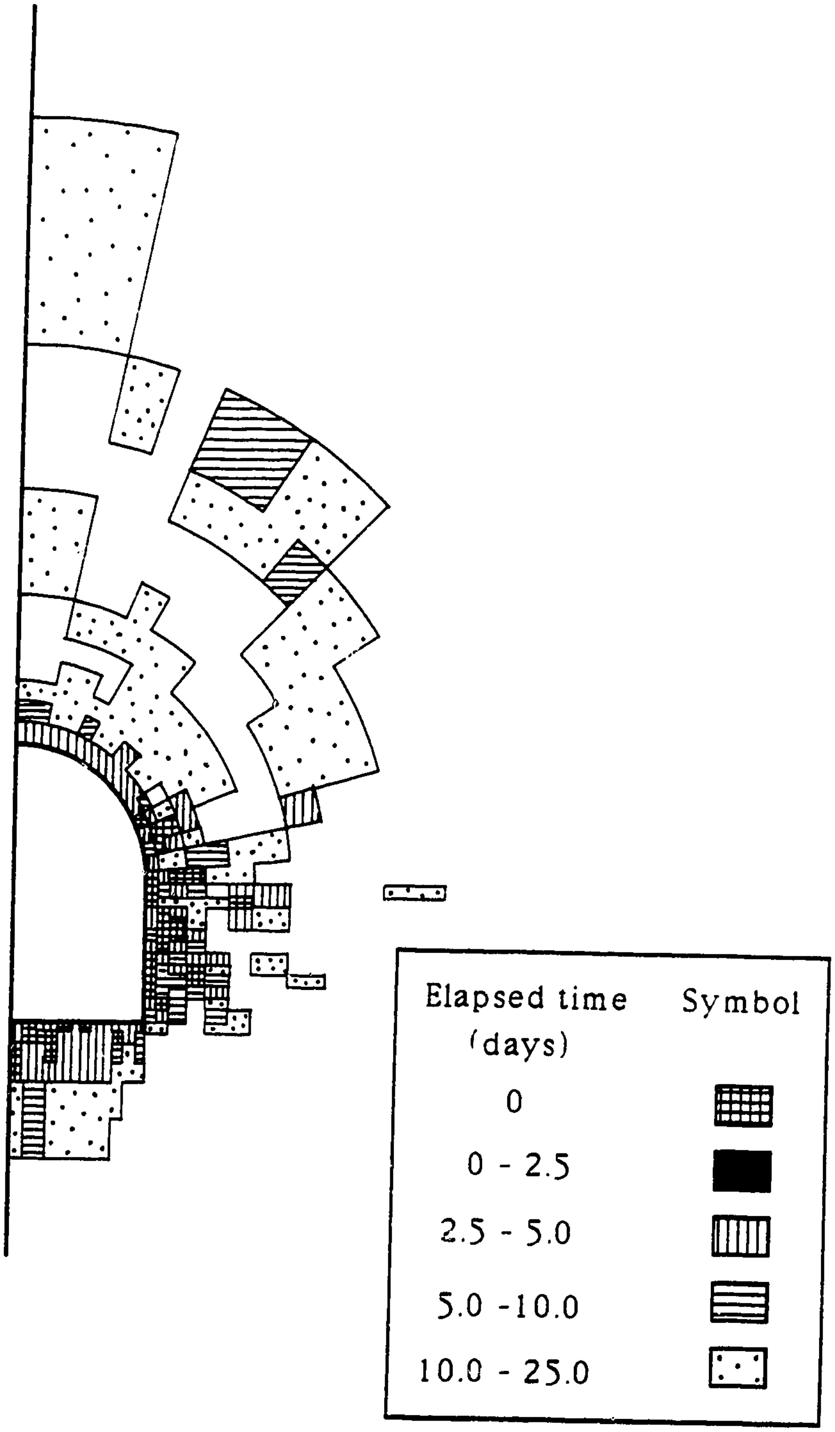
Elapsed time (days)
Symbol
0
0 - 2.5
2.5 - 5.0
5.0 -10.0
10.0 - 25.0

Figure 6.27 Development of plastic zones around tunnel (K_0 = 1.5)

7. Simple evaluation of softening effect in geotechnical engineering problems

7.1 Introduction

So far, a finite element method has been described to analyze time-dependent problems taking into consideration the effect of softening and its effectiveness has been demonstrated. The finite element method is no doubt a powerful and versatile tool, but performing a finite element analysis is often expensive and time-consuming, especially in analyzing a complex problem. For preliminary investigations, it is more desirable to conduct a simple analysis with simplified boundary conditions to obtain a rough estimate of the solution to the problem without losing physical insight into the problem.

In this chapter, some existing analytical methods which have been used in geotechnical engineering are modified to take into account softening in fissured, over-consolidated clays and mudstones. These are limit equilibrium analysis of slope stability, calculation of earth pressure and calculation of stress and displacement around a tunnel. For this purpose, the failure criterion with time-dependent strength parameters described in Chapter 3 is incorporated, with some modification, into these analysis methods. Since these analyses have been well established and can be found in geotechnical engineering text books (*e.g.*, Lambe and Whitman, 1979; Goodman, 1980), the detailed description of the fundamentals is not given in subsequent sections. For illustration, simple examples are given in later sections.

7.2 Slope stability

7.2.1 Infinite slip surface

Consider an infinite slope as shown in Figure 7.1. The ground water table is located at an elevation of z_w above the slip surface. Steady state seepage is assumed to be parallel to the slope surface. The available shear resistance along the slip surface, s, is expressed, using the failure criterion proposed in Chapter 3 and in terms of the factor of safety, F_s, as follows:

$$s = \frac{P\,\sigma_c}{F_s}\left(\frac{\sigma_n'}{\sigma_c} - Q\right)^{\frac{1}{R}} \tag{7.1}$$

where P, Q and R are strength parameters, σ_c is uniaxial compression strength, and σ_n' is the effective normal stress. The pore water pressure is expressed as:

$$u = \gamma_w\, z_w \cos^2 \beta \tag{7.2}$$

where γ_w is the unit weight of water.

From the equilibrium condition of resisting and driving forces acting on the slip surface, the following expression for F_s can be obtained using the pore pressure ratio, r_u, introduced by Bishop and Morgenstern (1960):

$$F_s = \frac{P\,\sigma_c}{\gamma\, z \sin\beta \cos\beta} \left\{ \frac{\gamma\, z}{\sigma_c} \left(\cos^2\beta - r_u \right) - Q \right\}^{\frac{1}{R}} \tag{7.3}$$

where γ is the unit weight of soil.

Fissured, over-consolidated clays and mudstones soften with time as discussed in Chapter 2. For natural slopes consisting of these materials, weathering can be a dominant cause for deterioration of the soil strength over a long period of time. This reduction in shear strength can be easily incorporated in the above calculation through reduction in the strength parameters P, Q and R with time. It is assumed that the variations of these strength parameters follow the same inverse-hyperbolic functions of time presented in Chapter 3. They are re-written as:

$$X = X_0 \left\{ 1 - \frac{t}{x\,t + t_{fs}\left(\frac{X_0}{X_0 - X_{fs}} - x \right)} \right\} \tag{7.4}$$

where X is strength parameter P, Q or R, and x is strength reduction-rate parameter **a**,**b** or **c** (see Equation (3.8)).

The variation of the factor of safety during softening can be computed by substituting variations of the strength parameters with time given by Equation (7.4) into Equation (7.3).

7.2.2 Circular slip surface

There are many methods of slices to handle a circular slip surface depending on the number of equilibrium conditions they satisfy. Among them, the method proposed by Bishop (1955) is used here. Bishop's simplified method has been known to provide an accurate estimate of the factor of safety for most cases, although it does not satisfy all the equilibrium conditions (Duncan and Wright, 1980). Further, it is simple and easy to carry out the analysis.

Consider the forces acting on a typical slice in a slope shown in Figure 7.2. From the equilibrium condition of over-all moment about the center of rotation together with the failure criterion, Equation (7.1), the following expression for F_s can be obtained:

$$F_s = \frac{1}{\sum_{i=1}^{n} w_i \sin \alpha_i} \sum_{i=1}^{n} l_i P \sigma_c \left(\frac{N'_i}{l_i \sigma_c} - Q \right)^{\frac{1}{R}} \tag{7.5}$$

where subscript 'i' denotes the i th slice and N'_i is effective normal force acting on the base of the i th slice. In order to determine the value of N'_i, another equilibrium condition is required. Bishop's simplified method considers the equilibrium of vertical forces for each slice neglecting the interslice shear forces. Thus, the following condition must be satisfied for each slice:

$$N'_i \cos \alpha_i + \frac{l_i P \sigma_c}{F_s} \left(\frac{N'_i}{l_i \sigma_c} - Q \right)^{\frac{1}{R}} \sin \alpha_i + l_i u_i \cos \alpha_i - w_i = 0 \tag{7.6}$$

The value of N'_i can be computed from this equation for an assumed value of F_s. Since F_s appears in the both equations above, an iterative method can be adopted to compute F_s. For this calculation, a computer program, STABNON, is developed from a program, STABGM, created by Duncan *et al.* (1985). It should be noted here that because of the nature of the proposed failure criterion not only linear but also non-linear types of failure criterion can be utilized in the analysis.

Following the same procedure as in the case of an infinite slope, the variation of the factor of safety due to softening can be computed.

7.3 Rankine earth pressure

Consider an element in semi-infinite soil mass having a horizontal surface, as shown in Figure 7.3(a). From symmetry, vertical and horizontal stresses acting on the element are principal stresses. Rankine states of stress are illustrated in Figure 7.3(b). Since the proposed failure criterion is expressed in terms of principal stresses as:

$$\sigma_1 = \sigma_3 + A\,\sigma_c \left(\frac{\sigma_3}{\sigma_c} - S \right)^{\frac{1}{B}} \tag{7.7}$$

the Rankine passive and active earth pressures, p_p and p_a, at a given depth are given simply by:

$$p_p = \sigma_v + A\,\sigma_c \left(\frac{\sigma_v}{\sigma_c} - S \right)^{\frac{1}{B}} \tag{7.8}$$

$$\sigma_v = p_a + A\,\sigma_c \left(\frac{p_a}{\sigma_c} - S \right)^{\frac{1}{B}} \tag{7.9}$$

where A, B and S are strength parameters, σ_c is uniaxial compression strength and σ_v is the vertical stress at a given depth. Because of the non-linearity of the failure criterion, the variation of these pressures with depth is non-linear. Further, predicted slip lines are also non-linear and their directions vary with depth.

Assuming that a retaining wall is rigid and that there are no shear forces between the vertical face of the retaining wall and the soil, the replacement of part of a semi-infinite soil mass by the retaining wall would not significantly change the stress field in the surrounding soil. Thus, a lateral pressure diagram along the vertical face of the retaining wall can be obtained using Equations (7.8) and (7.9) for the passive and active cases, respectively.

The variation of lateral pressure during softening can be computed by reduction in the strength parameters with time as in the previous section.

7.4 Stresses and displacements around tunnel

Suppose that a circular tunnel is excavated in a homogeneous, isotropic medium under a constant hydrostatic pressure, p_0, as shown in Figure 7.4. An elastic, perfectly-plastic and plane-strain, axisymmetric condition is assumed. The failure criterion for the medium is expressed by Equation (7.7). The differential equation of equilibrium to be satisfied for zero body forces is:

$$\frac{\partial \sigma_r}{\partial r} + \frac{\sigma_r - \sigma_\theta}{r} = 0 \qquad (7.10)$$

where σ_r and σ_θ are radial and tangential stresses, respectively, and r is a radial distance from the center of tunnel.

Stresses in the elastic zone around the tunnel ($r \geq R$) are obtained, by integrating the above differential equation, as:

$$\sigma_r = p_0 - (p_0 - \sigma_R)\left(\frac{R}{r} \right)^2 \qquad (7.11)$$

$$\sigma_\theta = p_0 + (p_0 - \sigma_R)\left(\frac{R}{r} \right)^2 \qquad (7.12)$$

where σ_R is the radial stress at the boundary between the elastic and plastic zone, R. In the plastic zone ($r \leq R$), stresses are calculated from the following equation:

$$\sigma_r = \sigma_c \left[\left\{ A \left(1 - \frac{1}{B} \right) \ln \left| \frac{r}{a} \right| + \left(\frac{p_s}{\sigma_c} - S \right)^{\frac{B-1}{B}} \right\}^{\frac{B}{B-1}} + S \right] \qquad (7.13)$$

where a is the tunnel radius and p_s is the support pressure. This equation is obtained by integrating Equation (7.10) together with Equation (7.7). The corresponding σ_θ is calculated from the following equation:

$$\sigma_\theta = \sigma_c \, M^{\frac{1}{B-1}} (M + A) + S \, \sigma_c \qquad (7.14)$$

where

$$M = \left\{ A \left(1 - \frac{1}{B} \right) \ln \left| \frac{r}{a} \right| + \left(\frac{p_s}{\sigma_c} - S \right)^{\frac{B-1}{B}} \right\}$$

The extent of plastic zone, R, can be determined, assuming the continuity condition of radial stress at R, as follows:

$$R = a \exp (N) \qquad (7.15)$$

where

$$N = \frac{1}{A\left(1 - \frac{1}{B}\right)}\left(\frac{\sigma_R}{\sigma_c} - S\right)^{\frac{B-1}{B}}\left\{1 - \left(\frac{p_s - S\,\sigma_c}{\sigma_R - S\,\sigma_c}\right)^{\frac{B-1}{B}}\right\}$$

The σ_R in the above equation is determined by solving the following equation:

$$2\,\sigma_R - 2\,p_0 + A\,\sigma_c\left(\frac{\sigma_R}{\sigma_c} - S\right)^{\frac{1}{B}} = 0 \tag{7.16}$$

Radial displacement due to excavation, u_r, in the elastic zone is computed from the following equation:

$$u_r = -\frac{p_0 - \sigma_R}{2\,G}\frac{R^2}{r} \tag{7.17}$$

where G is the shear modulus. The radial displacement is considered positive outwards from the center of tunnel.

In order to calculate radial displacements in the plastic zone, the following relation regarding plastic strains is assumed (Kaiser, 1980; Brown *et al.*, 1981):

$$\varepsilon_r^p + \beta\,\varepsilon_\theta^p = 0 \tag{7.18}$$

The parameter β controls the plastic volume change; β is one if no plastic volume change takes place. Further, it is assumed that elastic strain in the plastic zone is constant. By these assumptions and using the compatibility condition, the following expression for radial displacement in the plastic zone is obtained:

$$\frac{u_r}{r} = -\frac{p_0 - \sigma_R}{G(1+\beta)}\left\{\left(\frac{R}{r}\right)^{1+\beta} + \frac{\beta - 1}{2}\right\} \qquad (7.19)$$

Using Equations (7.11) to (7.15), (7.17) and (7.19) together with support pressure, in-situ stress and the properties of ground material, the stress and displacement around a tunnel can be computed. Following the same procedure as in the previous section, the variation of these variables with time during softening can be computed.

7.5 Examples

7.5.1 Slope stability analysis with an infinite slip surface

This example deals with the stability analysis of an infinite slope having an inclination of 15° as shown in Figure 7.1. The slope consists of a fissured, over-consolidated clay. The material properties are given in Table 7.1. These properties are identical to those of Brown London Clay. The slip surface is located at a depth of 6 m. A steady-seepage condition is maintained with the pore pressure ratio, r_u, of 0.5. The fully-softened condition is reached in 100 years. Using the equations derived in Section 7.2.1, a stability analysis is carried out.

Figure 7.5 shows the variation of shear strength with time. Three different reduction-rates of shear strength are considered which are denoted as Case 1, Case 2 and Case 3. Case 1 gives a linear reduction of shear strength with respect to time and Case 3 gives a more rapid initial reduction of shear strength. For reference, the shear stress acting along the slip surface is also given in Figure 7.5. It can be seen from this figure that the time required for the slope to fail is significantly affected by the reduction-rate. As can be expected, Case 3 gives the shortest lifetime and Case 1 gives the longest lifetime.

Figure 7.6 shows the variation of the factor of safety with time computed for Case 1 using three different values of pore pressure ratio. As can be expected from Figure 7.5, the factor of safety decreases linearly with time. The pore water pressure can be seen to have a significant influence on stability of the slope. The lifetime of the slope increases with decreasing pore pressure ratio. A slope with a ground water level below the slip surface does not fail.

Figure 7.7 shows the effect of slope angle on slope stability for a pore pressure ratio of 0.5. A decrease in slope angle results in a longer lifetime of the slope. Flattening the slope by 3 degrees results in a 35 years increase in the lifetime of the slope. A slope having an inclination less than 10° will not fail at the fully-softened condition.

7.5.2 Slope stability analysis with a circular slip surface

This example deals with a fissured, over-consolidated clay slope having a 1:2.5 inclination and a height of 7 m. The material properties are the same as in the infinite slip surface example. The pore pressure ratio is assumed as 0.3. Similar to the previous stability analysis, three different reduction-rates are considered: Case 1 gives a constant reduction with respect to time, Case 2 gives a slightly faster reduction and Case 3 gives the most rapid reduction in shear strength. The fully-softened condition is reached in 100 years.

The stability analysis is carried out using Bishop's simplified method as described in Section 7.2.2. The minimum value of the factor of safety for a given shear strength is determined by examining the results for different slip circles.

Figure 7.8 shows the variation of the factor of safety with time. As expected, Case 3 gives the shortest time to failure, 50 years, and Case 1 gives the longest time to failure, 82 years. The critical slip circles determined at the time of 0 and 50 years for Case 3 are given in Figure 7.9.

Figure 7.10 illustrates the influence of pore water pressure on the stability of a slope for Case 3. Three different values of pore pressure ratio have been assumed. The detrimental effect of pore water pressure on the stability can be observed. An increase in r_u by 0.1 results in a decrease in the lifetime of a slope by about 20 years.

7.5.3 Calculation of Rankine lateral earth pressure

This example deals with Rankine earth pressure acting on a retaining wall constructed upon excavation in a fissured, over-consolidated clay with an uniform surcharge of 0.1 MPa as shown in Figure 7.11. It is assumed that the wall is rigid and that no shear stress is developed between the vertical face of the wall and the soil. The soil properties are summarized in Table 7.2. The fully-softened condition is reached in 100 years after the construction of the retaining wall. A linear reduction of shear strength with respect to time is assumed. Using the equations presented in Section 7.3 Rankine lateral pressure can be computed.

Figure 7.12 shows the computed active lateral pressure distribution. Initially a large tension zone is developed down to about 5 m from the ground surface. As time goes by, lateral pressure at a given depth increases and the pressure diagram shifts rightward. At the bottom of the wall the computed lateral pressure is 5 kPa initially and increases to 120 kPa in 100 years. This would indicate that the stability of the retaining wall deteriorates with time.

7.5.4 Rock-support interaction analysis

This example analyzes stresses and displacements around a tunnel. Suppose that a circular tunnel, having a radius of 4 m, is driven at a depth of 250 m in mudstone bedrock. The bedrock material is assumed to behave in an elastic, perfectly-plastic manner with zero plastic volume change. The material properties are given in Table 7.3. A plane-strain, axisymmetric condition is assumed. It is also assumed that the bedrock material starts softening just after excavation and that the fully-softened condition is reached in one year. The shear strength decreases linearly with time during softening. Using the equations derived in Section 7.4 with the above data, stresses and displacements around the tunnel can be computed.

Figure 7.13 shows the distribution of radial and tangential stresses around the tunnel with zero support pressure or an unlined tunnel. It can be seen from the figure that a small plastic zone is formed initially and that as the softening progresses the plastic zone extends. At a time of 10 months the extent of the plastic zone reaches 5 times the tunnel radius. The magnitude of tangential stress decreases within the plastic zone with time and increases outside the plastic zone.

Figure 7.14 illustrates the variation of the ground convergence curve with time. It is seen that the plastic component in radial displacements increases with time and that the support pressure required to prevent yielding of the bedrock surrounding the tunnel increases with time. This suggests that in designing a tunnel support system it is important to recognize the softening effect.

7.6 Summary

In this chapter, some existing analytical methods - slope stability analysis, calculation of lateral earth pressure and calculation of stress and displacement around a tunnel were modified to take into account the effect of softening in terms of shear strength reduction with time. To achieve this, the failure criterion proposed in Chapter 3 was incorporated into these analytical methods and simple illustrations were calculated. The sensitivity of long-term stability and deformation to different rates of softening has been illustrated.

Table 7.1 Material properties for slope stability analysis

γ_t (MN/m^3)	σ_c (MPa)	P	Q	R
0.02	0.1	0.579	0.0	1.5

Table 7.2 Material properties for calculation of lateral earth pressure

γ_t (MN/m^3)	σ_c (MPa)	A_0	A_{fs}	B_0	S_0
0.02	0.206	3.525	1.04	1.762	-0.109

Table 7.3 Material properties for rock-support interaction analysis

γ_t (MN/m^3)	σ_c (MPa)	E' (MPa)	ν'	A_0	A_{fs}	B_0	S_0
0.02	7.0	200.0	0.2	2.57	1.04	1.53	-0.236

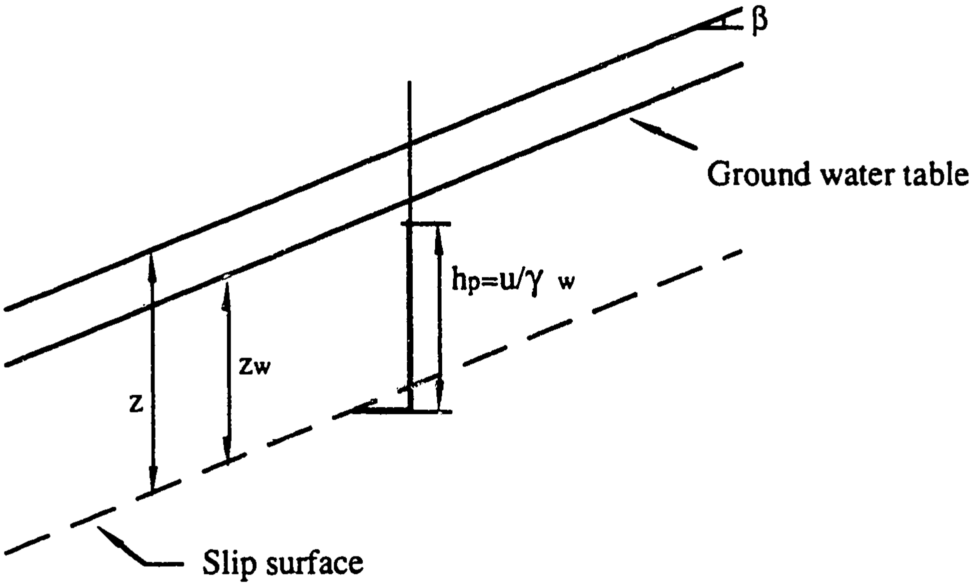
β
Ground water table
$h_p = u/\gamma_w$
zw
z
Slip surface

Figure 7.1 Slope with infinite slip surface

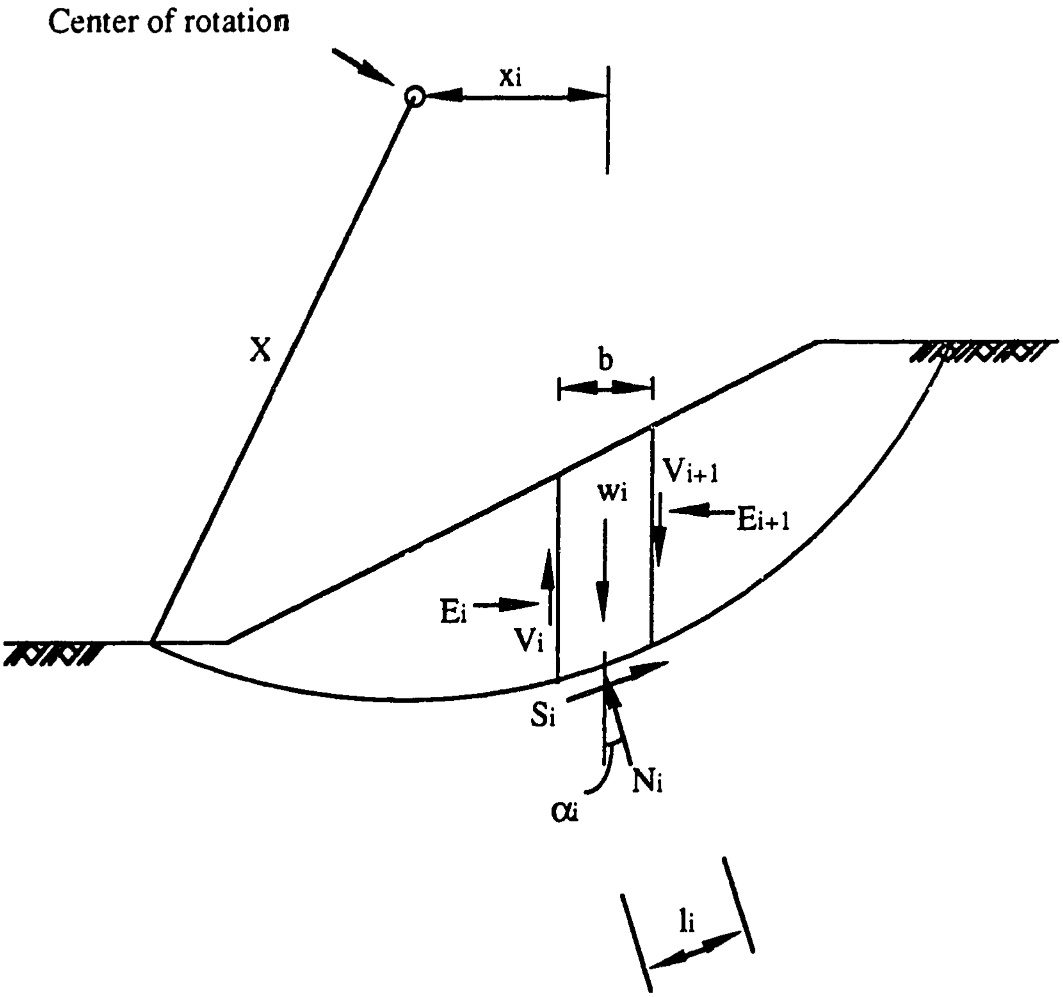
Center of rotation
xi
X
b
Vi+1
wi
Ei+1
Ei
Vi
Si
Ni
αi
li

Figure 7.2 Slope with circular slip surface

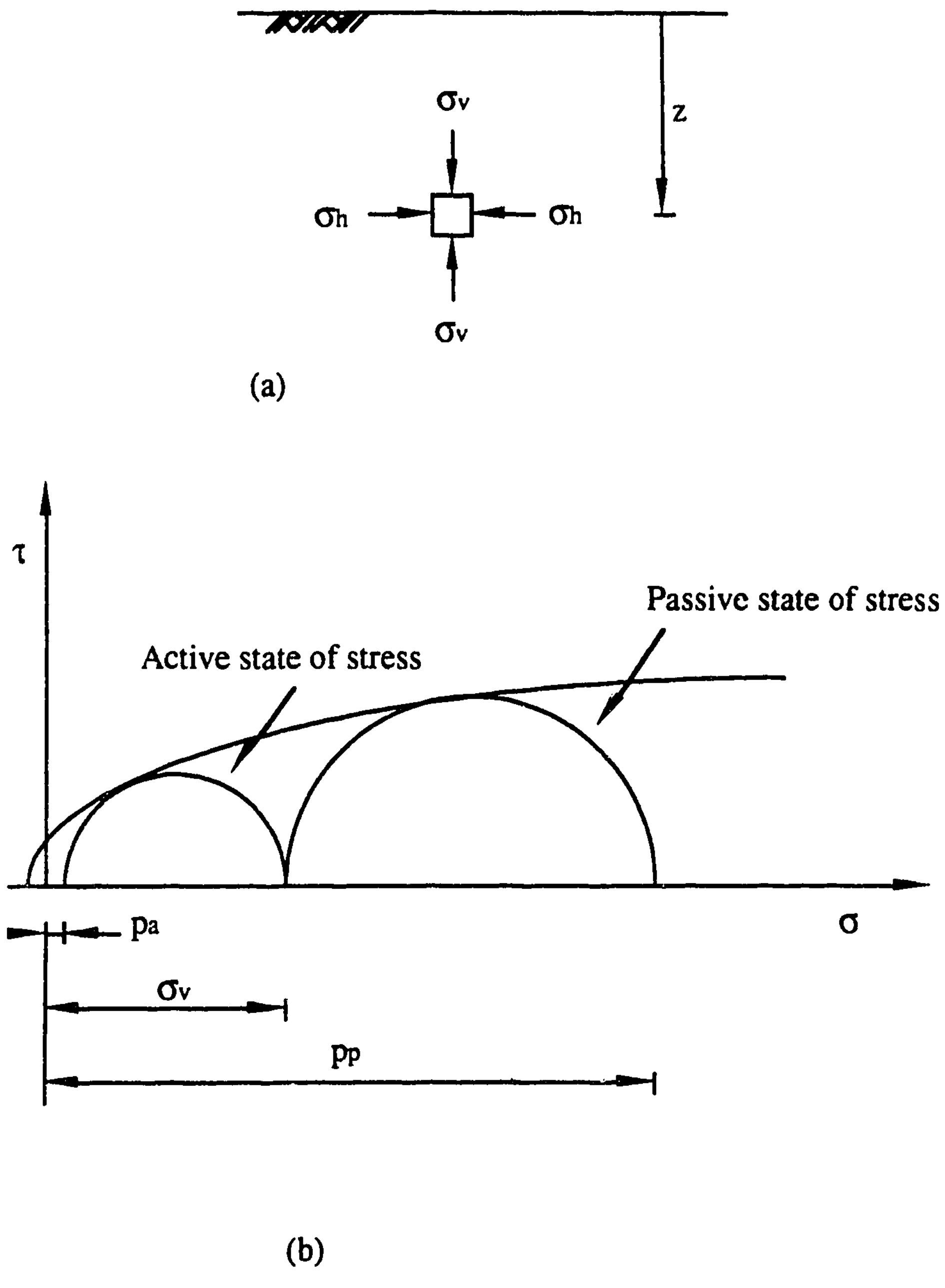
σv
z
σh
σh
σv
(a)
τ
Passive state of stress
Active state of stress
pa
σ
σv
pp
(b)

Figure 7.3 Rankine active and passive states of stresses in horizontal ground

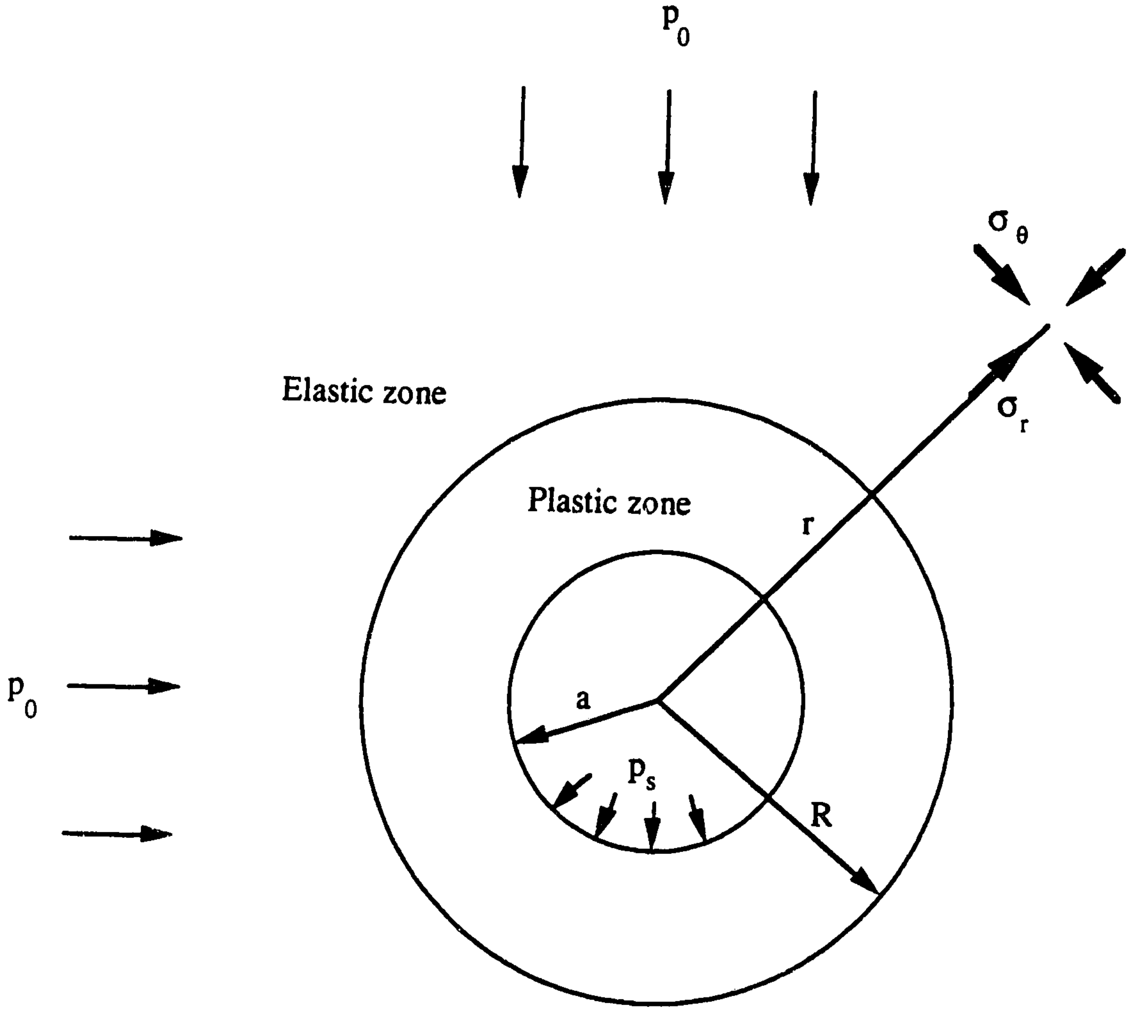
p_0
σ_θ
σ_r
Elastic zone
Plastic zone
r
p_0
a
p_s
R

Figure 7.4 Circular tunnel under hydrostatic stress field

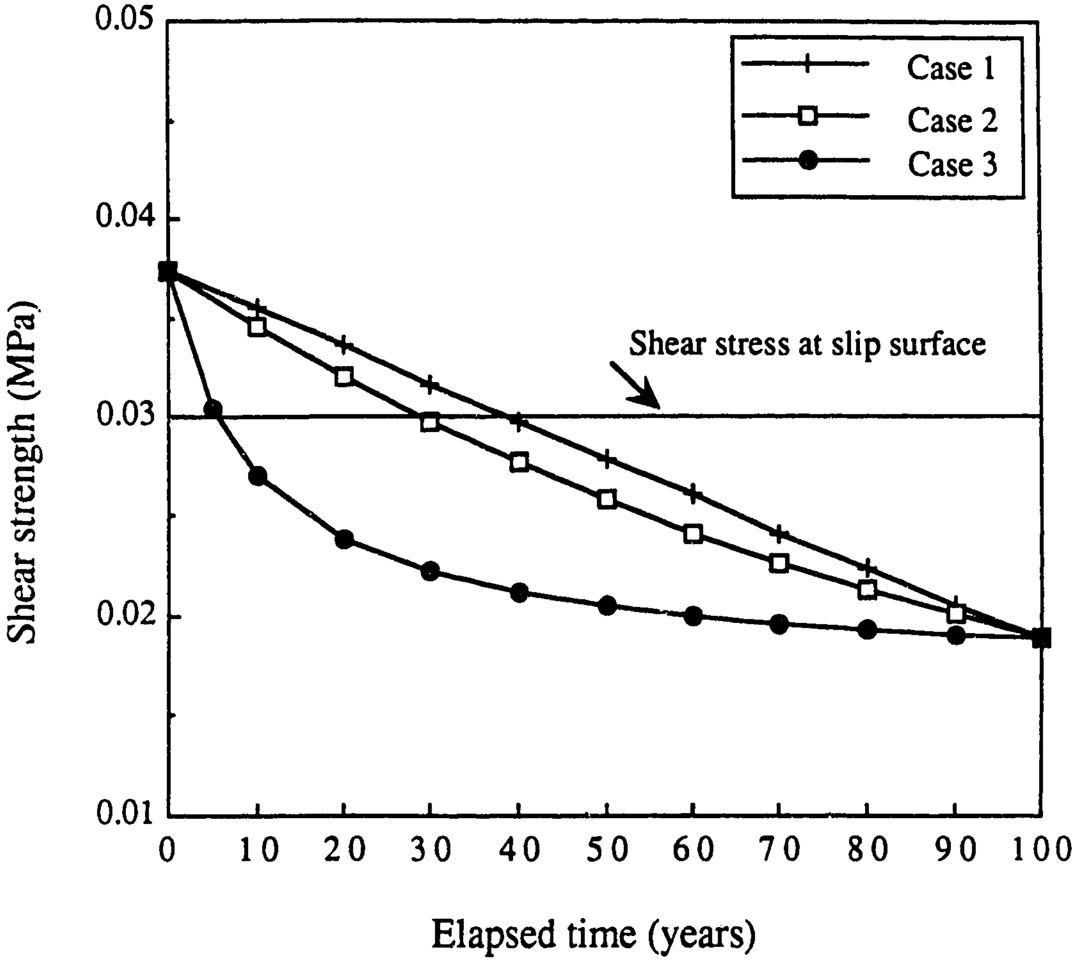

Figure 7.5 Variation with time of mobilized shear strength along slip surface

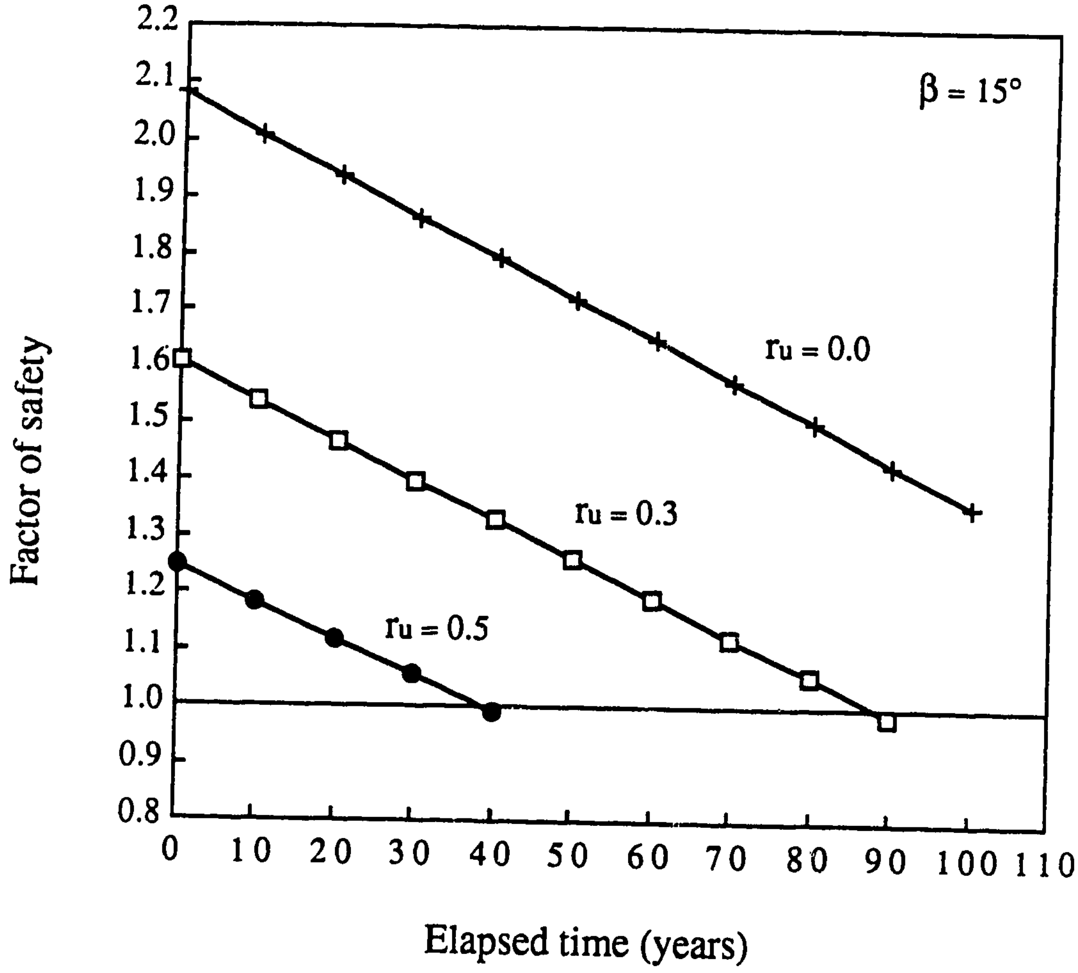

Figure 7.6 Variation of factor of safety with time for different values of r_u

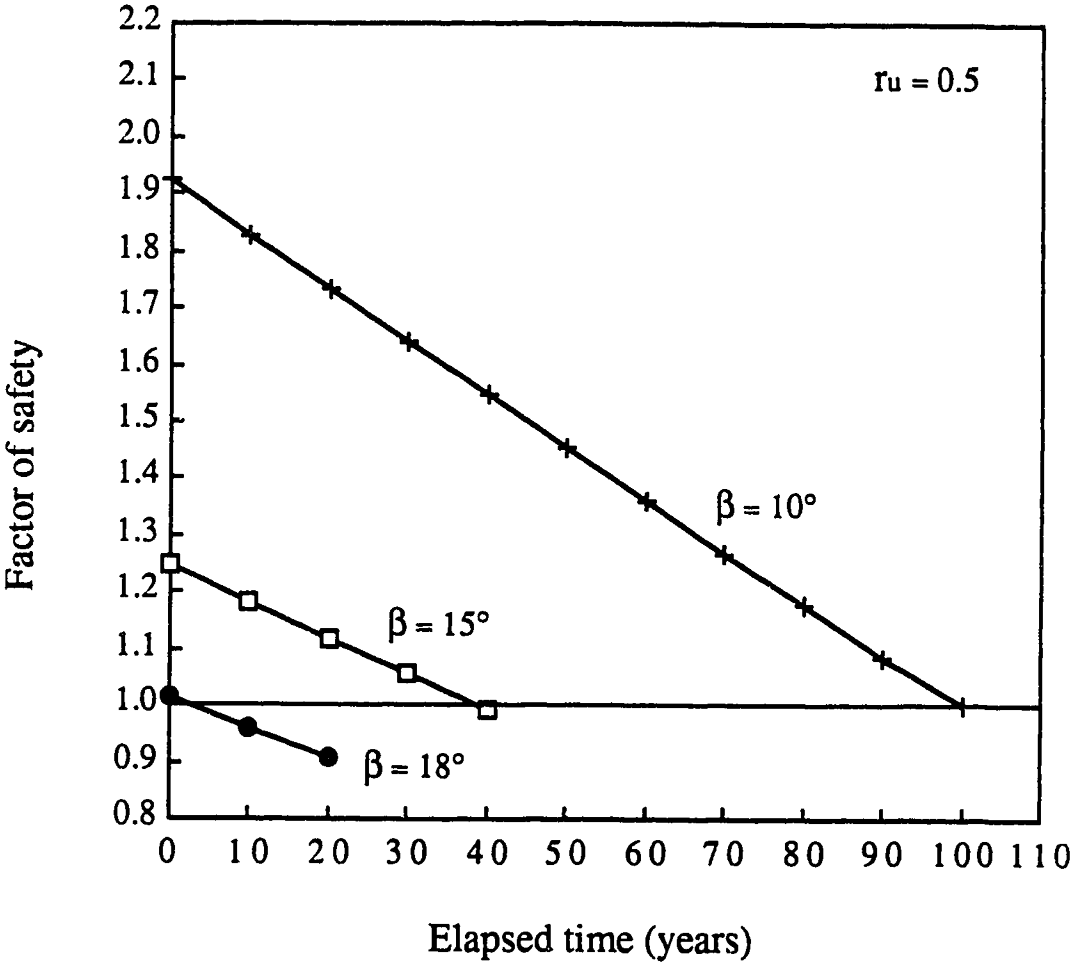

Figure 7.7 Variation of factor of safety with time for different slope angles

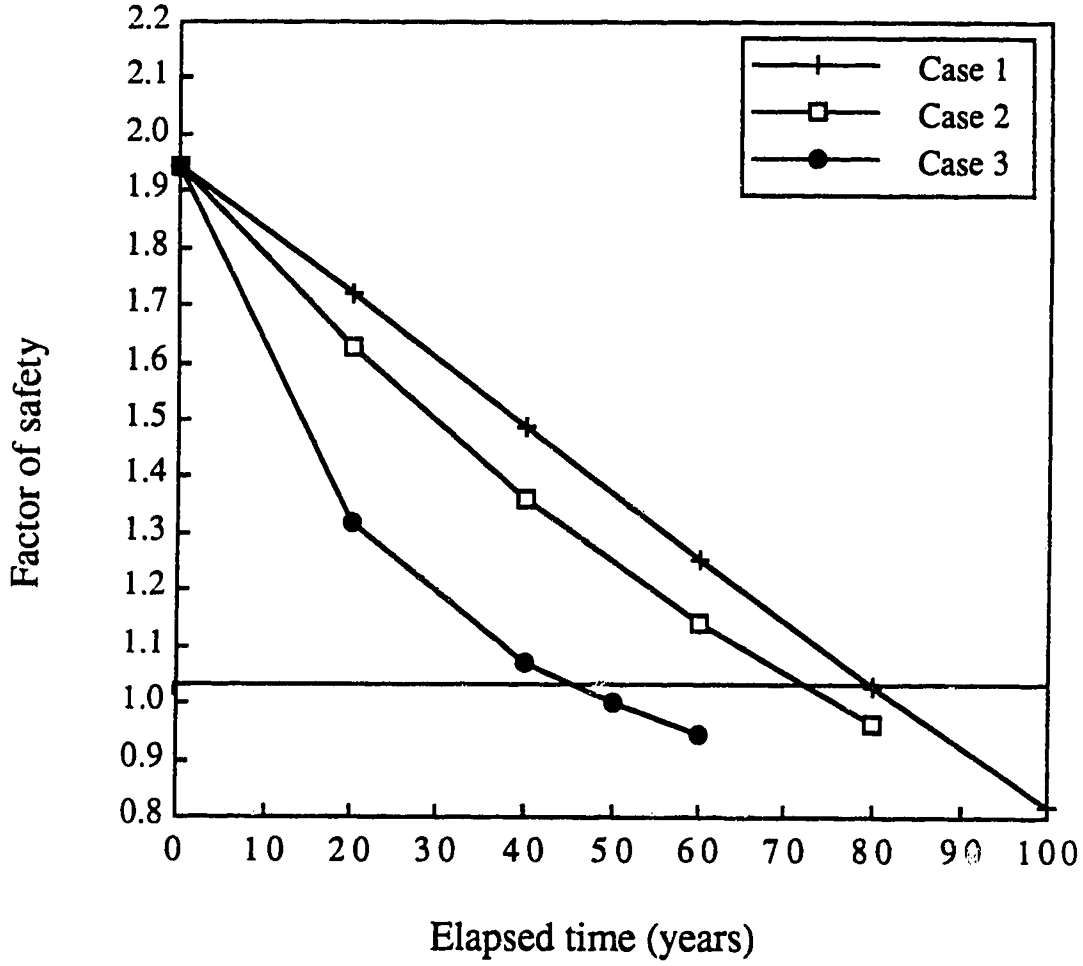

Figure 7.8 Variation of factor of safety with time

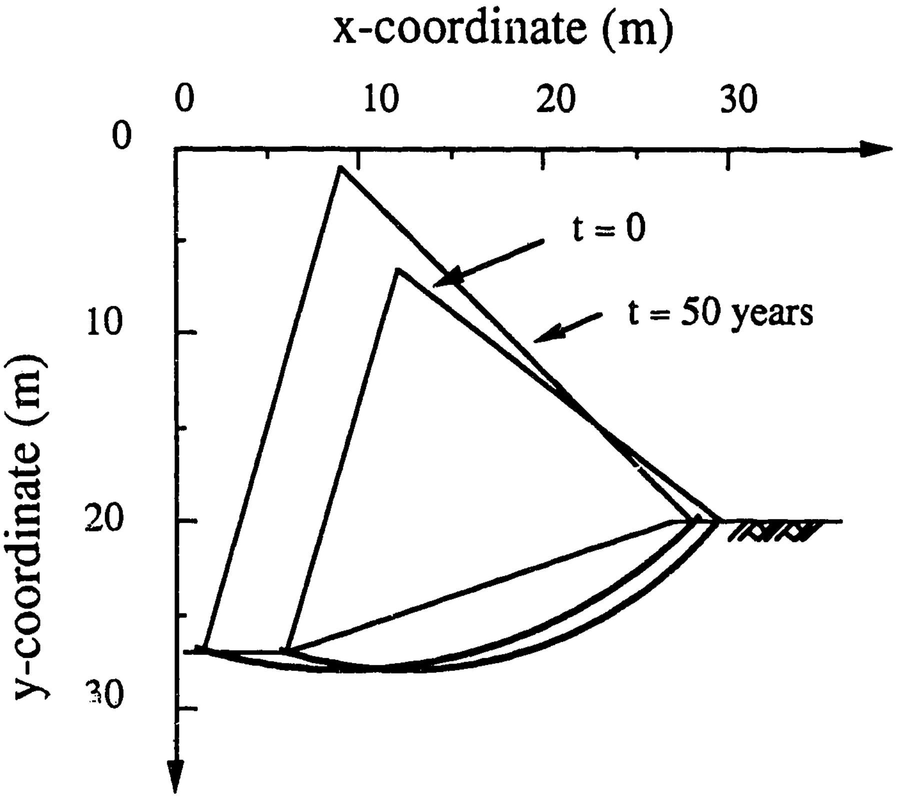

Figure 7.9 Critical slip circles at time of 0 and 50 years for Case 3

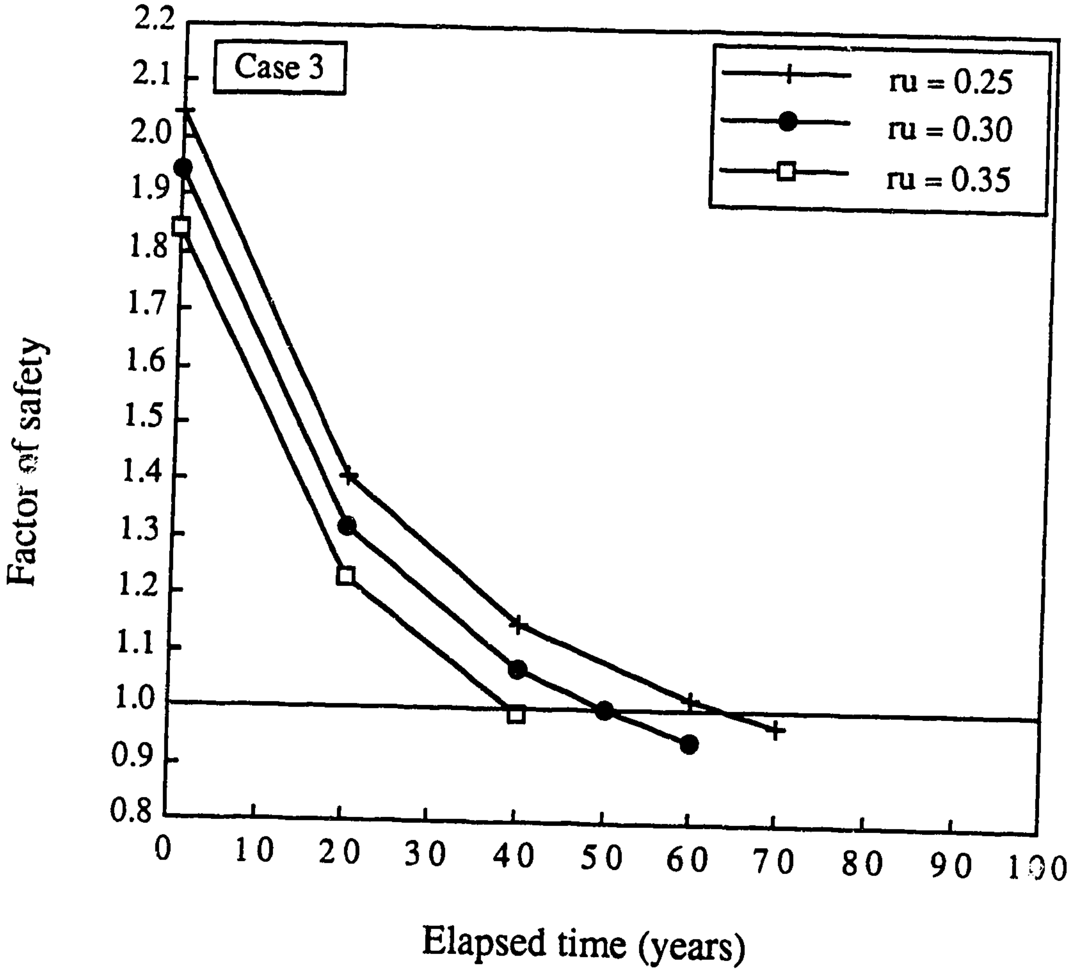

Figure 7.10 Variation of factor of safety with time for different values of r_u

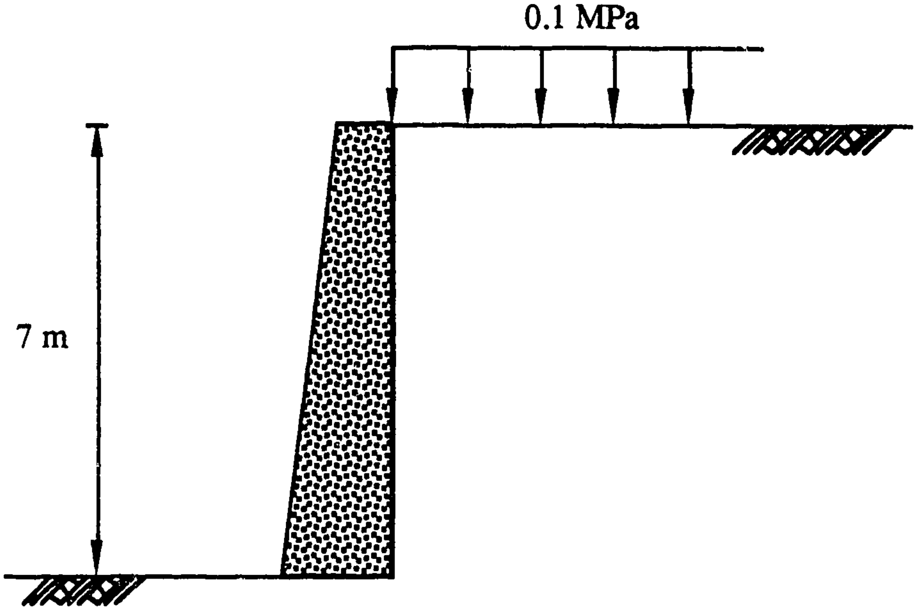

Figure 7.11 Retaining wall with horizontal ground surface

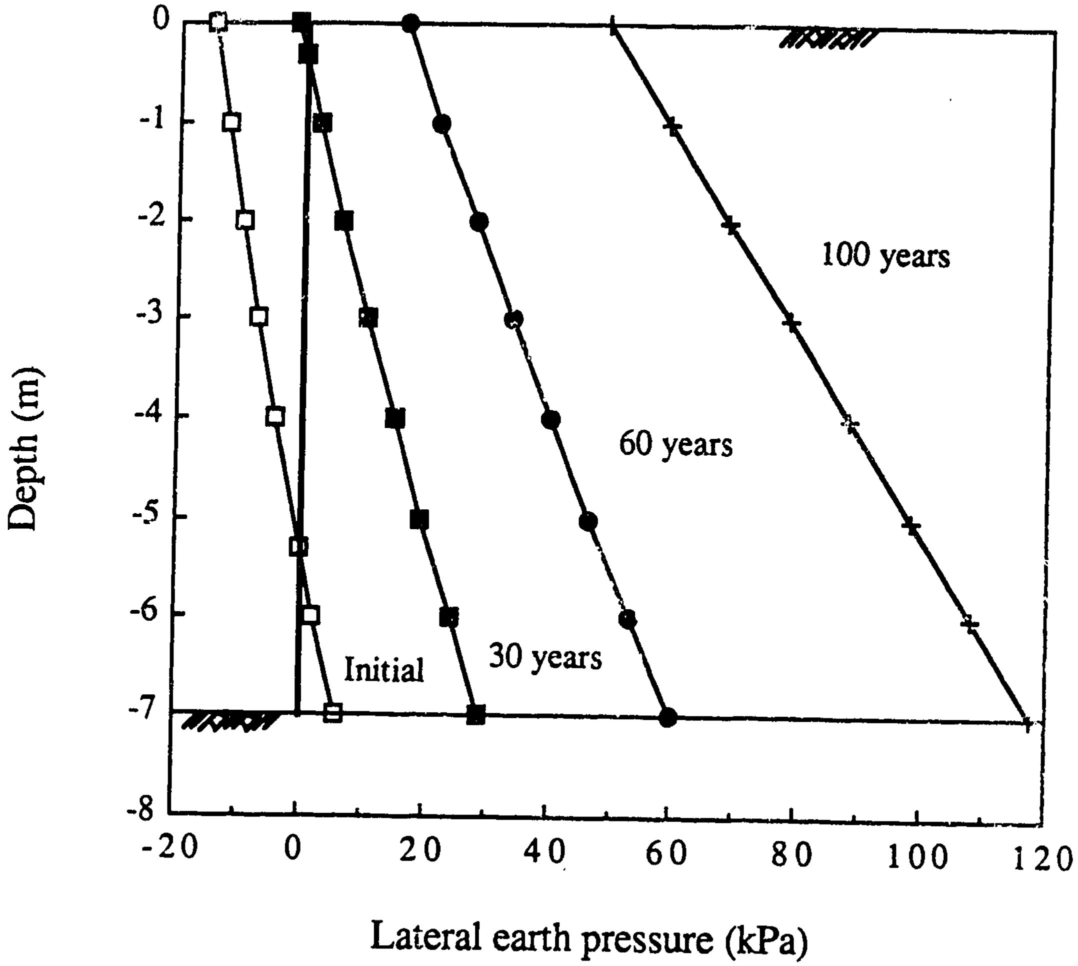

Figure 7.12 Active earth pressure distribution with depth

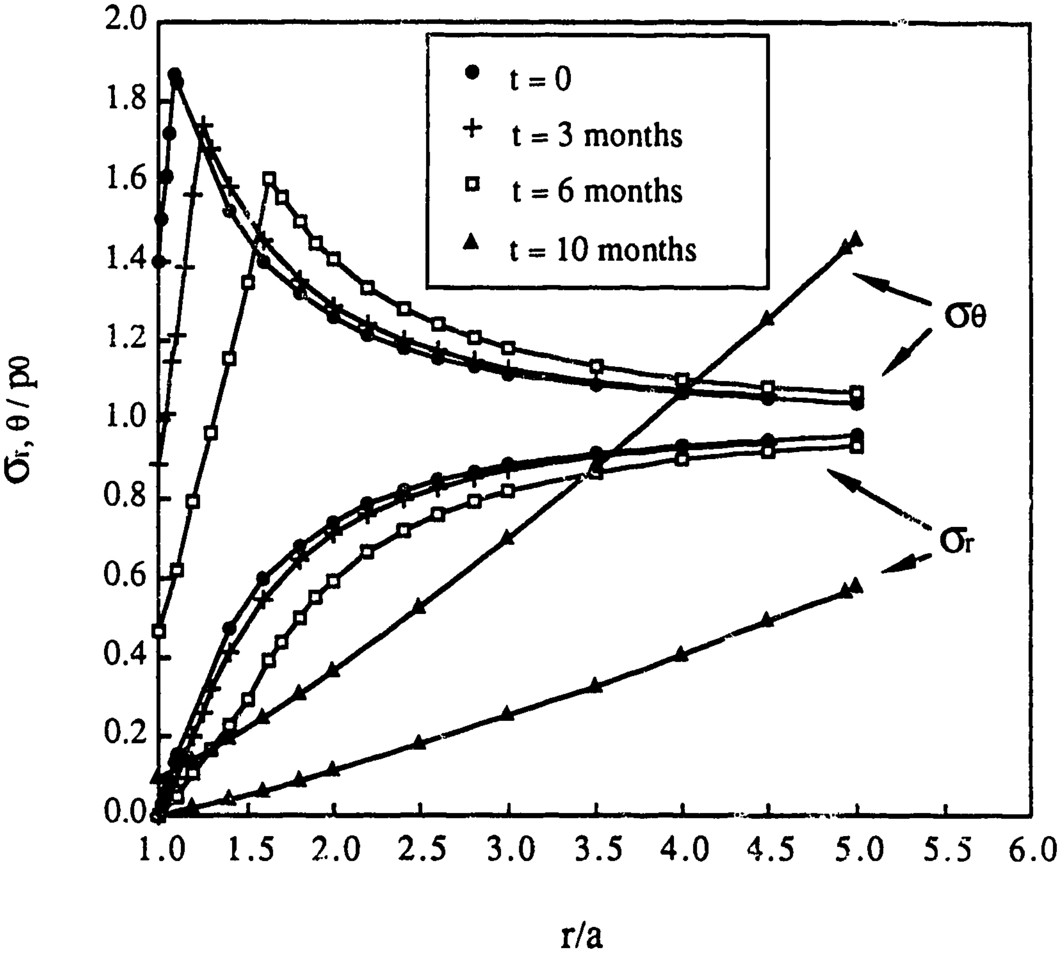

Figure 7.13 Variations with time of radial and tangential stresses around tunnel

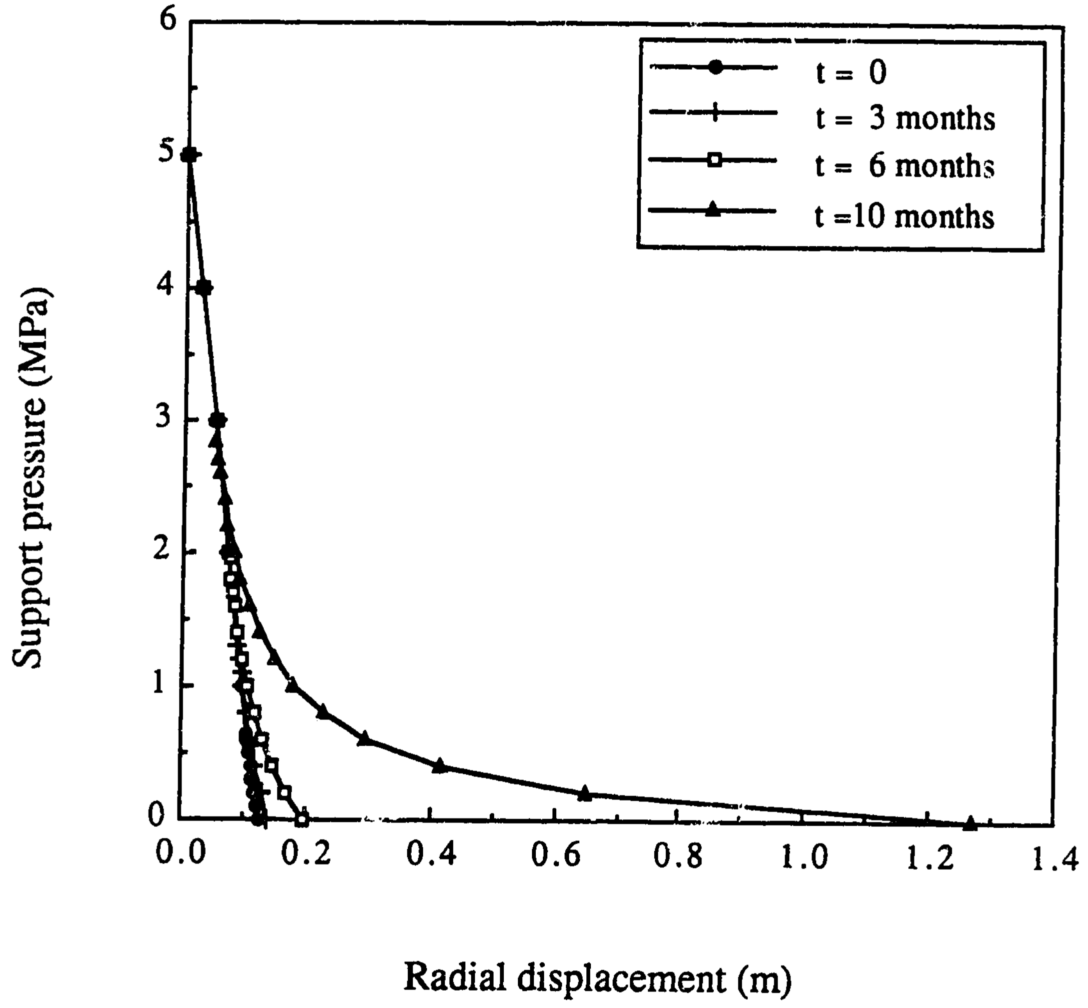

Figure 7.14 Variation with time of ground convergence curve

8. A comprehensive softening analysis

8.1 Introduction

Softening was discussed in detail in Chapter 2, and based upon the concepts developed there the finite element method to analyze softening effects was proposed and some examples were created in the subsequent chapters.

In this chapter a further discussion on softening is given and a more comprehensive analysis of softening by means of the finite element method is proposed. An example of softening in a slope is presented.

8.2 Further insight into softening

8.2.1 Internal and external softening

Softening mechanisms and their effects were discussed in detail in Chapter 2 and Terzaghi's softening mechanism was considered to be valid. The softening results from a deterioration of soil mass resistance due to uneven free-swelling which is initiated along fissures which are opened, during the process of pore water pressure equalization, in response to unloading stress paths imposed by excavation. The hard clay lump is transformed gradually into a softer clay within which the hard clay core may be retained. This softening is considered to be internal since no external agents are acting on the process except for the initial unloading. Stress change due to unloading is an important factor in initiating softening. It allows fissures to open. When a cutting is excavated, total stresses and pore water pressures in the ground are changed. For an elastic isotropic unloading, changes in effective stress after excavation can be represented using the first stress invariant, I_1', in terms of effective stress: the initial change in I_1' is theoretically zero and I_1' decreases with time toward the steady-state condition. Where negative pore water pressure is created due to excavation, fissures, which have been in a tightly interlocked state, will open later during swelling. Softening will start along these open fissures. Thus, it follows that softening takes place some time after I_1' starts decreasing.

Weathering effects such as slaking and freeze-thawing cause disintegration of the soil structure and also result in softening as described in Chapter 2. This softening due to weathering is considered to be external because during the process the energy for disintegrating the material comes from outside of the ground. Since weathering effects are generally restricted to relatively shallow depths below the ground surface, this softening is also restricted to the near ground surface. It is most likely that softening is more severe and its rate is much higher near the ground surface than at depth because at shallow depths internal as well as external softening take place.

8.2.2 Restriction on softening

Figure 8.1 shows stress paths and changes in pore water pressure at a representative point P before and after excavation in a fissured, over-consolidated clay. It is assumed that the ground is isotropic and fully-saturated and that the excavation is made in an undrained condition. Suppose that the stress state before excavation is represented by Point P (P') in the σ_1 (σ_1') and σ_3 (σ_3') stress space as shown in Figure 8.1(b). The excavation causes a reduction in total stresses and the resulting total stress state can be represented by Point A in the σ_1 and σ_3 stress space. The change in pore water pressure, Δu, due to total stress changes, $\Delta\sigma_1$ and $\Delta\sigma_3$, can be estimated as follows (Skempton, 1954):

$$\Delta u = B \{ \Delta\sigma_3 + A (\Delta\sigma_1 - \Delta\sigma_3) \} \tag{8.1}$$

where A, B are pore pressure parameters. Pore water pressure immediately after excavation, u_1, is $u_0 + \Delta u$ where u_0 is the pore water pressure before excavation, and the corresponding effective stress can be represented by Point B' in the σ_1' and σ_3' stress space since negative pore water pressure change is brought about in response to the undrained unloading. In Figure 8.1(c) changes in pore water pressure are shown for shallow and deep excavations denoted as S and D, respectively. Both excavations produce depressed pore water pressures in the ground. On average greater reductions in pore water pressure are brought about by a deeper excavation. The depressed pore water pressure equalizes with time toward the steady-state seepage condition, resulting in a gradual decrease in the effective stress towards Point A' in Figure 8.1(b). The excess pore water pressure, u_{exc}, is defined as the difference between u_1 and u_{ss} (pore water pressure at the steady-state condition) as shown in Figure 8.1(c). The stress path B'A' represents the swelling process. Assuming that softening does not take place, the soil element will remain stable since the effective stress state at the end of swelling does not reach the failure envelope, although it is seen that the drained condition is more dangerous than the undrained condition. In reality, however, the clay starts to soften some time after excavation, and the shear strength decreases with time toward the fully-softened condition as shown in Figure 8.1(b). The softening is unlikely to take place before the negative pore water pressure developed in the ground reaches zero or atmospheric pressure because as long as the negative pore water pressure remains the fissures stay closed. Referring to Figure 8.1(c), it seems to be reasonable to consider that the softening starts when the time t_p is reached. After the time t_p softening as well as swelling are occurring. When the equilibration of pore water pressure is achieved, softening alone will progress further. Depending on the stress state and shear strength retained during softening, the slope may or may not fail.

It can be seen from the above discussion that softening is restricted where negative pore water pressure is generated and that softening may be assumed to start when the negative pore water pressure becomes zero. Fissures may not be able to sustain high negative pore water pressures and therefore softening might actually start earlier. There is no experimental data to define this in detail.

The above discussion is taken into consideration in the subsequent finite element analysis.

8.3 Finite element analysis

8.3.1 Preliminary consideration

For a flat slope the changes in pore water pressure due to excavation may be approximated by:

$$\Delta u = \gamma \Delta z \tag{8.2}$$

where Δu is the change in pore water pressure, γ is the unit weight of the soil and Δz is the depth of soil excavated from above the point of interest (see Figure 8.2). Walbancke (1975) suggested, from the comparison with pore water pressures derived from two dimensional finite element analyses and field measurements, that this simple equation generally gives a reasonable approximation of pore water pressure changes due to excavation; noting that this equation tends to under-estimate pore water pressures near the crest of slope and over-estimate them at the base of the excavation as can be seen in Figure 8.2.

The variation with time in pore water pressure can be computed using consolidation theory. Considering its simplicity, one-dimensional swelling with a uniform value of the coefficient of swelling, C_s, is assumed here as adopted by Walbancke (*op. cit.*). It is further assumed that the initial consolidation pressure distributes uniformly through the drainage length at the location of interest and that pore water pressure before and after excavation is hydrostatic.

With these assumptions, isochrones for any location and time can be obtained. Figure 8.3 illustrates this analysis schematically. Further, by plotting points at which isochrones at various locations intersect the zero-pore water pressure line (for instance, Points A and B in Figure 8.3), a time contour can be obtained which consists of equi-time lines drawn through points of equal time when the pore water pressure reaches zero. Figure 8.4 shows the time contour obtained in this manner for a three to one cut slope having a 7 m depth. The coefficient of swelling of 3.5 m^2/year was assumed. As a boundary condition for solving the consolidation equation, swelling was restricted to the 14 m thick layer under the original ground surface. The time indicated in the figure is that required for the negative pore water pressure to become zero. It should be noted that these equi-time lines also represent time for softening to start after excavation. Softening can be seen to take place successively in the slope.

It should be kept in mind that external softening which could facilitate additional softening near the excavation face is not considered in this analysis.

8.3.2 Softening analysis

The finite element analysis here deals with a cutting of a three to one slope having a 7 m depth as shown in Figure 8.5. The excavation is performed in stages and in a fully-undrained condition. In reality, swelling as well as softening take place in the ground after excavation. However, in order to avoid the complexity associated with the inclusion of the swelling effect, the swelling process is not taken into account, and the pore water pressure is assumed to achieve the ultimate equilibrium condition - steady-state seepage condition - immediately after excavation. The ground consists of a fissured, over-consolidated clay and has a horizontal ground surface before excavation. The strength and deformation properties of the clay are summarized in Table 8.1. The constitutive model used in the analysis is an elastic, perfectly-plastic relation with no plastic volumetric changes. The finite element discretization of the ground is made with nine hundred and two four-node isoparametric elements and nine hundred and fifty nodal points. The boundary conditions are shown in Figure 8.6.

The computation begins with the application of the initial stresses in the ground. The K_0 value of 0.8 was applied. Then, the stepped excavation is modelled using an undrained effective stress analysis (Chan, 1986; Chan and Morgenstern, 1989). Skempton's pore pressure parameters A and B are assumed as 1/3 and 1, respectively, following Eigenbrod (1975). As mentioned earlier, the process of pore water pressure equilibration is not considered and the pore water pressures in the ground are assumed to attain their steady-state condition just after excavation. In the finite element analysis this is carried out by replacing the pore water pressures in the ground calculated in the excavation simulation by those of the steady-state condition which are obtained from a flow net analysis. Then, the softening scheme starts. According to the discussions presented in the previous section, softening is restricted to a certain region in the ground and begins at different times. Referring to

Figure 8.4, the ground is divided into five zones as shown in Figure 8.7: in Zone 1 no softening occurs, in Zone 2 softening starts immediately after excavation, in Zone 3 softening begins one year after excavation and so on. The time to reach the fully-softened condition is 100 years in all the softening zones. Figure 8.8 shows the input variation with time of shear strength retained at σ_3' of 0.05 MPa in each zones. The shear strength in the ordinate is the τ value at the tangent point between the failure envelope and the Mohr circle drawn for σ_3' of 0.05 MPa. The close-up of the initial part in the strength variation is given in the inset of the figure.

8.3.3 Results

Figures 8.9 and 8.10 show the variation with time in horizontal and vertical displacements, respectively. The displacements developed when the excavation is completed but before the pore water pressures are replaced are taken as zero. This allows one to evaluate the influence of the pore water pressure change on the slope behaviour. It can be seen from the figure that this pore water pressure replacement results in a large upward displacements at the both crest and toe (see displacements at elapsed time of zero). These displacements could have developed gradually with time if swelling had been taken into consideration in the analysis. In this example this pore water pressure change did not cause yielding in the ground as can be seen later. After the sudden movements due to the pore water pressure change, the slope remains still for a while. Horizontal displacement increases gradually initially at both locations 50 years after excavation and rapidly as the slope approaches its collapse, in association with the progression of yielding. Vertical displacement at the toe follows the same trend as the horizontal displacement but at the crest only a small downward displacement develops. The lifetime of the slope is calculated as 95 years. Beyond 95 years the solution did not achieve convergence in 30 iterations. Figure 8.11 shows the development of the plastic zone. Yielding initiates at the toe of the slope 50 years after excavation, then propagates with time as can be seen in the figure.

8.4 Commentary

The time-displacement relations obtained in the above analysis (Figures 8.9 and 8.10} may be seen as 'creep' since these results were calculated under a constant loading condition. There is a trend that time-dependent deformations are analyzed by employing creep or visco-plasticity because they provide a computationally convenient way to account for time effects. But considering that the time-displacement relations obtained here are the results of the progression of yielding due to softening, it can be considered that the finite element method used here provides a rational means of analyzing the time-dependent instability without loosing insight into the problem.

A more comprehensive finite element method to analyze the time-dependent instability can be formulated by unifying softening with swelling analyses. Figure 8.12 shows a simple flow chart of this unified finite element analysis. Suppose that a cutting is excavated in an undrained condition. First, an undrained analysis is carried out at t = 0 to establish the initial conditions for subsequent swelling and softening analyses. At this time, an element where negative pore water pressure is evaluated is registered as a 'softening potential' element which will undergo softening later. Then, equalization of the pore water pressure and associated deformation are [illegible]ated at subsequent time steps, which may employ a coupled or uncoupled elastic, plastic consolidation theory. As time goes by, pore water pressure equalizes toward the steady-state condition. During this process, the pore water pressure in a 'softening potential' element may reach zero. For this element, softening scheme is initiated: the shear strength reduction is computed and this reduced strength is used in evaluating the corresponding element stiffness matrices at the next time step. When the dissipation of excess pore water pressure is comp[illegible] the softening scheme alone progresses; that is, stiffness matrices [illegible]d to soil behaviour are modified, keeping pore water pressure constant as the final steady-state value in subsequent time steps. The computation continues until the solution can not achieve convergence or the fully-softened condition is reached. It should be noted that in the example analyzed in this chapter, where and when negative pore water pressure is generated and dissipates to zero were pre-determined as an approximation by using Terzaghi's consolidation theory and implemented in the finite element analysis as control data. Therefore, it can be seen that the example contains the essentials to portray the role of the softening mechanism.

8.5 Summary

This chapter extends the discussion on softening given in Chapter 2. Some restrictive conditions regarding where and when softening takes place are established.

A finite element analysis was carried out for a cut slope taking into account the concepts on softening developed so far. Time-dependent development of deformations and plastic zones are demonstrated.

A more comprehensive finite element method to analyze softening effects is proposed which unifies the softening analysis developed in this study with the analysis of swelling.

Table 8.1 Material properties of clay for excavation analysis

γ_t (MN/m^3)	σ_c (MPa)	A_0	A_{fs}	B_0	S_0
0.02	0.206	3.525	0.698	1.762	-0.109

Depth (m)	E' (MPa)	ν'
0 - 20.5	15.0	0.15
20.5 - 30.5	23.0	0.15
30.5 - 49.0	36.0	0.15

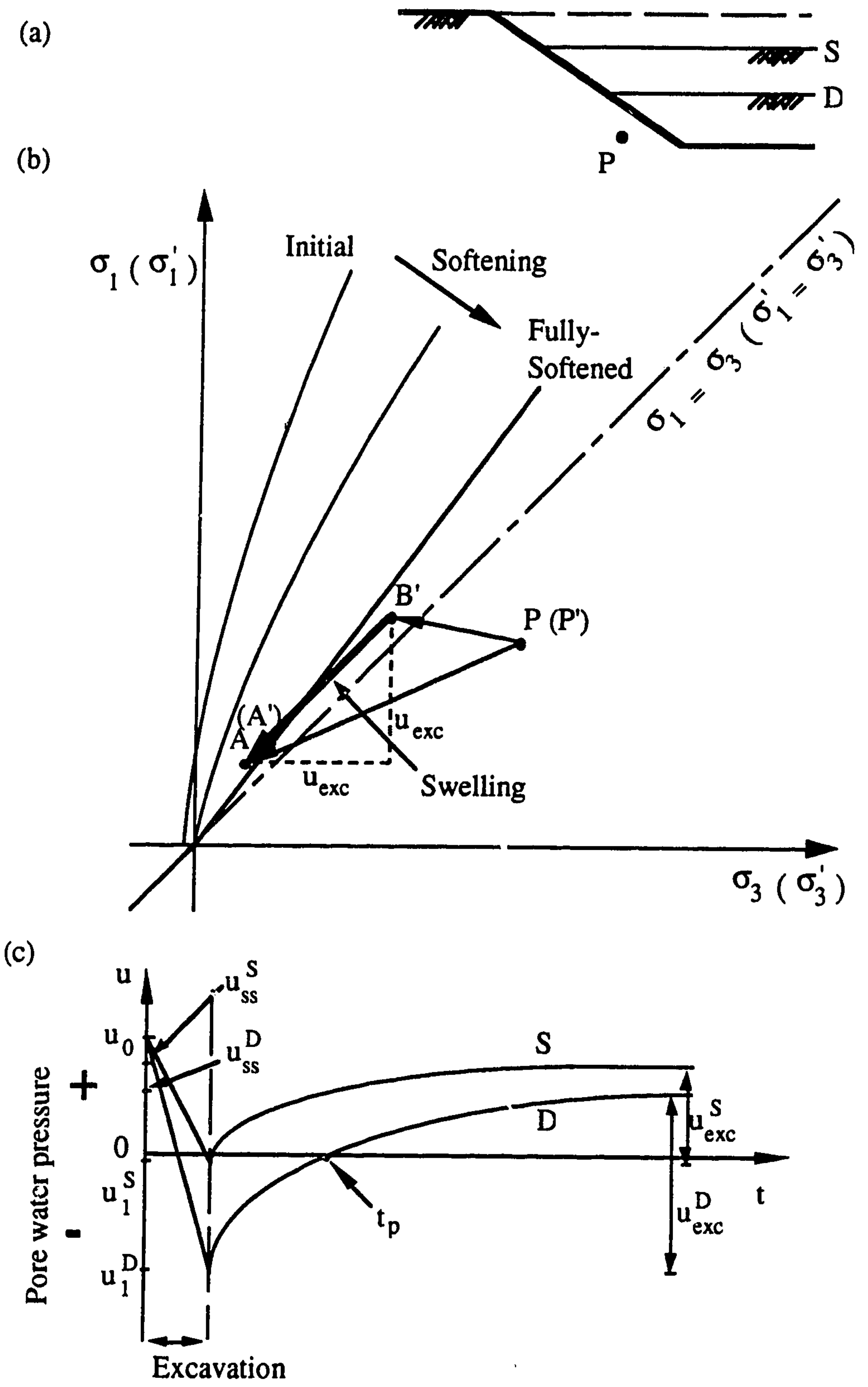
(a)
S
D
P
(b)
σ1 (σ'1)
Initial
Softening
Fully-Softened
σ1 = σ3 (σ'1 = σ'3)
B'
P (P')
(A')
A
u_exc
u_exc
Swelling
σ3 (σ'3)
(c)
u
u_ss^S
u_0
u_ss^D
S
D
+
0
-
u_1^S
u_1^D
Pore water pressure
u_exc^S
u_exc^D
t
t_p
Excavation

Figure 8.1 Stress paths and pore water pressure changes before and after excavation

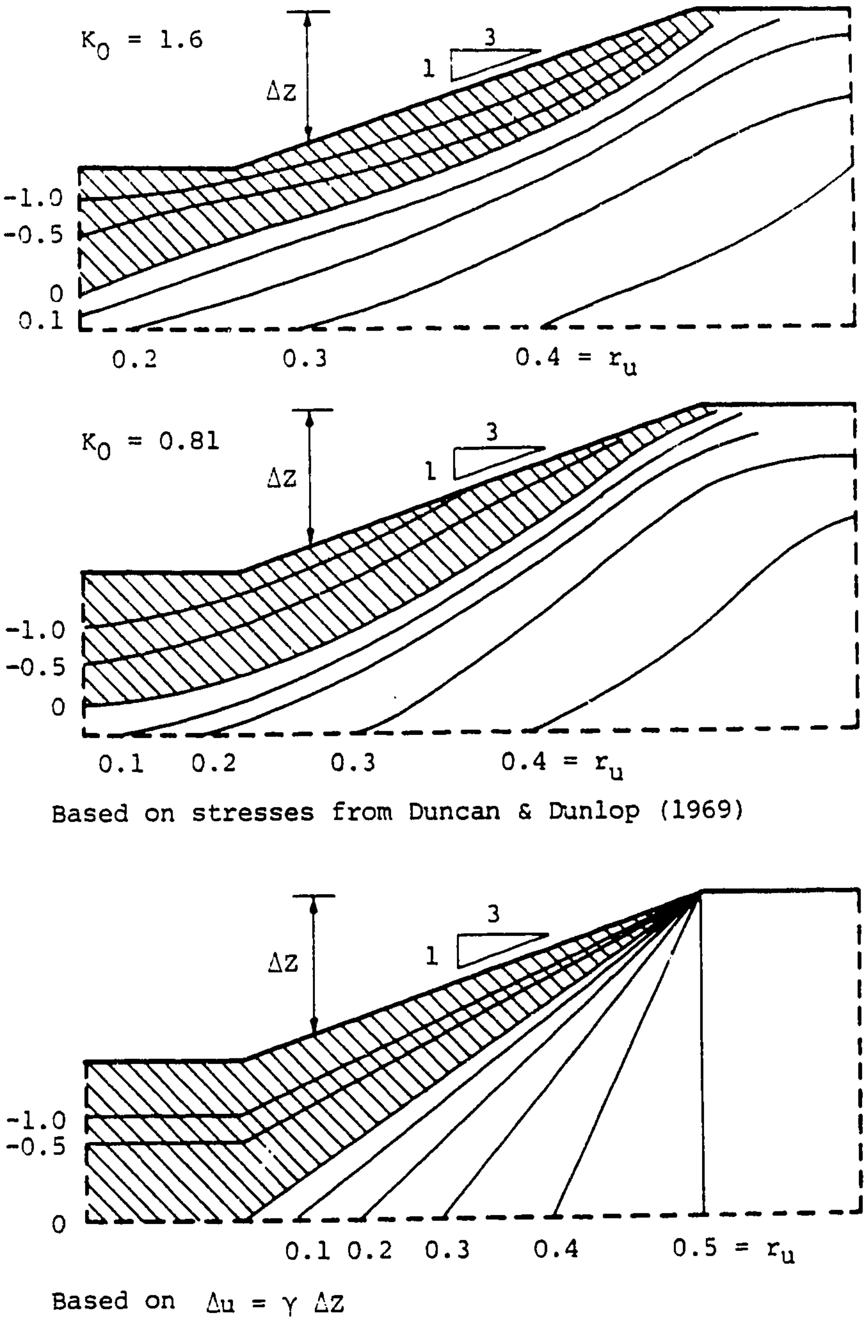
K$_0$ = 1.6
Δz
3
1
-1.0
-0.5
0
0.1
0.2
0.3
0.4 = r$_u$
K$_0$ = 0.81
Δz
3
1
-1.0
-0.5
0
0.1
0.2
0.3
0.4 = r$_u$
Δz
3
1
-1.0
-0.5
0
0.1
0.2
0.3
0.4
0.5 = r$_u$

Based on stresses from Duncan & Dunlop (1969)

Based on $\Delta u = \gamma \Delta z$

Figure 8.2 Pore water pressure at end of construction in 1:3 cut slope (modified after Walbanke, 1975)

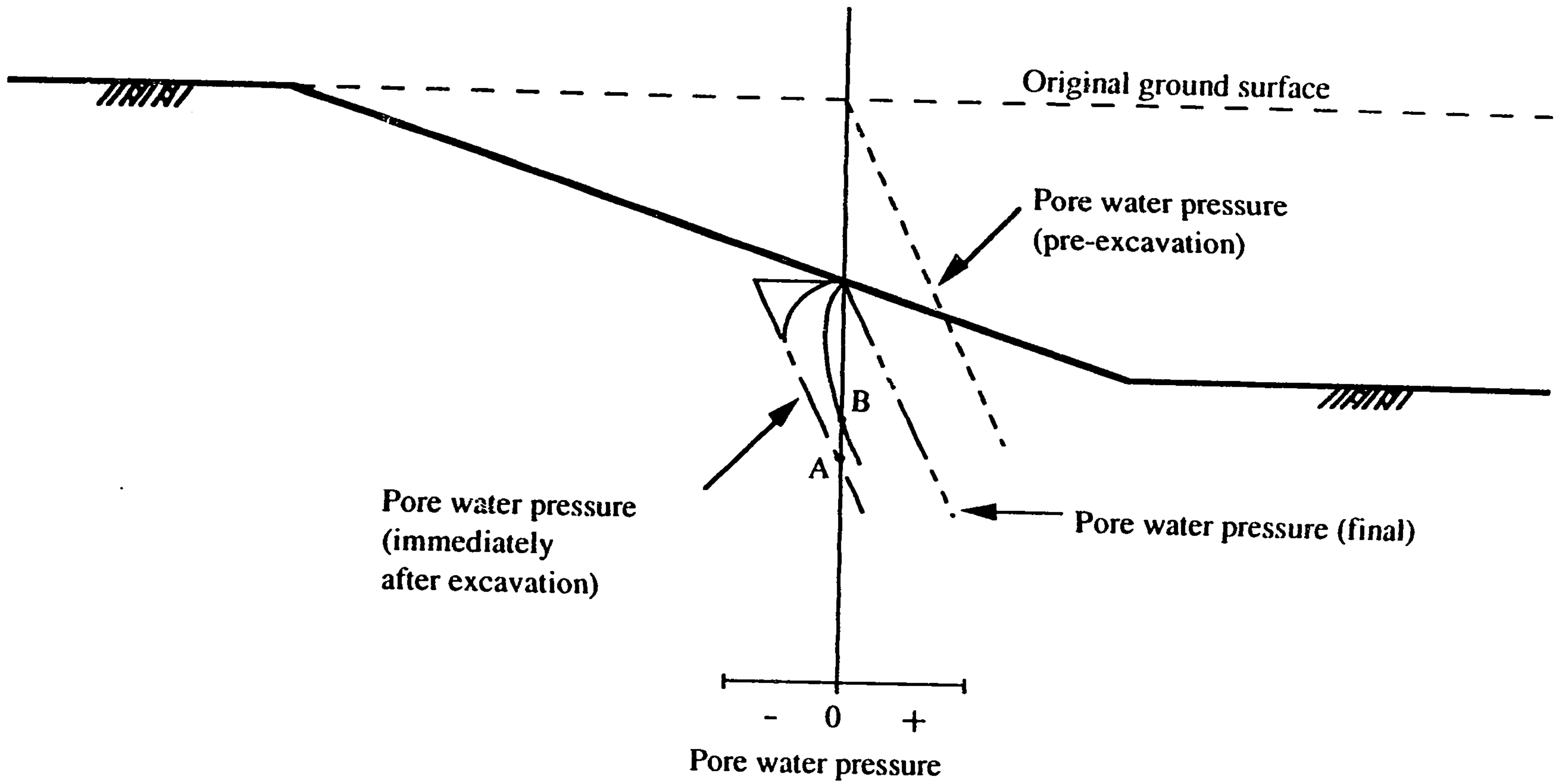
Original ground surface
Pore water pressure
(pre-excavation)
B
A
Pore water pressure
(immediately
after excavation)
Pore water pressure (final)
-
0
+
Pore water pressure

Figure 8.3 Calculation of variation in pore water pressure with time in cut slope

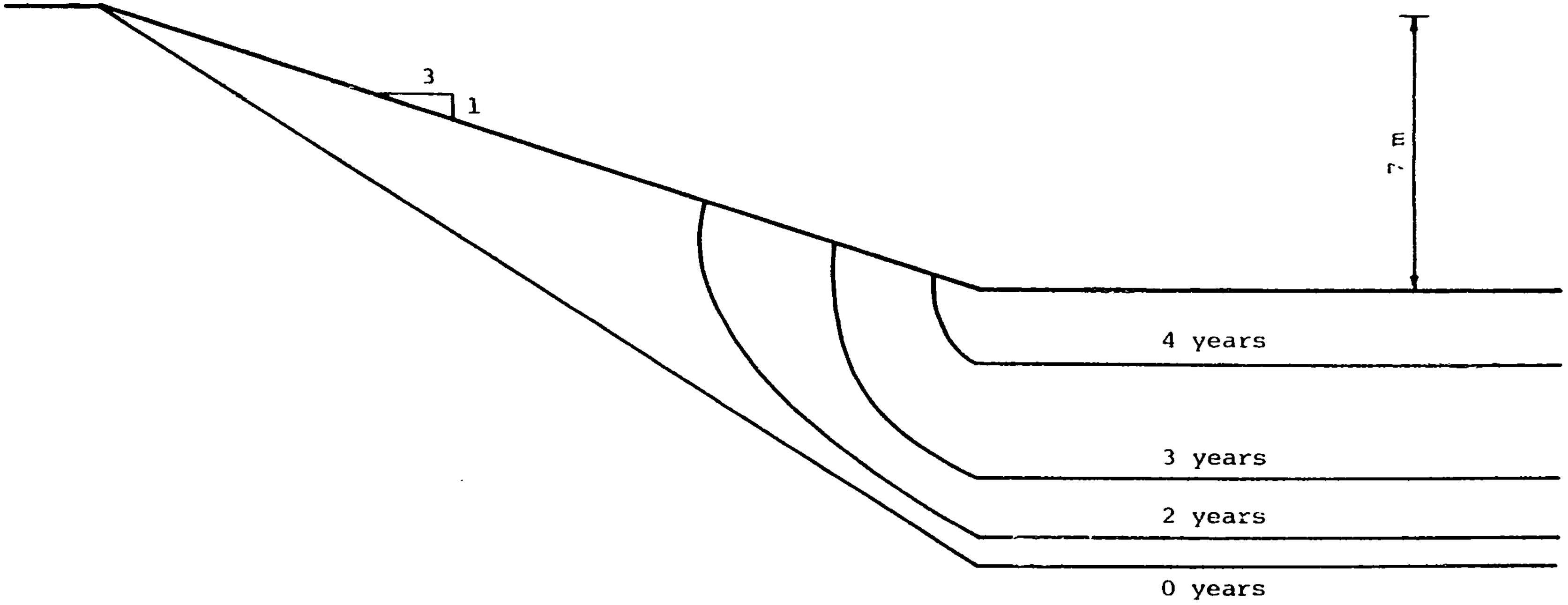
3
1
7 m
4 years
3 years
2 years
0 years

Figure 8.4 Time contour showing equi-time lines for 1:3 cut slope

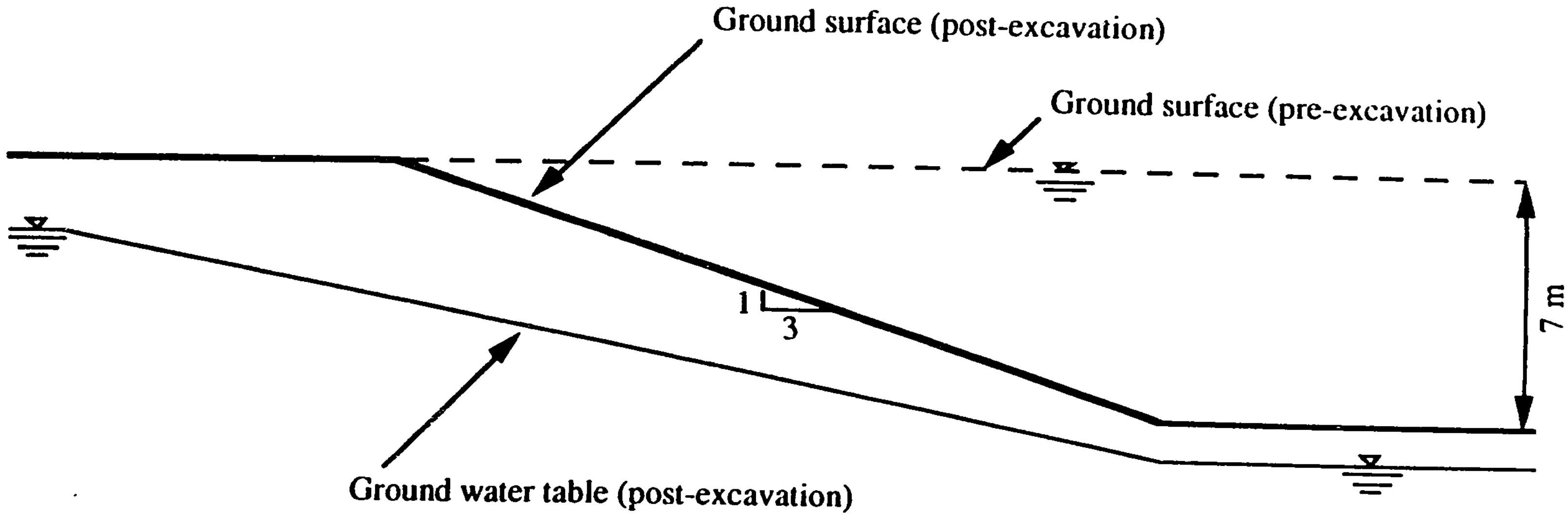
Ground surface (post-excavation)
Ground surface (pre-excavation)
1
3
7 m
Ground water table (post-excavation)

Figure 8.5 Ground condition of cut slope for finite element analysis

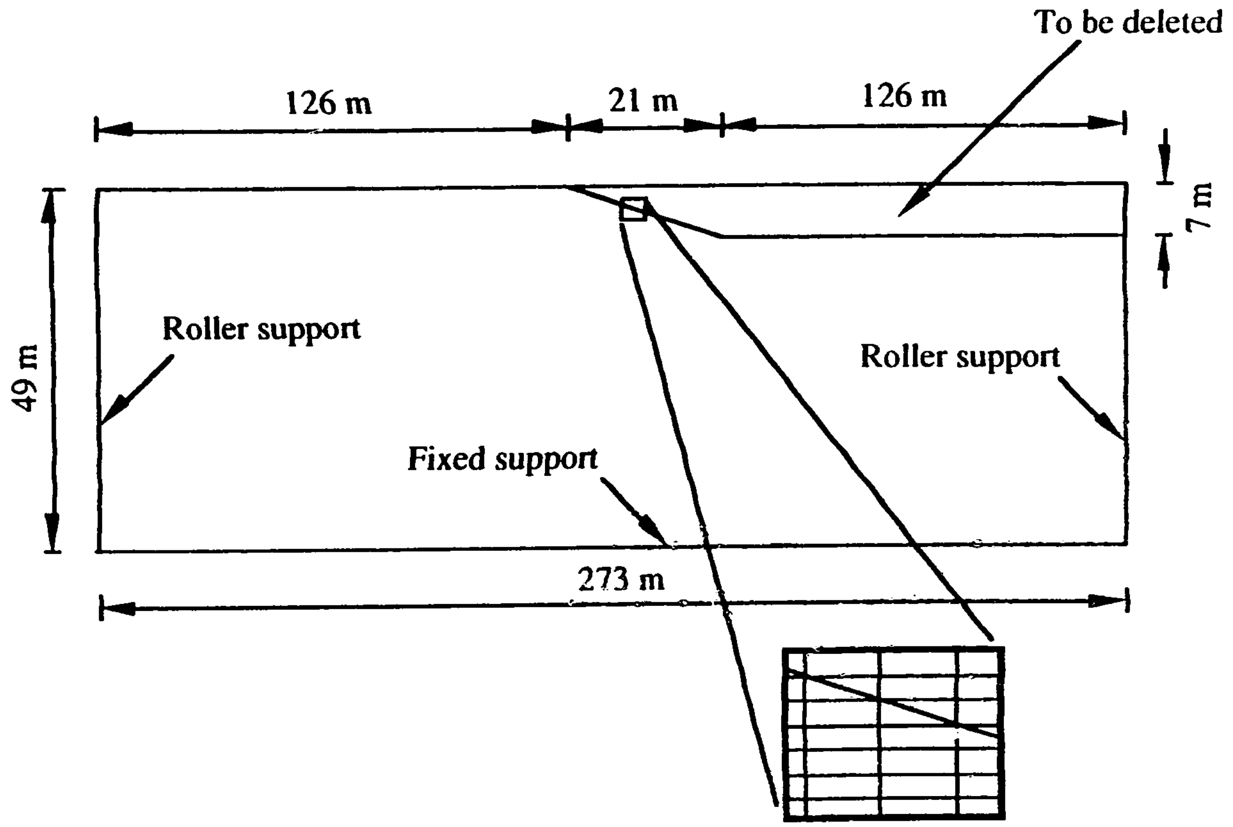
To be deleted
126 m
21 m
126 m
7 m
49 m
Roller support
Roller support
Fixed support
273 m

Figure 8.6 Finite element discretization of cut slope

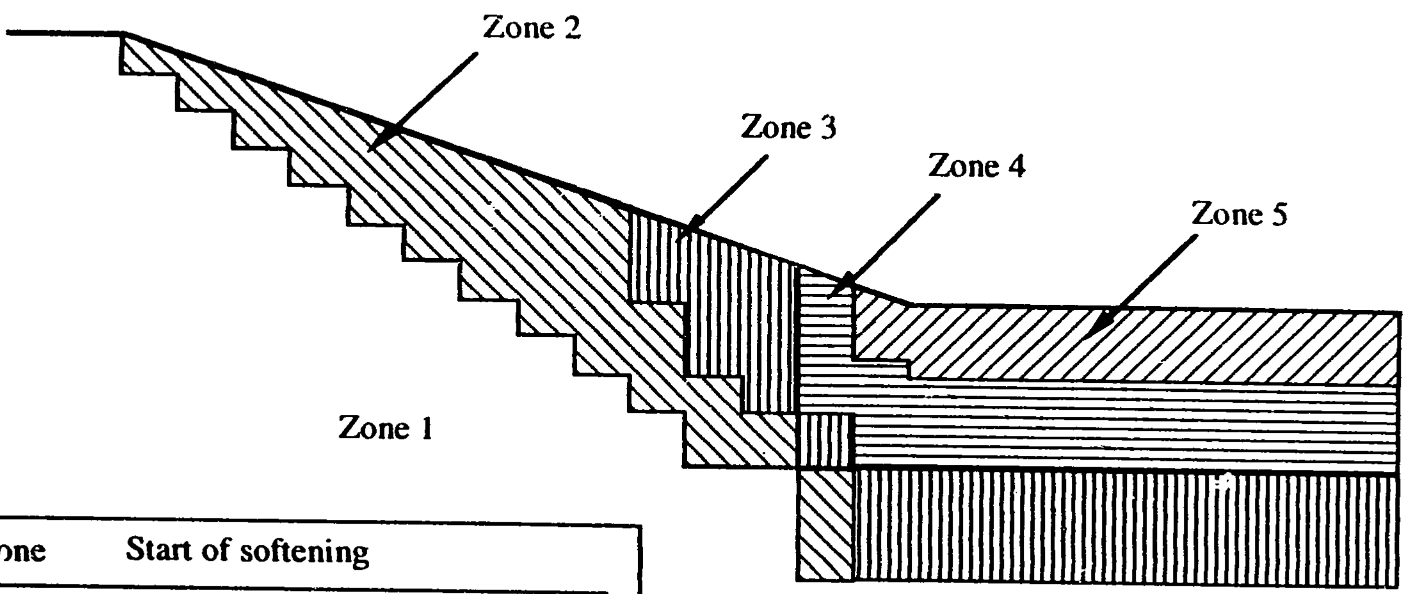
Zone 2
Zone 3
Zone 4
Zone 5
Zone 1

Zone	Start of softening
Zone 1	No
Zone 2	Immediately after excavation
Zone 3	2 years after excavation
Zone 4	3 years after excavation
Zone 5	4 years after excavation

Figure 8.7 Softening zones in ground for finite element analysis

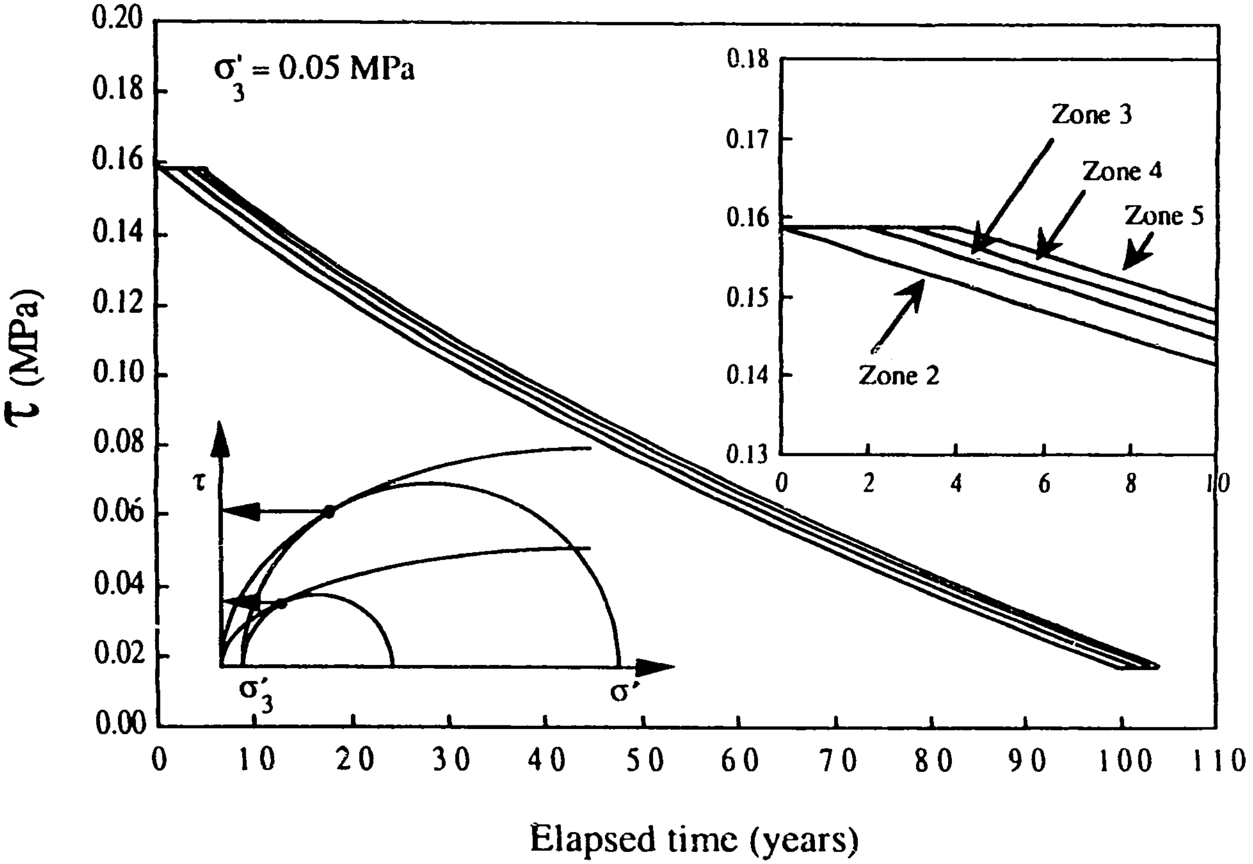

Figure 8.8 Input strength variation with time at σ_3' = 0.05 MPa

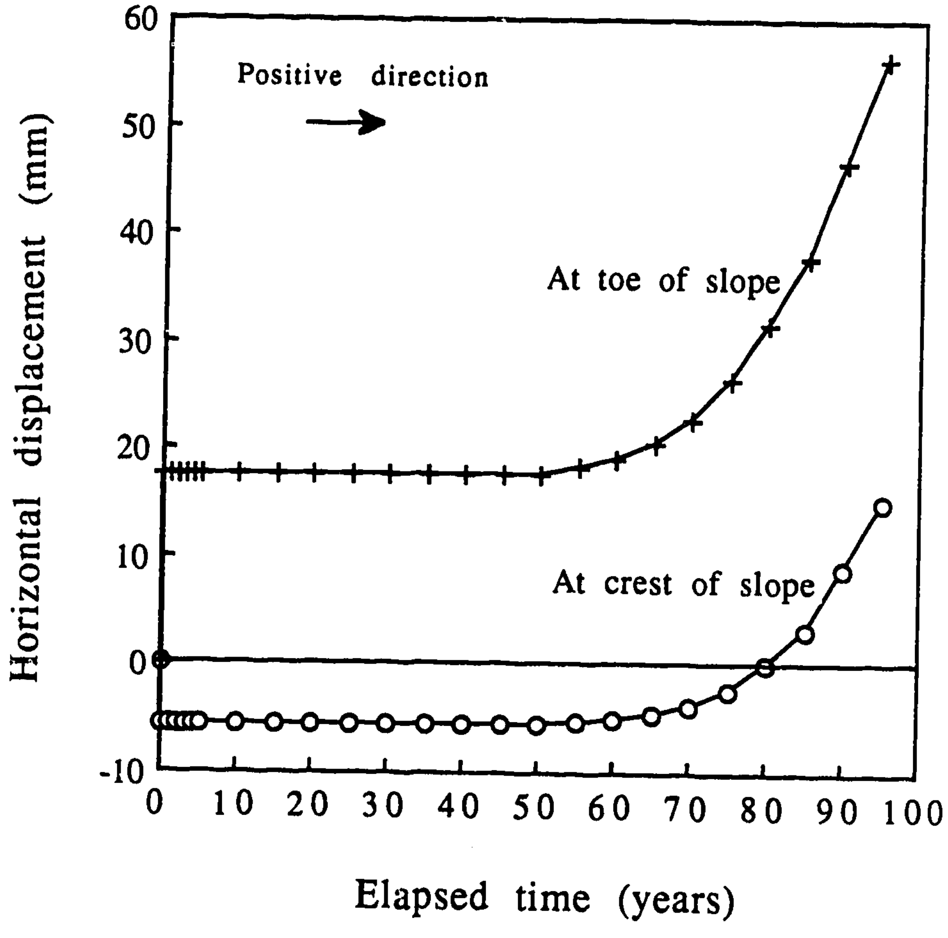

Figure 8.9 Variation with time in horizontal displacements at crest and toe of slope

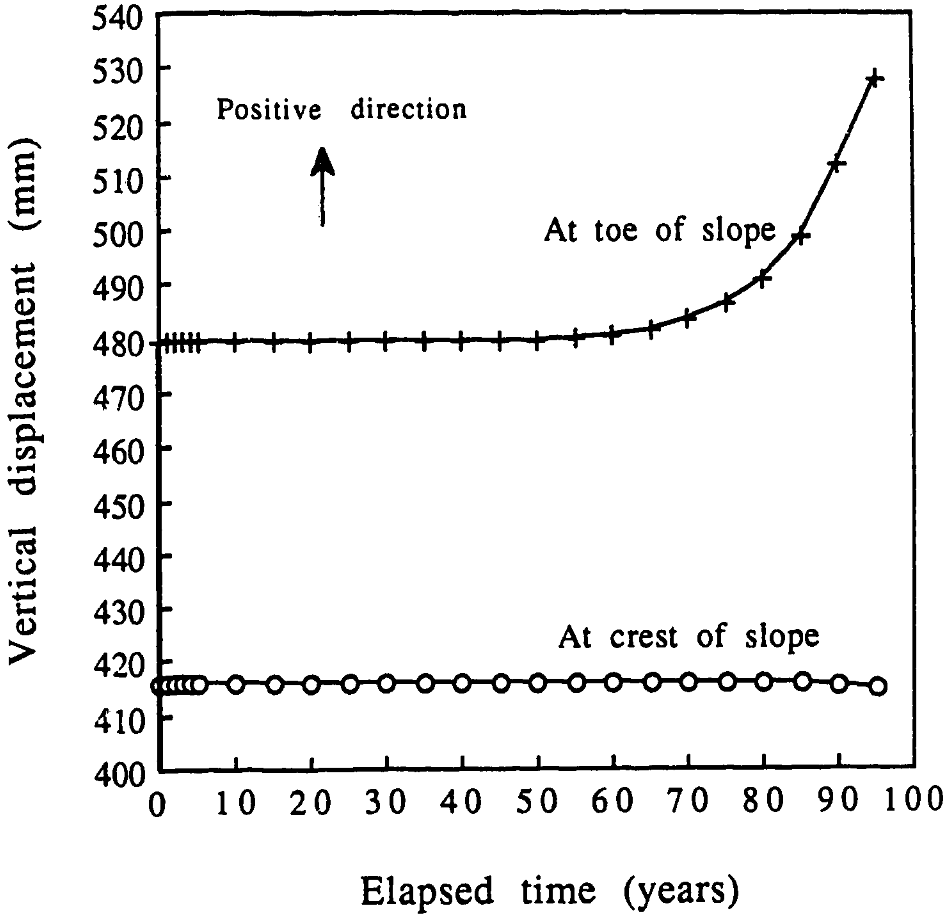

Figure 8.10 Variation with time in vertical displacements at crest and toe of slope

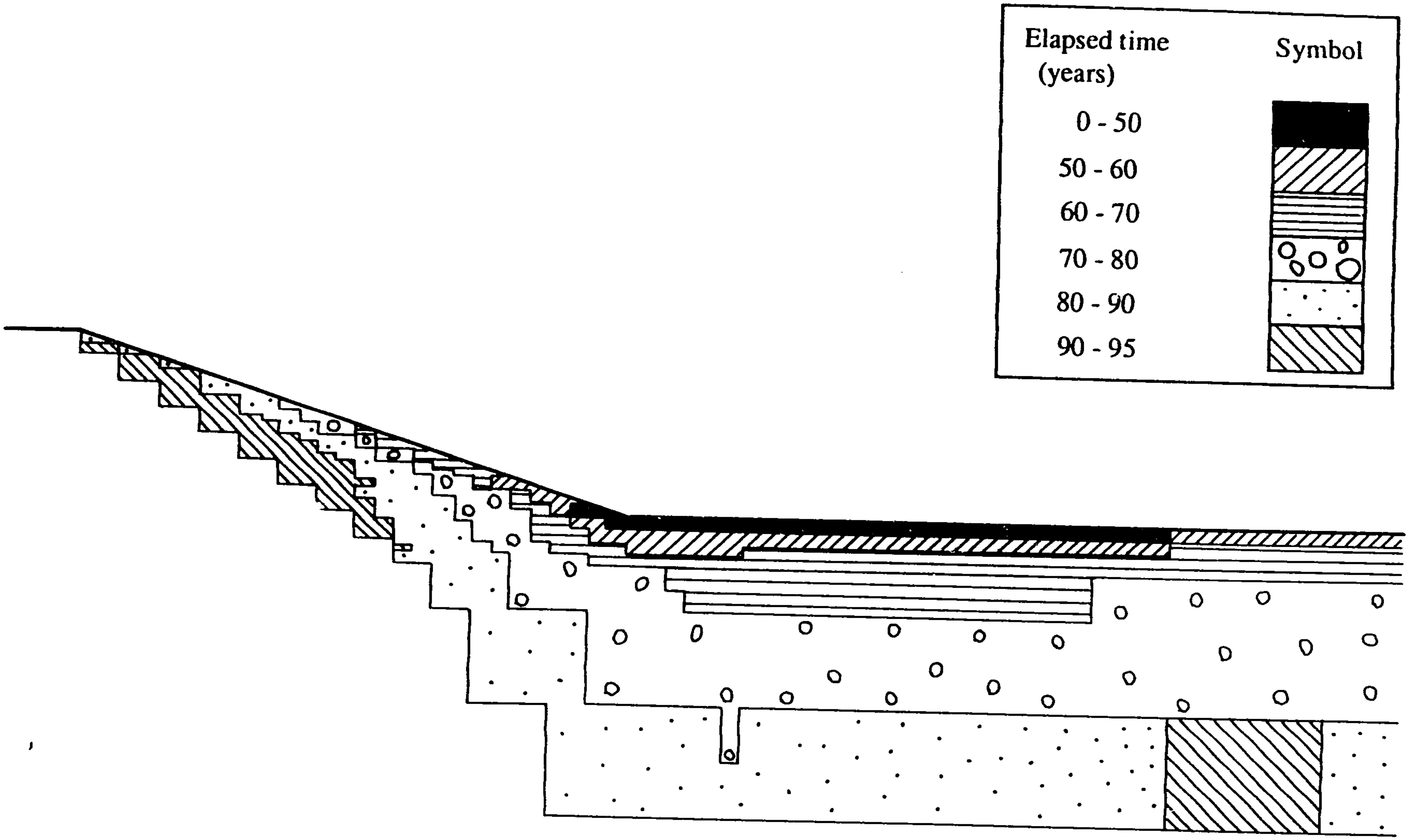
Elapsed time (years)
Symbol
0 - 50
50 - 60
60 - 70
70 - 80
80 - 90
90 - 95

Figure 8.11 Development of plastic zones in cut slope

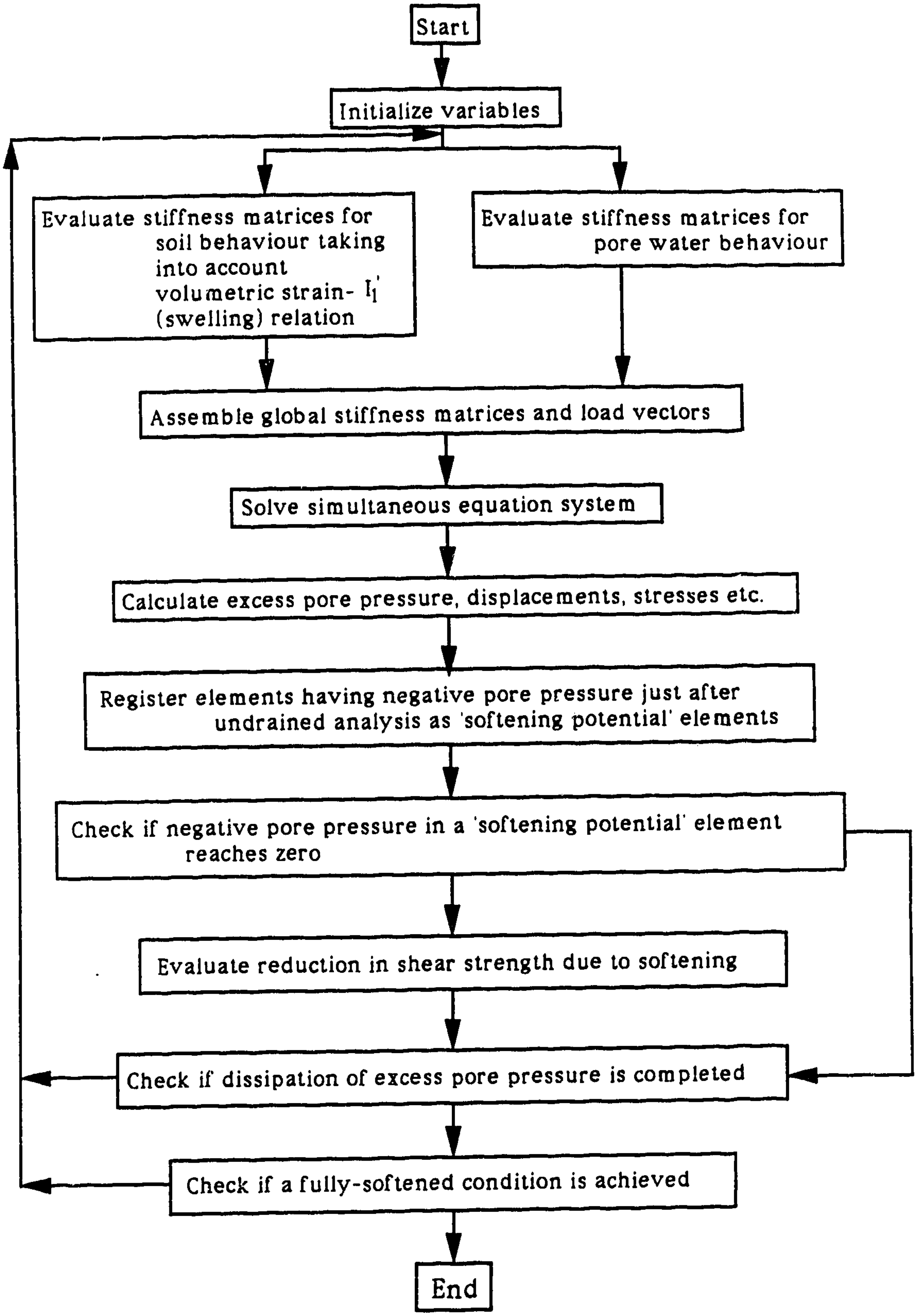
Start
Initialize variables
Evaluate stiffness matrices for soil behaviour taking into account volumetric strain- I_1' (swelling) relation
Evaluate stiffness matrices for pore water behaviour
Assemble global stiffness matrices and load vectors
Solve simultaneous equation system
Calculate excess pore pressure, displacements, stresses etc.
Register elements having negative pore pressure just after undrained analysis as 'softening potential' elements
Check if negative pore pressure in a 'softening potential' element reaches zero
Evaluate reduction in shear strength due to softening
Check if dissipation of excess pore pressure is completed
Check if a fully-softened condition is achieved
End

Figure 8.12 Flow chart of comprehensive swelling-softening analysis

9. Conclusions

9.1 Conclusions

Time-dependent instability observed in fissured, over-consolidated clays and mudstones was investigated in this dissertation. The main emphasis was placed upon understanding of softening mechanisms and their effects and development of a numerical method to analyze this problem.

Softening has been observed in field investigations of cut slopes and tunnels. The mechanism of softening described by Terzaghi appears to be valid. The softening results from a deterioration of soil mass resistance due to uneven swelling along open fissures. Unloading imposed by excavation initiates the softening. The hard clay lump is transformed with time into a softer clay within which the hard clay core may be retained. Softening also results from weathering effects which cause disintegration of the soil structure. Softening can be classified into internal and external processes. The effect of softening is to decrease the shear strength of material with time accompanied by a reduction of the dilatancy property. This shear strength reduction due to softening can be represented as a lowering of the failure envelope and a reduction in the high non-linearity at low stress levels. The rate of softening can be estimated from field observations or analyses of case histories. It is essential to carry out systematic experiments on these materials at low stress levels in order to gain physical insight into the mechanism of softening, but there exist only a few such experimental data in the literature.

A simple non-linear failure criterion was proposed for fissured, over-consolidated clays and mudstones which consists of maximum and minimum principal stresses, uniaxial compression strength and three strength parameters. These strength parameters can be determined from conventional strength tests such as triaxial compression tests. Usefulness of this failure criterion has been demonstrated through comparisons with experimental data taken from the literature. Further, using this failure criterion, shear strength reduction due to softening can be described rationally. The variation of shear strength during softening has been illustrated by interpolating the strength parameters from the initial to fully-softened values with an inverse-hyperbolic function.

The finite element method to analyze softening effects was developed according to an elastic-plastic finite element formulation based upon the principal of virtual work. The failure criterion with time-dependent strength parameters proposed in this research was incorporated in the finite element analysis. Elastic, perfectly-plastic and strain-softening relations are considered as constitutive models. The strain-softening model contains conventional shear strength and deformation parameters with only two extra parameters controlling post-peak behaviour. Examples were analyzed which demonstrate the usefulness of the proposed finite element method.

A high rock pressure problem encountered in tunnelling through mudstone bedrock was analyzed using the proposed finite element method, referring to an actual case history in Japan. The results show that undesirable influence of softening on the tunnel behaviour is developed over a long period of time. Relatively large stresses are induced at the floor and spring line with time. It is observed that the variation with time in these stresses is comparable to the field measurements, although the magnitude of the predicted stresses is smaller. This discrepancy in the stresses is attributed to neglecting swelling effects. It is indicated that this case history is dominated by swelling rather than softening.

Some existing analytical methods were modified to take into account the effect of softening by incorporating the proposed failure criterion with the time-dependent strength parameters. Simple examples were analyzed; slope stability, lateral earth pressure and stress and displacement around a tunnel. Sensitivity of the factor of safety and deformation on softening is illustrated. The analysis method can provide a simple and inexpensive means to evaluate the softening effect in geotechnical engineering problems.

A comprehensive finite element method to analyze softening effects is proposed. It unifies softening analysis developed in this research with swelling analysis. An example of analysis is presented which contains the essentials to describe the role of softening in the time-dependent instability, although it is an approximation of the proposed comprehensive analysis. There is a trend that time-dependent deformations observed in fissured, over-consolidated clays and mudstones are analyzed as creep or visco-plastic behaviour because they provide a computationally convenient way to account for time-dependency. However, it should be noted that time-displacement relations presented here are the results of softening not of creep or visco-plasticity. The analysis proposed in this research constitutes an alternate means to analyze time-dependent instability in fissured, over-consolidated clays and mudstones without losing physical insight into the problem.

9.2 Suggestions for future research

It would be valuable to explore more well-instrumented and documented case histories in various parts of the world in order to provide information for evaluating the rate of softening.

It would be necessary to investigate further the shear strength behaviour at low stress levels of fissured, over-consolidated clays and mudstones, particularly in relation to unloading stress paths, since there are only a few comprehensive experimental studies concerning this aspect.

Formulation of a more comprehensive softening analysis by means of the finite element method was suggested in Chapter 8. It couples softening with swelling analyses. The coupled analysis would provide an improved means of predicting the whole history of time-dependent instability in a cut slope and tunnel.

Modelling excavation in the finite element analysis required considerable patience. It has been felt during this research that things such as a proper mesh size and boundary effects may not be determined properly without trial and error, particularly for an elastic-plastic problem and that coping with these problems relies only on the experience of analyst. It would be valuable to establish some kind of criteria for excavation simulation.

In the course of this research, it has been strongly felt to be necessary to improve the development of versatile post-processing programs for interpreting and presenting calculation output efficiently.

References

Adachi, T., Ogawa, T. and Hayashi, M., 1981. "Mechanical properties of soft rock and rock mass". Proc. 10 th Int. Conf. Soil Mech. Found. Enging., Stockholm, Vol. 1, pp. 527-530.

Balmer, G., 1952. "A general analytic solution for Mohr's envelope". Proc. Amer. Soc. Testing Mat., Vol. 52, pp. 1260-1271.

Banks, D. C., 1971. "Study of clayshale slopes". 'Stability of Rock Slopes'. *Edited by* E. J. Cording, ASCE, pp. 303-328.

Bathe, K. J., 1982. "Finite Element Procedures in Engineering Analysis". Prentice-Hall, New Jersey.

Bieniawski, Z. T., 1974. "Estimating the strength of rock materials". Jour. South African Inst. Min. Metall., Vol. 74, No. 8, pp. 312-320.

Bishop, A. W., 1955. "The use of the slip circle in the stability analysis of earth slopes". Geotechnique, Vol. 5, pp. 7-17.

Bishop, A. W., 1966. "The strength of soils as engineering materials". Geotechnique, Vol. 16, pp. 91-130.

Bishop, A. W., 1967. "Progressive failure - with special reference to the mechanism causing it". Proc. Geotech. Conf., Oslo, Vol. 2, pp. 142-150.

Bishop, A. W. and Bjerrum, L., 1960. "The relevance of the triaxial test to the solution of stability problems". Proc. ASCE Res. Conf. Shear Strength of Cohesive Soils, Boulder, Colorado, pp. 437-501.

Bishop, A. W. and Morgenstern, N. R., 1960. "Stability coefficients for earth slopes". Geotechnique, Vol. 10, pp. 129-150.

Bishop, A. W., Webb, D. C. and Lewin, P. I., 1965. "Undisturbed samples of London Clay from Ashford Commonshaft, strength-effective stress relations". Geotechnique, Vol. 15, pp. 1-31.

Bjerrum, L., 1967. "Progressive failure in slopes in over-consolidated plastic clay and clay shales". Jour. of Soil Mech. Found. Div., ASCE, Vol. 93, pp. 3-49.

Botts, M. E., 1986. "The effects of slaking on the engineering behaviour of clayshales". Ph. D. Thesis, Univ. of Colorado, Boulder, U.S.A.

Bromhead, E. N., 1978. "Large landslides in London Clay at Herne Bay, Kent". Quar. J. Engng. Geology, Vol. 11, pp. 291-304.

Bromhead, E. N. and Dixon, N., 1984. "Pore water pressure observations in the coastal clay cliffs at the Isle of Sheppey, England". Proc. 4th Int. Symp. Landslides, Toronto, Vol. 1, pp. 385-390.

Brown, E. T., Bray, J. W., Ladanyi, B. and Hoek, E., 1981. "Ground response curves for rock tunnels". Jour. of Geotech. Engng. Div., ASCE, Vol. 109, pp. 15-39.

Burland, J. B. and Hancock, R. J. R., 1977. "Underground car park at the House of Commons, London: geotechnical aspects". Struct. Engr., Vol. 55, pp. 87-100.

Burnett, A. D. and Fookes, P. G., 1974. "A regional engineering geology study of the London clay in London and Hampshire basins". Qua. Jour. Eng. Geol., Vol. 7, pp. 257-295.

Calabresi, G. and Rampello, S., 1987. "Swelling of over-consolidated clays in excavations". Proc. 9th Euro. Conf. of SMFE, Dublin, Vol. 1, pp. 11-15.

Calabresi,G. and Scarpelli, G., 1985. "Effects of swelling caused by unloading in overconsolidated clays". Proc. 11th ICSMFE, San Francisco, Vol. 2, pp. 411-414.

Cassel, F. L., 1948. "Slips in fissured clay". Proc. 2nd ICSMFE, Rotterdam, Vol. 2, pp. 46-49.

Chan, D. H., 1986. "Finite element analysis of strain softening material". Ph. D. Thesis, Univ. of Alberta, Edmonton, Canada.

Chan, D. H. and Morgenstern, N. R., 1989. "An effective stress approach to undrained analysis". 'Numerical Methods in Geomechanics'. *Edited by* S. Pietruszczak and G. N. Pande, Elsevier Applied Science, London, pp. 740-750.

Chandler, R. J., 1967. "The strength of a stiff silty clay". Proc. Geotech. Conf., Oslo, Vol. 2, pp. 103-108.

Chandler, R. J., 1969. "The effect of weathering on the shear strength properties of Keuper Marl". Geotechnique, Vol. 19, pp. 321-334.

Chandler, R. J., 1972. "Lias clay: weathering processes and their effect on shear strength". Geotechnique, Vol. 22, pp. 403-431.

Chandler, R. J., 1974. "Lias clay: the long-term stability of cutting slopes". Geotechnique, Vol. 24, pp. 21-38.

Chandler, R. J., 1984. "Delayed failure and observed strengths of first-time slides in stiff clays: a review". Proc. 4th Int. Symp. on Landslides, Toronto, pp. 19-25.

Chandler, R. J. and Apted, J. P., 1988. "The effect of weathering on the strength of London Clay". Quar. J. Engng. Geology, Vol. 21, pp. 59-68.

Chandler, R. J. and Skempton, A. W., 1974. "The design of permanent cutting slopes in stiff fissured clays". Geotechnique, Vol. 24, No. 4, pp. 457-466.

De Alencar, J. A., 1988. "Deformation of dams on sheared foundations". Ph. D. Thesis, Univ. of Alberta, Edmonton, Canada.

de Beer, E. E., 1969. "Experimental data concerning clay slopes". Proc. 7th ICSMFE, Mexico, Vol. 2, pp. 517-525.

Denda, A., Watanabe, K., Kawasaki, H. and Nakazawa, A., 1987. "Mechanical characteristics of fully softened Tertiary sedimentary mudstone". Proc. 22 nd Japan National Conf. Soil Mech. Found. Engng., Niigata, Vol. 1, pp. 903-906. (in Japanese).

Desai, C. S. and Christian, J. T., 1977. "Numerical Methods in Geotechnical Engineering". McGraw-Hill, New York.

Dounias, G. T., 1987. "Progressive failure in embankment dams". Ph. D. Thesis, Univ. of London, London, U.K.

Dounias, G. T., Potts, D. M. and Vaughan, P. R., 1988. "The shear strength of soils containing undulating shear zones - a numerical study". Can. Geotech. Jour., Vol. 25, pp. 550-558.

Duncan, J. M. and Wright, S. G., 1980. "The accuracy of equilibrium methods of slope stability analysis". Engng. Geology, Vol. 16, pp. 5-17.

Duncan, J. M., Low, B. K. and Schaefer, V. R., 1985. "STABGM: A computer program for slope stability analysis of reinforced embankments and slopes". Dept. of Civil Engng., Virginia Polytech. Inst. State Univ., Backsburg, Virginia, USA.

Eigenbrod, K. D., 1972. "Progressive failure in overconsolidated clays and mudstones". Ph.D. Thesis, Univ. of Alberta, Edmonton, Canada.

Eigenbrod, K. D., 1975. "Analysis of the pore pressure changes following the excavation of a slope". Can. Geotech. Jour., Vol. 12, pp. 429-440.

Eigenbrod, K. D. and Morgenstern, N. R., 1971. "A slide in Cretaceous bedrock at Devon, Alberta", in 'Geotechnical Practice for Stability in Open Pit Mining'. *Edited by* C. O. Brawner and V. Milligan, AIME, New York, pp. 223-238.

Franklin, J. A. and Hoek, E., 1970. "Developments in triaxial testing technique". Rock Mech., Vol. 2, pp. 223-228.

Gates, R. H., 1972. "Progressive failure model for clay shale". Proc. Symp. Appl. FEM in Geotech. Engng., Vicksburg, pp. 327-348.

Gibo, S., 1987. "Shear strength parameters required for evaluation of stability of slopes". Tsuchi-To-Kiso, JSSMFE, No. 11, Vol. 35, pp. 27-32. (in Japanese).

Goodman, R. E., 1980. "Introduction to Rock Mechanics". John Wiley and Sons, New York.

Graham, J. and Au, V. C. S., 1985. "Effects of freeze-thaw and softening on a natural clay at low stresses". Can. Geotech. Jour., Vol. 22, pp. 69-78.

Graham, J. and Shields, D. H., 1985. "Influence of geology and geological processes on the geotechnical properties of a plastic soil". Engng. Geology, Vol. 22, pp. 109-126.

Griffith, A. A., 1921. "The phenomena of rupture and flow in solids". Phil. Trans. Roy. Soc. London, Ser. A, 221, pp. 163-198.

Griffith, A. A., 1924. "Theory of rupture". 1st Int. Congr. Appl. Mech., Delft, pp. 55-63.

Henkel, D. J., 1956. "Discussion" on 'Earth movement affecting L.T.E. railway in deep cutting east of Uxbridge'., Proc. Inst. Civil Engineers, Vol. 5, pp. 320-324.

Henkel, D. J., 1957. "Investigation into two long-term failures in London Clay slopes at Wood Green and Northolt". Proc. 4th ICSMFE, London, Vol. 2, pp. 315-320.

Hirano, I., Takeda, N., Honma, N. and Sato, M., 1983. "Measurement and analysis of tunnel excavated in expansive stone". Proc. 15th Japan National Symp. on Rock Mechanics, JSCE, pp. 81-85.

Hobbs, D. W., 1966. "A study of the behaviour of broken rock under triaxial compression, and its application to mine roadways". Int. Jour. Rock Mech. Mining Sci., Vol. 3, pp. 11-43.

Hoeg, K., 1972. "Finite element analysis of strain-softening clay". Jour. of Soil Mech. Found. Div., ASCE, Vol. 98, pp. 43-58.

Hoek, E., 1968. "Brittle failure of rock". In 'Rock Mechanics in Engineering Practice', *Edited by* K. G. Stagg and O. C. Zienkiewicz, London, John Wiley and Sons, pp. 99-124.

Hoek, E., 1983. "Strength of jointed rock masses". 23rd Rankine Lecture, Geotechnique, Vol. 33, No. 3, pp. 187-223.

Hoek, E. and Bray, J. W., 1981. "Rock slope engineering". Revised 3rd edition, Inst. of Mining and Metallurgy, London, U.K.

Hoek, E. and Brown, E. T., 1980. "Empirical strength criterion for rock masses". Jour. of Geotech. Div., ASCE, Vol. 106, No. GT9, pp. 1013-1035.

Jaeger, J. C., 1970. "Behaviour of closely jointed rock". In 'Rock Mechanics - Theory and Practice'. Proc. 11th Symp. Rock Mech., Berkeley, California, pp. 57-68.

James, P. M., 1970. "Time effects and progressive failure in clay slope". Ph.D. Thesis, Univ. of London, London, U.K.

Kaiser, P. K., 1980. "Effect of stress-history on the deformation behaviour of underground openings". Proc. 13th Can. Rock Mech. Symposium, Toronto, pp. 133-140.

Katzenbach, R., 1981. "Entwicklungstendenzen beim Bau und der Berechnung oberflächennaher Tunnel in bebautem Stadtgebiet". Mitteilungen der Versuchsanstalt für Bodenmechanik und Grundban der Technischen Hochschule Darmstadt, Heft. 24.

Kawamoto, O. and Tanaka, T., 1988. "Elasto-plastic analysis of unstable slopes in the typical case records". Tsuchi-To-Kiso, JSSMFE, No.5, Vol. 36, pp. 49-54. (in Japanese).

Kjartanson, B. H., 1978. "A study of delayed failure of a cut slope in stiff clay". M. Sc. Thesis, Univ. of Alberta, Edmonton, Canada.

Komiya, Y. and Shinjo, T., 1984. "On the compression properties of mudstones". Proc. 16th Japan National Symp. on Rock Mechanics, JSCE, pp. 67-72.

Ladd, C. C., 1960. "Mechanisms of swelling by compacted clay". High. Res. Board, Bulletin 245, pp. 10-26.

Lambe, T. W. and Whitman, R. V., 1979. "Soil Mechanics, SI version". John Wiley and Sons, New York.

Lo, K. Y. and Lee, C. F., 1973. "Stress analysis and slope stability in strain-softening materials". Geotechnique, Vol. 23, pp. 1-11.

Lutton, R. J. and Banks, D. C., 1970. "Study of clayshale slopes along the Panama Canal: East Culebra and West Culebra Slides and the Model Slope". U.S.A.E.W.E.S., Tech. Rept. S-70-9, Report 1, Vicksburg, U.S.A.

Marsland, A., 1971. The shear strength of stiff fissured clays in "Stress-strain Behaviour of Soils", Roscoe Memorial Symp., Foulis, Henley-on-Thames, U.K., pp. 59-68.

Matsumoto, T. and Ko, H. Y., 1982. "Finite element analysis of strain-softening soils". Proc. 4th Int. Conf. Num. Meth. in Geomechanics, Edmonton, Vol. 1, pp. 213-222.

McClintock, F. A. and Walsh, J. B., 1962. "Friction on Griffith cracks under pressure". Proc. 4th US Congr. Appl. Mech., Berkeley, Vol. 2, pp. 1015-1021.

McGown, A., Roberts, A. G. and Woodrow, L. K. R., 1987. "Long-term pore water pressure variations within coastal cliffs in North Kent". Proc. 9th Euro. Conf. SMFE, Dublin, Vol. 1, pp. 455-460.

Moore, I. D. and Rowe, R. K., 1988. "Numerical models for evaluating progressive failure in earth structures - a review". Computers and Geotechnics, Vol. 6, pp. 217-239.

Morgenstern, N. R., 1977. "Slopes and excavations in heavily over-consolidated clay", State-of-the-Art report. Proc. 9th ICSMFE, Tokyo, Vol. 2, pp. 547-604.

Morgenstern, N. R. and Eigenbrod, K. D., 1974. "Classification of argillaceous soils and rocks". Jour. of Geotech. Div., ASCE, Vol. 100, pp. 1137-1156.

Moriwaki, Y., 1974. "Causes of slaking in argillaceous materials". Ph. D. Thesis, Univ. of California, Berkeley, California.

Muir Wood, A. W., 1971. "Engineering aspects of coastal landslides". Proc. Inst. Civil Eng., Vol. 50, pp. 257-276.

Murrell, A. F., 1965. "The effect of triaxial stress systems on the strength of rocks at atmospheric temperatures". Jour. Geophysics, Vol. 10, pp. 231-281.

Nakano, R., 1967. "On weathering and change of properties of Tertiary mudstone related to landslide". Soils and Foundations, No. 1, Vol. 7, pp. 1-4.

Nakano, R., 1974. "On the design of water tunnels in relation with the type and magnitude of rock load with special reference to the mechanism and prediction of squeezing-swelling rock pressure". Bulletin, National Res. Inst. of Agri. Engng., Ministry of Agri. and Forestry, Japan, No. 12, pp. 89-133. (in Japanese).

Nakano, R., 1979. "Geotechnical properties of mudstone of Neogene Tertiary in Japan with special reference to the mechanism of squeezing swelling rock pressure in tunnelling". Proc. Int. Symp. on Soil Mech., Oaxaca, Vol. 1, pp. 75-92.

Nakano, R., 1981. "On the mechanism of swelling rock pressure on tunnels driven through mudstone". Proc. Int. Symp. on Weak Rock, Tokyo, Vol. 2, pp. 1007-1012.

Nayak, G. C. and Zienkiewicz, O. C., 1972. "Elasto-plastic stress analysis. A generalization for various constitutive relations including strain softening". Int. Jour. Num. Meth. in Engng., Vol. 5, pp. 113-135.

Nelson, J. D. and Thompson, E. G., 1974. "Creep failure of slopes in clay and clayshale". Proc. 12th Annual Engng. Geol. and Soil Engng. Symp., Boise, pp. 177-195.

Nelson, J. D. and Thompson, E. G., 1977. "A theory of creep failure in overconsolidated clay". Jour. of Geotech. Engng. Div.,ASCE, Vol. 103, pp. 1281-1291.

Ohtsuka, M. and Takano, A., 1980. "Displacement due to tunnel excavation and geological characteristics in swelling mudstone". Tsuchi-to-Kiso, JSSMFE, No. 7, Vol. 28, pp. 29-36. (in Japanese).

Owen, D. R. J. and Hinton, E., 1980. "Finite Elements in Plasticity: Theory and Practice". Pineridge Press Limited, Swansea, U.K.

Patton, F. D., 1966. "Multiple modes of shear failure in rock". Proc. 1st Congr. of Int. Soc. Rock Mech., Lisbon, Vol. 1, pp. 509-514.

Petterson, R. and Peters, N., 1963. "Heave of spillway structures on clay shales". Can. Geotech. J., Vol. 1, No. 1, pp. 5-15.

Pietruszczak, S. and Mroz, Z., 1981. "Finite element analysis of deformation of strain-softening materials". Int. Jour. Num. Meth. in Engng., Vol. 17, pp. 327-334.

Pietruszczak, S. and Stolle, D. F. E., 1985. "Deformation of strain-softening materials". Computers and Geotechnics, Vol. 1, pp. 99-115.

Prevost, J. H., 1974. "Soil stress-strain-strength models based on plasticity theory". Ph. D. Thesis, Stanford Univ., Stanford, California, USA.

Prevost, J. H. and Hoeg, K., 1975. "Soil mechanics and plasticity analysis of strain softening". Geotechnique, Vol. 25, pp. 279-297.

Rankine, W. J. M., 1857. "On the stability of loose earth". Phil. Trans. Roy. Soc. London, 147, pp. 9-27.

Scarpelli, G. and Calabresi, G., 1984. "A typical earthflow in a weathered clay at Todi". Proc. 6th Int. Symp. on Landslides, Toronto, Vol. 3, pp. 119-121.

Schwartz, A. E., 1964. "Failure of rock in the triaxial shear test". Proc. 6th Symp. Rock Mech., Rolla, Missouri, pp. 109-135.

Shinjo, T., 1976. "Shear strength characteristics of Shimajiri mudstone". Memoirs of Dept. of Agri. Engng., Univ. of Ryukyus, Vol. 23, pp. 237-254. (in Japanese).

Sidharta, A. S., 1985. "Prediction of creep failure of excavations in overconsolidated clay with pore pressure dissipation". Ph. D. Thesis, Colorado State Univ., Fort Collins, Colorado, U.S.A.

Simmons, J. V., 1981. "Shearband yielding and strain weakening". Ph. D. Thesis, Univ. of Alberta, Edmonton, Canada.

Simpson, B., Calabresi, G., Sommer, H. and Wallays, M., 1979. "Design parameters for stiff clays". Proc. 7th Euro. Conf. SMFE, Brighton, England, Vol. 5, pp. 91-125.

Skempton, A. W., 1948. "The rate of softening of stiff fissured clays with special reference to London Clay". Proc. 2nd ICSMFE, Rotterdam, Vol. 2, pp. 50-53.

Skempton, A. W., 1954. "The pore-pressure coefficients A and B". Geotechnique, Vol. 4, pp. 143-147.

Skempton, A. W., 1970. "First time slides in over-consolidated clays". Geotechnique, Vol. 20, pp. 320-324.

Skempton, A. W., 1977. "Slope stability of cuttings in Brown London Clay". Proc. 9th ICSMFE, Tokyo, Vol. 3, pp. 261-270.

Skempton, A. W. and DeLory, F. A., 1957. "Stability of natural slopes in London Clay". Proc. 4th ICSMFE, London, Vol. 2, pp. 378-381.

Skempton, A. W. and Petley, D. J., 1967. "The strength along structural discontinuities in stiff clays". Proc. Geotech. Conf., Oslo, Vol. 2, pp. 3-20.

Tanaka, T. and Kawamoto, O., 1989. "Plastic collapse analysis of slopes of strain softening materials". 'Numerical Models in Geomechanics'. *Edited by* S. Pietruszczak and G. N. Pange, Elsevier Applied Science, London, pp. 667-674.

Terzaghi, K., 1936. "Stability of slopes in natural clay". Proc. ICSM, Harvard, Vol. 1, pp. 161-165.

Terzaghi, K. and Peck, R. B., 1948. "Soil Mechanics in Engineering Practice", John Wiley & Sons, N.Y.

Thomson, S. and Kjartanson, B. H., 1985. "A study of delayed failure of a cut slope in stiff clay". Can. Geotech. J., Vol. 22, pp. 195-207.

Thomson, S. and Tweedie, R. W., 1978. "The Edgerton landslide". Can. Geotech. Jour., Vol. 15, pp. 510-521.

Tweedie, R. W., 1976. "An investigation of the Edgerton Landslide, Wainwright, Alberta". M. Sc. Thesis, Univ. of Alberta, Edmonton, Canada.

Vaughan, P. R. and Walbancke, H. J., 1973. "Pore pressure changes and the delayed failure of cutting slopes in overconsolidated clay". Geotechnique, Vol. 23, pp. 531-539.

Vermeer, P. A. and De Borst, R., 1984. "Non-associated plasticity for soils, concrete and rock". Heron, Vol. 29, No. 3.

Walbancke, H. J., 1975. "Pore pressure in clay embankments and cuttings". Ph. D. Thesis, Univ. of London, London, U.K.

Ward, W. H., Samuels, S. G. and Butler, M. E., 1960. "Further studies of the properties of London Clay". Geotechnique, Vol. 10, pp. 33-58.

Watanabe, K., Denda, A., Kawasaki, H. and Nakazawa, A., 1988. "Constitutive equation of tertiary sedimentary mudstone considering strain hardening and strain softening". Proc. 6th Int. Conf. Num. Meth. in Geomechanics, Innsbruck, Vol. 1, pp. 385-390.

Watanabe, K., Kawasaki, H., Denda, A. and Nakazawa, A., 1987. "Elasto-plastic behaviour of Tertiary sedimentary mudstone considering strain hardening and strain softening". Proc. 22nd Japan National Conf. Soil Mech. Found. Engng., Niigata, Vol. 1, pp. 907-910. (in Japanese).

Wawersik, W. R., 1968. "Detailed analysis of rock failure in laboratory compression tests". Ph. D. thesis, Univ. of Minnesota, Minneapolis, Minnesota.

Yoshinaka, R. and Yamabe, T., 1980. "Strength criterion of rocks". Soils and Foundations, JSSMFE, Vol. 20, No. 4, pp. 113-126.

Zienkiewicz, O. C., 1977. "The Finite Element Method". Third revised edition, McGraw-Hill, U.K.

Appendix

Determination of strength parameters A, B and S

The failure criterion is written as:

$$\sigma_1 = \sigma_3 + A\,\sigma_c \left(\frac{\sigma_3}{\sigma_c} - S \right)^{\frac{1}{B}} \tag{A1}$$

Initially, the following condition must be satisfied:

$$A \left(- S \right)^{\frac{1}{B}} = 1 \tag{A2}$$

Substituting Equation (A2) into Equation (A1) for A, one can obtain the following equation:

$$y = a\,x \tag{A3}$$

where

$$y = \ln \left(\frac{\sigma_1 - \sigma_3}{\sigma_c} \right)$$

$$x = \ln \left(1 - \frac{\sigma_3}{S\,\sigma_C} \right)$$

$$a = \frac{1}{B}$$

By the application of the least squares method, the parameter B and the coefficient of determination r^2 are given as follows:

$$B = \frac{\sum_{i=1}^{N} x_i^2}{\sum_{i=1}^{N} x_i \, y_i} \tag{A4}$$

$$r^2 = \frac{\left\{\sum_{i=1}^{N} x_i \, y_i\right\}^2 \left\{\sum_{i=1}^{N} x_i^2 - \frac{\left(\sum_{i=1}^{N} x_i\right)^2}{N}\right\}}{\left\{\sum_{i=1}^{N} y_i^2 - \frac{\left(\sum_{i=1}^{N} y_i\right)^2}{N}\right\}\left(\sum_{i=1}^{N} x_i^2\right)^2} \tag{A5}$$

where N is the total number of data set. A value of B is calculated for an arbitrary value of S. By using an iterative method for various values of S, the values of B and S are determined which give the best correlation, $r^2=1$. Then, the value of A is computed using Equation (A2) with these values of B and S.

To determine the strength parameters from direct shear test results, it is necessary first to estimate maximum and minimum principal stresses. For this purpose, the following relations, derived by Balmer (1952), are used:

$$\sigma = \sigma_3 + \frac{\sigma_1 - \sigma_3}{1 + \frac{\partial \sigma_1}{\partial \sigma_3}} \tag{A6}$$

$$\tau = \frac{\sigma_1 - \sigma_3}{1 + \frac{\partial \sigma_1}{\partial \sigma_3}} \sqrt{\frac{\partial \sigma_1}{\partial \sigma_3}} \tag{A7}$$

$$\tan \phi_i = \frac{\frac{\partial \sigma_1}{\partial \sigma_3} - 1}{2\sqrt{\frac{\partial \sigma_1}{\partial \sigma_3}}} \qquad \text{(A8)}$$

$$c_i = \tau - \sigma \tan \phi_i \qquad \text{(A9)}$$

It can be assumed that relation between σ and τ in the entire data obtained experimentally is approximated to be linear or non-linear. When the linear relation is assumed as:

$$\tau = c + \sigma \tan \phi \qquad \text{(A10)}$$

σ_1 and σ_3 can be calculated as follows (Hoek, 1983):

$$\sigma_3 = \frac{\{ \sigma^2 + (\tau - c) \tau \} - \tau \sqrt{\sigma^2 + (\tau - c)^2}}{\sigma} \qquad \text{(A11)}$$

$$\sigma_1 = \frac{\{ \sigma^2 + (\tau - c) \tau \} + \tau \sqrt{\sigma^2 + (\tau - c)^2}}{\sigma} \qquad \text{(A12)}$$

When the non-linear relation is assumed as:

$$\tau = p (\sigma - q)^r \qquad \text{(A13)}$$

σ_1 and σ_3 can be calculated as follows:

$$\sigma_3 = \sigma - \tau N_1 \qquad \text{(A14)}$$

$$\sigma_1 = \sigma + \tau N_1 N_2^2 \qquad \text{(A15)}$$

where

$$N_1 = p r (\sigma - q)^{r - 1} - \sqrt{p^2 r^2 (\sigma - q)^{2(r - 1)} + 1}$$

$$N_2 = p\,r(\sigma - q)^{r-1} + \sqrt{p^2\,r^2\,(\sigma - q)^{2(r-1)} + 1}$$

After the calculation of the values of σ_1 and σ_3 using the above equations, the parameters A, B and S are determined according to the method described earlier.

Determination of strength parameters P, Q and R

The alternative failure criterion is written as:

$$\tau = P\,\sigma_c \left(\frac{\sigma}{\sigma_c} - Q \right)^{\frac{1}{R}} \qquad \text{(A16)}$$

Re-writing the above equation,

$$y = a\,x + b \qquad \text{(A17)}$$

where

$$y = \ln \frac{\tau}{\sigma_c}$$

$$x = \ln \left(\frac{\sigma}{\sigma_c} - Q \right)$$

$$a = \frac{1}{R}$$

$$b = \ln P$$

The value of the parameter Q is computed by solving the following equation:

$$Q + A(Q - S)^{\frac{1}{B}} = 0 \qquad \text{(A18)}$$

where A, B and S are strength parameters in Equation (A1). The values of P and R are given as:

$$R = \frac{\sum_{i=1}^{N} x_i^2 - \frac{\left(\sum_{i=1}^{N} x_i\right)^2}{N}}{\sum_{i=1}^{N} x_i\, y_i - \frac{\left(\sum_{i=1}^{N} x_i \sum_{i=1}^{N} y_i\right)}{N}} \tag{A19}$$

$$\ln P = \frac{\sum_{i=1}^{N} y_i}{N} - B\,\frac{\sum_{i=1}^{N} x_i}{N} \tag{A20}$$

The values of R and P are calculated for values of σ and τ given by substituting arbitrary values of σ_3 into Equations (A1), (A6) and (A7).